COMPUTATION AND CHARACTERISTICS OF INFLATIONARY THREE-POINT FUNCTIONS

A THESIS
submitted by

V. SREENATH

for the award of the degree
of

DOCTOR OF PHILOSOPHY

DEPARTMENT OF PHYSICS
INDIAN INSTITUTE OF TECHNOLOGY MADRAS
MARCH 2015

Dedicated to

my mother

Smt. Sathy Vijayakumar

THESIS CERTIFICATE

This is to certify that the thesis titled **Computation and characteristics of inflationary three-point functions**, submitted by **V. Sreenath**, to the Indian Institute of Technology, Madras, for the award of the degree of **Doctor of Philosophy**, is a bona fide record of the research work done by him under my supervision. The contents of this thesis, in full or in parts, have not been submitted to any other Institute or University for the award of the degree.

Dr. L. Sriramkumar
Research Guide
Associate Professor
Department of Physics
Indian Institute of Technology Madras
Chennai 600 036

Place: Chennai
Date: 05 March 2015

ACKNOWLEDGEMENTS

This thesis would not have been complete without the help and support of a lot of people. First of all, I am grateful to Dr. L. Sriramkumar, my thesis supervisor, without whom I could not have completed this thesis. I would like to thank him for guiding me through my Ph. D. and for ensuring that I get a good start in my career. I also appreciate and is thankful for the love and care that he showered up on me during the years of my Ph. D. Thank you very much sir for being there for me.

I would like to thank Profs. Suresh Govindarajan, Ghanashyam Date, James F. Libby and Anil Prabhakar, members of the doctoral committee, for their valuable suggestions. Prof. Suresh has been a constant source of guidance from the beginning of my Ph. D. I would like to thank him for all the help that he has provided. I am thankful to Prof. Ghanashyam Date for his continued support for my future aspirations. Prof. G. Markandeyulu was the head of the department when I joined the institute. I would like to thank him for supporting and guiding me at times when it mattered most. I would also like to thank Prof. P. B. Sunil Kumar, current Head of the department, for the support he has provided. I am also grateful to various other faculty members in our department for their support and guidance at various instances of my life as a Graduate student. I would like to thank Prof. S. Lakshmi Bala for her timely advice and support and Dr. Dawood Kothawala for his support. I would also like to thank my collaborators Dr. Rakesh Tibrewala and Dr. Dhiraj Kumar Hazra for helping me in my learning process.

As a Ph. D. student, I had to go through various administrative procedures. My sincere thanks to the department office staff, administrative and other staff of the institute for assisting me in these and making the process smooth. I would like to thank people behind various institute facilities such as HPCE, CC, various sports facilities, institute transport and so on for making this journey comfortable. I am also thankful to CCW and institute hospital for making my stay in the institute pleasant.

I have been lucky to have Jaffino, Debika and Rathul as my lab mates. Thanks a lot for making our lab a joyous place to work. I would like to thank Debika for painstakingly

reading through my thesis and for her suggestions in improving it. I would like to thank my batch mates: Rajasekhar, Sreeja, Dinesh, Ramanjaneyulu, Pranati, Mridula, Kapil, Imran and Sasibhushan for their companionship. These five years of my life would have been difficult if for not the constant company of my friends. I am thankful to my friends: Raman, Pradheesh, Pramod, Pattambi, Minakshi, Dhanya, Priyanka, Ganga, Prasanth, Resmi, Rebin, Jinu, Vasu, Krishnadas, Subeesh, Anoop, Prathyusha, Balu, Ankur, Gokul, Basith, Jafar, Deepak, Swetambar and many others for being there for me when it mattered most.

I thank all my teachers, beginning from my kindergarten to my masters, for opening the gates of knowledge to me. I would like to thank all my friends and teachers at Chinmaya mission for introducing me to the teachings of Swami Chinmayananda on Bhagavad Geeta and Upanishads, from which I draw my inspiration.

I am thankful to my parents for making me what I am. I am grateful to my father for his love and blessings. My mother, who has never faltered in the face of a challenge, has been a constant source of inspiration for me. Without her love and affection, I would not have been able to reach this stage in life. I also thank my sisters Remya and Dhanya for all the love and support. I also thank all other family members for their love and blessings.

Last but not the least I bow down to the countless sacrifices of all those known and unknown people which have helped me in my growth.

ABSTRACT

KEYWORDS: Inflation, Non-Gaussianity, Consistency relations

Over the last decade, it has been realized that non-Gaussianities and, in particular, the scalar bi-spectrum can provide a powerful handle to arrive at a much smaller class of viable inflationary models. Such an expectation has been corroborated to a substantial extent by the strong constraints that have been arrived at from the Planck data on the three non-Gaussianity parameters, *viz.* ($f_{\rm NL}^{\rm loc}$, $f_{\rm NL}^{\rm eq}$, $f_{\rm NL}^{\rm ortho}$), that are commonly used to characterize the scalar bi-spectrum. While a considerable amount of effort has been dedicated to understanding the generation and imprints of the scalar bi-spectrum, a rather limited amount of attention has been paid to investigating the three-point functions involving the tensor perturbations. This thesis aims at the numerical computation of the three-point functions in general, with specific focus on understanding their behavior in the squeezed limit. In what follows, we shall provide a brief outline of the various issues that we have dealt with in this thesis.

On the scalar consistency relation away from slow roll: The non-Gaussianity parameter $f_{\rm NL}$, which is often used to characterize the amplitude of the scalar bi-spectrum, can be expressed completely in terms of the scalar spectral index $n_{\rm s}$ in the squeezed limit, wherein one of the wavenumbers involved is much larger than the other two. This relation, while it is largely discussed in the context of slow roll inflation, is actually expected to hold in any single field model of inflation, irrespective of the dynamics of the underlying model, provided inflation occurs on the attractor at late times. In this work, we explicitly examine the validity of the consistency relation, analytically as well as numerically, *away from slow roll*. Analytically, we arrive at the relation in the simple case of power law inflation and the non-trivial but analytically tractable example of the Starobinsky model involving a linear potential with a sudden change in its slope (which leads to a brief period of fast roll). We then numerically evaluate the scalar bi-spectrum for an arbitrary triangular configuration of the wavenumbers in inflationary models that lead to the following features in the scalar power spectrum due to departures from slow roll: (i) a sharp cut off at

large scales, (ii) a burst of oscillations over an intermediate range of scales and (iii) small, but repeated, modulations extending over a wide range of scales, and explicitly illustrate that, in the squeezed limit, the consistency condition is indeed satisfied even in situations consisting of strong deviations from slow roll.

Numerical evaluation of the inflationary three-point functions involving tensors: In this work, utilizing the Maldacena formalism and extending the earlier efforts to compute the scalar bi-spectrum, we construct a numerical procedure to evaluate the three-point scalar-tensor cross-correlations as well as the tensor bi-spectrum in single field inflationary models involving the canonical scalar field. We illustrate the accuracy of the adopted procedure by comparing the numerical results with the analytical results that can be obtained in the simpler cases of power law and slow roll inflation. We also carry out such a comparison in the case of the Starobinsky model, which provides a non-trivial and interesting (but, nevertheless, analytically tractable) scenario involving a brief period of deviation from slow roll. We then utilize the code we have developed to evaluate the three-point correlation functions of interest (and the corresponding non-Gaussianity parameters that we introduce) for an arbitrary triangular configuration of the wavenumbers in three different classes of inflationary models which lead to features in the scalar power spectrum, as have been recently considered by the Planck team. We also discuss the contributions to the three-point functions during preheating in inflationary models with a quadratic minimum.

Examining the consistency relations involving tensors: In this work, we consider the consistency relations associated with the three-point cross-correlations involving scalars and tensors as well as the tensor bi-spectrum in inflationary models driven by a single, canonical, scalar field. Characterizing the cross-correlations in terms of the dimensionless non-Gaussianity parameters $C^{\mathcal{R}}_{\rm NL}$ and $C^{\gamma}_{\rm NL}$ that we had introduced earlier, we express the consistency relations governing the cross-correlations as relations between these non-Gaussianity parameters and the scalar or tensor spectral indices, in a fashion similar to that of the purely scalar case. We also discuss the corresponding relation for the non-Gaussianity parameter $h_{\rm NL}$ used to describe the tensor bi-spectrum. We analytically establish these consistency relations explicitly in the following two situations: a simple example involving a specific case of power law inflation and the non-trivial scenario arising in the Starobinsky model. We also numerically verify the consistency relations in three types of inflationary models that permit deviations from slow roll and lead to scalar power spectra with features which typically result in an improved fit to the data than the more conventional, nearly scale invariant, spectra.

Contents

List of Figures

Chapter 1

Introduction and background

1.1 The standard cosmological model and beyond

Cosmology as a scientific theory, supported by empirical evidence, has taken giant strides over the last century. With an array of satellite and terrestrial missions dedicated to high quality observations of astrophysical and cosmological phenomena over a wide range of length scales, today, we are in an unprecedented position to test our theories against various cosmological data. Due to this reason, it is often said that we are in an era of precision cosmology. The universe as we know today is best described by a theory known as the standard cosmological model, which has its roots in the discovery of the expansion of the universe in the early part of the last century. Since then, various observations have broadened our understanding of the universe. The standard cosmological model can be said to be based on the following four aspects (in this context, see the texts [1] and the references therein).

In order to describe the universe, it proves to be convenient to assume that it is homogeneous and isotropic. Originally, it was considered to be so for theoretical convenience. However, in the modern viewpoint, this assumption, which is often referred to as the cosmological principle, is based on observations such as the exceedingly isotropic nature of the Cosmic Microwave Background (CMB) [2, 3, 4, 5, 6]. It is also supported by the observations of the large scale structure in the universe [7, 8]. The observed distribution of matter in the universe seems to suggest that the universe is indeed homogeneous and isotropic on length scales of the order of $100\,\mathrm{Mpc}$ or so (see, for instance, Ref. [9]).

Secondly, the expansion of the universe and the behaviour of the energy densities of matter and radiation suggest that the universe underwent a hot radiation dominated phase in its early stages. During this regime, the radiation was strongly coupled to mat-

ter. As the universe expanded, it cooled down, and transited from a radiation dominated epoch to a regime of matter domination. Moreover, as the universe transited to the matter dominated phase, the photons decoupled from the electrons and started streaming freely. It is this stream of photons which we observe today as the CMB. The discovery of the CMB gave great impetus to the development of the theory that is now popularly referred to as the hot big bang model. The hot epoch of the early universe is also responsible for the formation of light elements, a phenomenon that is known as big bang nucleosynthesis. The physics at these energy scales being well understood, we have a good theoretical grasp of the phenomenon. The theoretical understanding is corroborated to a large extent by the observations of the abundances of the light elements in the universe (see, for example, Refs. [10, 11]).

Thirdly, though the CMB is highly isotropic, it contains tiny anisotropies at the level of one part in 10^5 [2, 5, 6]. According to the by-now conventional picture, it is these anisotropies in the CMB that grow through gravitational instability to form the structures that we see around us today. However, within the hot big bang model, the scales of cosmological interest are well outside the causally connected domains during the early epochs of radiation domination. As a result, the hot big bang model is unable to provide a causal mechanism for the origin of structures in the universe. As we shall describe in some detail below, often, an epoch of accelerated expansion, referred to as inflation, is invoked to explain the origin of perturbations in the early universe (see the texts [1] and the reviews [12]). We should hasten to clarify that the inflationary scenario does not necessarily form a part of the standard cosmological model. Within the standard cosmological model, it is *assumed* that the primordial perturbations are adiabatic in nature, with a nearly scale invariant power spectrum. It is these perturbations which, in turn, are supposed to lead to the observed anisotropies in the CMB and the large scale structure.

Lastly, observations of distant supernovae suggest that the universe is currently undergoing a period of accelerated expansion [13, 14]. Such an accelerated expansion cannot be achieved by ordinary matter and one requires a source with a relatively peculiar equation of state to drive the rapid expansion. It is believed that a cosmological constant or, more generically, dark energy is responsible for this behaviour.

In summary, these four elements, supported by various other observations, indicate that ours is a spatially flat, homogeneous and isotropic, expanding universe. The observations also suggest that there was an early phase when the seeds for the formation of large scale structure were sown. This epoch was followed by eras of radiation and matter domination and, more recently, by a cosmological constant (or dark energy) dominated

regime, which is supposed to be driving the current epoch of accelerated expansion. The model of our universe based on these aspects is known as the standard cosmological model [1]. Since the observations point to the fact that roughly 70% of the energy density of the universe is in form of cosmological constant (Λ), while 25% is in the form of pressureless Cold Dark Matter (CDM), the standard cosmological model is also called the ΛCDM model (for the recent constraints from the CMB data on the cosmological parameters, see, for example, Refs. [15, 16]).

On cosmological scales, the Newtonian theory of gravitation ceases to be valid and one needs to consider a relativistic theory to describe gravity. Amongst the relativistic theories of gravitation, Einstein's general theory of relativity proves to be the simplest and seems to be consistent with the various data available at hand (in this context, see, for instance, Ref. [17]). Hence, in the standard cosmological model, the dynamics of the universe is assumed to be governed by Einstein's general theory of relativity. Throughout this thesis, we shall assume that gravity is described by the general theory of relativity.

An impressive feat of the standard cosmological model is that it has been able to account for a large set of observations with just six parameters, four of which describe the background, while two characterize the primordial perturbations [15, 16]. In spite of its success, the model leaves us with a few open questions. For instance, according to the model, about 95% of the universe consists of dark matter and dark energy. But, as the names indicate, we seem to know nothing beyond their equations of state and we are fairly in the dark about the nature of these constituents. The other crucial issue, which this thesis will focus on, is the physical process that might have sown the seeds for the formation of structures in the universe. As we mentioned before, within the standard model, the scales of cosmological interest are well outside the causally connected domain during the early stages of the radiation dominated era. Hence, we require a mechanism to bring these scales inside the Hubble radius at early times and lead to the generation of perturbations. Such a mechanism is provided by the inflationary paradigm, according to which, the universe went through a period of accelerated expansion at a very early stage [1, 12]. Though there exist some alternatives to inflation, such as the bouncing model which assumes that the universe underwent a phase of contraction before it entered the current expanding phase (see, for instance, the early efforts [18] and the more recent reviews [19]), none of them seem to perform as effectively against the various cosmological data as inflation is capable of. As we shall discuss later in this chapter, inflation can be easily achieved with the help of scalar fields that are slowly rolling down a relatively flat potential. However, the ease with which inflation can be accomplished also leads to a situation wherein

many models perform almost equally well against the cosmological data [20, 21].

Often, inflationary models are compared with the cosmological data at the level of the power spectra. Over the last decade, it has been realized that non-Gaussianities and, in particular, the scalar three-point function, also referred to as the scalar bi-spectrum, can provide a powerful handle on arriving at a much smaller class of viable inflationary models (for initial efforts in this direction, see, for example, Refs. [22]; for more recent work, see Refs. [23, 24, 25]). Such an expectation has been corroborated to a substantial extent by the strong constraints that have been arrived at from the Planck data on the non-Gaussianity parameters that are commonly used to characterize the scalar bi-spectrum (for earlier work, *i.e.* prior to Planck, towards arriving at observational constraints, see, for instance, Refs. [26, 27]; for the constraints from Planck, see Refs. [28, 29]). While a considerable amount of effort has been dedicated to understanding the generation and imprints of the scalar bi-spectrum, a rather limited amount of attention has been paid to investigating the three-point functions involving the tensor perturbations [30, 31, 32, 33, 34]. Broadly, this thesis can be said to be aimed at investigating the properties of the three-point functions involving scalars as well as tensors generated during inflation and the possible contributions to these correlation functions due to non-trivial post-inflationary dynamics such as preheating.

The remainder of this chapter is organized as follows. In the following two sections, we shall quickly describe the need for the inflationary paradigm and discuss how inflation can be achieved using a scalar field. In Sec. 1.4, we shall consider cosmological perturbation theory at the linear order. After describing the action governing the scalar and the tensor perturbations at the second order, we shall discuss the definitions of the scalar and the tensor power spectra and also arrive at the power spectra in the slow roll approximation. We shall also briefly discuss the current constraints on inflationary models at the level of power spectra. In Sec. 1.5, we shall outline the formalism due to Maldacena for the calculation of the inflationary three-point functions. We shall also utilize the formalism to arrive at all the three-point functions in the slow roll approximation. We shall further discuss the recent constraints on the scalar bi-spectrum arrived at from the CMB data. In Sec. 1.6, we shall sketch the basic aspects of preheating. Finally, we shall conclude this chapter with Sec. 1.7 wherein we describe the organization of this thesis.

Notations and conventions

Before we proceed, for convenience and clarity, let us summarize certain notations and conventions that we shall follow throughout this thesis. We shall work with units such that $\hbar = c = 1$ and assume the Planck mass to be $M_{_{\rm Pl}} = (8\,\pi\,G)^{-1/2}$. We shall always work with the $(3 + 1)$-dimensional, spatially flat, Friedmann-Lemaître-Robertson-Walker (or, simply, FLRW, hereafter) universe. We shall choose the metric signature to be $(-, +, +, +)$. Greek indices shall be used to denote the spacetime coordinates, while Latin indices shall represent the spatial coordinates (except for the index k which shall be reserved for representing the wavenumber of the perturbations). The quantities a and H shall denote the scale factor and the Hubble parameter associated with the FLRW universe. At various stages, we shall use different notions of time in the Friedmann universe, *viz.* the cosmic time t, the conformal time η, or the number of e-folds N, as is convenient. Finally, an overdot and an overprime shall denote differentiation with respect to the cosmic and the conformal time coordinates, respectively.

1.2 The horizon problem and the need for inflation

The so-called horizon problem is the primary issue that plagues the hot big bang model [1, 12]. In this section, we shall describe the problem and thereby motivate the need for a phase of accelerated expansion in the early universe.

As we had discussed in the previous section, the universe as we know today, on averaging over sufficiently large volumes, is homogeneous and isotropic. Upon combining with the fact that it is spatially flat and expanding, it can be described by the FLRW line-element, which is given by

$$\mathrm{d}s^2 = -\mathrm{d}t^2 + a^2(t)\,\mathrm{d}\boldsymbol{x}^2, \tag{1.1}$$

where, as we mentioned, t denotes the cosmic time coordinate, while $\boldsymbol{x}$ represents the spatial coordinates, and $a(t)$ is the scale factor describing the expansion of the universe. In such a background, the size of the causally connected region, which is the distance that light would have traveled from the big bang to a given time t, *viz.* the horizon, is defined as

$$h(t) = a(t)\int_0^t \frac{\mathrm{d}\tilde{t}}{a(\tilde{t})}. \tag{1.2}$$

When we observe the CMB, we are in fact looking at the sky as it was at the time of last scattering. If we assume that the universe was matter dominated from the time of

decoupling, say, $t_{\rm dec}$, till today, say, t_0, the linear dimension of the backward light cone on the last scattering surface as observed today is given by

$$\ell_{\rm B} = a(t_{\rm dec}) \int_{t_{\rm dec}}^{t_0} \frac{{\rm d}\tilde{t}}{a(\tilde{t})} \simeq 3\,(t_{\rm dec}^2\, t_0)^{1/3}. \tag{1.3}$$

Assuming that the universe was dominated by radiation till the time of decoupling, the size of the forward light cone at $t_{\rm dec}$ is found to be

$$\ell_{\rm F} = a(t_{\rm dec}) \int_{0}^{t_{\rm dec}} \frac{{\rm d}\tilde{t}}{a(\tilde{t})} \simeq 2\, t_{\rm dec}. \tag{1.4}$$

If we now evaluate the ratio of these backward and forward light cones at the time of decoupling, we obtain that

$$R \equiv \frac{\ell_{\rm B}}{\ell_{\rm F}} = \frac{3}{2}\left(\frac{t_0}{t_{\rm dec}}\right)^{1/3} \simeq 70, \tag{1.5}$$

where we have set $t_{\rm dec} \simeq 10^5\,{\rm years}$ and $t_0 \simeq 10^{10}\,{\rm years}$. This implies that the linear dimension of the causally connected region at the time of decoupling was about 70 times smaller than the size of surface of last scattering that we can observe today. Despite the fact that there exist regions of the sky that were not causally connected at the time of decoupling, we find that the temperature of the CMB is virtually the same in all the directions of the sky. This is essentially the horizon problem.

We can also state the horizon problem in another way. As we shall discuss, the homogeneity of the background FLRW universe allows us to decompose the perturbations into Fourier modes to study their evolution. The physical wavelength associated with these modes, say, $\lambda_{\rm P}$, is always proportional to the scale factor, *i.e.* $\lambda_{\rm P} \propto a$. If we assume that the scale factor goes as $a \propto t^q$, which is the case during radiation and matter domination wherein $q = 1/2$ and $q = 2/3$, respectively, then the Hubble radius behaves as $H^{-1} \propto a^{1/q}$. Therefore, in such situations, the ratio of the physical wavelength to the Hubble radius is given by

$$\frac{\lambda_{\rm p}}{H^{-1}} \propto a^{(q-1)/q}. \tag{1.6}$$

This implies that, for $q < 1$, *as we go back in time*, the Hubble radius shrinks faster in size than the physical wavelengths. Or, equivalently, the physical wavelengths are larger than the Hubble radius at early times (see Fig. 1.1). Hence, within the hot big bang model, there can exist no causal mechanism to explain the extent of isotropy of the CMB.

In order to overcome the horizon problem, we need to bring the physical wavelengths associated with the modes of cosmological interest inside the Hubble radius at sufficiently

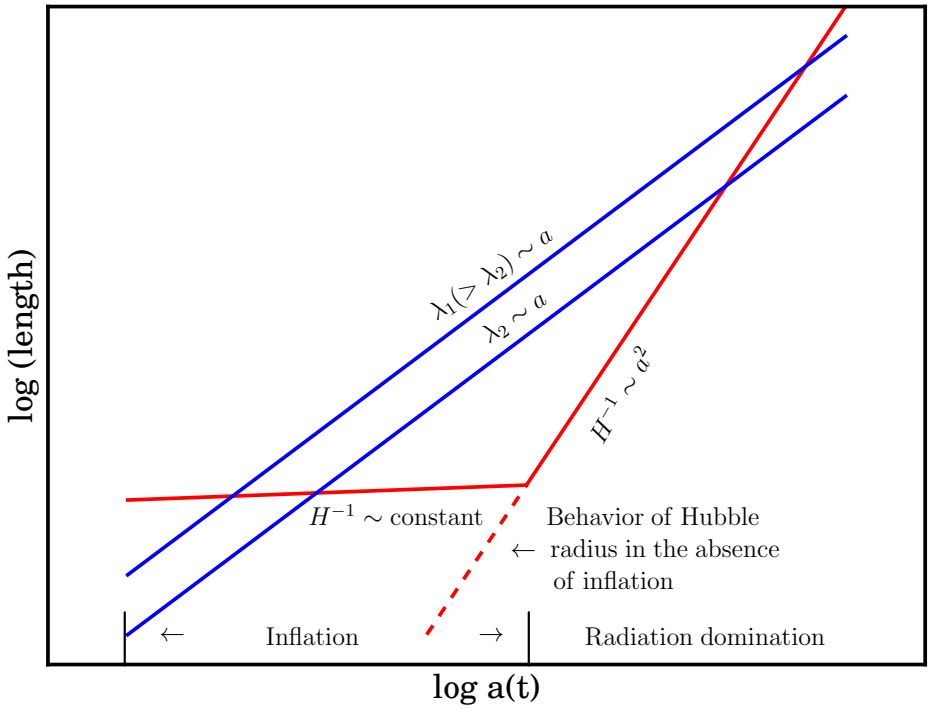

Figure 1.1: A schematic illustration of the evolution of physical wavelengths associated with the Fourier modes of the perturbations (in blue) and the Hubble radius (in red) in a FLRW universe during the inflationary and the radiation dominated epochs. It should be clear from the figure that, in the absence of inflation, the wavelengths of the modes will be well outside the Hubble radius at early times. A phase of accelerated expansion wherein the Hubble radius remains roughly a constant, as it occurs in, say, slow roll inflation, can bring the modes inside the Hubble radius.

early times. Evidently, this would be possible if there exists an epoch in the early universe wherein the physical wavelengths shrink faster than the Hubble radius *as we go back in time*, *i.e.* when

$$-\frac{\mathrm{d}}{\mathrm{d}t}\left(\frac{\lambda_{\mathrm{p}}}{H^{-1}}\right) < 0, \tag{1.7}$$

which is equivalent to the condition $\ddot{a} > 0$. In other words, we can overcome the horizon problem if the universe undergoes a period of accelerated expansion during its early stages. It is such a phase of rapid expansion that is referred to as inflation.

As we shall describe in the following section, it is not possible to achieve inflation with ordinary forms of matter and one need to resort to scalar fields to drive the accelerated expansion. However, before we turn to the discussion on achieving the phase of accelerated expansion, let us evaluate the extent of inflation that is required in order to overcome

the horizon problem. Let us assume that inflation in the form of exponential (*i.e.* de Sitter) expansion took place over a time t_i to t_f, such that $0 < t_{\rm i} < t_{\rm f} < t_{\rm dec}$, resulting in a rapid growth of the scale factor by the amount A. Upon including the expansion due to inflation, the linear dimension of the forward light cone at decoupling can be shown to be

$$\ell_{\rm FI} = a(t_{\rm dec}) \int_0^{t_{\rm dec}} \frac{{\rm d}\tilde{t}}{a(\tilde{t})} \simeq A\, t_i \left(\frac{t_{\rm dec}}{t_f}\right)^{1/2}. \tag{1.8}$$

Let us assume that inflation took place at a relatively high energy scale of, say, $10^{16}\,{\rm GeV}$. In such a scenario, if we calculate the ratio of the forward and the backward light cones at decoupling, one finds that $\ell_{\rm FI}/\ell_{\rm B} \simeq A/10^{26}$. This implies that the horizon problem can be surmounted if the universe is rapidly stretched by a factor of 10^{26} during inflation. Such a conclusion is often expressed in terms of e-folds, which is defined as

$$N = \int_{\rm t_i}^{\rm t} {\rm d}t\, H. \tag{1.9}$$

Since during inflation $N = \log A = \log\left(10^{26}\right) \simeq 60$, it is often said that one requires about 60 e-folds of inflation to overcome the horizon problem.

1.3 Driving inflation with scalar fields

Having discussed the need for inflation and the duration of inflation required to overcome the horizon problem, let us turn our attention to the issue of how we can achieve inflation. As we had discussed earlier, the simplest of the relativistic theories to describe the dynamics of gravity is Einstein's general theory of relativity. In the theory, the evolution of the metric is governed by the Einstein's equations. For the case of the FLRW line element (1.1), the Einstein's equations reduce to the Friedmann equations, which are given by

$$H^2 = \frac{8\,\pi\,G}{3}\,\rho, \tag{1.10a}$$

$$\frac{\ddot{a}}{a} = -\frac{4\,\pi\,G}{3}\,(\rho + 3\,p), \tag{1.10b}$$

where $H = \dot{a}/a$, while ρ and p are the total energy density and pressure of all the constituents in the universe. Evidently, in order to achieve accelerated expansion, *i.e.* $\ddot{a} > 0$, we require that $(\rho + 3\,p) < 0$. This is not possible with ordinary forms of matter such as non-relativistic matter or radiation which possess positive (or vanishing) energy densities and pressure.

Consider a scalar field ϕ that is described by the action

$$S[\phi] = \int \mathrm{d}^4x\,\sqrt{-g}\,\left[\frac{1}{2}\,\partial_\mu\phi\,\partial^\mu\phi - V(\phi)\right], \tag{1.11}$$

where $V(\phi)$ is the potential that governs the dynamics of the field. If we assume that the field is homogeneous, the energy density and pressure associated with the scalar field are given by

$$\rho = \frac{\dot{\phi}^2}{2} + V(\phi), \tag{1.12a}$$

$$p = \frac{\dot{\phi}^2}{2} - V(\phi). \tag{1.12b}$$

From these expressions for the energy density and pressure and the second Friedmann equation (1.10b), it should be clear that, if the scalar field is the dominant source of matter in the universe, then the condition $\dot{\phi}^2 < V(\phi)$ leads to accelerated expansion wherein $\ddot{a} > 0$. In other words, it is possible to drive inflation with a scalar field provided the kinetic energy of the field is sub-dominant to the potential energy. It is useful to note that the scalar field that drives inflation is often referred to as the inflaton.

In a FLRW universe, the equation of motion governing the homogeneous scalar field ϕ is given by

$$\ddot{\phi} + 3\,H\,\dot{\phi} + V_\phi = 0, \tag{1.13}$$

where $V_\phi = \mathrm{d}V/\mathrm{d}\phi$. While, as we discussed above, inflation can be achieved when the kinetic energy of the scalar field is sub-dominant to the potential energy, inflation can be guaranteed if $\dot{\phi}^2 \ll V(\phi)$, *i.e.* when the field is rolling slowly down the potential. Moreover, the velocity of the field should remain small for a sufficiently long period of time in order to ensure that inflation lasts long enough to overcome the horizon problem. This would be possible if the acceleration of the field remains suitably small as well, say, $\ddot{\phi} \ll 3H\dot{\phi}$. These two conditions lead to what is known as the slow roll approximation. This approximation is often described in terms of a hierarchy of parameters referred to as the slow roll parameters. They are given by [35]

$$\epsilon_1 = -\frac{\dot{H}}{H^2}, \tag{1.14a}$$

$$\epsilon_{i+1} = \frac{\mathrm{d}\ln|\epsilon_i|}{dN} \quad \text{for } i > 1. \tag{1.14b}$$

Slow roll approximation amounts to assuming that the parameters ϵ_i are approximately constant and much smaller than unity. It should be noted that inflation will be terminated when $\epsilon_1 \simeq 1$.

1.4 Inflationary perturbation theory at the linear order

Inflation, in addition to solving various issues plaguing the hot big bang model, such as the horizon problem that we had discussed, also provides a causal mechanism for the generation of the primordial perturbations [1, 12]. As is common knowledge, fluctuations can be non-zero even when the mean values of quantum operators vanish. It is the quantum fluctuations associated with the inflaton that prove to be responsible for the origin of the perturbations. The inflationary epoch amplifies and converts the tiny quantum fluctuations into classical perturbations which, in turn, leave their imprints as anisotropies in the CMB. As we have already pointed out, observations of the CMB indicate that the anisotropies at the epoch of decoupling are very small, about one part in 10^5. This implies that the deviation from homogeneity at earlier times would be even smaller. Therefore, the generation and evolution of perturbations in the early universe can be studied using the methods of perturbation theory.

Perturbations to the homogeneous and isotropic FLRW metric can be decomposed based on their transformation properties under rotations of the spatial coordinates on, say, hypersurfaces of constant time. Based on these properties, one can easily show that the perturbations in the metric tensor and, equivalently, in the matter, characterized by the stress-energy tensor, can be classified into scalars, vectors and tensors. The scalar perturbations are the dominant of the three and are primarily responsible for the anisotropies in the CMB and inhomogeneities in the universe. Vector perturbations can be generated by rotational velocity fields and, hence, they are also referred to as vorticity modes. The tensor perturbations are basically gravitational waves and, as is well known, they can be generated even in the absence of sources.

In $(3+1)$-dimensions, one finds that there exist two independent degrees of freedom associated with each class of perturbation. In this thesis, we shall be focusing on inflationary scenarios driven by scalar fields. In such a situation, due to the absence of vector sources, the vector perturbations are not produced at all. Hence, throughout this thesis, we shall only be concerned with the scalar and the tensor perturbations. Since scalar fields do not possess any isotropic stress, effectively, there arises only one independent scalar degree of freedom, which we shall represent by the curvature perturbation $\mathcal{R}$. The two tensor degrees of freedom correspond to the two polarizations of the gravitational waves. We shall represent the tensor perturbations as γ_{ij}, which are essentially the perturbations to the spatial components of the metric tensor. The tensor perturbations are transverse and traceless, *i.e.* they satisfy the conditions $\partial_j\gamma_{ij} = \gamma_{ii} = 0$, which reduce the number of

true degrees of freedom associated with γ_{ij} to two. Moreover, at the linear order in the perturbations, it can be shown that the scalars and tensors evolve independently. However, as we shall discuss, there can exist cross-correlations between the scalars and tensors at the higher orders in the perturbations.

A simple and straightforward way to arrive at the equations governing the perturbations and study their evolution would be to perturb the Einstein's equations up to a given order and then analyze the resultant equations. However, in order to evaluate the correlation functions beyond the two-point functions using perturbative methods of quantum field theory, we shall require the actions governing the perturbations at the higher orders. In this thesis, we shall focus on the three-point functions generated during inflation and for the purpose we shall require the action describing the perturbations at the third order. For this reason, we shall also obtain the linear equations of motion from the corresponding quadratic action. In the following three subsections, after briefly introducing the so-called Arnowitt-Deser-Misner (ADM) formalism and discussing the scalar and the tensor perturbations to the FLRW metric, we shall arrive at the quadratic action describing these perturbations. In the subsequent two subsections, we shall quickly discuss the quantization of the perturbations and the definitions of the power spectra and outline the evaluation of the power spectrum in the slow roll approximation. In the last two subsections, we shall describe the procedure to evaluate the inflationary power spectra numerically and briefly discuss the recent constraints from the cosmological data on the inflationary parameters.

1.4.1 The ADM formalism

In order to arrive at the actions governing the perturbations, we shall make use of the ADM formalism [36]. Recall that, in the ADM formalism, the spacetime metric is expressed in terms of the lapse function N, the shift vector N^i and the spatial metric h_{ij} as follows:

$$ds^2 = -N^2 \left(\mathrm{d}x^0\right)^2 + h_{ij} \left(N^i \,\mathrm{d}x^0 + \mathrm{d}x^i\right) \left(N^j \,\mathrm{d}x^0 + \mathrm{d}x^j\right), \tag{1.15}$$

where x^0 and x^i denote the time and the spatial coordinates, respectively. The system of our interest is Einsteinian gravity which is sourced by a canonical and minimally coupled scalar field, *viz.* the inflaton ϕ, that is described by the potential $V(\phi)$. In such a case, the action describing the complete system can be written in terms of the metric variables N,

N^i and h_{ij} and the scalar field ϕ as follows [23, 24, 25, 37]:

$$
\begin{aligned}
S[N, N^i, h_{ij}, \phi] \;=\; & \int \mathrm{d}x^0 \int \mathrm{d}^3\boldsymbol{x}\, N\, \sqrt{h} \left\{ \frac{M_{_{\rm Pl}}^2}{2} \left[\frac{1}{N^2}\, \left(E_{ij}E^{ij} - E^2\right) + {}^{(3)}\!R \right] \right. \\
& + \left[\frac{1}{2\,N^2}\, \left(\partial_0\phi\right)^2 - \frac{N^i}{N^2}\, \partial_0\phi\, \partial_i\phi - \frac{1}{2}\, h^{ij}\, \partial_i\phi\, \partial_j\phi \right. \\
& \left. \left. + \frac{N^iN^j}{2\,N^2}\, \partial_i\phi\, \partial_j\phi - V(\phi) \right] \right\},
\end{aligned}
\tag{1.16}
$$

where $\partial_0\phi = \partial\phi/\partial x^0$, $h \equiv \det\,(h_{ij})$ and ${}^{(3)}\!R$ is the spatial curvature associated with the metric h_{ij}. The quantity E_{ij} is given by

$$
E_{ij} = \frac{1}{2}\, \left(\partial_0 h_{ij} - \nabla_i N_j - \nabla_j N_i\right),
\tag{1.17}
$$

with $E = h_{ij}\, E^{ij}$. As is well known, the variation of the action (1.16) with respect to the Lagrange multipliers N and N^i leads to the so-called Hamiltonian and momentum constraints, respectively. Solving these constraint equations and substituting the solutions back in the original action (1.16) permits us to arrive at the action governing the dynamical variables of interest up to a given order in the perturbations.

1.4.2 The scalar and the tensor perturbations

When the scalar and the tensor perturbations are taken into account, it proves to be convenient to work in a specific gauge to arrive at the action governing the perturbations. We shall choose to work in the so-called co-moving gauge [23]. In such a gauge, the perturbation in the scalar field is assumed to be absent, *i.e.* $\delta\phi = 0$, so that the scalar field ϕ actually depends only on time. Upon taking into account the scalar perturbation described by the curvature perturbation $\mathcal{R}$ and the tensor perturbation characterized by γ_{ij}, the spatially flat FLRW metric can be expressed as [23]

$$
\mathrm{d}s^2 = -\mathrm{d}t^2 + h_{ij}(t, \boldsymbol{x})\, \mathrm{d}x^i\, \mathrm{d}x^j,
\tag{1.18}
$$

where the quantity h_{ij} is given by

$$
h_{ij} = a^2(t)\, \mathrm{e}^{2\,\mathcal{R}(t,\boldsymbol{x})}\, \left[\mathrm{e}^{\gamma(t,\boldsymbol{x})}\right]_{ij}.
\tag{1.19}
$$

These assumptions for the scalar field ϕ and the spatial metric h_{ij} as well as the solutions to the Hamiltonian and momentum constraint equations allow us to arrive at the action describing the perturbations, *viz.* the quantities $\mathcal{R}$ and γ_{ij}, at a given order [23, 24].

1.4.3 Actions at the quadratic order

The action at the quadratic order governing the perturbations can be arrived at using the ADM formalism sketched in Sec. 1.4.1. For instance, working in the comoving gauge, one can show that the actions at the quadratic order governing the curvature perturbation $\mathcal{R}$ and the tensor perturbation γ_{ij} are given by [12, 23, 24]

$$\mathcal{S}^2_{\mathcal{R}\mathcal{R}}[\mathcal{R}] = \frac{1}{2}\int \mathrm{d}\eta \int \mathrm{d}^3\boldsymbol{x}\ z^2\ \left[\mathcal{R}'^2 - (\partial\mathcal{R})^2\right], \tag{1.20a}$$

$$\mathcal{S}^2_{\gamma\gamma}[\gamma_{ij}] = \frac{M_{_{\rm Pl}}^2}{8}\int \mathrm{d}\eta \int \mathrm{d}^3\boldsymbol{x}\ a^2\ \left[\gamma_{ij}'^2 - (\partial\gamma_{ij})^2\right], \tag{1.20b}$$

where $z = \sqrt{2\,\epsilon_1}\,M_{_{\rm Pl}}\,a$, with ϵ_1 being the first slow roll parameter. These actions at the quadratic order will, obviously, lead to the linear equations of motion. In Fourier space, the modes, say, f_k and g_k, associated with the scalar and the tensor modes are found to satisfy the differential equations

$$f_k'' + 2\,\frac{z'}{z}\,f_k' + k^2\,f_k = 0, \tag{1.21a}$$

$$g_k'' + 2\,\frac{a'}{a}\,g_k' + k^2\,g_k = 0, \tag{1.21b}$$

respectively.

1.4.4 Quantization of the perturbations and the power spectra

As we mentioned, in the inflationary paradigm, the primordial perturbations are generated due to quantum fluctuations. On quantization, the curvature perturbation $\hat{\mathcal{R}}$ and the tensor perturbation $\hat{\gamma}_{ij}$ can be written in terms of the scalar and tensor Fourier modes as follows:

$$\begin{aligned}\hat{\mathcal{R}}(\eta,\mathbf{x}) &= \int \frac{\mathrm{d}^3\boldsymbol{k}}{(2\,\pi)^{3/2}}\,\hat{\mathcal{R}}_{\boldsymbol{k}}(\eta)\,\mathrm{e}^{i\,\boldsymbol{k}\cdot\boldsymbol{x}}\\ &= \int \frac{\mathrm{d}^3\boldsymbol{k}}{(2\,\pi)^{3/2}}\,\left(\hat{a}_{\boldsymbol{k}}\,f_k(\eta)\,\mathrm{e}^{i\,\boldsymbol{k}\cdot\boldsymbol{x}} + \hat{a}^\dagger_{\mathbf{k}}\,f_k^*(\eta)\,\mathrm{e}^{-i\,\boldsymbol{k}\cdot\boldsymbol{x}}\right), \end{aligned}\tag{1.22a}$$

$$\begin{aligned}\hat{\gamma}_{ij}(\eta,\mathbf{x}) &= \int \frac{\mathrm{d}^3\boldsymbol{k}}{(2\,\pi)^{3/2}}\,\hat{\gamma}^{\boldsymbol{k}}_{ij}(\eta)\,\mathrm{e}^{i\,\boldsymbol{k}\cdot\boldsymbol{x}}\\ &= \sum_s \int \frac{\mathrm{d}^3\boldsymbol{k}}{(2\,\pi)^{3/2}}\,\left(\hat{b}^s_{\boldsymbol{k}}\,\varepsilon^s_{ij}(\boldsymbol{k})\,g_k(\eta)\,\mathrm{e}^{i\,\boldsymbol{k}\cdot\boldsymbol{x}} + \hat{b}^{s\dagger}_{\mathbf{k}}\,\varepsilon^{s*}_{ij}(\boldsymbol{k})\,g_k^*(\eta)\,\mathrm{e}^{-i\,\boldsymbol{k}\cdot\boldsymbol{x}}\right). \end{aligned}\tag{1.22b}$$

In these decompositions, the pairs of operators $(\hat{a}_{\boldsymbol{k}}, \hat{a}^\dagger_{\boldsymbol{k}})$ and $(\hat{b}^s_{\boldsymbol{k}}, \hat{b}^{s\dagger}_{\boldsymbol{k}})$ represent the annihilation and creation operators corresponding to the scalar and the tensor modes associated

with the wavevector $\boldsymbol{k}$, and they satisfy the standard commutation relations. The quantity $\varepsilon_{ij}^{s}(\boldsymbol{k})$ represents the polarization tensor of gravitational waves with their helicity being denoted by the index s. The transverse and traceless nature of gravitational waves leads to the conditions $\varepsilon_{ii}^{s}(\boldsymbol{k}) = k_i\, \varepsilon_{ij}^{s}(\boldsymbol{k}) = 0$. We shall work with the normalization condition $\varepsilon_{ij}^{r}(\boldsymbol{k})\, \varepsilon_{ij}^{s*}(\boldsymbol{k}) = 2\, \delta^{rs}$ [23].

It is often convenient to rewrite the modes in terms of the Mukhanov-Sasaki variables, *viz.* $v_k = z\, f_k$ and $u_k = M_{_{\rm Pl}}\, a\, g_k/\sqrt{2}$. In terms of these new variables, the equations of motion governing the scalar and the tensor perturbations reduce to

$$v_k'' + \left(k^2 - \frac{z''}{z}\right)\, v_k \;\; = \;\; 0, \tag{1.23a}$$

$$u_k'' + \left(k^2 - \frac{a''}{a}\right)\, u_k \;\; = \;\; 0, \tag{1.23b}$$

respectively. The scalar and the tensor power spectra, *viz.* $\mathcal{P}_{_{\rm S}}(k)$ and $\mathcal{P}_{_{\rm T}}(k)$, are defined as follows:

$$\langle\, \hat{\mathcal{R}}_{\boldsymbol{k}}(\eta)\, \hat{\mathcal{R}}_{\boldsymbol{k}'}(\eta)\, \rangle \;\; = \;\; \frac{(2\,\pi)^2}{2\, k^3}\, \mathcal{P}_{_{\rm S}}(k)\, \delta^{(3)}(\boldsymbol{k} + \boldsymbol{k}'), \tag{1.24a}$$

$$\langle\, \hat{\gamma}_{ij}^{\boldsymbol{k}}(\eta)\, \hat{\gamma}_{mn}^{\boldsymbol{k}'}(\eta)\, \rangle \;\; = \;\; \frac{(2\,\pi)^2}{2\, k^3}\, \frac{\Pi_{ij,mn}^{\boldsymbol{k}}}{4}\, \mathcal{P}_{_{\rm T}}(k)\, \delta^{(3)}(\boldsymbol{k} + \boldsymbol{k}'), \tag{1.24b}$$

where the expectation values on the left hand sides are to be evaluated in the specified initial quantum state of the perturbations, and the quantity $\Pi_{ij,mn}^{\boldsymbol{k}}$ is given by [30, 33]

$$\Pi_{ij,mn}^{\boldsymbol{k}} = \sum_{s}\, \varepsilon_{ij}^{s}(\boldsymbol{k})\, \varepsilon_{mn}^{s*}(\boldsymbol{k}). \tag{1.25}$$

The vacuum state $|0\rangle$ associated with the quantized perturbations is defined as the state that satisfies the conditions $\hat{a}_{\boldsymbol{k}}|0\rangle = 0$ and $\hat{b}_{\boldsymbol{k}}^{s}|0\rangle = 0$ for all $\boldsymbol{k}$ and s. If one assumes the initial state of the perturbations to be the vacuum state $|0\rangle$, then, on making use of the decompositions (1.22) in the above definitions, the inflationary scalar and tensor power spectra $\mathcal{P}_{_{\rm S}}(k)$ and $\mathcal{P}_{_{\rm T}}(k)$ can be expressed as

$$\mathcal{P}_{_{\rm S}}(k) \;\; = \;\; \frac{k^3}{2\,\pi^2}\, |f_k|^2, \tag{1.26a}$$

$$\mathcal{P}_{_{\rm T}}(k) \;\; = \;\; 4\, \frac{k^3}{2\,\pi^2}\, |g_k|^2. \tag{1.26b}$$

The amplitudes $|f_k|$ and $|g_k|$ on the right hand sides of the above expressions are to be evaluated when the modes are sufficiently outside the Hubble radius. It is useful to note

here that the scalar and tensor spectral indices $n_{\rm S}$ and $n_{\rm T}$ are defined as

$$n_{\rm S}(k) = 1 + \frac{{\rm d}\ln \mathcal{P}_{\rm S}(k)}{{\rm d}\ln k}, \tag{1.27a}$$

$$n_{\rm T}(k) = \frac{{\rm d}\ln \mathcal{P}_{\rm T}(k)}{{\rm d}\ln k}. \tag{1.27b}$$

1.4.5 The power spectra in slow roll inflation

Let us now turn to the evaluation of the power spectra in the slow roll approximation. The Mukhanov-Sasaki equations (1.23) resemble that of a parametric oscillator with time dependent frequencies. At the leading order in the slow roll approximation, one can show that the quantities z''/z and a''/a are given by [1, 12]

$$\frac{z''}{z} \simeq \frac{2 + 3\,\epsilon_1 + 3\,\epsilon_2/2}{\eta^2}, \tag{1.28a}$$

$$\frac{a''}{a} \simeq \frac{2 + 3\,\epsilon_1}{\eta^2}, \tag{1.28b}$$

where ϵ_2 is the second slow roll parameter that is related to the first parameter ϵ_1 as follows: $\epsilon_2 = \dot{\epsilon}_1/(H\epsilon_1)$.

On treating the slow roll parameters as constants, one finds that the solutions to the variables (v_k, u_k) that satisfy the standard Bunch-Davies initial conditions in the sub-Hubble regime, *i.e.* $[v_k(\eta), u_k(\eta)] \to (1/\sqrt{2\,k})\ \exp -(i\,k\,\eta)$ as $k\,\eta \to -\infty$, are given by [1, 12, 38]

$$[v_k(\eta), u_k(\eta)] = \left(\frac{-\pi\,\eta}{4}\right)^{1/2}\ {\rm e}^{i\,\pi\,(\nu_{\rm S,T}+1/2)/2}\ H^{(1)}_{\nu_{\rm S,T}}(-k\,\eta), \tag{1.29}$$

where $H^{(1)}_{\nu}(x)$ denotes the Hankel function of the first kind, while $\nu_{\rm S} = 3/2 + \epsilon_1 - \epsilon_2/2$ and $\nu_{\rm T} = 3/2 + \epsilon_1$ are the indices of the Hankel function for the scalar and the tensor modes. In the super-Hubble limit, *i.e.* as $k\,\eta \to 0$, the scalar and tensor power spectra associated with the above modes can be obtained to be [39]

$$\mathcal{P}_{\rm S}(k) = \frac{H^2}{8\,\pi^2\,M_{\rm Pl}^2\,\epsilon_1}\left[1 - 2\,\epsilon_1\,(C+1) - \epsilon_2\,C - (2\,\epsilon_1 + \epsilon_2)\,\ln\left(\frac{k}{k_*}\right)\right], \tag{1.30a}$$

$$\mathcal{P}_{\rm T}(k) = \frac{2\,H^2}{\pi^2\,M_{\rm Pl}^2}\left[1 - 2\,\epsilon_1\,(C+1) - 2\,\epsilon_1\,\ln\left(\frac{k}{k_*}\right)\right], \tag{1.30b}$$

where $C = \gamma_{\rm E} - 2 + \ln 2$, with $\gamma_{\rm E}$ being the Euler constant [40], and k_* denotes a suitable pivot scale at which the amplitudes of the power spectra are often quoted. These power

spectra lead to the following spectral indices: $n_{_{\rm S}} = 1 - 2\,\epsilon_1 - \epsilon_2$ and $n_{_{\rm T}} = -2\,\epsilon_1$, which correspond to nearly scale invariant spectra. It is useful to note that, if one ignores the weak scale dependence in the above expressions, one arrives at the following standard slow roll result for the tensor-to-scalar ratio: $r = \mathcal{P}_{_{\rm T}}(k)/\mathcal{P}_{_{\rm S}}(k) \simeq 16\,\epsilon_1$.

1.4.6 A few words on the numerical evaluation of inflationary power spectra

In the case of models which are not analytically tractable, one needs to resort to numerical methods for evaluating the power spectra. Note that the coefficients of the equations governing the scalar and the tensor perturbations, *viz.* Eqs. (1.21), depend on the background variables. Evidently, one needs to first solve the equation (1.13) describing the homogeneous scalar field before we go on to solve the equations governing the perturbations.

To solve the differential equations numerically, it proves to be efficient to work with e-folds as the independent variable. In terms of e-folds, the differential equation (1.13) governing the background scalar field can be expressed as

$$\phi_{NN} + \left(3 - \frac{\phi_N^2}{2M_{_{\rm Pl}}^2}\right)\,\phi_N + \left(3\,M_{_{\rm Pl}}^2 - \frac{\phi_N^2}{2}\right)\,\frac{V_\phi}{V} = 0, \tag{1.31}$$

where each suffix N denotes a derivative with respect to the e-fold. This equation is usually solved for by assuming that the field starts on the inflationary attractor. Moreover, the initial value of the field is chosen to be such that the required number of 60 or so e-folds is achieved before inflation is terminated at the bottom of the potential.

The solution to the scalar field allows us to construct the coefficients involving the background quantities that arise in the equations (1.21) describing the perturbations. The perturbation equations can then be integrated with suitable initial conditions to arrive at the power spectra. As in case of the background scalar field, one again works with e-folds as the independent variable. In terms of e-folds, the equations (1.21) that govern the evolution of the perturbations are given by

$$f^k_{NN} + \left(1 + \frac{2\,z_N}{z} + \frac{H_N}{H}\right)\,f^k_N + \frac{k^2}{a^2\,H^2}\,f^k \;=\; 0, \tag{1.32a}$$

$$g^k_{NN} + \left(3 + \frac{H_N}{H}\right)\,g^k_N + \frac{k^2}{a^2\,H^2}\,g^k \;=\; 0, \tag{1.32b}$$

where, for convenience, we have denoted f_k and g_k as f^k and g^k and, as we mentioned, the suffix N represents differentiation with respect to the e-fold. The initial conditions that

are required to solve these two equations are provided by the standard Bunch-Davies initial conditions. In the analytical derivation of the power spectra in slow roll inflation discussed in the previous sub-section, we had imposed these initial conditions in the extreme sub-Hubble domain, *i.e.* as $k/(aH) \to \infty$. Moreover, we had evaluated the power spectra in the super-Hubble limit, *i.e.* as $k/(aH) \to 0$. Obviously, these limits are impossible to implement numerically. Therefore, in the numerical analysis, one imposes the initial conditions when the modes are sufficiently inside the Hubble radius and evolves the perturbations on to super-Hubble scales. Apart from some peculiar instances, it is found that the amplitude of the curvature and the tensor perturbations always settle down to a constant value soon after the modes leave the Hubble radius. This is evident, for instance, in Fig. (1.2), wherein we have plotted the evolution of the curvature perturbation for a specific mode in a typical inflationary model such as the one described by the quadratic potential. Due to this reason, it proves to be sufficient to evolve the modes until a time when they are suitably outside the Hubble radius. Various investigations suggest that it suffices to impose the initial conditions when $k/(a\,H) \simeq 100$ and evaluate the power spectra when $k/(a\,H) \simeq 10^{-5}$ [41].

1.4.7 Observational constraints at the level of power spectrum

While comparing inflationary models with the data, one often considers the following power law forms for the primordial scalar and tensor power spectra:

$$\mathcal{P}_{_{\rm S}}(k) = \mathcal{A}_{_{\rm S}} \left(\frac{k}{k_*}\right)^{n_{_{\rm S}}-1}, \tag{1.33a}$$

$$\mathcal{P}_{_{\rm T}}(k) = \mathcal{A}_{_{\rm T}} \left(\frac{k}{k_*}\right)^{n_{_{\rm T}}}, \tag{1.33b}$$

where $\mathcal{A}_{_{\rm S}}$ and $\mathcal{A}_{_{\rm T}}$ represent the scalar and the tensor amplitudes, while the spectral indices $n_{_{\rm S}}$ and $n_{_{\rm T}}$ are assumed to be constants. The quantity k_* denotes the so-called pivot scale at which the amplitudes of the power spectra are quoted. The scalar amplitude $\mathcal{A}_{_{\rm S}}$ is well constrained by the data and its value is referred to as the COBE normalization [42]. Often, one ignores the weak scale dependence of the tensor power spectra and the tensor power is referred to in terms of the tensor-to-scalar ratio r, quoted at the pivot scale. The primordial spectra are compared with the CMB data using Boltzmann codes such as COSMOMC [43] or CLASS [44]. The template power law spectra (1.33) are found to lead to a good fit to the recent Planck data as is illustrated in Fig. 1.3 [6, 15, 16, 21]. Fig. 1.4 shows the joint constraint on the parameters r and $n_{_{\rm S}}$ arrived at from the most

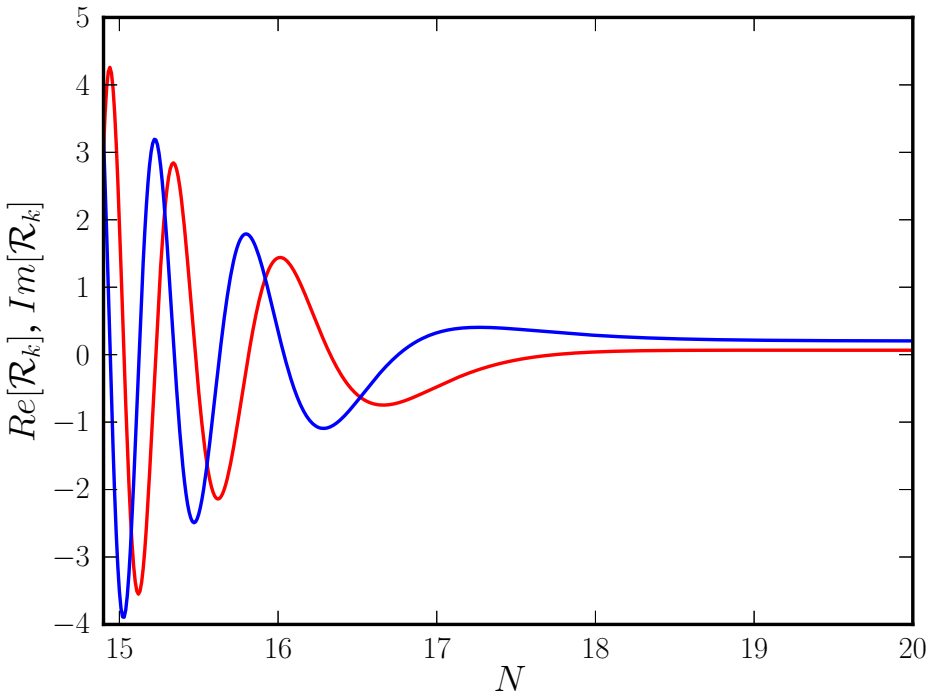

Figure 1.2: The evolution of the real (in blue) and the imaginary (in red) parts of the curvature perturbation f_k for a typical cosmological scale in the case of inflation driven by the quadratic potential has been plotted as a function of e-folds. The evolution has been plotted for a mode that leaves the Hubble radius around 18 e-folds. Note that the mode oscillates when it is inside the Hubble radius, but quickly settles down to a constant value when outside. It is due to this reason that it proves to be sufficient to evaluate the power spectrum at an instant when the mode is on super-Hubble scales.

recent Planck data [21]. The figure suggests that the data point to a scalar spectral index of about $n_{\rm s} \simeq 0.96$ and an upper bound of $r \simeq 0.1$ for the tensor-to-scalar ratio. It is notable that the central spot in the r-$n_{\rm s}$ plane is occupied by the Starobinsky model that is governed by an action which is a quadratic function of the spacetime curvature [45].

Instead of working with template power spectra, one can carry out a more detailed analysis of comparing specific models with the data and examine as to how the Bayesian evidence for the various models [46] contrast with respect to, say, the above-mentioned Starobinsky model. Recent comprehensive efforts in this direction seems to suggest that potentials with a plateau are preferred by the data [47, 48, 49]. It is important to note that it is the essentially the increasingly tighter constraint on the upper limit of the tensor-to-scalar ratio r that is responsible for ruling out classes of inflationary models such as the

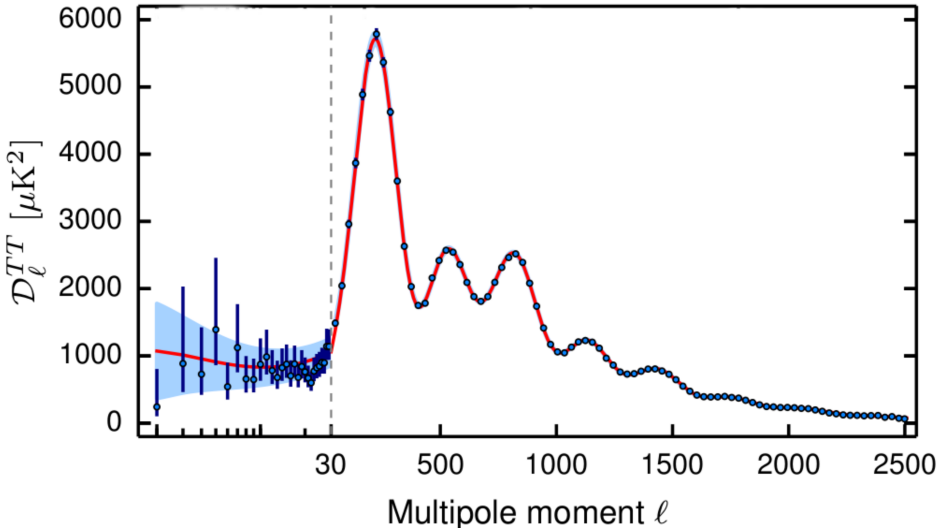

Figure 1.3: The observed and the theoretical CMB temperature angular power spectra have been plotted as a function of multipoles (figure from Ref. [21]). The blue dots with the error bars denote the recent Planck data, while the red curve represents the best fit curve associated with a nearly scale invariant power spectrum.

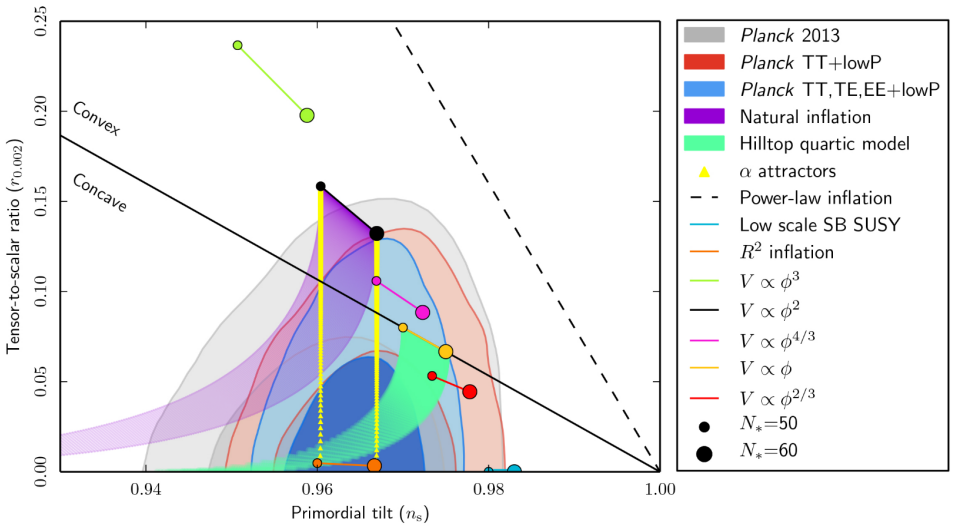

Figure 1.4: Joint constraint on the inflationary parameters r and $n_{\rm S}$ arrived at from the recent Planck temperature and polarization data as well as other cosmological data (figure from Ref. [21]). Constraints indicate that large field models, which lead to $r \gtrsim 0.1$, are beginning to be completely ruled out by the data.

large field models. The claims of BICEP2 [50, 51] about the detection of the imprints of the primordial tensor modes in the B-mode polarization of the CMB had provided hope on arriving at rather strong constraints on the inflationary models. But, it has since been realized that the signals detected by BICEP2 can be attributed to emissions from foreground dust [52, 53]. More accurate measurements of the CMB polarization are expected to yield additional constraints on the inflationary models. However, all these constraints are nevertheless expected to leave sufficient room for a relatively large class of inflationary models to remain viable. In such a situation, it is believed that, to lift the degeneracy amongst the prevailing models, we will have to turn to constraints on quantities beyond the power spectra.

1.5 The Maldacena formalism for evaluating the inflationary three-point functions

The statistical properties of the primordial perturbations are described by their moments. If the primordial perturbations were Gaussian, all its statistical properties would have been contained in the variance or the power spectrum. However, if the perturbations were non-Gaussian, either its odd moments will be non-zero or its even moments will have a different functional form. Hence, the first evidence for the non-Gaussian nature of the primordial perturbations would be non-zero three-point functions. Amongst the different approaches available, the so-called Maldacena formalism is the most complete formalism to calculate the three-point functions generated during inflation [23]. In this section, after introducing the various three-point functions, we shall briefly summarize the essential aspects of the Maldacena formalism to evaluate the three-point functions involving scalars as well as tensors. We shall also present the results for the three-point functions in the slow roll approximation and discuss the recent constraints on the non-Gaussianity parameters often used to characterize the scalar three-point function.

1.5.1 The three-point functions: Definitions

The scalar bi-spectrum, the two scalar-tensor three-point cross-correlations and the tensor bi-spectrum in Fourier space, *viz.* $\mathcal{B}_{\mathcal{R}\mathcal{R}\mathcal{R}}(\boldsymbol{k}_1, \boldsymbol{k}_2, \boldsymbol{k}_3)$, $\mathcal{B}^{m_3 n_3}_{\mathcal{R}\mathcal{R}\gamma}(\boldsymbol{k}_1, \boldsymbol{k}_2, \boldsymbol{k}_3)$, $\mathcal{B}^{m_2 n_2 m_3 n_3}_{\mathcal{R}\gamma\gamma}(\boldsymbol{k}_1, \boldsymbol{k}_2, \boldsymbol{k}_3)$ and $\mathcal{B}^{m_1 n_1 m_2 n_2 m_3 n_3}_{\gamma\gamma\gamma}(\boldsymbol{k}_1, \boldsymbol{k}_2, \boldsymbol{k}_3)$, evaluated towards the end of inflation at the conformal

time, say, $\eta_{\rm e}$, are defined as [23, 30, 31, 32, 33]

$$\langle\, \hat{\mathcal{R}}_{\boldsymbol{k}_1}(\eta_{\rm e})\, \hat{\mathcal{R}}_{\boldsymbol{k}_2}(\eta_{\rm e})\, \hat{\mathcal{R}}_{\boldsymbol{k}_3}(\eta_{\rm e})\,\rangle \equiv (2\,\pi)^3\, \mathcal{B}_{\mathcal{R}\mathcal{R}\mathcal{R}}(\boldsymbol{k}_1, \boldsymbol{k}_2, \boldsymbol{k}_3)\, \delta^{(3)}\,(\boldsymbol{k}_1 + \boldsymbol{k}_2 + \boldsymbol{k}_3)\,, \tag{1.34a}$$

$$\langle\, \hat{\mathcal{R}}_{\boldsymbol{k}_1}(\eta_{\rm e})\, \hat{\mathcal{R}}_{\boldsymbol{k}_2}(\eta_{\rm e})\, \hat{\gamma}^{\boldsymbol{k}_3}_{m_3 n_3}(\eta_{\rm e})\,\rangle \equiv (2\,\pi)^3\, \mathcal{B}^{m_3 n_3}_{\mathcal{R}\mathcal{R}\gamma}(\boldsymbol{k}_1, \boldsymbol{k}_2, \boldsymbol{k}_3)\, \delta^{(3)}\,(\boldsymbol{k}_1 + \boldsymbol{k}_2 + \boldsymbol{k}_3)\,, \tag{1.34b}$$

$$\langle\, \hat{\mathcal{R}}_{\boldsymbol{k}_1}(\eta_{\rm e})\, \hat{\gamma}^{\boldsymbol{k}_2}_{m_2 n_2}(\eta_{\rm e})\, \hat{\gamma}^{\boldsymbol{k}_3}_{m_3 n_3}(\eta_{\rm e})\,\rangle \equiv (2\,\pi)^3\, \mathcal{B}^{m_2 n_2 m_3 n_3}_{\mathcal{R}\gamma\gamma}(\boldsymbol{k}_1, \boldsymbol{k}_2, \boldsymbol{k}_3)\, \delta^{(3)}\,(\boldsymbol{k}_1 + \boldsymbol{k}_2 + \boldsymbol{k}_3)\,, \tag{1.34c}$$

$$\langle\, \hat{\gamma}^{\boldsymbol{k}_1}_{m_1 n_1}(\eta_{\rm e})\, \hat{\gamma}^{\boldsymbol{k}_2}_{m_2 n_2}(\eta_{\rm e})\, \hat{\gamma}^{\boldsymbol{k}_3}_{m_3 n_3}(\eta_{\rm e})\,\rangle \equiv (2\,\pi)^3\, \mathcal{B}^{m_1 n_1 m_2 n_2 m_3 n_3}_{\gamma\gamma\gamma}(\boldsymbol{k}_1, \boldsymbol{k}_2, \boldsymbol{k}_3)\, \delta^{(3)}\,(\boldsymbol{k}_1 + \boldsymbol{k}_2 + \boldsymbol{k}_3)\,. \tag{1.34d}$$

For convenience, hereafter, we shall write these correlators as

$$\mathcal{B}_{\mathsf{ABC}}(\boldsymbol{k}_1, \boldsymbol{k}_2, \boldsymbol{k}_3) = (2\,\pi)^{-9/2}\, G_{\mathsf{ABC}}(\boldsymbol{k}_1, \boldsymbol{k}_2, \boldsymbol{k}_3), \tag{1.35}$$

where A, B and C refer to either $\mathcal{R}$ or γ.

1.5.2 The actions governing the three-point functions

As we mentioned, the most comprehensive method to study the generation of non-Gaussianities during inflation is the approach due to Maldacena. The primary aim of Maldacena's approach is to obtain the cubic order action that governs the scalar and the tensor perturbations using the ADM formalism [36]. Then, based on the action, one arrives at the corresponding three-point functions using the standard rules of perturbative quantum field theory [23, 24, 25, 30, 31, 32, 33].

We had pointed out that, while the scalars and the tensors evolve independently at the linear order in the perturbations, they interact at the higher orders. Therefore, in the comoving gauge, at the cubic order in the perturbations, apart from the terms such as $\mathcal{R}\mathcal{R}\mathcal{R}$ and $\gamma\gamma\gamma$, the action governing the perturbations will also consist of terms of the form $\mathcal{R}\mathcal{R}\gamma$ and $\mathcal{R}\gamma\gamma$. The terms involving $\mathcal{R}\mathcal{R}\mathcal{R}$ and $\gamma\gamma\gamma$ will evidently lead to the scalar and the tensor bi-spectra. Similarly, the terms involving $\mathcal{R}\mathcal{R}\gamma$ and $\mathcal{R}\gamma\gamma$ will lead to the two three-point scalar-tensor cross-correlations. The actions that lead to these correlations are found to be (see, for example, Refs. [23, 30, 31, 32, 33])

$$\begin{aligned} S^3_{\mathcal{R}\mathcal{R}\mathcal{R}}[\mathcal{R}] \;=\; & M_{_{\rm Pl}}^2 \int {\rm d}\eta \int {\rm d}^3\boldsymbol{x}\, \Big[a^2\, \epsilon_1^2\, \mathcal{R}\, \mathcal{R}'^2 + a^2\, \epsilon_1^2\, \mathcal{R}\, (\partial\mathcal{R})^2 - 2\, a\, \epsilon_1\, \mathcal{R}'\, \partial_i\mathcal{R}\, \partial_i\chi \\ & + \frac{a^2}{2}\, \epsilon_1\, \epsilon_2'\, \mathcal{R}^2\, \mathcal{R}' + \frac{\epsilon_1}{2}\, \partial_i\mathcal{R}\, \partial_i\chi\, \partial^2\chi + \frac{\epsilon_1}{4}\, \partial^2\mathcal{R}\, (\partial\chi)^2 \\ & + a\, \mathcal{F}^1(\mathcal{R})\, \frac{\delta\mathcal{L}^2_{\mathcal{R}\mathcal{R}}}{\delta\mathcal{R}}\Big], \end{aligned} \tag{1.36a}$$

$$S^3_{\mathcal{R}\mathcal{R}\gamma}[\mathcal{R},\gamma_{ij}] = M_{_{\rm Pl}}^2 \int {\rm d}\eta \int {\rm d}^3\boldsymbol{x} \left[a^2\,\epsilon_1\,\gamma_{ij}\,\partial_i\mathcal{R}\,\partial_j\mathcal{R} + \frac{1}{4}\,\partial^2\gamma_{ij}\,\partial_i\chi\,\partial_j\chi + \frac{a\,\epsilon_1}{2}\,\gamma'_{ij}\,\partial_i\mathcal{R}\,\partial_j\chi + \mathcal{F}^2_{ij}(\mathcal{R})\,\frac{\delta\mathcal{L}^2_{\gamma\gamma}}{\delta\gamma_{ij}} + \mathcal{F}^3(\mathcal{R},\gamma_{ij})\,\frac{\delta\mathcal{L}^2_{\mathcal{R}\mathcal{R}}}{\delta\mathcal{R}}\right], \tag{1.36b}$$

$$S^3_{\mathcal{R}\gamma\gamma}[\mathcal{R},\gamma_{ij}] = \frac{M_{_{\rm Pl}}^2}{4} \int {\rm d}\eta \int {\rm d}^3\boldsymbol{x} \left[\frac{a^2\,\epsilon_1}{2}\,\mathcal{R}\,\gamma'_{ij}\,\gamma'_{ij} + \frac{a^2\,\epsilon_1}{2}\,\mathcal{R}\,\partial_l\gamma_{ij}\,\partial_l\gamma_{ij} - a\,\gamma'_{ij}\,\partial_l\gamma_{ij}\,\partial_l\chi + \mathcal{F}^4_{ij}(\mathcal{R},\gamma_{mn})\,\frac{\delta\mathcal{L}^2_{\gamma\gamma}}{\delta\gamma_{ij}}\right], \tag{1.36c}$$

$$S^3_{\gamma\gamma\gamma}[\gamma_{ij}] = \frac{M_{_{\rm Pl}}^2}{2} \int {\rm d}\eta \int {\rm d}^3\boldsymbol{x} \left[\frac{a^2}{2}\,\gamma_{lj}\,\gamma_{im}\,\partial_l\partial_m\gamma_{ij} - \frac{a^2}{4}\,\gamma_{ij}\,\gamma_{lm}\,\partial_l\partial_m\gamma_{ij}\right], \tag{1.36d}$$

where the quantities $\mathcal{F}^1(\mathcal{R})$, $\mathcal{F}^2_{ij}(\mathcal{R})$, $\mathcal{F}^3(\mathcal{R},\gamma_{ij})$ and $\mathcal{F}^4_{ij}(\mathcal{R},\gamma_{mn})$ are given by

$$\mathcal{F}^1(\mathcal{R}) = \frac{1}{2\,a\,H}\left\{\left[a^2\,H\,\epsilon_2\,\mathcal{R}^2 + 4\,a\,H\,\mathcal{R}\,\mathcal{R}' + \partial_i\mathcal{R}\,\partial_i\chi - \frac{1}{H}\,(\partial\mathcal{R})^2\right]\,\frac{\delta\mathcal{L}^2_{\mathcal{R}\mathcal{R}}}{\delta\mathcal{R}} + \left[\partial_i\mathcal{R}\,\partial^2\chi + \partial^2\mathcal{R}\,\partial_i\chi\right]\,\delta_{ij}\,\partial_j\left[\partial^{-2}\left(\frac{\delta\mathcal{L}^2_{\mathcal{R}\mathcal{R}}}{\delta\mathcal{R}}\right)\right] + \frac{1}{H}\,\delta_{im}\,\delta_{jn}\,\partial_i\mathcal{R}\,\partial_j\mathcal{R}\,\partial_m\partial_n\left[\partial^{-2}\left(\frac{\delta\mathcal{L}^2_{\mathcal{R}\mathcal{R}}}{\delta\mathcal{R}}\right)\right]\right\}, \tag{1.37a}$$

$$\mathcal{F}^2_{ij}(\mathcal{R}) = -\frac{1}{a^2\,H^2}\,\partial_i\mathcal{R}\,\partial_j\mathcal{R} + \frac{1}{a^2\,H}\,(\partial_i\chi\,\partial_j\mathcal{R} + \partial_j\chi\,\partial_i\mathcal{R}), \tag{1.37b}$$

$$\mathcal{F}^3(\mathcal{R},\gamma_{ij}) = -\frac{1}{4\,a\,H}\,\gamma'_{ij}\,\partial^{-2}\partial_i\partial_j\mathcal{R}, \tag{1.37c}$$

$$\mathcal{F}^4_{ij}(\mathcal{R},\gamma_{mn}) = \frac{1}{aH}\,\gamma'_{ij}\,\mathcal{R}. \tag{1.37d}$$

In these actions, the quantity χ is determined by the relation $\partial^2\chi = a\,\epsilon_1\,\mathcal{R}'$, while the quantities $\mathcal{L}^2_{\mathcal{R}\mathcal{R}}$ and $\mathcal{L}^2_{\gamma\gamma}$ are the second order Lagrangian densities corresponding to the actions (1.20a) and (1.20b), respectively. One can show that the terms involving $\delta\mathcal{L}^2_{\mathcal{R}\mathcal{R}}/\delta\mathcal{R}$ or $\delta\mathcal{L}^2_{\gamma\gamma}/\delta\gamma_{ij}$ and the quantities $\mathcal{F}^1(\mathcal{R})$, $\mathcal{F}^2_{ij}(\mathcal{R})$, $\mathcal{F}^3(\mathcal{R},\gamma_{ij})$ and $\mathcal{F}^4_{ij}(\mathcal{R},\gamma_{mn})$ can be removed by the following field redefinitions (for further details, see Refs. [23, 31]):

$$\mathcal{R} \rightarrow \mathcal{R} + \mathcal{F}^1(\mathcal{R}) + \mathcal{F}^3(\mathcal{R},\gamma_{ij}), \tag{1.38}$$

$$\gamma_{ij} \rightarrow \gamma_{ij} + \mathcal{F}^2_{ij}(\mathcal{R}) + \mathcal{F}^4_{ij}(\mathcal{R},\gamma_{mn}), \tag{1.39}$$

thereby reducing the actions to simpler forms.

1.5.3 Generation of three-point functions during inflation

In order to calculate the three-point correlation functions using the methods of quantum field theory, one requires the interaction Hamiltonian corresponding to the above actions.

One can show that, at the cubic order, the interaction Hamiltonian $H_{\rm int}$ is related to the interaction Lagrangian $L_{\rm int}$ through the relation: $H_{\rm int} = -L_{\rm int}$ [23, 24, 25, 30, 31, 32, 33]. In what follows, we shall refer to $H_{\rm int}$ corresponding to the various actions as H_{ABC}, where each of $(\mathsf{A}, \mathsf{B}, \mathsf{C})$ can be either a $\mathcal{R}$ or a γ. Given the interaction Hamiltonian, $\hat{H}_{ABC}$, the corresponding three-point function can be evaluated using the standard rules of perturbative quantum field theory.

The scalar bi-spectrum

At the leading order in perturbation theory, the scalar bi-spectrum can be expressed in terms of the corresponding interaction Hamiltonian as follows [23]:

$$\langle \hat{\mathcal{R}}_{\boldsymbol{k}_1}(\eta_{\rm e})\, \hat{\mathcal{R}}_{\boldsymbol{k}_2}(\eta_{\rm e})\, \hat{\mathcal{R}}_{\boldsymbol{k}_3}(\eta_{\rm e})\rangle \;=\; -i \int_{\eta_{\rm i}}^{\eta_{\rm e}} {\rm d}\eta\, \langle [\hat{\mathcal{R}}_{\boldsymbol{k}_1}(\eta_{\rm e})\, \hat{\mathcal{R}}_{\boldsymbol{k}_2}(\eta_{\rm e})\, \hat{\mathcal{R}}_{\boldsymbol{k}_3}(\eta_{\rm e}), \hat{H}_{\mathcal{R}\mathcal{R}\mathcal{R}}(\eta)]\rangle, \quad (1.40)$$

where the expectation value has to be calculated in the perturbative vacuum. Note that the action (1.36a) which governs the scalar three-point function contains six terms. Therefore, the scalar bi-spectrum receives a contribution from each of these 'vertices'. In fact, there also occurs a seventh term which arises due to the field redefinition that we mentioned above. The scalar bi-spectrum can be evaluated from the above expression upon using the Fourier decomposition of the curvature perturbation, the expression for $\hat{H}_{\mathcal{R}\mathcal{R}\mathcal{R}}$ and Wick's theorem [23, 24, 25]. One can show that the complete contribution to the scalar bi-spectrum in the perturbative vacuum can be written as [37, 54, 55]

$$\begin{aligned} G_{\mathcal{R}\mathcal{R}\mathcal{R}}(\boldsymbol{k}_1, \boldsymbol{k}_2, \boldsymbol{k}_3) \;&\equiv\; \sum_{C=1}^{7} G_{\mathcal{R}\mathcal{R}\mathcal{R}\,(C)}(\boldsymbol{k}_1, \boldsymbol{k}_2, \boldsymbol{k}_3) \\ &\equiv\; M_{\rm Pl}^2 \sum_{C=1}^{6} \Big\{ [f_{k_1}(\eta_{\rm e})\, f_{k_2}(\eta_{\rm e})\, f_{k_3}(\eta_{\rm e})]\; \mathcal{G}^{C}_{\mathcal{R}\mathcal{R}\mathcal{R}}(\boldsymbol{k}_1, \boldsymbol{k}_2, \boldsymbol{k}_3) \\ &\qquad + \text{complex conjugate} \Big\} + G_{\mathcal{R}\mathcal{R}\mathcal{R}(7)}(\boldsymbol{k}_1, \boldsymbol{k}_2, \boldsymbol{k}_3), \end{aligned} \quad (1.41)$$

where f_k are the Fourier modes in terms of which we had decomposed the curvature perturbation at the linear order in the perturbations [cf. Eq. (1.22a)]. In the above expression, the quantities $\mathcal{G}^{C}_{\mathcal{R}\mathcal{R}\mathcal{R}}(\boldsymbol{k}_1, \boldsymbol{k}_2, \boldsymbol{k}_3)$ with $C = (1, 6)$ correspond to the six vertices in the interaction Hamiltonian (obtained from the third order action), and are described by the

integrals

$$\mathcal{G}^{1}_{\mathcal{R}\mathcal{R}\mathcal{R}}(\boldsymbol{k}_1,\boldsymbol{k}_2,\boldsymbol{k}_3) = 2\,i\int_{\eta_{\rm i}}^{\eta_{\rm e}}{\rm d}\eta\; a^2\,\epsilon_1^2\,\left(f^*_{k_1}\,f'^*_{k_2}\,f'^*_{k_3}+\text{two permutations}\right), \tag{1.42a}$$

$$\mathcal{G}^{2}_{\mathcal{R}\mathcal{R}\mathcal{R}}(\boldsymbol{k}_1,\boldsymbol{k}_2,\boldsymbol{k}_3) = -2\,i\,\left(\boldsymbol{k}_1\cdot\boldsymbol{k}_2+\text{two permutations}\right)\int_{\eta_{\rm i}}^{\eta_{\rm e}}{\rm d}\eta\; a^2\,\epsilon_1^2\,f^*_{k_1}\,f^*_{k_2}\,f^*_{k_3}, \tag{1.42b}$$

$$\mathcal{G}^{3}_{\mathcal{R}\mathcal{R}\mathcal{R}}(\boldsymbol{k}_1,\boldsymbol{k}_2,\boldsymbol{k}_3) = -2\,i\int_{\eta_{\rm i}}^{\eta_{\rm e}}{\rm d}\eta\; a^2\,\epsilon_1^2\left[\left(\frac{\boldsymbol{k}_1\cdot\boldsymbol{k}_2}{k_2^2}\right)\,f^*_{k_1}\,f'^*_{k_2}\,f'^*_{k_3}+\text{five permutations}\right], \tag{1.42c}$$

$$\mathcal{G}^{4}_{\mathcal{R}\mathcal{R}\mathcal{R}}(\boldsymbol{k}_1,\boldsymbol{k}_2,\boldsymbol{k}_3) = i\int_{\eta_{\rm i}}^{\eta_{\rm e}}{\rm d}\eta\; a^2\,\epsilon_1\,\epsilon_2'\,\left(f^*_{k_1}\,f^*_{k_2}\,f'^*_{k_3}+\text{two permutations}\right), \tag{1.42d}$$

$$\mathcal{G}^{5}_{\mathcal{R}\mathcal{R}\mathcal{R}}(\boldsymbol{k}_1,\boldsymbol{k}_2,\boldsymbol{k}_3) = \frac{i}{2}\int_{\eta_{\rm i}}^{\eta_{\rm e}}{\rm d}\eta\; a^2\,\epsilon_1^3\left[\left(\frac{\boldsymbol{k}_1\cdot\boldsymbol{k}_2}{k_2^2}\right)\,f^*_{k_1}\,f'^*_{k_2}\,f'^*_{k_3}+\text{five permutations}\right], \tag{1.42e}$$

$$\mathcal{G}^{6}_{\mathcal{R}\mathcal{R}\mathcal{R}}(\boldsymbol{k}_1,\boldsymbol{k}_2,\boldsymbol{k}_3) = \frac{i}{2}\int_{\eta_{\rm i}}^{\eta_{\rm e}}{\rm d}\eta\; a^2\,\epsilon_1^3\left\{\left[\frac{k_1^2\,(\boldsymbol{k}_2\cdot\boldsymbol{k}_3)}{k_2^2\,k_3^2}\right]\,f^*_{k_1}\,f'^*_{k_2}\,f'^*_{k_3}+\text{two permutations}\right\}. \tag{1.42f}$$

These integrals are to be evaluated from a sufficiently early time, say, $\eta_{\rm i}$, when the initial conditions are imposed on the modes until very late times, say, towards the end of inflation at $\eta_{\rm e}$. The additional, seventh term $G_7(\boldsymbol{k}_1,\boldsymbol{k}_2,\boldsymbol{k}_3)$ arises due to the field redefinition and its contribution to the bi-spectrum $G(\boldsymbol{k}_1,\boldsymbol{k}_2,\boldsymbol{k}_3)$ is given by

$$G_{\mathcal{R}\mathcal{R}\mathcal{R}\,(7)}(\boldsymbol{k}_1,\boldsymbol{k}_2,\boldsymbol{k}_3) = \frac{\epsilon_2(\eta_{\rm e})}{2}\,\left(|f_{k_1}(\eta_{\rm e})|^2\,|f_{k_2}(\eta_{\rm e})|^2+\text{two permutations}\right). \tag{1.43}$$

The scalar-tensor cross-correlations

The two three-point scalar-tensor cross-correlations can be expressed in terms of the corresponding interaction Hamiltonians $\hat{H}_{\mathcal{R}\mathcal{R}\gamma}$ and $\hat{H}_{\mathcal{R}\gamma\gamma}$ [obtained from the actions (1.36b) and (1.36c)] as follows [23]:

$$\langle\hat{\mathcal{R}}_{\boldsymbol{k}_1}(\eta_{\rm e})\,\hat{\mathcal{R}}_{\boldsymbol{k}_2}(\eta_{\rm e})\,\hat{\gamma}^{\boldsymbol{k}_3}_{m_3n_3}(\eta_{\rm e})\rangle = -i\int_{\eta_{\rm i}}^{\eta_{\rm e}}{\rm d}\eta\;\langle[\hat{\mathcal{R}}_{\boldsymbol{k}_1}(\eta_{\rm e})\,\hat{\mathcal{R}}_{\boldsymbol{k}_2}(\eta_{\rm e})\,\hat{\gamma}^{\boldsymbol{k}_3}_{m_3n_3}(\eta_{\rm e}),\hat{H}_{\mathcal{R}\mathcal{R}\gamma}(\eta)]\rangle, \tag{1.44}$$

$$\langle\hat{\mathcal{R}}_{\boldsymbol{k}_1}(\eta_{\rm e})\,\hat{\gamma}^{\boldsymbol{k}_2}_{m_2n_2}(\eta_{\rm e})\,\hat{\gamma}^{\boldsymbol{k}_3}_{m_3n_3}(\eta_{\rm e})\rangle = -i\int_{\eta_{\rm i}}^{\eta_{\rm e}}{\rm d}\eta\;\langle[\hat{\mathcal{R}}_{\boldsymbol{k}_1}(\eta_{\rm e})\,\hat{\gamma}^{\boldsymbol{k}_2}_{m_2n_2}(\eta_{\rm e})\,\hat{\gamma}^{\boldsymbol{k}_3}_{m_3n_3}(\eta_{\rm e}),\hat{H}_{\mathcal{R}\gamma\gamma}(\eta)]\rangle. \tag{1.45}$$

One can show that the scalar-scalar-tensor cross-correlation $G^{m_3n_3}_{\mathcal{R}\mathcal{R}\gamma}(\boldsymbol{k}_1,\boldsymbol{k}_2,\boldsymbol{k}_3)$, when

evaluated in the perturbative vacuum, can be written as [30, 31, 32, 56]

$$
\begin{aligned}
G^{m_3 n_3}_{\mathcal{R}\mathcal{R}\gamma}(\boldsymbol{k}_1, \boldsymbol{k}_2, \boldsymbol{k}_3) &= \sum_{C=1}^{3} G^{m_3 n_3}_{\mathcal{R}\mathcal{R}\gamma\,(C)}(\boldsymbol{k}_1, \boldsymbol{k}_2, \boldsymbol{k}_3) \\
&= M_{_{\rm Pl}}^2\, \Pi^{\boldsymbol{k}_3}_{m_3 n_3, ij}\, \hat{n}_{1i}\, \hat{n}_{2j} \sum_{C=1}^{3} \big[f_{k_1}(\eta_{\rm e})\, f_{k_2}(\eta_{\rm e})\, g_{k_3}(\eta_{\rm e}) \\
&\quad \times \mathcal{G}^{C}_{\mathcal{R}\mathcal{R}\gamma}(\boldsymbol{k}_1, \boldsymbol{k}_2, \boldsymbol{k}_3) + \text{complex conjugate}\big], \qquad (1.46)
\end{aligned}
$$

where the quantities $\mathcal{G}^{C}_{\mathcal{R}\mathcal{R}\gamma}(\boldsymbol{k}_1, \boldsymbol{k}_2, \boldsymbol{k}_3)$ are described by the integrals

$$
\mathcal{G}^{1}_{\mathcal{R}\mathcal{R}\gamma}(\boldsymbol{k}_1, \boldsymbol{k}_2, \boldsymbol{k}_3) = -2\, i\, k_1\, k_2 \int_{\eta_{\rm i}}^{\eta_{\rm e}} {\rm d}\eta\, a^2\, \epsilon_1\, f^{*}_{k_1}\, f^{*}_{k_2}\, g^{*}_{k_3}, \qquad (1.47a)
$$

$$
\mathcal{G}^{2}_{\mathcal{R}\mathcal{R}\gamma}(\boldsymbol{k}_1, \boldsymbol{k}_2, \boldsymbol{k}_3) = \frac{i}{2}\, \frac{k_3^2}{k_1\, k_2} \int_{\eta_{\rm i}}^{\eta_{\rm e}} {\rm d}\eta\, a^2\, \epsilon_1^2\, f'^{*}_{k_1}\, f'^{*}_{k_2}\, g^{*}_{k_3}, \qquad (1.47b)
$$

$$
\mathcal{G}^{3}_{\mathcal{R}\mathcal{R}\gamma}(\boldsymbol{k}_1, \boldsymbol{k}_2, \boldsymbol{k}_3) = \frac{i}{2}\, \frac{1}{k_1\, k_2} \int_{\eta_{\rm i}}^{\eta_{\rm e}} {\rm d}\eta\, a^2\, \epsilon_1^2\, \left[k_1^2\, f^{*}_{k_1}\, f'^{*}_{k_2} + k_2^2\, f'^{*}_{k_1}\, f^{*}_{k_2}\right]\, g'^{*}_{k_3}. \qquad (1.47c)
$$

Note that, for a given wavevector $\boldsymbol{k}$, $\hat{\boldsymbol{n}}$ denotes the unit vector $\hat{\boldsymbol{n}} = \boldsymbol{k}/k$. Hence, the quantities $\hat{n}_{1i}$ and $\hat{n}_{2i}$ represent the components of the unit vectors $\hat{\boldsymbol{n}}_1 = \boldsymbol{k}_1/k_1$ and $\hat{\boldsymbol{n}}_2 = \boldsymbol{k}_2/k_2$ along the i-spatial direction.

Similarly, the scalar-tensor-tensor cross-correlation $G^{m_2 n_2 m_3 n_3}_{\mathcal{R}\gamma\gamma}(\boldsymbol{k}_1, \boldsymbol{k}_2, \boldsymbol{k}_3)$, evaluated in the perturbative vacuum, can be expressed as [30, 31, 32, 56]

$$
\begin{aligned}
G^{m_2 n_2 m_3 n_3}_{\mathcal{R}\gamma\gamma}(\boldsymbol{k}_1, \boldsymbol{k}_2, \boldsymbol{k}_3) &= \sum_{C=1}^{3} G^{m_2 n_2 m_3 n_3}_{\mathcal{R}\gamma\gamma\,(C)}(\boldsymbol{k}_1, \boldsymbol{k}_2, \boldsymbol{k}_3) \\
&= M_{_{\rm Pl}}^2\, \Pi^{\boldsymbol{k}_2}_{m_2 n_2, ij}\, \Pi^{\boldsymbol{k}_3}_{m_3 n_3, ij} \sum_{C=1}^{3} \big[f_{k_1}(\eta_{\rm e})\, g_{k_2}(\eta_{\rm e})\, g_{k_3}(\eta_{\rm e}) \\
&\quad \times \mathcal{G}^{C}_{\mathcal{R}\gamma\gamma}(\boldsymbol{k}_1, \boldsymbol{k}_2, \boldsymbol{k}_3) + \text{complex conjugate}\big], \qquad (1.48)
\end{aligned}
$$

with the quantities $\mathcal{G}^{C}_{\mathcal{R}\gamma\gamma}(\boldsymbol{k}_1, \boldsymbol{k}_2, \boldsymbol{k}_3)$ being given by

$$
\mathcal{G}^{1}_{\mathcal{R}\gamma\gamma}(\boldsymbol{k}_1, \boldsymbol{k}_2, \boldsymbol{k}_3) = \frac{i}{4} \int_{\eta_{\rm i}}^{\eta_{\rm e}} {\rm d}\eta\, a^2\, \epsilon_1\, f^{*}_{k_1}\, g'^{*}_{k_2}\, g'^{*}_{k_3}, \qquad (1.49a)
$$

$$
\mathcal{G}^{2}_{\mathcal{R}\gamma\gamma}(\boldsymbol{k}_1, \boldsymbol{k}_2, \boldsymbol{k}_3) = -\frac{i}{4}\, (\boldsymbol{k}_2 \cdot \boldsymbol{k}_3) \int_{\eta_{\rm i}}^{\eta_{\rm e}} {\rm d}\eta\, a^2\, \epsilon_1\, f^{*}_{k_1}\, g^{*}_{k_2}\, g^{*}_{k_3}, \qquad (1.49b)
$$

$$
\mathcal{G}^{3}_{\mathcal{R}\gamma\gamma}(\boldsymbol{k}_1, \boldsymbol{k}_2, \boldsymbol{k}_3) = -\frac{i}{4} \int_{\eta_{\rm i}}^{\eta_{\rm e}} {\rm d}\eta\, a^2\, \epsilon_1\, f'^{*}_{k_1} \left[\frac{\boldsymbol{k}_1 \cdot \boldsymbol{k}_2}{k_1^2}\, g^{*}_{k_2}\, g'^{*}_{k_3} + \frac{\boldsymbol{k}_1 \cdot \boldsymbol{k}_3}{k_1^2}\, g'^{*}_{k_2}\, g^{*}_{k_3}\right]. \qquad (1.49c)
$$

The tensor bi-spectrum

The tensor bi-spectrum $\mathcal{B}_{\gamma\gamma\gamma}^{m_1n_1m_2n_2m_3n_3}(\boldsymbol{k}_1, \boldsymbol{k}_2, \boldsymbol{k}_3)$ can be expressed in terms of the Hamiltonian $\hat{H}_{\gamma\gamma\gamma}$ as [32, 33, 56]

$$\langle \hat{\gamma}_{m_1n_1}^{\boldsymbol{k}_1}(\eta_{\rm e})\, \hat{\gamma}_{m_2n_2}^{\boldsymbol{k}_2}(\eta_{\rm e})\, \hat{\gamma}_{m_3n_3}^{\boldsymbol{k}_3}(\eta_{\rm e})\rangle = -i \int_{\eta_{\rm i}}^{\eta_{\rm e}} {\rm d}\eta\, \langle [\hat{\gamma}_{m_1n_1}^{\boldsymbol{k}_1}(\eta_{\rm e})\, \hat{\gamma}_{m_2n_2}^{\boldsymbol{k}_2}(\eta_{\rm e})\, \hat{\gamma}_{m_3n_3}^{\boldsymbol{k}_3}(\eta_{\rm e}), \hat{H}_{\gamma\gamma\gamma}(\eta)]\rangle. \tag{1.50}$$

The corresponding quantity $G_{\gamma\gamma\gamma}^{m_1n_1m_2n_2m_3n_3}(\boldsymbol{k}_1, \boldsymbol{k}_2, \boldsymbol{k}_3)$ can be arrived in the same fashion as the scalar bi-spectrum and the scalar-tensor cross-correlations from the corresponding action $S^3_{\gamma\gamma\gamma}[\gamma_{ij}]$ [cf. Eq. (1.36d)]. One finds that the tensor bi-spectrum $G_{\gamma\gamma\gamma}^{m_1n_1m_2n_2m_3n_3}(\boldsymbol{k}_1, \boldsymbol{k}_2, \boldsymbol{k}_3)$, calculated in the perturbative vacuum, can be written as [23, 32, 33, 56]

$$\begin{aligned} G_{\gamma\gamma\gamma}^{m_1n_1m_2n_2m_3n_3}(\boldsymbol{k}_1, \boldsymbol{k}_2, \boldsymbol{k}_3) \;=\; & M_{\rm Pl}^2 \Big[\big(\Pi_{m_1n_1,ij}^{\boldsymbol{k}_1}\, \Pi_{m_2n_2,im}^{\boldsymbol{k}_2}\, \Pi_{m_3n_3,lj}^{\boldsymbol{k}_3} \\ & - \frac{1}{2}\, \Pi_{m_1n_1,ij}^{\boldsymbol{k}_1}\, \Pi_{m_2n_2,ml}^{\boldsymbol{k}_2}\, \Pi_{m_3n_3,ij}^{\boldsymbol{k}_3}\big)\, k_{1m}\, k_{1l} + \text{five permutations}\Big] \\ & \times \big[g_{k_1}(\eta_{\rm e})\, g_{k_2}(\eta_{\rm e})\, g_{k_3}(\eta_{\rm e})\, \mathcal{G}_{\gamma\gamma\gamma}(\boldsymbol{k}_1, \boldsymbol{k}_2, \boldsymbol{k}_3) \\ & + \text{complex conjugate}\big], \end{aligned} \tag{1.51}$$

where the quantity $\mathcal{G}_{\gamma\gamma\gamma}(\boldsymbol{k}_1, \boldsymbol{k}_2, \boldsymbol{k}_3)$ is described by the integral

$$\mathcal{G}^1_{\gamma\gamma\gamma}(\boldsymbol{k}_1, \boldsymbol{k}_2, \boldsymbol{k}_3) = -\frac{i}{4} \int_{\eta_{\rm i}}^{\eta_{\rm e}} {\rm d}\eta\, a^2\, g^*_{k_1}\, g^*_{k_2}\, g^*_{k_3}, \tag{1.52}$$

and we should emphasize that (k_{1i}, k_{2i}, k_{3i}) denote the components of the three wavevectors $(\boldsymbol{k}_1, \boldsymbol{k}_2, \boldsymbol{k}_3)$ along the i-spatial direction[1].

1.5.4 The three-point functions in the slow roll approximation

We shall now turn to the evaluation of the three-point functions in slow roll inflation. As we have discussed, at the leading order in the slow approximation, the first two slow roll parameters, *viz.* ϵ_1 and ϵ_2, can be assumed to be constant. In order to evaluate the three-point functions, apart from the slow roll parameters, we shall require the behavior of the scale factor and the scalar and the tensor mode functions f_k and g_k. It proves to be

[1]Such an emphasis seems essential to avoid confusion between k_1, k_2 and k_3 which denote the wavenumbers associated with the wavevectors $\boldsymbol{k}_1$, $\boldsymbol{k}_2$ and $\boldsymbol{k}_3$, and the quantity k_i which represents the component of the wavevector $\boldsymbol{k}$ along the i-spatial direction. We have made similar clarifications below wherever we are concerned some confusion in the notation may arise.

sufficient to assume that the scale factor as well as the modes f_k and g_k are given by their de Sitter forms. The de Sitter limit of the mode functions can be obtained by setting the slow roll parameters in the index of Hankel function in (1.29) to zero and are given by

$$f_k(\eta) = \frac{i\,H_0}{2\,M_{_{\rm Pl}}\sqrt{k^3\,\epsilon_1}}\,(1+i\,k\,\eta)\,\mathrm{e}^{-i\,k\,\eta}, \tag{1.53a}$$

$$g_k(\eta) = \frac{\sqrt{2}}{M_{_{\rm Pl}}}\frac{i\,H_0}{\sqrt{2\,k^3}}\,(1+i\,k\,\eta)\,\mathrm{e}^{-i\,k\,\eta}. \tag{1.53b}$$

To arrive at the three-point functions, it is now a matter of substituting these quantities in the various integrals and calculating the integrals involved. All the integrals prove to be straightforward to calculate. However, there are two points that need to be noted. Firstly, all the integrands oscillate highly in the extreme sub-Hubble domain, *i.e.* as $k\,\eta \to -\infty$, and one needs to regulate the integrals by introducing a cut-off of the form $\mathrm{e}^{\kappa\,k\,\eta}$, where κ is a small positive quantity. Theoretically, such a cut-off proves to be essential in order to identify the correct perturbative vacuum. Secondly, the integrals corresponding to certain contributions to the three-point functions can diverge in the super-Hubble limit, *i.e.* as $k\,\eta \to 0$, and they need to be handled with care. One can easily show that though some integrals may diverge in the late time limit, the complete contribution to the three-point function remains perfectly finite.

The scalar bi-spectrum

As we have discussed, the slow roll approximation amounts to assuming the slow roll parameters to be much smaller than unity. Hence, while evaluating the scalar bi-spectrum, at the leading order in the slow roll parameters, we need to consider only the contributions due to the first three vertices and the contribution due to the field redefinition. Upon substituting the mode (1.53a) in the expressions (1.42a), (1.42b), (1.42c) and (1.43), carrying out the integrals involved, and making use of Eq. (1.41), one finds that the scalar bi-spectrum can be expressed as the sum of the four contributions as follows:

$$\begin{aligned} G_{\mathcal{R}\mathcal{R}\mathcal{R}}(\boldsymbol{k}_1,\boldsymbol{k}_2,\boldsymbol{k}_3) &= G_{\mathcal{R}\mathcal{R}\mathcal{R}\,(1)}(\boldsymbol{k}_1,\boldsymbol{k}_2,\boldsymbol{k}_3) + G_{\mathcal{R}\mathcal{R}\mathcal{R}\,(2)}(\boldsymbol{k}_1,\boldsymbol{k}_2,\boldsymbol{k}_3) \\ &\quad + G_{\mathcal{R}\mathcal{R}\mathcal{R}\,(3)}(\boldsymbol{k}_1,\boldsymbol{k}_2,\boldsymbol{k}_3) + G_{\mathcal{R}\mathcal{R}\mathcal{R}\,(7)}(\boldsymbol{k}_1,\boldsymbol{k}_2,\boldsymbol{k}_3), \end{aligned} \tag{1.54}$$

where the different contributions are given by

$$\begin{aligned} G_{\mathcal{R}\mathcal{R}\mathcal{R}\,(1)}(\boldsymbol{k}_1,\boldsymbol{k}_2,\boldsymbol{k}_3) &= \frac{H_0^4}{16\,M_{_{\rm Pl}}^4\,\epsilon_1}\,\frac{1}{(k_1\,k_2\,k_3)^3} \\ &\quad \times\left[k_2^2\,k_3^2\left(\frac{1}{k_{_{\rm T}}}+\frac{k_1}{k_{_{\rm T}}^2}\right)+\text{two permutations}\right], \end{aligned} \tag{1.55a}$$

$$
\begin{aligned}
G_{\mathcal{R}\mathcal{R}\mathcal{R}\,(2)}(\boldsymbol{k}_1,\boldsymbol{k}_2,\boldsymbol{k}_3) &= \frac{H_0^4}{16\,M_{_{\rm Pl}}^4\,\epsilon_1}\,\frac{\boldsymbol{k}_1\cdot\boldsymbol{k}_2+\boldsymbol{k}_2\cdot\boldsymbol{k}_3+\boldsymbol{k}_3\cdot\boldsymbol{k}_1}{(k_1\,k_2\,k_3)^3} \\
&\quad\times\left[-k_{_{\rm T}}+\frac{(k_1k_2+k_2k_3+k_3k_1)}{k_{_{\rm T}}}+\frac{k_1k_2k_3}{k_{_{\rm T}}^2}\right], \qquad (1.55b)\\
G_{\mathcal{R}\mathcal{R}\mathcal{R}\,(3)}(\boldsymbol{k}_1,\boldsymbol{k}_2,\boldsymbol{k}_3) &= \frac{-H_0^4}{16\,M_{_{\rm Pl}}^4\,\epsilon_1}\,\frac{1}{(k_1\,k_2\,k_3)^3} \\
&\quad\times\left[\frac{\boldsymbol{k}_1\cdot\boldsymbol{k}_2}{k_2^2}\,\left(\frac{1}{k_{_{\rm T}}}+\frac{k_1}{k_{_{\rm T}}^2}\right)+\text{five permutations}\right], \qquad (1.55c)\\
G_{\mathcal{R}\mathcal{R}\mathcal{R}\,(7)}(\boldsymbol{k}_1,\boldsymbol{k}_2,\boldsymbol{k}_3) &= \frac{H_0^4}{32\,M_{_{\rm Pl}}^4}\,\frac{\epsilon_2}{\epsilon_1^2}\left[\frac{1}{k_1^3k_2^3}+\frac{1}{k_2^3k_3^3}+\frac{1}{k_3^3k_1^3}\right], \qquad (1.55d)
\end{aligned}
$$

with $k_{_{\rm T}}=k_1+k_2+k_3$.

The scalar-scalar-tensor cross-correlation

Note that the second and the third of the three integrals (1.47) depend quadratically on the first slow parameter, while the first depends linearly. Hence, it is the first term which dominates in slow roll approximation. On using the scalar and the tensor modes (1.53), evaluating the integral involved and finally using Eq. (1.46), we obtain the scalar-scalar-tensor three-point function to be

$$
\begin{aligned}
G^{m_3n_3}_{\mathcal{R}\mathcal{R}\gamma}(\boldsymbol{k}_1,\boldsymbol{k}_2,\boldsymbol{k}_3) &= \frac{H_0^4}{4\,M_{_{\rm Pl}}^4\,\epsilon_1}\,\frac{k_1\,k_2}{(k_1\,k_2\,k_3)^3}\,\Pi^{\boldsymbol{k}_3}_{m_3n_3,ij}\,\hat{n}_{1i}\,\hat{n}_{2j} \\
&\quad\times\left[-k_{_{\rm T}}+\frac{k_1\,k_2+k_2\,k_3+k_3\,k_1}{k_{_{\rm T}}}+\frac{k_1\,k_2\,k_3}{k_{_{\rm T}}^2}\right]. \qquad (1.56)
\end{aligned}
$$

The scalar-tensor-tensor cross-correlation

The contributions from the three vertices to the scalar-tensor-tensor correlation are of the same order in first slow roll parameter and, hence, we need to evaluate all of them in the slow roll approximation. Upon performing the integrals (1.49) using the modes (1.53) and substituting the resultant expressions in Eq. (1.48), one can express the scalar-tensor-tensor three-point function as

$$
\begin{aligned}
G^{m_2n_2m_3n_3}_{\mathcal{R}\gamma\gamma}(\boldsymbol{k}_1,\boldsymbol{k}_2,\boldsymbol{k}_3) &= G^{m_2n_2m_3n_3}_{\mathcal{R}\gamma\gamma\,(1)}(\boldsymbol{k}_1,\boldsymbol{k}_2,\boldsymbol{k}_3)+G^{m_2n_2m_3n_3}_{\mathcal{R}\gamma\gamma\,(2)}(\boldsymbol{k}_1,\boldsymbol{k}_2,\boldsymbol{k}_3) \\
&\quad+G^{m_2n_2m_3n_3}_{\mathcal{R}\gamma\gamma\,(3)}(\boldsymbol{k}_1,\boldsymbol{k}_2,\boldsymbol{k}_3), \qquad (1.57)
\end{aligned}
$$

where the three contributions are given by

$$G^{m_2n_2m_3n_3}_{\mathcal{R}\gamma\gamma\,(1)}(\boldsymbol{k}_1,\boldsymbol{k}_2,\boldsymbol{k}_3) = \frac{H_0^4}{8\,M_{_{\rm Pl}}^4}\frac{k_2^2\,k_3^2}{(k_1\,k_2\,k_3)^3}\,\Pi^{\boldsymbol{k}_2}_{m_2n_2,ij}\,\Pi^{\boldsymbol{k}_3}_{m_3n_3,ij}\,\left[\frac{1}{k_{_{\rm T}}}+\frac{k_1}{k_{_{\rm T}}^2}\right], \tag{1.58a}$$

$$G^{m_2n_2m_3n_3}_{\mathcal{R}\gamma\gamma\,(2)}(\boldsymbol{k}_1,\boldsymbol{k}_2,\boldsymbol{k}_3) = \frac{H_0^4}{8\,M_{_{\rm Pl}}^4}\frac{\boldsymbol{k}_2\cdot\boldsymbol{k}_3}{(k_1k_2k_3)^3}\,\Pi^{\boldsymbol{k}_2}_{m_2n_2,ij}\,\Pi^{\boldsymbol{k}_3}_{m_3n_3,ij} \times\left[-k_{_{\rm T}}+\frac{k_1\,k_2+k_2\,k_3+k_3\,k_1}{k_{_{\rm T}}}+\frac{k_1\,k_2\,k_3}{k_{_{\rm T}}^2}\right], \tag{1.58b}$$

$$G^{m_2n_2m_3n_3}_{\mathcal{R}\gamma\gamma\,(3)}(\boldsymbol{k}_1,\boldsymbol{k}_2,\boldsymbol{k}_3) = -\frac{H_0^4}{8\,M_{_{\rm Pl}}^4}\frac{1}{(k_1k_2k_3)^3}\,\Pi^{\boldsymbol{k}_2}_{m_2n_2,ij}\,\Pi^{\boldsymbol{k}_3}_{m_3n_3,ij} \times\left[(\boldsymbol{k}_1\cdot\boldsymbol{k}_2)\,k_3^2\,\left(\frac{1}{k_{_{\rm T}}}+\frac{k_2}{k_{_{\rm T}}^2}\right)+(\boldsymbol{k}_1\cdot\boldsymbol{k}_3)\,k_2^2\,\left(\frac{1}{k_{_{\rm T}}}+\frac{k_3}{k_{_{\rm T}}^2}\right)\right]. \tag{1.58c}$$

The tensor bi-spectrum

The tensor bi-spectrum can be evaluated in a similar way in the slow roll approximation. It can be arrived at upon using the tensor mode (1.53b), carrying out the integral (1.52) and substituting the result in the expression (1.51). The tensor bi-spectrum in the slow roll approximation can be written as

$$G^{m_1n_1m_2n_2m_3n_3}_{\gamma\gamma\gamma}(\boldsymbol{k}_1,\boldsymbol{k}_2,\boldsymbol{k}_3) = \frac{H_0^4}{2\,M_{_{\rm Pl}}^4}\frac{1}{(k_1\,k_2\,k_3)^3}\,\Big[\big(\Pi^{\boldsymbol{k}_1}_{m_1n_1,ij}\,\Pi^{\boldsymbol{k}_2}_{m_2n_2,im}\,\Pi^{\boldsymbol{k}_3}_{m_3n_3,lj} -\frac{1}{2}\,\Pi^{\boldsymbol{k}_1}_{m_1n_1,ij}\,\Pi^{\boldsymbol{k}_2}_{m_2n_2,ml}\,\Pi^{\boldsymbol{k}_3}_{m_3n_3,ij}\big)\,k_{1m}\,k_{1l} +\text{five permutations}\Big] \times\left[-k_{_{\rm T}}+\frac{k_1\,k_2+k_2\,k_3+k_3\,k_1}{k_{_{\rm T}}}+\frac{k_1\,k_2\,k_3}{k_{_{\rm T}}^2}\right]. \tag{1.59}$$

1.5.5 Observational constraints on non-Gaussianities

Needless to say, it will be interesting to arrive at constraints on the extent of primordial non-Gaussianities from the CMB and other cosmological data and thereby converge on, possibly, a smaller class of viable inflationary models than are permitted by the power spectra. As in the case of the primordial spectra, such constraints are usually arrived at by assuming certain template scalar bi-spectra. There are three templates that are usually assumed, which are referred to as the local, equilateral and the orthogonal templates [25]. While the local form is largely independent of the wavenumbers and peaks in the squeezed limit of the bi-spectrum (wherein one of the wavenumbers is much smaller

that the other two), the equilateral form peaks in the equilateral limit (wherein the three wavenumbers are equal). The orthogonal form has a shape which is represented by neither the local or the equilateral forms. The local shape is generated in multi-field models of inflation and in certain post-inflationary scenarios such as the curvaton scenario. The equilateral shape is produced in inflationary models involving non-canonical scalar fields, whereas generating the orthogonal shape requires a special class of models involving higher derivatives of the field. The local, the equilateral and the orthogonal shapes are expressed in terms of the scalar power spectra as follows [5, 25]:

$$G^{\rm loc}_{\mathcal{R}\mathcal{R}\mathcal{R}}(\boldsymbol{k}_1,\boldsymbol{k}_2,\boldsymbol{k}_3) = f^{\rm loc}_{\rm NL}\,\frac{6}{5}\,\left[\frac{\left(2\,\pi^2\right)^2}{k_1^3\,k_2^3\,k_3^3}\right]\,\left[k_1^3\,\mathcal{P}_{\rm S}(k_2)\,\mathcal{P}_{\rm S}(k_3) + \text{two permutations}\right], \tag{1.60a}$$

$$\begin{aligned} G^{\rm eq}_{\mathcal{R}\mathcal{R}\mathcal{R}}(\boldsymbol{k}_1,\boldsymbol{k}_2,\boldsymbol{k}_3) = {} & f^{\rm eq}_{\rm NL}\,\frac{3}{5}\,\left[\frac{\left(2\,\pi^2\right)^2}{k_1^3\,k_2^3\,k_3^3}\right]\,\Big[6\,k_2\,k_3^2\,\mathcal{P}_{\rm S}(k_1)\,\mathcal{P}^{2/3}_{\rm S}(k_2)\,\mathcal{P}^{1/3}_{\rm S}(k_3) \\ & - 3\,k_3^3\,\mathcal{P}_{\rm S}(k_1)\,\mathcal{P}_{\rm S}(k_2) - 2\,k_1\,k_2\,k_3\,\mathcal{P}^{2/3}_{\rm S}(k_1)\,\mathcal{P}^{2/3}_{\rm S}(k_2)\,\mathcal{P}^{2/3}_{\rm S}(k_3) \\ & + \text{five permutations}\Big], \end{aligned} \tag{1.60b}$$

$$\begin{aligned} G^{\rm orth}_{\mathcal{R}\mathcal{R}\mathcal{R}}(\boldsymbol{k}_1,\boldsymbol{k}_2,\boldsymbol{k}_3) = {} & f^{\rm orth}_{\rm NL}\,\frac{3}{5}\,\left[\frac{\left(2\,\pi^2\right)^2}{k_1^3\,k_2^3\,k_3^3}\right]\,\Big[18\,k_2\,k_3^2\,\mathcal{P}_{\rm S}(k_1)\,\mathcal{P}^{2/3}_{\rm S}(k_2)\,\mathcal{P}^{1/3}_{\rm S}(k_3) \\ & - 9\,k_3^3\,\mathcal{P}_{\rm S}(k_1)\,\mathcal{P}_{\rm S}(k_2) - 8\,k_1\,k_2\,k_3\,\mathcal{P}^{2/3}_{\rm S}(k_1)\,\mathcal{P}^{2/3}_{\rm S}(k_2)\,\mathcal{P}^{2/3}_{\rm S}(k_3) \\ & + \text{five permutations}\Big]. \end{aligned} \tag{1.60c}$$

The quantities $(f^{\rm loc}_{\rm NL}, f^{eq}_{\rm NL}, f^{\rm ortho}_{\rm NL})$ are dimensionless parameters which reflect the amplitude associated with the three shapes. It is these parameters that are expected to be constrained by the data.

The constraints from Planck on these non-Gaussianity parameters are given by: $f^{\rm loc}_{\rm NL} = 0.8 \pm 5.0$, $f^{\rm eq}_{\rm NL} = -4 \pm 43$ and $f^{\rm ortho}_{\rm NL} = -26 \pm 21$ [29]. Note that the constraints are consistent with a Gaussian primordial perturbation at 2-σ. From the expressions for the scalar bi-spectrum that we had obtained earlier in the slow roll case, it can be shown that the corresponding non-Gaussianity parameter $f_{\rm NL}$ (for the relation between the scalar bi-spectrum and the non-Gaussianity parameter, see Subsec. 2.2.1) is of the order of the first slow roll parameter ϵ_1. Therefore, the above constraints from Planck on the non-Gaussianity parameters suggest that slow roll models involving the canonical scalar field which are consistent with the data at the level of the power spectra are also consistent at the level of non-Gaussianities.

1.6 Preheating

As the field rolls down the potential, typically, the first slow roll parameter ϵ_1 steadily increases and inflation is terminated when the parameter becomes greater than unity. At the end of inflation, the inflaton, which is coupled to the other standard model fields, is expected to decay into relativistic particles described by these fields. These relativistic particles are then supposed to thermalize, thus leading to the radiation dominated era as described by the hot big bang model. In many models, soon after inflation comes to an end, the scalar field oscillates at the minimum of the potential with an ever decreasing amplitude. This phase of damped oscillatory motion soon after inflation is referred to as preheating [57, 58].

In this phase, as the scalar field oscillates at the minimum of the potential, the fields coupled to the inflaton can undergo parametric resonance which may lead to a rapid production of particles. Such a phenomenon can, in principle, enhance the amplitude of the otherwise frozen, primordial perturbations [12]. Moreover, recently, it has been shown that the constraints on the inflationary models can depend on the details of reheating [59]. In such a situation, clearly, post inflationary scenarios such as preheating need to be taken into account while considering the imprints of the primordial perturbations on the CMB or the large scale structure in order to arrive at meaningful constraints on the inflationary models.

1.7 Organization of the thesis

The rest of the thesis, consisting of four more chapters, is organized as follows. In Chap. 2, we shall investigate the consistency relation obeyed by scalar bi-spectrum in the squeezed limit in inflationary models permitting deviations from slow roll. In Chap. 3, we shall discuss a numerical procedure to compute the three-point functions involving tensors for an arbitrary triangular configuration of the wavenumbers. We shall also make use of the code developed based on the procedure to evaluate the three-point functions in a class of inflationary models that lead to features in the scalar power spectrum. In Chap. 4, we shall examine the validity of consistency relations obeyed by the three-point functions involving tensors. Finally, we shall conclude the thesis in Chap. 5 with a discussion of the results obtained and a brief outlook.

Chapter 2

On the scalar consistency relation away from slow roll

2.1 Introduction

Over the past two decades, cosmologists have dedicated a considerable amount of attention to hunting down credible models of inflation. As discussed before, the inflationary scenario, which is often invoked to resolve puzzles such as the horizon problem that plague the hot big bang model, is well known to provide an attractive mechanism for the origin of perturbations in the early universe [1, 12]. In the modern viewpoint, it is the primordial perturbations generated during inflation that leave their signatures as anisotropies in the CMB and later lead to the formation of the large scale structure. Ever since the discovery of the CMB anisotropies by COBE [2], there has been a constant endeavor to utilize cosmological observations to arrive at stronger and stronger constraints on models of inflation. While the CMB anisotropies have been measured with ever increasing precision by missions such as WMAP [3, 4, 5], Planck [6, 15, 20, 21] and by BICEP2 [50, 51], it would be fair to say that we still seem rather far from converging on a small class of well motivated and viable inflationary models (in this context, see Refs. [47, 48, 49]).

The difficulty in arriving at a limited set of credible models of inflation seems to lie in the simplicity and efficiency of the inflationary scenario. Inflation can be easily achieved with the aid of one or more scalar fields that are slowly rolling down a relatively flat potential. Due to this reason, a plethora of models of inflation have been proposed, which give rise to the required 60 or so e-folds of accelerated expansion that is necessary to overcome the horizon problem. Moreover, there always seem to exist sufficient room to tweak the model parameters in such a way so as to result in a nearly scale invariant power

spectrum of the scalar perturbations that lead to a good fit to the CMB data. In such a situation, non-Gaussianities in general and the scalar bi-spectrum in particular have been expected to lift the degeneracy prevailing amongst the various inflationary models. For convenience, the extent of non-Gaussianity associated with the scalar bi-spectrum is often expressed in terms of the parameter commonly referred to as $f_{_{\rm NL}}$ [60], a quantity which is a dimensionless ratio of the scalar bi-spectrum to the power spectrum. The expectation regarding non-Gaussianities alluded to above has been largely corroborated by the strong limits that have been arrived at by the Planck mission on the value of the $f_{_{\rm NL}}$ parameter [29]. As we had pointed out in Subsec. 1.5.5, these bounds suggest that the observed perturbations are consistent with a Gaussian primordial distribution. Also, the strong constraints imply that exotic models which lead to large levels of non-Gaussianities are ruled out by the data.

Despite the strong bounds that have been arrived at on the amplitude of the scalar bi-spectrum, there exist many models of inflation that remain consistent with the cosmological data at hand. The so-called scalar consistency relation is expected to play a powerful role in this regard, ruling out, for instance, many multi-field models of inflation, if it is confirmed observationally (for early discussion in this context, see, for instance, Refs. [23, 61]; for recent discussions, see Refs. [62]; for similar results that involve the higher order correlation functions, see, for example, Refs. [63]). According to the consistency condition, in the squeezed limit of the three-point functions wherein one of the wavenumbers associated with the perturbations is much smaller than the other two, the three-point functions can be completely expressed in terms of the two-point functions[1]. In the squeezed limit, for instance, the scalar non-Gaussianity parameter $f_{_{\rm NL}}$ can be expressed completely in terms of the scalar spectral index $n_{_{\rm S}}$ as $f_{_{\rm NL}} = 5\,(n_{_{\rm S}} - 1)/12$ [23, 61]. As we shall briefly outline later, the consistency conditions are expected to hold [64] whenever the amplitude of the perturbations freeze on super-Hubble scales, a behavior which is true in single field models where inflation occurs on the attractor at late times (see Refs. [65]; in this context, also see Refs. [66, 67]). While the scalar consistency relation has been established in the slow roll scenario, we find that there has been only a limited effort in explicitly examining the relation in situations consisting of periods of fast roll [68, 69]. Moreover, it has been shown that there can be deviations from the consistency relation under certain conditions, particularly when the field is either evolving

[1]It should be added here that, in a fashion similar to that of the purely scalar case, one can also arrive at consistency conditions for the other three-point functions which involve tensors (in this context, see Chap. 4).

away from the attractor [70] or when the perturbations are in an excited state above the Bunch-Davies vacuum [71]. In this chapter [72], our aim is to verify the validity of the scalar consistency relation in inflationary models which exhibit non-trivial dynamics. By considering a few examples, we shall explicitly show, analytically and numerically, that the scalar consistency relation holds even in scenarios involving strong deviations from slow roll.

The remainder of this chapter is organized as follows. In the next section, we shall quickly introduce the scalar non-Gaussianity parameter $f_{_{\rm NL}}$. We shall also briefly revisit the proof of the scalar consistency relation in the squeezed limit. In the succeeding section, we shall explicitly verify the validity of the consistency condition analytically in the cases of power law inflation and the Starobinsky model which is described by a linear potential with a sudden change in its slope. We shall then evaluate the scalar bi-spectrum numerically for an arbitrary triangular configuration of the wavenumbers in three inflationary models that lead to features in the scalar power spectrum, and examine the consistency condition in the squeezed limit. We shall conclude the chapter with a brief discussion on the results we obtain.

2.2 The scalar bi-spectrum in the squeezed limit

In this section, we shall first introduce the scalar non-Gaussianity parameter and arrive at an expression for the quantity in terms of the scalar bi-spectrum and power spectrum. We shall also sketch a simple proof of the consistency relation obeyed by the non-Gaussianity parameter in the squeezed limit of the scalar bi-spectrum.

2.2.1 The scalar non-Gaussianity parameter $f_{_{\rm NL}}$

In order to compare the primordial three-point functions with the data, it proves to be convenient to quantify the extent of non-Gaussianity in the scalar bi-spectrum in terms of a dimensionless parameter. This parameter, known as the scalar non-Gaussianity parameter $f_{_{\rm NL}}$, is introduced through the relation [60]

$$\mathcal{R}(\eta, \boldsymbol{x}) = \mathcal{R}_{_{\rm G}}(\eta, \boldsymbol{x}) - \frac{3\, f_{_{\rm NL}}}{5}\, \left[\mathcal{R}^2_{_{\rm G}}(\eta, \boldsymbol{x}) - \left\langle \mathcal{R}^2_{_{\rm G}}(\eta, \boldsymbol{x})\right\rangle\right], \tag{2.1}$$

where $\mathcal{R}_{_{\rm G}}$ denotes the Gaussian part of the curvature perturbation.

Recall that the scalar bi-spectrum is defined through the relation (1.34a). Upon Fourier transforming the above expression for $\mathcal{R}$ and using Wick's theorem (which applies to

Gaussian random variables), one can arrive at the following expression for the dimensionless non-Gaussianity parameter $f_{_{\rm NL}}$ in terms of the bi-spectrum $G_{\mathcal{R}\mathcal{R}\mathcal{R}}(\boldsymbol{k}_1, \boldsymbol{k}_2, \boldsymbol{k}_3)$ [cf. Eq. (1.35)] and the scalar power spectrum $\mathcal{P}_{_{\rm S}}(k)$ [cf. Eq. (1.26a)]:

$$f_{_{\rm NL}}(\boldsymbol{k}_1, \boldsymbol{k}_2, \boldsymbol{k}_3) = -\frac{10}{3}\,\frac{1}{(2\,\pi)^4}\,(k_1\,k_2\,k_3)^3\,G_{\mathcal{R}\mathcal{R}\mathcal{R}}(\boldsymbol{k}_1, \boldsymbol{k}_2, \boldsymbol{k}_3) \times \left[k_1^3\,\mathcal{P}_{_{\rm S}}(k_2)\,\mathcal{P}_{_{\rm S}}(k_3) + \text{two permutations}\right]^{-1}. \tag{2.2}$$

In the next subsection, we shall outline a derivation of the consistency relation obeyed by the non-Gaussianity parameter $f_{_{\rm NL}}$ in the squeezed limit.

2.2.2 The consistency relation

The squeezed limit refers to the case wherein one of the wavenumbers of the triangular configuration vanishes, say, $k_3 \to 0$, leading to $\boldsymbol{k}_2 = -\boldsymbol{k}_1$. Or, equivalently, one of the modes is assumed to possess a wavelength which is much larger than the other two. The long wavelength mode would be well outside the Hubble radius. In models of inflation driven by a single scalar field, the amplitude of the curvature perturbation freezes on super-Hubble scales, provided the inflaton evolves on the attractor at late times [66, 70]. As a result, the long wavelength mode simply acts as a background as far as the other two modes are concerned. If $\mathcal{R}^{_{\rm B}}$ is the amplitude of the curvature perturbation associated with the long wavelength mode, then the unperturbed part of the original FLRW metric (1.1) will be modified to

$$\mathrm{d}s^2 = -\mathrm{d}t^2 + a^2(t)\,\mathrm{e}^{2\,\mathcal{R}^{_{\rm B}}}\,\mathrm{d}\boldsymbol{x}^2. \tag{2.3}$$

In other words, the effect of the long wavelength mode is to modify the scale factor locally, which is equivalent to a spatial transformation of the form $\boldsymbol{x}' = \Lambda\,\boldsymbol{x}$, with the components of the matrix Λ being given by $\Lambda_{ij} = \mathrm{e}^{\mathcal{R}^{_{\rm B}}}\,\delta_{ij}$. Under such a transformation, the modes of the curvature perturbation transform as $\mathcal{R}_{\boldsymbol{k}} \to \det\,(\Lambda^{-1})\,\mathcal{R}_{\Lambda^{-1}\boldsymbol{k}}$. Further, we have $|\Lambda^{-1}\,\boldsymbol{k}| = (1 - \mathcal{R}^{_{\rm B}})\,k$ and $\delta^{(3)}(\Lambda^{-1}\,\boldsymbol{k}_1 + \Lambda^{-1}\,\boldsymbol{k}_2) = \det\,(\Lambda)\,\delta^{(3)}(\boldsymbol{k}_1 + \boldsymbol{k}_2)$. Utilizing these relations, the scalar two-point function can be written, up to the leading order in $\mathcal{R}^{_{\rm B}}$, as

$$\langle\hat{\mathcal{R}}_{\boldsymbol{k}_1}\,\hat{\mathcal{R}}_{\boldsymbol{k}_2}\rangle_k = \frac{(2\,\pi)^2}{2\,k_1^3}\,\mathcal{P}_{_{\rm S}}(k_1)\,\left[1 - (n_{_{\rm S}} - 1)\,\mathcal{R}^{_{\rm B}}\right]\,\delta^{(3)}(\boldsymbol{k}_1 + \boldsymbol{k}_2), \tag{2.4}$$

where the suffix k on the two-point function indicates that the correlator has been evaluated in the presence of a long wavelength perturbation and the quantity $n_{_{\rm S}}$ is the scalar spectral index defined by the relation (1.27a). Upon using the above expression for the

scalar power spectrum, we can write the scalar three-point function in the squeezed limit as [32, 61, 64, 72]

$$\begin{aligned}\langle\, \hat{\mathcal{R}}_{\boldsymbol{k}_1}\, \hat{\mathcal{R}}_{\boldsymbol{k}_2}\, \hat{\mathcal{R}}_{\boldsymbol{k}_3}\, \rangle_{k_3} &\equiv \langle\, \langle\, \hat{\mathcal{R}}_{\boldsymbol{k}_1}\, \hat{\mathcal{R}}_{\boldsymbol{k}_2}\, \rangle_{k_3}\, \hat{\mathcal{R}}_{\boldsymbol{k}_3}\, \rangle \\ &= -\frac{(2\,\pi)^{5/2}}{4\, k_1^3\, k_3^3}\, (n_{_{\rm S}} - 1)\, \mathcal{P}_{_{\rm S}}(k_1)\, \mathcal{P}_{_{\rm S}}(k_3)\, \delta^3(\boldsymbol{k}_1 + \boldsymbol{k}_2). \end{aligned} \tag{2.5}$$

On making use of this expression for the scalar bi-spectrum in the squeezed limit and the definition of the scalar non-Gaussianity parameter (2.2), one can immediately arrive at the consistency relation for $f_{_{\rm NL}}$ [23, 61, 62], *viz.* $f_{_{\rm NL}} = 5\,(n_{_{\rm S}} - 1)/12$.

2.3 Analytically examining the validity of the condition away from slow roll

As was outlined in the previous section, the only requirement for the validity of the consistency relation is the existence of a unique clock during inflation. Hence, in principle, this relation should be valid for any single field model of inflation irrespective of the detailed dynamics, if the field is evolving on the attractor at late times. Therefore, it should be valid even away from slow roll. In this section, we shall analytically examine the validity of the consistency condition in scenarios consisting of deviations from slow roll. After establishing the relation first in the simple case of power law inflation, we shall consider the Starobinsky model which involves a brief period of fast roll.

2.3.1 The simple example of power law inflation

We shall first consider the case of power law inflation with no specific constraints on the power law index, so that the behavior of the scale factor can be far different from that of its behavior in slow roll inflation. In power law inflation, the scale factor can be written as

$$a(\eta) = a_1\, \left(\frac{\eta}{\eta_1}\right)^{\gamma+1}, \tag{2.6}$$

where a_1 and η_1 are constants, and $\gamma < -2$. In such a background, the Fourier modes f_k associated with the curvature perturbation that satisfy the Bunch-Davies initial conditions are found to be [54, 73]

$$f_k(\eta) = \frac{1}{\sqrt{2\,\epsilon_1}\, M_{_{\rm Pl}}\, a(\eta)}\, \sqrt{\frac{-\pi\,\eta}{4}}\, {\rm e}^{-i\,\pi\,\gamma/2}\, H^{(1)}_{-(\gamma+1/2)}(-k\,\eta), \tag{2.7}$$

where the first slow roll parameter ϵ_1 is a constant given by $\epsilon_1 = (\gamma + 2)/(\gamma + 1)$. Note that $H_\nu^{(1)}(x)$ denotes the Hankel function of the first kind [40], while the scale factor $a(\eta)$ is given by Eq. (2.6). For real arguments, the Hankel functions of the first and the second kinds, *viz.* $H_\nu^{(1)}(x)$ and $H_\nu^{(2)}(x)$, are complex conjugates of each other [40]. Moreover, as $x \to 0$, the Hankel function has the following form

$$\lim_{x\to 0} H_\nu^{(1)}(x) = \frac{i}{\pi\,\nu}\left[\Gamma(1-\nu)\,\mathrm{e}^{-i\,\pi\,\nu}\,\left(\frac{x}{2}\right)^{\nu} - \Gamma(1+\nu)\,\left(\frac{x}{2}\right)^{-\nu}\right]. \tag{2.8}$$

Upon using this behavior, one can show that the corresponding scalar power spectrum, evaluated at late times, *i.e.* as $\eta \to 0$, is given by

$$\mathcal{P}_{_{\rm S}}(k) = \frac{1}{2\,\pi^3\,M_{_{\rm Pl}}^2\,\epsilon_1}\,\left(\frac{|\eta_1|^{\gamma+1}}{a_1}\right)^2\,\left|\Gamma[-(\gamma+1/2)]\right|^2\,\left(\frac{k}{2}\right)^{2\,(\gamma+2)}, \tag{2.9}$$

where $\Gamma(x)$ represents the Gamma function [40]. The scalar spectral index corresponding to such a power spectrum is evidently a constant and can be easily determined to be $n_{_{\rm S}} = 2\,\gamma + 5$. If the consistency condition is true, it would then imply that the scalar non-Gaussianity parameter has the value $f_{_{\rm NL}} = 5\,(\gamma + 2)/6$ in the squeezed limit.

Let us now evaluate the scalar bi-spectrum in the squeezed limit using the Maldacena formalism and see whether it indeed leads to the above consistency condition for $f_{_{\rm NL}}$. From Sec. 1.5.3, it should be clear that, in order to arrive at the complete scalar bi-spectrum, we first need to carry out the integrals (1.42) associated with the six vertices, calculate the corresponding contributions $G_{\mathcal{R}\mathcal{R}\mathcal{R}\,(C)}(\boldsymbol{k}_1, \boldsymbol{k}_2, \boldsymbol{k}_3)$ for $C = (1, 6)$, and lastly add the contribution $G_{\mathcal{R}\mathcal{R}\mathcal{R}\,(7)}(\boldsymbol{k}_1, \boldsymbol{k}_2, \boldsymbol{k}_3)$ [cf. Eq. (1.43)] that arises due to the field redefinition. However, since ϵ_1 is a constant in power law inflation, the second slow roll parameter ϵ_2 vanishes identically. As a result, the contributions corresponding to the fourth term that is determined by the integral (1.42d) as well as the seventh term $G_{\mathcal{R}\mathcal{R}\mathcal{R}\,(7)}(\boldsymbol{k}_1, \boldsymbol{k}_2, \boldsymbol{k}_3)$ prove to be zero. Moreover, in the squeezed limit of our interest, *i.e.* as $k_3 \to 0$, the amplitude of the mode f_{k_3} freezes and hence its time derivative goes to zero. Therefore, terms that are either multiplied by the wavenumber corresponding to the long wavelength mode or explicitly involve the time derivative of the long wavelength mode do not contribute, as both vanish in the squeezed limit. Due to these reasons, we find that it is only the first and the second terms, determined by the integrals (1.42a) and (1.42b), that contribute in power law inflation. After an integration by parts, we find that, in the

squeezed limit, these two integrals can be combined to be expressed as

$$\lim_{k_3\to 0}\, \left[\mathcal{G}^{1}_{\mathcal{R}\mathcal{R}\mathcal{R}}(\boldsymbol{k},-\boldsymbol{k},\boldsymbol{k}_3) + \mathcal{G}^{2}_{\mathcal{R}\mathcal{R}\mathcal{R}}(\boldsymbol{k},-\boldsymbol{k},\boldsymbol{k}_3)\right] = \lim_{k_3\to 0}\, 2\,i\,\epsilon_1^2\, f^{*}_{k_3}\, \left[\left(a^2\, f'^{*}_{k}\, f^{*}_{k}\right)^{0}_{-\infty} + 2\,k^2\, \int_{-\infty}^{0} \mathrm{d}\eta\, a^2\, f^{*2}_{k}\right], \quad (2.10)$$

where we have set $\eta_{\rm i} = -\infty$ and $\eta_{\rm e} = 0$. One can show that the derivative f'_k can be written as

$$f'_k(\eta) = \frac{-k}{\sqrt{2\,\epsilon_1}\, M_{_{\rm Pl}}\, a(\eta)}\, \sqrt{\frac{-\pi\,\eta}{4}}\, \mathrm{e}^{-i\,\pi\,\gamma/2}\, H^{(1)}_{-(\gamma+3/2)}(-k\,\eta). \quad (2.11)$$

Therefore, upon using this expression for the derivative f'_k, the behavior (2.8), the following asymptotic form of the Hankel function

$$\lim_{x\to\infty}\, H^{(1)}_{\nu}(x) = \sqrt{\frac{2}{\pi\,x}}\, \mathrm{e}^{i\,(x-\pi\,\nu/2-\pi/4)} \quad (2.12)$$

and the integral [40]

$$\int \mathrm{d}x\, x\, \left[H^{(1)}_{\nu}(x)\right]^2 = \frac{x^2}{2}\, \left\{\left[H^{(1)}_{\nu}(x)\right]^2 - H^{(1)}_{\nu-1}(x)\, H^{(1)}_{\nu+1}(x)\right\}, \quad (2.13)$$

we find that the bi-spectrum in the squeezed limit can be written as

$$\lim_{k_3\to 0}\, k^3\, k_3^3\, G_{\mathcal{R}\mathcal{R}\mathcal{R}}(\boldsymbol{k},-\boldsymbol{k},\boldsymbol{k}_3) = -8\,\pi^4\,(\gamma+2)\,\mathcal{P}_{_{\rm S}}(k)\,\mathcal{P}_{_{\rm S}}(k_3). \quad (2.14)$$

This expression and the definition (2.2) for the scalar non-Gaussianity parameter then leads to $f_{_{\rm NL}} = 5\,(\gamma+2)/6$, which is the result suggested by the consistency relation. We should add here that such a result has been arrived at earlier using a slightly different approach (see the third reference in Refs. [62]).

2.3.2 A non-trivial example involving the Starobinsky model

The second example that we shall consider is the Starobinsky model. In the Starobinsky model, the inflaton rolls down a linear potential which changes its slope suddenly at a particular value of the scalar field [74]. The governing potential is given by

$$V(\phi) = \begin{cases} V_0 + A_{+}\,(\phi-\phi_0) & \text{for} \quad \phi > \phi_0, \\ V_0 + A_{-}\,(\phi-\phi_0) & \text{for} \quad \phi < \phi_0, \end{cases} \quad (2.15)$$

where V_0, A_{+}, A_{-} and ϕ_0 are constants. An important aspect of the Starobinsky model is the assumption that it is the constant V_0 which dominates the value of the potential

around ϕ_0. Due to this reason, the scale factor always remains rather close to that of de Sitter. This in turn implies that the first slow roll parameter ϵ_1 remains small throughout the domain of interest. However, the discontinuity in the slope of the potential at ϕ_0 causes a transition to a brief period of fast roll before slow roll is restored at late times. One finds that the transition leads to large values for the second slow roll parameter ϵ_2 and, importantly, the quantity $\dot{\epsilon}_2$ grows to be even larger. In fact, it behaves as a Dirac delta function *at* the transition. As we shall discuss, it is this behavior that leads to the most important contribution to the scalar bi-spectrum in the model [37, 75, 76].

Clearly, it would be convenient to divide the evolution of the background quantities and the perturbation variables into two phases, before and after the transition at ϕ_0. In what follows, we shall represent the various quantities corresponding to the epochs before and after the transition by a plus sign and a minus sign respectively (in the superscript or subscript, as is convenient), while the values of the quantities at the transition will be denoted by a zero. Let us quickly list out the behavior of the different quantities which we shall require to establish the consistency relation.

The first slow roll parameter before and after the transition is found to be [37, 74, 75, 76]

$$\epsilon_{1+}(\eta) \simeq \frac{A_+^2}{18\, M_{_{\rm Pl}}^2\, H_0^4}, \tag{2.16a}$$

$$\epsilon_{1-}(\eta) \simeq \frac{A_-^2}{18\, M_{_{\rm Pl}}^2\, H_0^4}\, \left[1 - \frac{\Delta A}{A_-}\, \left(\frac{\eta}{\eta_0}\right)^3\right]^2, \tag{2.16b}$$

where $\Delta A = A_- - A_+$, H_0 is the Hubble parameter determined by the relation $H_0^2 \simeq V_0/(3\, M_{_{\rm Pl}}^2)$, and η_0 denotes the conformal time when the transition takes place. The second slow roll parameter is given by

$$\epsilon_{2+}(\eta) = 4\, \epsilon_{1+}, \tag{2.17a}$$

$$\epsilon_{2-}(\eta) = \frac{6\, \Delta\, A}{A_-}\, \frac{(\eta/\eta_0)^3}{1\, -\, (\Delta\, A/A_-)\, (\eta/\eta_0)^3} + 4\, \epsilon_{1-}. \tag{2.17b}$$

In fact, to determine the modes associated with the scalar perturbations and to evaluate the dominant contribution to the scalar bi-spectrum, we shall also require the behavior of the quantity $\dot{\epsilon}_2$. One can show that $\dot{\epsilon}_2$ can be expressed as

$$\dot{\epsilon}_2 = -\frac{2\, V_{\phi\,\phi}}{H} + 12\, H\, \epsilon_1 - 3\, H\, \epsilon_2 - 4\, H\, \epsilon_1^2 + 5\, H\, \epsilon_1 \epsilon_2 - \frac{H}{2}\, \epsilon_2^2, \tag{2.18}$$

where $V_{\phi\phi} = {\rm d}^2V/{\rm d}\phi^2$ and it should be stressed that this is an exact relation. It should be clear that the first term in the above expression involving $V_{\phi\phi}$ will lead to a Dirac delta

function due to the discontinuity in the first derivative of the potential in the case of the Starobinsky model. Hence, the dominant contribution to $\dot{\epsilon}_2$ *at the transition* can be written as [75, 76]

$$\begin{aligned}\dot{\epsilon}_2^0 &\simeq \frac{2\,\Delta\,A}{H_0}\,\delta^{(1)}(\phi\,-\,\phi_0)\\ &= \frac{6\,\Delta\,A}{A_+\,a_0}\,\delta^{(1)}(\eta\,-\,\eta_0),\end{aligned} \tag{2.19}$$

where a_0 denotes the value of the scale factor when $\eta = \eta_0$. Post transition, the dominant contribution to $\dot{\epsilon}_2$ is found to be [37]

$$\begin{aligned}\dot{\epsilon}_{2-} &\simeq -3\,H\,\epsilon_{2-} - \frac{H}{2}\,\epsilon_{2-}^2\\ &\simeq -\frac{18\,H_0\,\Delta\,A}{A_-}\,\frac{(\eta/\eta_0)^3}{\left[1-(\Delta\,A/A_-)\,(\eta/\eta_0)^3\right]^2}.\end{aligned} \tag{2.20}$$

Due to the fact that the potential is linear and also since the first slow roll parameter remains small, the modes f_k governing the curvature perturbation can be described by the conventional de Sitter modes to a good approximation before the transition. For the same reasons, one finds that the scalar modes can be described by the de Sitter modes soon after the transition as well. However, due to the transition, the modes after the transition are related by the Bogoliubov transformations to the modes before the transition. Therefore, the scalar mode and its time derivative before the transition can be written as [37, 74, 75, 76]:

$$f_k^+(\eta) = \frac{i\,H_0}{2\,M_{_{\rm Pl}}\,\sqrt{k^3\,\epsilon_{1+}}}\,(1+i\,k\,\eta)\,\mathrm{e}^{-i\,k\,\eta}, \tag{2.21a}$$

$$f_k^{+\prime}(\eta) = \frac{i\,H_0}{2\,M_{_{\rm Pl}}\,\sqrt{k^3\,\epsilon_{1+}}}\,\left[\frac{3\,\epsilon_{1+}}{\eta}\,(1+i\,k\,\eta)+k^2\,\eta\right]\mathrm{e}^{-i\,k\,\eta}, \tag{2.21b}$$

whereas the mode and its derivative after the transition can be expressed as follows:

$$f_k^-(\eta) = \frac{i\,H_0\,\alpha_k}{2\,M_{_{\rm Pl}}\,\sqrt{k^3\,\epsilon_{1-}}}\,(1+i\,k\,\eta)\,\mathrm{e}^{-i\,k\,\eta} - \frac{i\,H_0\,\beta_k}{2\,M_{_{\rm Pl}}\,\sqrt{k^3\,\epsilon_{1-}}}\,(1-i\,k\,\eta)\,\mathrm{e}^{i\,k\,\eta}, \tag{2.22a}$$

$$\begin{aligned}f_k^{-\prime}(\eta) &= \frac{i\,H_0\,\alpha_k}{2\,M_{_{\rm Pl}}\,\sqrt{k^3\epsilon_{1-}}}\,\left[\left(\epsilon_{1-}+\frac{\epsilon_{2-}}{2}\right)\,\frac{1}{\eta}\,(1+i\,k\,\eta)+k^2\,\eta\right]\mathrm{e}^{-i\,k\,\eta}\\ &- \frac{i\,H_0\,\beta_k}{2\,M_{_{\rm Pl}}\,\sqrt{k^3\epsilon_{1-}}}\,\left[\left(\epsilon_{1-}+\frac{\epsilon_{2-}}{2}\right)\,\frac{1}{\eta}\,(1-i\,k\,\eta)+k^2\,\eta\right]\mathrm{e}^{i\,k\,\eta},\end{aligned} \tag{2.22b}$$

with α_k and β_k denoting the Bogoliubov coefficients. Upon matching the above modes and their time derivatives at the transition, the Bogoliubov coefficients can be determined

to be

$$\alpha_k = 1 + \frac{3\,i\,\Delta A}{2\,A_+}\,\frac{k_0}{k}\left(1+\frac{k_0^2}{k^2}\right), \tag{2.23a}$$

$$\beta_k = -\frac{3\,i\,\Delta A}{2\,A_+}\,\frac{k_0}{k}\left(1+\frac{i\,k_0}{k}\right)^2 \mathrm{e}^{2\,i\,k/k_0}, \tag{2.23b}$$

where $k_0 = -1/\eta_0 = a_0\,H_0$ denotes the mode that leaves the Hubble radius at the transition. At late times, the scalar mode behaves as

$$f_k^{-}(\eta_{\rm e}) = \frac{i\,H_0}{2\,M_{_{\rm Pl}}\sqrt{k^3\,\epsilon_{1-}(\eta_{\rm e})}}\,(\alpha_k - \beta_k)\,, \tag{2.24}$$

where $\epsilon_{1-}(\eta_{\rm e}) = A_-^2/(18\,M_{_{\rm Pl}}^2\,H_0^4)$. Therefore, the scalar power spectrum, evaluated as $\eta \to 0$, can be expressed as

$$\begin{aligned}\mathcal{P}_{_{\rm S}}(k) &= \left(\frac{H_0}{2\,\pi}\right)^2\left(\frac{3\,H_0^2}{A_-}\right)^2|\alpha_k-\beta_k|^2\\ &= \left(\frac{H_0}{2\,\pi}\right)^2\left(\frac{3\,H_0^2}{A_-}\right)^2\left[\mathcal{I}(k)+\mathcal{I}_{\rm c}(k)\,\cos\left(\frac{2\,k}{k_0}\right)+\mathcal{I}_{\rm s}(k)\,\sin\left(\frac{2\,k}{k_0}\right)\right],\end{aligned} \tag{2.25}$$

where the quantities $\mathcal{I}(k)$, $\mathcal{I}_{\rm c}(k)$ and $\mathcal{I}_{\rm s}(k)$ are given by

$$\mathcal{I}(k) = 1+\frac{9}{2}\left(\frac{\Delta A}{A_+}\right)^2\left(\frac{k_0}{k}\right)^2+9\left(\frac{\Delta A}{A_+}\right)^2\left(\frac{k_0}{k}\right)^4+\frac{9}{2}\left(\frac{\Delta A}{A_+}\right)^2\left(\frac{k_0}{k}\right)^6, \tag{2.26a}$$

$$\mathcal{I}_{\rm c}(k) = \frac{3\,\Delta A}{2\,A_+}\left(\frac{k_0}{k}\right)^2\left[\left(\frac{3\,A_-}{A_+}-7\right)-\frac{3\,\Delta A}{A_+}\left(\frac{k_0}{k}\right)^4\right], \tag{2.26b}$$

$$\mathcal{I}_{\rm s}(k) = -\frac{3\,\Delta A}{A_+}\,\frac{k_0}{k}\left[1+\left(\frac{3\,A_-}{A_+}-4\right)\left(\frac{k_0}{k}\right)^2+\frac{3\,\Delta A}{A_+}\left(\frac{k_0}{k}\right)^4\right]. \tag{2.26c}$$

Note that, because of the features in the power spectrum, the corresponding scalar spectral index $n_{_{\rm S}}$ depends on the wavenumber k, and is found to be

$$\begin{aligned}n_{_{\rm S}}(k) &= \frac{1}{2}\left[\mathcal{I}(k)+\mathcal{I}_{\rm c}(k)\,\cos\left(\frac{2\,k}{k_0}\right)+\mathcal{I}_{\rm s}(k)\,\sin\left(\frac{2\,k}{k_0}\right)\right]^{-1}\\ &\quad\times\left[\mathcal{J}(k)+\mathcal{J}_{\rm c}(k)\,\cos\left(\frac{2\,k}{k_0}\right)+\mathcal{J}_{\rm s}(k)\,\sin\left(\frac{2\,k}{k_0}\right)\right],\end{aligned} \tag{2.27}$$

where $\mathcal{J}(k)$, $\mathcal{J}_{\rm c}(k)$ and $\mathcal{J}_{\rm s}(k)$ are given by

$$\mathcal{J}(k) = 2 - 9\left(\frac{\Delta A}{A_+}\right)^2\left(\frac{k_0}{k}\right)^2 - 54\left(\frac{\Delta A}{A_+}\right)^2\left(\frac{k_0}{k}\right)^4 - 45\left(\frac{\Delta A}{A_+}\right)^2\left(\frac{k_0}{k}\right)^6, \tag{2.28a}$$

$$\mathcal{J}_{\rm c}(k) = -\frac{3\,\Delta A}{A_+}\left[4 + \left(\frac{15\,A_-}{A_+} - 23\right)\left(\frac{k_0}{k}\right)^2 + \frac{12\,\Delta A}{A_+}\left(\frac{k_0}{k}\right)^4 - \frac{15\,\Delta A}{A_+}\left(\frac{k_0}{k}\right)^6\right], \tag{2.28b}$$

$$\mathcal{J}_{\rm s}(k) = -\frac{6\,\Delta A}{A_+}\,\frac{k_0}{k}\left[\left(\frac{3\,A_-}{A_+} - 7\right) - 2\left(\frac{3\,A_-}{A_+} - 4\right)\left(\frac{k_0}{k}\right)^2 - \frac{15\,\Delta A}{A_+}\left(\frac{k_0}{k}\right)^4\right]. \tag{2.28c}$$

If the consistency condition is indeed satisfied, then the scalar non-Gaussianity parameter, as predicted by the relation, would prove to be

$$\begin{aligned} f_{\rm NL}(k) &= \frac{5}{12}\,[n_{\rm s}(k) - 1] \\ &= \frac{5}{24}\left[\mathcal{I}(k) + \mathcal{I}_{\rm c}(k)\,\cos\left(\frac{2\,k}{k_0}\right) + \mathcal{I}_{\rm s}(k)\,\sin\left(\frac{2\,k}{k_0}\right)\right]^{-1} \\ &\quad\times\left\{[\mathcal{J}(k) - 2\,\mathcal{I}(k)] + [\mathcal{J}_{\rm c}(k) - 2\,\mathcal{I}_{\rm c}(k)]\,\cos\left(\frac{2\,k}{k_0}\right)\right. \\ &\quad\left. + [\mathcal{J}_{\rm s}(k) - 2\,\mathcal{I}_{\rm s}(k)]\,\sin\left(\frac{2\,k}{k_0}\right)\right\}. \end{aligned} \tag{2.29}$$

Let us now examine whether we do arrive at the same result upon using the Maldacena formalism to compute the scalar bi-spectrum. It is known that, when there exist deviations from slow roll, it is the fourth vertex that leads to the most dominant contribution to the bi-spectrum. In other words, we need to focus on the contribution $G_{\mathcal{R}\mathcal{R}\mathcal{R}\,(4)}(\boldsymbol{k}_1, \boldsymbol{k}_2, \boldsymbol{k}_3)$ that is governed by the integral (1.42d). Notice that the integral involves the quantity ϵ_2'. In the Starobinsky model, at the level of approximation that we are working in, $\epsilon_{2+} = 4\,\epsilon_{1+}$, with ϵ_1 being a constant [cf. Eqs. (2.16a) and (2.17a)]. Hence, ϵ_2' as well as the integral $\mathcal{G}^4_{\mathcal{R}\mathcal{R}\mathcal{R}}(\boldsymbol{k}_1, \boldsymbol{k}_2, \boldsymbol{k}_3)$ vanish during the initial slow roll phase, prior to the transition. However, as we discussed above, due to the discontinuity at ϕ_0, $\dot{\epsilon}_2$ is described by a delta function at the transition [cf. Eq. (2.19)], whereas post transition, it is given by Eq. (2.20). Since the mode f_k and its derivative are continuous, the contribution due to the delta function at the transition can be easily evaluated using the modes f_k^+ and the corresponding derivative $f_k^{+\prime}$ [cf. Eqs. (2.21)]. Since we are interested in the squeezed limit, the contribution at the transition can be written as

$$\lim_{k_3\to 0}\mathcal{G}^0_{\mathcal{R}\mathcal{R}\mathcal{R}\,(4)}(\boldsymbol{k}, -\boldsymbol{k}, \boldsymbol{k}_3) = \lim_{k_3\to 0}\frac{12\,i\,a_0^2\,\epsilon_{1+}\,\Delta A}{A_+}\left[f_k^{+*}(\eta_0)\,f_k^{+\prime *}(\eta_0)\,f^*_{k_3}(\eta_0)\right]. \tag{2.30}$$

The corresponding contribution to the bi-spectrum can be easily evaluated using the late time behavior (2.24) of the mode f_k. The contribution after the transition is governed by the integral

$$\lim_{k_3\to 0} \mathcal{G}^{-}_{\mathcal{R}\mathcal{R}\mathcal{R}\,(4)}(\boldsymbol{k}, -\boldsymbol{k}, \boldsymbol{k}_3) = \lim_{k_3\to 0} 2\,i \int_{\eta_0}^{\eta_e} \mathrm{d}\eta\, a^2\, \epsilon_{1-}\, \epsilon'_{2-}\, f_k^{-*}\, f_k^{-\prime *}\, f_{k_3}^{-*}. \tag{2.31}$$

We find that the resulting integral, arrived at upon making use of the behavior (2.16b) and (2.20) of the slow roll parameters and the modes (2.22), can be easily evaluated. On adding the above two contributions at the transition and post transition, we can show that the bi-spectrum in the squeezed limit can be written as

$$\begin{aligned}\lim_{k_3\to 0} G_{\mathcal{R}\mathcal{R}\mathcal{R}\,(4)}(\boldsymbol{k}, -\boldsymbol{k}, \boldsymbol{k}_3) \;\; = \;\; & -\frac{81\,H_0^{12}}{8\,A_+^2\,A_-^2}\Bigg\{[\mathcal{J}(k) - 2\,\mathcal{I}(k)] + [\mathcal{J}_{\rm c}(k) - 2\,\mathcal{I}_{\rm c}(k)]\,\cos\left(\frac{2\,k}{k_0}\right) \\ & + [\mathcal{J}_{\rm s}(k) - 2\,\mathcal{I}_{\rm s}(k)]\,\sin\left(\frac{2\,k}{k_0}\right)\Bigg\},\end{aligned} \tag{2.32}$$

where the quantities $[\mathcal{I}(k), \mathcal{I}_{\rm c}(k), \mathcal{I}_{\rm s}(k)]$ and $[\mathcal{J}(k), \mathcal{J}_{\rm c}(k), \mathcal{J}_{\rm s}(k)]$ are given by Eqs. (2.26) and (2.28).

There are a few points concerning this result that require emphasis. The above bi-spectrum goes to a constant value at large scales, while it is found to oscillate with a constant amplitude in the small scale limit. In the equilateral limit, the contribution at the transition is known to lead to a term that grows linearly with k at large wavenumbers [75, 76]. This essentially arises due to the infinitely sharp transition in the Starobinsky model. In the squeezed limit, we do not encounter such a growing term, but the sharpness of the transition is reflected in the oscillations of a fixed amplitude that persist indefinitely. Clearly, one can expect these oscillations to die down at suitably large wavenumbers if one smoothens the transition [76]. As far as our primary concern here, *viz.* the validity of the consistency condition, we find that upon making use of the expression (2.32) for the bi-spectrum and (2.25) for the power spectrum, we indeed recover the $f_{\rm NL}$ as given by Eq. (2.29). This implies that the consistency relation does hold even in the case of the infinitely sharp Starobinsky model. Moreover, it is important to appreciate the point that while it is the contribution at the transition that dominates the amplitude of the non-Gaussianity parameter at large wavenumbers, the contribution after the transition proves to be important for establishing the consistency relation at small wavenumbers. This suggests that the contribution after the transition is essential in order to arrive at the complete bi-spectrum in the Starobinsky model [37, 76].

2.4 Numerical verification of the relation during deviations from slow roll

In this section, we shall numerically examine the validity of the consistency relation in three models that lead to features in the scalar power spectrum due to deviations from slow roll. We shall investigate three models that result in the following types of features: (i) a sharp drop in power at low multipoles, roughly associated with the Hubble scale today (see Refs. [77, 78, 79]; for recent discussions, see Ref. [80]), (ii) a burst of oscillations around scales corresponding to the multipoles of $\ell \simeq 20$–40 [81, 82, 83] and (iii) small and repeated modulations extending over a wide range of scales [84, 85, 86, 87, 88, 89, 90]. Such features are known to result in a better fit to the cosmological data than the more simple and conventional, nearly scale invariant, spectra. It should be highlighted that it is essentially these three types of spectra that have been considered by the Planck team while examining the possibility of features in the primordial spectrum [20, 21]. We should also clarify that, though the fit to the data improves in the presence of features, the Bayesian evidence does not necessarily alter significantly, as the improvement in the fit is typically achieved at the cost of a few extra parameters [20, 21, 46, 47, 48, 76]. Nevertheless, we believe that the possibility of features require to be explored further since repeated exercises towards model independent reconstruction of the primordial power spectrum seem to point to their presence [91].

2.4.1 Inflationary models of interest

In what follows, we shall first briefly describe three models that lead to the above mentioned power spectra with features. We shall then numerically evaluate the scalar non-Gaussianity parameter $f_{\rm NL}$ for an arbitrary triangular configuration of wavenumbers in these models. Using the numerical results, we shall then go on to verify whether the consistency relation is indeed valid in these cases involving deviations from slow roll.

Punctuated inflation

Measurements of the CMB anisotropies from the very early days of COBE have consistently indicated lower power at the quadrapole than that expected from a nearly scale invariant power spectrum. There have been various attempts to construct inflationary models which achieve this drop in power at large scales (see Refs. [77, 78, 79]; for more recent efforts in this direction, see Refs. [80]). One such model is punctuated inflation [79].

It corresponds to a situation wherein a short period of departure from inflation is sandwiched between two epochs of slow roll inflation.

Such a background behavior can be produced by the following potential which contains a point of inflection:

$$V(\phi) = \frac{m^2}{2}\,\phi^2 - \frac{\sqrt{2\,\lambda\,(n-1)}\,m}{n}\,\phi^n + \frac{\lambda}{4}\,\phi^{2\,(n-1)}, \tag{2.33}$$

where $n \geq 3$. This potential is known to arise in certain minimal supersymmetric extensions to the standard model of particle physics. Amongst the three scenarios which lead to features in the power spectrum due to deviation from slow roll that we shall consider, punctuated inflation is an extreme case wherein inflation is interrupted for a brief period of time. We shall repeatedly consider this scenario in this thesis and, throughout, we shall work with $n = 3$ and $m/M_{_{\rm Pl}} = 1.5012 \times 10^{-7}$. The parameter λ can be expressed in terms of the point of inflection in the potential, say, ϕ_0, as

$$\lambda = \frac{2\,m^2}{(n-1)\,\phi_0^{2\,(n-2)}}, \tag{2.34}$$

and we shall set $\phi_0/M_{_{\rm Pl}} = 1.95964$. Also, we shall assume that the field starts from rest at a sufficiently large value in order to achieve the required number of e-folds. In Fig. 2.1, we have plotted the scalar power spectrum generated in the model for the above values of the parameters [79].

Quadratic potential with a step

It has been repeatedly noticed that a burst of oscillations in the power spectrum over intermediate scales improves the fit to the CMB data around the multipoles $\ell = 22$–40 [81, 82, 83]. Such a burst of oscillations can be generated with the introduction of a step in a potential that otherwise admits only slow roll. The step causes a brief period of fast roll which leads to oscillations in the power spectrum over scales which leave the Hubble radius during this period. We shall consider the case wherein a step has been introduced in the conventional quadratic potential. The complete potential is given by

$$V(\phi) = \frac{m^2}{2}\,\phi^2\,\left[1 + \alpha\,\tanh\,\left(\frac{\phi - \phi_0}{\Delta\phi}\right)\right], \tag{2.35}$$

where, evidently, ϕ_0, α and $\Delta\phi$ represent the location, the height and the width of the step, respectively [81, 82, 83]. Throughout this thesis, we shall work with the following values of potential parameters: $m/M_{_{\rm Pl}} = 7.147378 \times 10^{-6}$, $\alpha = 1.606 \times 10^{-3}$, $\phi_0/M_{_{\rm Pl}} = 14.67$

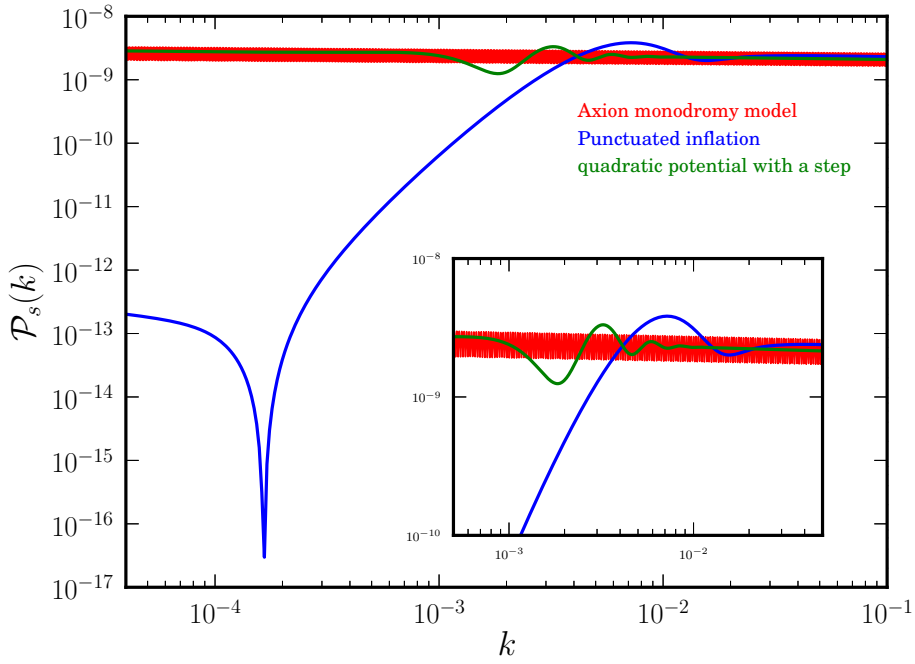

Figure 2.1: The scalar power spectra with features in the three models of our interest that permit deviations from slow roll. While punctuated inflation leads to a sharp drop in power at large scales (in blue), a step in the quadratic potential results in a burst of oscillations at intermediate scales (in green), whereas the axion monodromy model leads to continued oscillations running over a wide range of scales (in red).

and $\Delta\phi/M_{\rm Pl} = 3.11 \times 10^{-2}$. The scalar power spectrum corresponding to these values (see Fig. 2.1) is known to fit the WMAP and the Planck data better than the more conventional, nearly scale invariant, primordial spectrum [82, 83].

Axion monodromy model

While punctuated inflation and the quadratic potential with the step lead to localized features in the primordial power spectrum, models which contain oscillatory terms in the potential lead to modulations extending over a wide range of scales. A classic example of such models is the so-called axion monodromy model [86, 88, 89]. In this thesis, we shall consider a particular case of the axion monodromy model wherein the linear potential is modulated by a cosine term. The potential in such an example is given by

$$V(\phi) = \lambda \left[\phi + \alpha \cos\left(\frac{\phi}{\beta} + \delta\right)\right], \tag{2.36}$$

where $1/\beta$ represents the frequency of the oscillations in the potential and δ is a phase. The repeated modulations in the power spectrum generated by the oscillations in the potential (see Fig. 2.1) has been shown to result in an improved fit to the CMB data [86, 88, 89]. The parameters that give rise to the best fit to the data are known to be: $\lambda/M_{_{\rm Pl}}^3 = 2.512 \times 10^{-10}$, $\alpha/M_{_{\rm Pl}} = 1.83979 \times 10^{-4}$, $\beta/M_{_{\rm Pl}} = 4.50299 \times 10^{-4}$ and $\delta = 0.336033$ [88].

2.4.2 $f_{_{\rm NL}}$ for an arbitrary triangular configuration of the wavenumbers

It should be clear from the Maldacena formalism that, in order to arrive at the scalar bi-spectrum and the non-Gaussianity parameter, one first requires the behavior of the background quantities (such as, say, the scale factor and the slow roll parameters) and the scalar modes. Then, it is a matter of computing the various integrals that govern the scalar bi-spectrum. Given an inflaton potential and the initial conditions for the scalar field, the evolution of the background quantities can be arrived at by solving equation (1.31) which governs the dynamics of the field. Once we have the solution to the background, the scalar modes can be obtained by solving the corresponding differential equation, *viz.* Eq. (1.21a), with the standard Bunch-Davies initial conditions. With these at hand, the integrals involved, *i.e.* Eqs. (1.42), can be evaluated and substituted in the expression (1.41) to obtain the bi-spectrum. Since the scalar modes have been computed, the corresponding power spectrum can also be evaluated and substituted in the expression (2.2) to arrive at the non-Gaussianity parameter $f_{_{\rm NL}}(\boldsymbol{k}_1, \boldsymbol{k}_2, \boldsymbol{k}_3)$. In order to carry out the numerical computations, we have made use of the Fortran 90 code BI-spectra and Non-Gaussianity Operator, or simply, BINGO [54]. The code is based on the Maldacena formalism, and it efficiently computes all the various contributions to the bi-spectrum in the manner described above. We should add here that we have independently reproduced the results from BINGO using a different code as well. The latter code was originally used to calculate the scalar-tensor three-point functions and the tensor bi-spectrum [56], and it has been modified suitably to calculate the scalar bi-spectrum and the corresponding non-Gaussianity parameter. We shall discuss the latter code in detail in the next chapter.

In the context of power spectrum (see Subsec. 1.4.6), it is well known that it is sufficient to evolve the modes from a time when they are sufficiently inside the Hubble radius, say, from $k/(a\,H) = 10^2$, till they are well outside, say, when $k/(a\,H) = 10^{-5}$ [41]. One finds that, in order to arrive at the bi-spectrum, it suffices to carry out the integrals involved over roughly the same domain in time [56, 55, 92, 93]. However, two points need to be

emphasized in this regard. Firstly, in the case of the bi-spectrum, while evaluating for an arbitrary triangular configuration, one needs to make sure that the integrals are carried out from a time when the largest of the three modes (in terms of wavelength) is well inside the Hubble radius to a time when the smallest of the three is sufficiently outside. To achieve the accuracy we desire (say, of the order of 2–3% or better), we perform the integrals from the time when the largest mode satisfies the condition $k/(a\,H) = 10^2$ until a time when the smallest mode satisfies the condition $k/(a\,H) = 10^{-5}$. (This is so barring the case of the axion monodromy model wherein we have to integrate from deeper inside the Hubble radius—actually, from $k/(a\,H) = 250$ for the values of the parameters that we work with—to take into account the resonances that occur in the model [86].) Secondly, due to continued oscillations in the sub-Hubble domain, it is well known that the integrals require a cut-off in order for them to converge. We have introduced a cut-off of the form $\exp\,-[\kappa\,k/(a\,H)]$ and have worked with $\kappa = 0.1$, which is known to lead to consistent results [55, 56].

Before we go on to consider the consistency relation in the squeezed limit, let us make use of BINGO to understand the shape and structure of the bi-spectrum or, equivalently, the non-Gaussianity parameter $f_{_{\rm NL}}$, for an arbitrary triangular configuration of the wavenumbers. Usually, the scalar bi-spectrum and the parameter $f_{_{\rm NL}}$ are illustrated as density plots, plotted as a function of the ratios k_3/k_1 and k_2/k_1, for a fixed value of k_1 (in this context, see, for instance, Ref. [55]). While the actual value of k_1 will not play a significant role in simple slow roll scenarios, the structure of the bi-spectrum revealed in such density plots will depend on choice of k_1 in models which lead to features. In Fig. 2.2, we have plotted the scalar non-Gaussianity parameter arising in the three inflationary models of our interest, for suitable values of the quantity k_1. We find that, in the cases of punctuated inflation and the quadratic potential with a step, since the features are localized over a small range of scales, the structure of the plot changes to a certain extent with the choice of k_1. However, in the case of axion monodromy model, because of the reason that the oscillations extend over a wide range of scales, the choice of k_1 does not alter the structure of the plots significantly.

In Figs. 2.3, 2.4 and 2.5, we have attempted to capture the complete structure and shape of the bi-spectrum (actually, the corresponding non-Gaussianity parameter $f_{_{\rm NL}}$) using three-dimensional contour plots. We have made use of Mayavi and Python to create the three-dimensional plots [94]. We have plotted the parameter $f_{_{\rm NL}}$ for a wide range of the wavenumbers k_1, k_2 and k_3, over the allowed domain wherein the corresponding wavevectors satisfy the triangularity condition. It is known that the triangularity

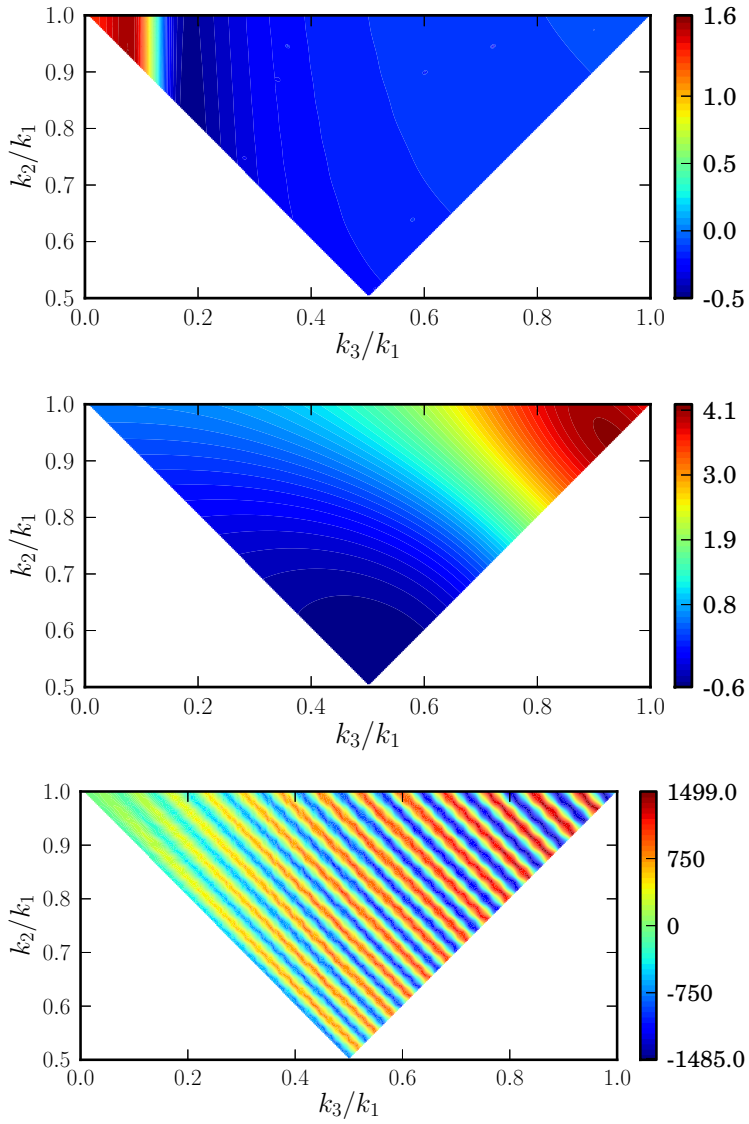

Figure 2.2: Density plots of the scalar non-Gaussianity parameter $f_{\rm NL}$, plotted as function of k_3/k_1 and k_2/k_1, with fixed values of k_1, in the three models of our interest, *viz.* punctuated inflation (on top), quadratic potential with a step (in the middle) and axion monodromy model (at the bottom). We have chosen the wavenumber k_1 to be $10^{-3}\,\mathrm{Mpc}^{-1}$ in the case of punctuated inflation, while we have set it to be $2 \times 10^{-3}\,\mathrm{Mpc}^{-1}$ for the other two models. We find that, when the features are localized, as in the cases of punctuated inflation and the quadratic potential with a step, the structure of $f_{\rm NL}$ varies considerably with the choice of k_1. However, in the case of the axion monodromy model, wherein there arises continued oscillations, the shape of $f_{\rm NL}$ is more or less independent of the choice of k_1.

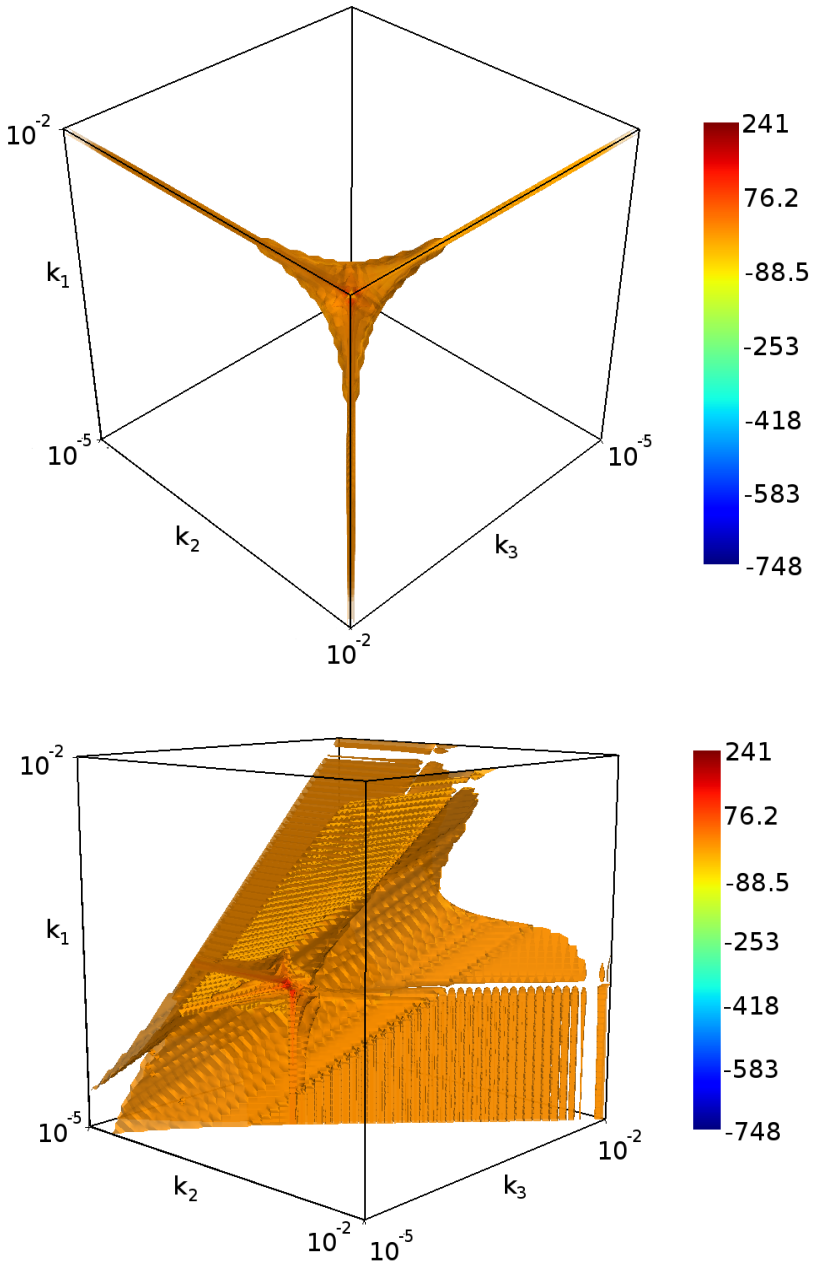

Figure 2.3: Three-dimensional contour plots of the non-Gaussianity parameter $f_{\rm NL}$, plotted against the three wavenumbers k_1, k_2 and k_3, in the case of punctuated inflation. We have shown two different projections of the plots in the figure. The projection in the top clearly indicates the symmetry along the three different axes, as is expected in an isotropic background. The figure at the bottom illustrates the fact that the allowed wavenumbers are confined to a 'tetrapyd' and that the bi-spectrum peaks in the equilateral limit, *i.e.* along the line $k_1 = k_2 = k_3$.

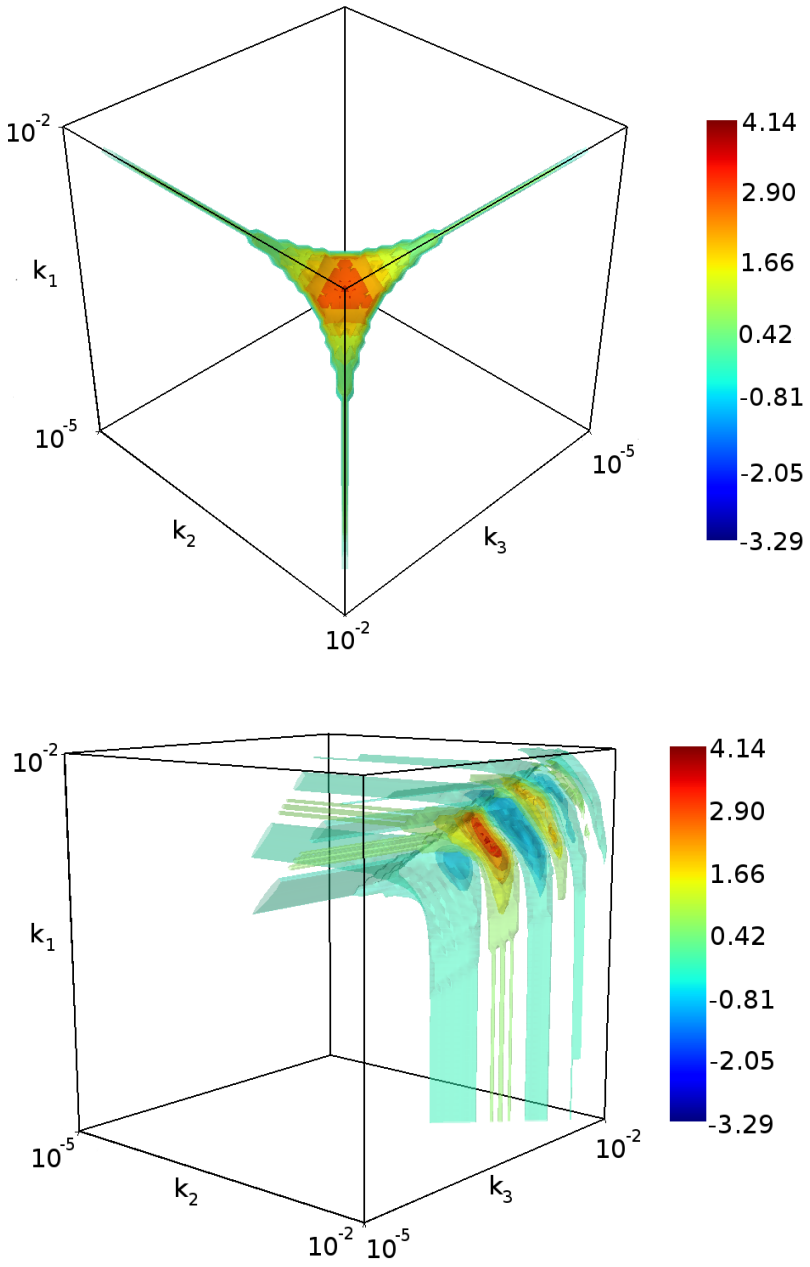

Figure 2.4: Three-dimensional contour plots of the parameter $f_{\rm NL}$, plotted against the three wavenumbers k_1, k_2 and k_3, in the case of the quadratic potential with a step. As in the previous figure, we have shown two different views to illustrate the symmetry along the three axis and the fact that the wavenumbers of interest are confined to a 'tetrapyd'.

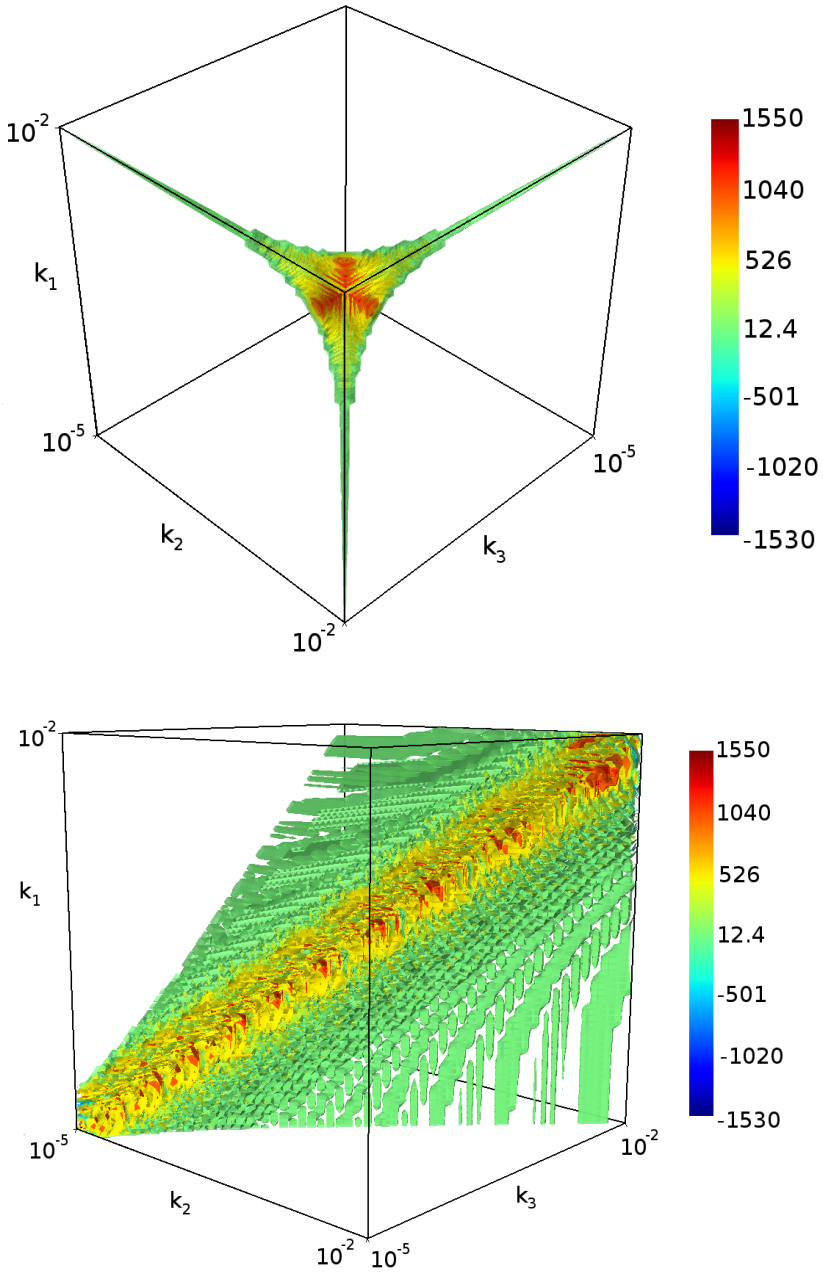

Figure 2.5: Three-dimensional contour plots of the parameter $f_{\rm NL}$, plotted as in the last two figures, in the case of the axion monodromy model.

condition restricts the wavenumbers to a 'tetrapyd', as is evident from the figures. In the figures, we have presented two projections of the three-dimensional plot. One of the views clearly shows the fact that the bi-spectrum is symmetric along the three axes, as is expected in an isotropic background. The second illustrates the fact that the non-Gaussianity parameter peaks in the equilateral limit, *i.e.* when $k_1 = k_2 = k_3$.

2.4.3 $f_{\rm NL}$ in the squeezed limit

Let us now turn to examine the consistency relation in the three models of our interest. Towards this end, we have made use of BINGO to evaluate the non-Gaussianity parameter $f_{\rm NL}$ in the squeezed limit, using the Maldacena formalism. As we had pointed out, BINGO can be made use of to evaluate the power spectrum as well. Using the expression (1.27a) and the scalar power spectrum, we arrive at the scalar spectral index $n_{\rm S}$, which we then utilize to verify the consistency condition $f_{\rm NL}(k) = 5\,[n_{\rm S}(k) - 1]/12$. Before we go on to illustrate the results for the three models that we are focusing on, a couple of points concerning the squeezed limit needs to be made. We should stress that we choose the wavenumber of the squeezed mode to be smallest wavenumber that is numerically tenable in the sense that the mode is sufficiently inside the Hubble radius at a time close to when the integration of the background begins. Moreover, it should be noted that, since the squeezed mode has a finite and non-zero wavenumber, in the squeezed limit of our interest, the numerically evaluated bi-spectrum is expected to be more accurate at larger wavenumbers than the smaller ones. In Fig. 2.6, we have plotted the quantity $f_{\rm NL}$ obtained from the Maldacena formalism as well as the quantity arrived at from the consistency relation. It is clear from the figure that the two quantities match very well (they match at the level of a few percent) thus confirming the validity of the consistency relation even in scenarios displaying highly nontrivial dynamics.

2.5 Discussion

At the level of the three-point function, the consistency condition relates the scalar bi-spectrum to the power spectrum in the squeezed limit wherein the wavelength of one of the three modes is much longer than the other two. As we had discussed, the consistency condition applies to any situation wherein the amplitude of the long wavelength mode freezes. Since the amplitude of the curvature perturbation settles down to a constant value on super-Hubble scales in most single field models of inflation, the consistency

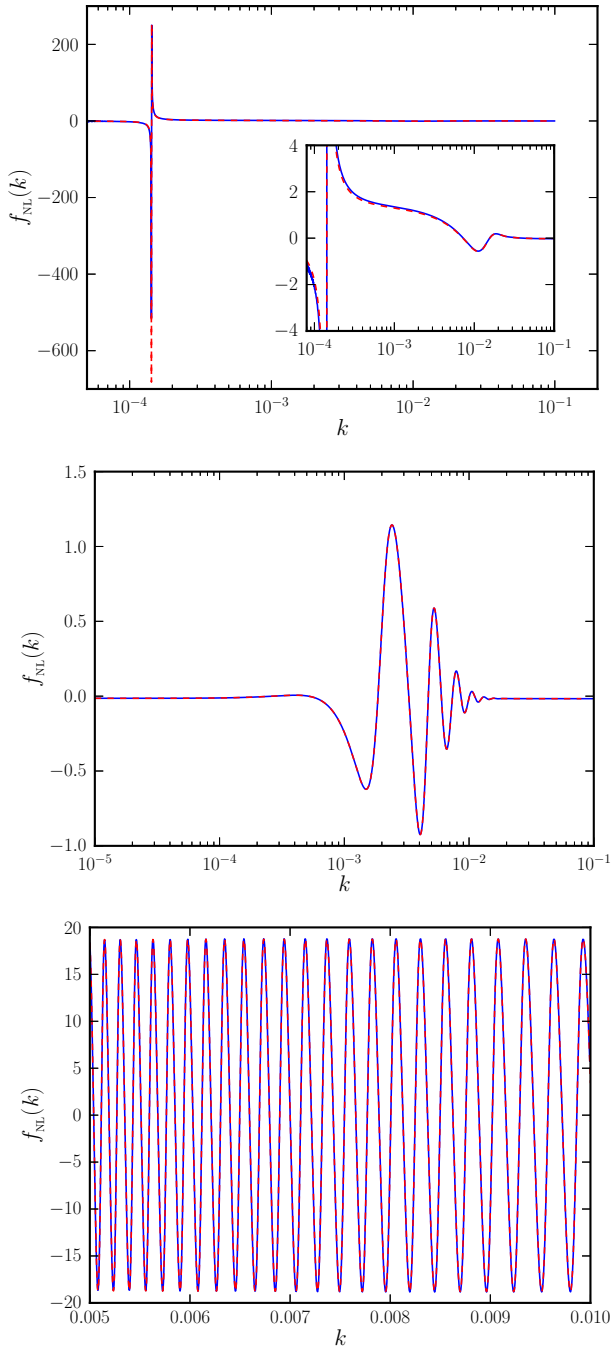

Figure 2.6: The behavior of the non-Gaussianity parameter $f_{\rm NL}$ in the squeezed limit has been plotted as a function of k for the case of punctuated inflation (on top), the quadratic potential with a step (in the middle) and axion monodromy model (at the bottom). The blue curve represents the $f_{\rm NL}$ calculated using the Maldacena formalism, while the red dashed line corresponds to the same quantity arrived at from the consistency relation. The excellent match between the two curves indicate that the consistency relation is valid even in non-trivial scenarios involving brief departures from inflation.

relation is expected to be valid in such models. It is easy to analytically establish the consistency relation in slow roll scenarios. In contrast, one needs to often resort to numerical methods to analyze situations involving departures from slow roll. In this chapter, we had examined the validity of the scalar consistency condition, analytically as well as numerically, in a class of models permitting deviations from slow roll. We find that the condition is indeed satisfied even in situations consisting of strong departures from slow roll, such as the punctuated inflationary scenario.

Chapter 3

Numerical evaluation of the three-point functions involving tensors

3.1 Introduction

Most of the efforts towards understanding non-Gaussianities generated by the inflationary models and arriving at constraints from the observational data have focused on the scalar bi-spectrum and the corresponding non-Gaussianity parameter $f_{\rm NL}$ (for the theoretical efforts, see, for instance, Refs. [23, 24, 25]; for efforts on arriving at observational constraints, see, for example, Refs. [26, 27, 28, 29]). There have also been some theoretical efforts aimed at analyzing the behavior of the tensor bi-spectrum (see, for example, Refs. [23, 33, 34]). But, we find that there have been relatively limited attempts at studying the scalar-tensor cross-correlations (see, for instance, Refs. [23, 30, 31]). It will be interesting to closely examine the behavior of these quantities and, eventually, try to arrive at observational constraints on the corresponding non-Gaussianity parameters that can be constructed to characterize these quantities. The fact that tensors remain to be detected at the level of the power spectrum could have been a dissuading factor in the limited attention devoted to the cross-correlations and the tensor bi-spectrum. However, it is important to bear in mind that popular models, such as those described by the quadratic and quartic potentials involving the canonical scalar field, are being ruled out by the Planck data primarily by the upper limits on the tensor-to-scalar ratio [20, 47]. We believe that the three-point functions involving the scalars and the tensors can play a similar role leading to additional constraints on the inflationary models.

The aims of this chapter can be said to be three-fold. Firstly, we shall describe our efforts [56] to devise a numerical procedure to evaluate the three-point scalar-tensor cross-correlations and the tensor bi-spectrum as well as the corresponding non-Gaussianity pa-

rameters that we introduce. Secondly, utilizing the developed numerical procedure, we shall evaluate these quantities in the models which lead to features in the scalar power spectrum (see Subsec. 2.4.1) but do not permit analytical calculation of these quantities. Thirdly, we shall consider the contribution to these quantities during the period of preheating, *viz.* the epoch which immediately follows inflation [57, 58].

The plan of this chapter is as follows. In the next section, along the lines of the definition of scalar non-Gaussianity parameter, we shall introduce parameters to quantify the extent of non-Gaussianity in the three-point scalar-tensor cross-correlations and the tensor bi-spectrum. In Sec. 3.3, we shall outline the numerical procedure that we adopt for evaluating the scalar-tensor cross-correlations and the tensor bi-spectrum. We shall begin by showing that as in the case of the scalar bi-spectrum (in this context, see, for instance, Refs. [54, 55]), the super-Hubble contributions to the other three-point correlation functions too turn out to be negligible. Further, as in the pure scalar case, one needs to introduce a suitable cut-off in the sub-Hubble domain in order to deal with the continued oscillations that would otherwise arise. Under these conditions, we shall illustrate that it proves to be sufficient to evolve the scalar and the tensor modes from sufficiently inside the Hubble radius to a suitably late time when they are well outside, and evaluate the integrals involved over this period. In order to demonstrate the accuracy of the numerical procedure, we shall compare our numerical results with the analytical results available in the cases of power law and slow roll inflation as well as in the case of the Starobinsky model [37, 74, 75]. In Sec. 3.4, we shall use the validated numerical code to study the three-point functions that arise in three types of models which involve deviations from slow roll, *viz.* the punctuated inflationary scenario [79], the quadratic potential with a step [82, 81, 83] and the axion monodromy model [86, 88, 89], that we had discussed in the last chapter. In Sec. 3.5, we shall consider the contributions to the cross-correlations and the tensor bi-spectrum during preheating and show that the contributions prove to be completely insignificant. We shall conclude this chapter in Sec. 3.6 with a quick summary of the results we have obtained. We shall relegate some of the details pertaining to the evaluation of the three-point functions in the Starobinsky model to Appendix A.

3.2 Non-Gaussianity parameters for the three-point functions involving tensors

Recall that, often, the scalar bi-spectrum is essentially characterized by the dimensionless non-Gaussianity parameters $f_{\rm NL}$ (see Subsecs.1.5.5 and 2.2.1). The basic set of three

non-Gaussianity parameters, *viz.* $(f_{\rm NL}^{\rm loc}, f_{\rm NL}^{\rm eq}, f_{\rm NL}^{\rm ortho})$, do not always capture the complete structure of the scalar bi-spectrum, in particular, when there exist deviations from the conventional scenario of slow roll inflation driven by the canonical scalar field (and, of course, the assumption that the perturbations are in the standard Bunch-Davies vacuum [1, 12, 38]). Nonetheless, they prove to be a convenient tool in understanding the amplitude and shape of the scalar bi-spectrum in many situations.

In a similar manner, the cross-correlations and the tensor bi-spectrum can be characterized by parameters that are suitable dimensionless ratios of the three-point functions and the scalar or the tensor power spectra. We can generalize the conventional way of introducing the $f_{\rm NL}$ parameter to write the scalar and tensor perturbations $\mathcal{R}$ and γ_{ij} as follows:

$$\begin{aligned}
\mathcal{R}(\eta,\boldsymbol{x}) &= \mathcal{R}_{\rm G}(\eta,\boldsymbol{x}) - \frac{3\,f_{\rm NL}}{5}\,\left[\mathcal{R}^2_{\rm G}(\eta,\boldsymbol{x}) - \left\langle\mathcal{R}^2_{\rm G}(\eta,\boldsymbol{x})\right\rangle\right] \\
&\quad - C^{\mathcal{R}}_{\rm NL}\,\mathcal{R}_{\rm G}(\eta,\boldsymbol{x})\,\gamma^{\rm G}_{\bar{m}\bar{n}}(\eta,\boldsymbol{x}), \qquad (3.1a)\\
\gamma_{ij}(\eta,\boldsymbol{x}) &= \gamma^{\rm G}_{ij}(\eta,\boldsymbol{x}) - h_{\rm NL}\,\left[\gamma^{\rm G}_{ij}(\eta,\boldsymbol{x})\,\gamma^{\rm G}_{\bar{m}\bar{n}}(\eta,\boldsymbol{x}) - \langle\gamma^{\rm G}_{ij}(\eta,\boldsymbol{x})\,\gamma^{\rm G}_{\bar{m}\bar{n}}(\eta,\boldsymbol{x})\rangle\right] \\
&\quad - C^{\gamma}_{\rm NL}\,\gamma^{\rm G}_{ij}(\eta,\boldsymbol{x})\,\mathcal{R}_{\rm G}(\eta,\boldsymbol{x}), \qquad (3.1b)
\end{aligned}$$

where $\mathcal{R}_{\rm G}$ and $\gamma^{\rm G}_{ij}$ denote the Gaussian quantities. Note that the overbars on the indices of the Gaussian tensor perturbation imply that the indices should be summed over all allowed values[1]. Upon using the above definitions along with the Wick's theorem to calculate the three-point functions (but retaining terms only to the linear order in the non-Gaussianity parameters), we find that we can write the parameters $C^{\mathcal{R}}_{\rm NL}$, $C^{\gamma}_{\rm NL}$ and $h_{\rm NL}$ as follows:

$$\begin{aligned}
C^{\mathcal{R}}_{\rm NL}(\boldsymbol{k}_1,\boldsymbol{k}_2,\boldsymbol{k}_3) &= -\frac{4}{(2\,\pi^2)^2}\,\left[k_1^3\,k_2^3\,k_3^3\,G^{m_3n_3}_{\mathcal{R}\mathcal{R}\gamma}(\boldsymbol{k}_1,\boldsymbol{k}_2,\boldsymbol{k}_3)\right] \\
&\quad \times \left(\Pi^{\boldsymbol{k}_3}_{m_3n_3,\bar{m}\bar{n}}\right)^{-1}\,\left\{\left[k_1^3\,\mathcal{P}_{\rm S}(k_2) + k_2^3\,\mathcal{P}_{\rm S}(k_1)\right]\,\mathcal{P}_{\rm T}(k_3)\right\}^{-1}, \qquad (3.2a)
\end{aligned}$$

[1]It should be apparent that such a procedure is required to 'remove' the additional polarization indices that would otherwise occur when the parameters $C^{\mathcal{R}}_{\rm NL}$, $C^{\gamma}_{\rm NL}$ and $h_{\rm NL}$ are introduced in the above fashion. Also, clearly, this procedure is not unique, and there exist other ways of 'removing' the additional indices.

$$C^{\gamma}_{_{\rm NL}}(\boldsymbol{k}_1,\boldsymbol{k}_2,\boldsymbol{k}_3) = -\frac{4}{(2\,\pi^2)^2}\,\left[k_1^3\,k_2^3\,k_3^3\,G^{m_2n_2m_3n_3}_{\mathcal{R}\gamma\gamma}(\boldsymbol{k}_1,\boldsymbol{k}_2,\boldsymbol{k}_3)\right] \times\left\{\mathcal{P}_{_{\rm S}}(k_1)\,\left[\Pi^{\boldsymbol{k}_2}_{m_2n_2,m_3n_3}\,k_3^3\,\mathcal{P}_{_{\rm T}}(k_2)+\Pi^{\boldsymbol{k}_3}_{m_3n_3,m_2n_2}\,k_2^3\,\mathcal{P}_{_{\rm T}}(k_3)\right]\right\}^{-1}, \tag{3.2b}$$

$$h_{_{\rm NL}}(\boldsymbol{k}_1,\boldsymbol{k}_2,\boldsymbol{k}_3) = -\frac{4^2}{(2\,\pi^2)^2}\,\left[k_1^3\,k_2^3\,k_3^3\,G^{m_1n_1m_2n_2m_3n_3}_{\gamma\gamma\gamma}(\boldsymbol{k}_1,\boldsymbol{k}_2,\boldsymbol{k}_3)\right] \times\,\left[\Pi^{\boldsymbol{k}_1}_{m_1n_1,m_3n_3}\,\Pi^{\boldsymbol{k}_2}_{m_2n_2,\bar{m}\bar{n}}\,k_3^3\,\mathcal{P}_{_{\rm T}}(k_1)\,\mathcal{P}_{_{\rm T}}(k_2)+\text{five permutations}\right]^{-1}, \tag{3.2c}$$

where the quantity $\Pi^{\boldsymbol{k}}_{m_1n_1,m_2n_2}$ is defined in Eq. (1.25). While we notice that a parameter such as $h_{_{\rm NL}}$ to characterize the tensor bi-spectrum has been discussed earlier (see, for instance, Refs. [30, 33]), to our knowledge, the non-Gaussianity parameters $C^{\mathcal{R}}_{_{\rm NL}}$ and $C^{\gamma}_{_{\rm NL}}$ describing the cross-correlations do not seem to have been considered before in the literature. In retrospect though, the introduction and the utility of these parameters in helping to characterize and eventually constrain inflationary models seem evident.

3.3 The numerical procedure for evaluating the three-point functions

For a general inflationary model, it proves to be difficult to analytically calculate the scalar-tensor cross-correlations and the tensor bi-spectrum. It is therefore useful to develop a numerical approach to evaluate these three-point correlations. It is evident from the discussion in Subsec. 1.5.3 that the three-point functions involve integrals over the background quantities as well as the scalar and the tensor modes from the early stages of inflation till its very end. Recently, in the context of the scalar bi-spectrum, it was shown that the corresponding super-Hubble contributions prove to be negligible and it suffices to carry out the integrals numerically over a suitably smaller domain in time [55]. We find that similar arguments apply for the other three-point functions too. In this section, we shall first show that the super-Hubble contributions to the three-point functions of our interest here are indeed insignificant and then, based on this result, go on to construct a numerical method to evaluate the correlation functions. We shall also illustrate the accuracy of our numerical procedure by comparing them with the analytical results that can be obtained in the cases of power law inflation, the quadratic potential and the non-trivial scenario involving departures from slow roll that occurs in the Starobinsky model [37, 74, 75].

3.3.1 Insignificance of the super-Hubble contributions

As we had described earlier, the evolution of scalar and the tensor modes are governed by the Mukhanov-Sasaki equations (1.23). During slow roll inflation, we can show that $z''/z \simeq a''/a \simeq 2\,\mathcal{H}^2$, where $\mathcal{H} = a\,H$ denotes the conformal Hubble parameter [1, 12]. On super-Hubble scales during inflation, *i.e.* when $k/\mathcal{H} \ll 1$, we can ignore the k^2 term in the above equations in comparison to z''/z and a''/a, thereby obtaining the following solutions for f_k and g_k:

$$f_k(\eta) = A_k + B_k \int^{\eta} \frac{d\tilde{\eta}}{z^2(\tilde{\eta})}, \tag{3.3a}$$

$$g_k(\eta) = \frac{\sqrt{2}}{M_{_{\rm Pl}}} \left(C_k + D_k \int^{\eta} \frac{{\rm d}\tilde{\eta}}{a^2(\tilde{\eta})}\right), \tag{3.3b}$$

where A_k, B_k, C_k and D_k are k-dependent constants that are determined by the initial conditions imposed on the modes at early times when they are well inside the Hubble radius. Moreover, the overall factor of $\sqrt{2}/M_{_{\rm Pl}}$ has been introduced in the solution for g_k by convention, so as to ensure that the resulting tensor power spectrum [cf. Eq. (1.26b)] is dimensionless. The first terms in the above expressions for f_k and g_k are the growing (actually, constant) solutions, while the second represent the decaying (*i.e.* the sub-dominant) ones. Therefore, at late times, we have

$$f_k \simeq A_k, \tag{3.4a}$$

$$g_k \simeq \sqrt{2}\,C_k/M_{_{\rm Pl}} \tag{3.4b}$$

and, since the derivative of the first terms vanish, we also have, at the leading order,

$$f_k' \simeq B_k/z^2 = \bar{B}_k/\left(a^2\,\epsilon_1\right), \tag{3.5a}$$

$$g_k' \simeq \sqrt{2}\,D_k/\left(M_{_{\rm Pl}}\,a^2\right), \tag{3.5b}$$

where $\bar{B}_k = B_k/(2\,M_{_{\rm Pl}}^2)$. Let us now make use of the above super-Hubble behavior of the modes to arrive at the corresponding contributions to the three point functions $G^{m_3 n_3}_{\mathcal{R}\mathcal{R}\gamma}(\boldsymbol{k}_1, \boldsymbol{k}_2, \boldsymbol{k}_3)$, $G^{m_2 n_2 m_3 n_3}_{\mathcal{R}\gamma\gamma}(\boldsymbol{k}_1, \boldsymbol{k}_2, \boldsymbol{k}_3)$ and $G^{m_1 n_1 m_2 n_2 m_3 n_3}_{\gamma\gamma\gamma}(\boldsymbol{k}_1, \boldsymbol{k}_2, \boldsymbol{k}_3)$.

Let us first focus on $G^{m_3 n_3}_{\mathcal{R}\mathcal{R}\gamma}(\boldsymbol{k}_1, \boldsymbol{k}_2, \boldsymbol{k}_3)$. Let $\eta_{\rm s}$ denote the conformal time when the largest of the three wavenumbers k_1, k_2 and k_3 is well outside the Hubble radius (in this context, we would refer the reader to Fig. 1 of Ref. [55]). It is then straightforward to show using the above behavior of the modes that the super-Hubble contributions to

$G^{m_3n_3}_{\mathcal{R}\mathcal{R}\gamma}(\boldsymbol{k}_1,\boldsymbol{k}_2,\boldsymbol{k}_3)$ are given by

$$
\begin{aligned}
G^{m_3n_3\,(\mathrm{se})}_{\mathcal{R}\mathcal{R}\gamma\,(1)}(\boldsymbol{k}_1,\boldsymbol{k}_2,\boldsymbol{k}_3) &\simeq -4\,i\,\Pi^{\boldsymbol{k}_3}_{m_3n_3,ij}\,k_{1i}\,k_{2j}\,|A_{k_1}|^2\,|A_{k_2}|^2\,|C_{k_3}|^2 \\
&\quad\times\left[I(\eta_{\mathrm{e}},\eta_{\mathrm{s}})-I^*(\eta_{\mathrm{e}},\eta_{\mathrm{s}})\right], \qquad (3.6a)\\
G^{m_3n_3(\mathrm{se})}_{\mathcal{R}\mathcal{R}\gamma\,(2)}(\boldsymbol{k}_1,\boldsymbol{k}_2,\boldsymbol{k}_3) &\simeq i\,\Pi^{\boldsymbol{k}_3}_{m_3n_3,ij}\,k_{1i}\,k_{2j}\,\left[k_3^2/\left(k_1^2\,k_2^2\right)\right]\,|C_{k_3}|^2\,J(\eta_{\mathrm{e}},\eta_{\mathrm{s}}) \\
&\quad\times\left(A_{k_1}\,A_{k_2}\,\bar{B}^*_{k_1}\,\bar{B}^*_{k_2}-A^*_{k_1}\,A^*_{k_2}\,\bar{B}_{k_1}\,\bar{B}_{k_2}\right), \qquad (3.6b)\\
G^{m_3n_3\,(\mathrm{se})}_{\mathcal{R}\mathcal{R}\gamma\,(3)}(\boldsymbol{k}_1,\boldsymbol{k}_2,\boldsymbol{k}_3) &\simeq i\,\Pi^{\boldsymbol{k}_3}_{m_3n_3,ij}\,\left[k_{1i}\,k_{2j}/\left(k_1^2\,k_2^2\right)\right]\,K(\eta_{\mathrm{e}},\eta_{\mathrm{s}}) \\
&\quad\times\Bigg[k_1^2\,|A_{k_1}|^2\,\left(A_{k_2}\,\bar{B}^*_{k_2}\,C_{k_3}\,D^*_{k_3}-A^*_{k_2}\,\bar{B}_{k_2}\,C^*_{k_3}\,D_{k_3}\right) \\
&\quad+k_2^2\,|A_{k_2}|^2\,\left(A_{k_1}\,\bar{B}^*_{k_1}\,C_{k_3}\,D^*_{k_3}-A^*_{k_1}\,\bar{B}_{k_1}\,C^*_{k_3}\,D_{k_3}\right)\Bigg], \qquad (3.6c)
\end{aligned}
$$

where the super-script (se) implies that they correspond to the contributions over the time domain η_{s} to η_{e}, and the quantities $I(\eta_{\mathrm{e}},\eta_{\mathrm{s}})$, $J(\eta_{\mathrm{e}},\eta_{\mathrm{s}})$ and $K(\eta_{\mathrm{e}},\eta_{\mathrm{s}})$ are described by the integrals

$$
\begin{aligned}
I(\eta_{\mathrm{e}},\eta_{\mathrm{s}}) &= \int_{\eta_{\mathrm{s}}}^{\eta_{\mathrm{e}}}\mathrm{d}\eta\;a^2\,\epsilon_1, \qquad (3.7a)\\
J(\eta_{\mathrm{e}},\eta_{\mathrm{s}}) &= \int_{\eta_{\mathrm{s}}}^{\eta_{\mathrm{e}}}\frac{\mathrm{d}\eta}{a^2}, \qquad (3.7b)\\
K(\eta_{\mathrm{e}},\eta_{\mathrm{s}}) &= \int_{\eta_{\mathrm{s}}}^{\eta_{\mathrm{e}}}\frac{\mathrm{d}\eta}{a^2}\,\epsilon_1. \qquad (3.7c)
\end{aligned}
$$

Note that, since $I(\eta_{\mathrm{e}},\eta_{\mathrm{s}})$ is real, the term $G^{m_3n_3\,(\mathrm{se})}_{\mathcal{R}\mathcal{R}\gamma\,(1)}(\boldsymbol{k}_1,\boldsymbol{k}_2,\boldsymbol{k}_3)$ vanishes identically and, hence, the super-Hubble contributions arise only due to the other two terms.

In a similar fashion, we can show that the super-Hubble contributions to the quantity $G^{m_2n_2m_3n_3}_{\mathcal{R}\gamma\gamma}(\boldsymbol{k}_1,\boldsymbol{k}_2,\boldsymbol{k}_3)$ are given by

$$
\begin{aligned}
G^{m_2n_2m_3n_3\,(\mathrm{se})}_{\mathcal{R}\gamma\gamma\,(1)}(\boldsymbol{k}_1,\boldsymbol{k}_2,\boldsymbol{k}_3) &\simeq \frac{i}{M_{\mathrm{Pl}}^2}\,\Pi^{\boldsymbol{k}_2}_{m_2n_2,ij}\,\Pi^{\boldsymbol{k}_3}_{m_3n_3,ij}\,|A_{k_1}|^2\,K(\eta_{\mathrm{e}},\eta_{\mathrm{s}}) \\
&\quad\times\left(C_{k_2}\,C_{k_3}\,D^*_{k_2}\,D^*_{k_3}-C^*_{k_2}\,C^*_{k_3}\,D_{k_2}\,D_{k_3}\right), \qquad (3.8a)\\
G^{m_2n_2m_3n_3\,(\mathrm{se})}_{\mathcal{R}\gamma\gamma\,(2)}(\boldsymbol{k}_1,\boldsymbol{k}_2,\boldsymbol{k}_3) &\simeq -\frac{i}{M_{\mathrm{Pl}}^2}\,\Pi^{\boldsymbol{k}_2}_{m_2n_2,ij}\,\Pi^{\boldsymbol{k}_3}_{m_3n_3,ij}\,(\boldsymbol{k}_2\cdot\boldsymbol{k}_3)\,|A_{k_1}|^2\,|C_{k_2}|^2\,|C_{k_3}|^2 \\
&\quad\times\left[I(\eta_{\mathrm{e}},\eta_{\mathrm{s}})-I^*(\eta_{\mathrm{e}},\eta_{\mathrm{s}})\right], \qquad (3.8b)\\
G^{m_2n_2m_3n_3\,(\mathrm{se})}_{\mathcal{R}\gamma\gamma\,(3)}(\boldsymbol{k}_1,\boldsymbol{k}_2,\boldsymbol{k}_3) &\simeq -\frac{i}{M_{\mathrm{Pl}}^2}\,\Pi^{\boldsymbol{k}_2}_{m_2n_2,ij}\,\Pi^{\boldsymbol{k}_3}_{m_3n_3,ij}\,J(\eta_{\mathrm{e}},\eta_{\mathrm{s}}) \\
&\quad\times\Bigg[\frac{\boldsymbol{k}_1\cdot\boldsymbol{k}_2}{k_1^2}\,|C_{k_2}|^2\,\left(A_{k_1}\,\bar{B}^*_{k_1}\,C_{k_3}\,D^*_{k_3}-A^*_{k_1}\,\bar{B}_{k_1}\,C^*_{k_3}\,D_{k_3}\right) \\
&\quad+\frac{\boldsymbol{k}_1\cdot\boldsymbol{k}_3}{k_1^2}\,|C_{k_3}|^2\,\left(A_{k_1}\,\bar{B}^*_{k_1}\,C_{k_2}\,D^*_{k_2}-A^*_{k_1}\,\bar{B}_{k_1}\,C^*_{k_2}\,D_{k_2}\right)\Bigg]. \qquad (3.8c)
\end{aligned}
$$

Clearly, the contribution $G^{m_2n_2m_3n_3\,(\mathrm{se})}_{\mathcal{R}\gamma\gamma\,(2)}(\boldsymbol{k}_1,\boldsymbol{k}_2,\boldsymbol{k}_3)$ vanishes for the same reason as $G^{m_3n_3\,(\mathrm{se})}_{\mathcal{R}\mathcal{R}\gamma\,(1)}(\boldsymbol{k}_1,\boldsymbol{k}_2,\boldsymbol{k}_3)$ had and, as a result, it is only the remaining two terms that contribute on super-Hubble scales to $G^{m_2n_2m_3n_3}_{\mathcal{R}\gamma\gamma}(\boldsymbol{k}_1,\boldsymbol{k}_2,\boldsymbol{k}_3)$.

Lastly, let us turn to the tensor bi-spectrum, *viz.* $G^{m_1n_1m_2n_2m_3n_3}_{\gamma\gamma\gamma}(\boldsymbol{k}_1,\boldsymbol{k}_2,\boldsymbol{k}_3)$. In this case, we have, on super-Hubble scales

$$G^{m_1n_1m_2n_2\,(\mathrm{se})}_{\gamma\gamma\gamma\,(1)}(\boldsymbol{k}_1,\boldsymbol{k}_2,\boldsymbol{k}_3) = -\frac{2\,i}{M_{_{\mathrm{Pl}}}^4}\,\left(\Pi^{\boldsymbol{k}_1}_{m_1n_1,ij}\,\Pi^{\boldsymbol{k}_2}_{m_2n_2,im}\,\Pi^{\boldsymbol{k}_3}_{m_3n_3,lj}\,k_{1m}\,k_{1l} + \text{five permutations}\right) \times |C_{k_1}|^2\,|C_{k_2}|^2\,|C_{k_3}|^2\,\left[L(\eta_{_{\mathrm{e}}},\eta_{_{\mathrm{s}}}) - L^*(\eta_{_{\mathrm{e}}},\eta_{_{\mathrm{s}}})\right], \tag{3.9a}$$

$$G^{m_1n_1m_2n_2\,(\mathrm{se})}_{\gamma\gamma\gamma\,(2)}(\boldsymbol{k}_1,\boldsymbol{k}_2,\boldsymbol{k}_3) = \frac{i}{M_{_{\mathrm{Pl}}}^4}\,\left(\Pi^{\boldsymbol{k}_1}_{m_1n_1,ij}\,\Pi^{\boldsymbol{k}_2}_{m_2n_2,ml}\,\Pi^{\boldsymbol{k}_3}_{m_3n_3,ij}\,k_{1m}\,k_{1l} + \text{five permutations}\right) \times |C_{k_1}|^2\,|C_{k_2}|^2\,|C_{k_3}|^2\,\left[L(\eta_{_{\mathrm{e}}},\eta_{_{\mathrm{s}}}) - L^*(\eta_{_{\mathrm{e}}},\eta_{_{\mathrm{s}}})\right], \tag{3.9b}$$

where the quantity $L(\eta_{_{\mathrm{e}}},\eta_{_{\mathrm{s}}})$ is described by the integral

$$L(\eta_{_{\mathrm{e}}},\eta_{_{\mathrm{s}}}) = \int_{\eta_{_{\mathrm{s}}}}^{\eta_{_{\mathrm{e}}}} \mathrm{d}\eta\; a^2. \tag{3.10}$$

We should mention that we have expressed the quantity $G^{m_1n_1m_2n_2m_3n_3}_{\gamma\gamma\gamma}(\boldsymbol{k}_1,\boldsymbol{k}_2,\boldsymbol{k}_3)$ [cf. Eq. (1.51)] as two separate terms above for convenience. Both of the above expressions obviously vanish since $L(\eta_{_{\mathrm{e}}},\eta_{_{\mathrm{s}}})$ is real. In other words, the super-Hubble contributions to the tensor bi-spectrum and the corresponding non-Gaussianity parameter $h_{_{\mathrm{NL}}}$ are identically zero.

It is now worthwhile to estimate the extent of the super-Hubble contributions to the other two non-Gaussianity parameters $C^{\mathcal{R}}_{_{\mathrm{NL}}}$ and $C^{\gamma}_{_{\mathrm{NL}}}$. In order to carry out such an estimate, let us focus on power law inflation wherein the scale factor is given by (2.6). In such a situation, the first slow roll parameter is a constant and is given by $\epsilon_1 = (\gamma+2)/(\gamma+1)$. Also, since $z''/z = a''/a$ in power law inflation, the solutions to the scalar and the tensor modes f_k and g_k are exactly the same functions, barring overall constants. In fact, the solutions to the Mukhanov-Sasaki equations (1.23) can be expressed in terms of the Bessel functions $J_\nu(x)$ as follows (see, for instance, Refs. [54, 73]):

$$v_k(\eta) = u_k(\eta) = \sqrt{-k\,\eta}\;\left[\mathcal{A}_k\,J_\nu(-k\,\eta) + \mathcal{B}_k\,J_{-\nu}(-k\,\eta)\right], \tag{3.11}$$

where $\nu = \gamma + 1/2$. The quantities $\mathcal{A}_k$ and $\mathcal{B}_k$ are k-dependent constants which are determined by demanding that the above solutions satisfy the Bunch-Davies initial conditions at early times [1, 12, 38]. They are found to be

$$\mathcal{A}_k = -\mathcal{B}_k\,\mathrm{e}^{-i\,\pi\,(\gamma+1/2)}, \tag{3.12a}$$

$$\mathcal{B}_k = \sqrt{\frac{\pi}{k}}\,\frac{\mathrm{e}^{i\,\pi\,\gamma/2}}{2\cos{(\pi\,\gamma)}}. \tag{3.12b}$$

In the super-Hubble limit, *i.e.* as $-k\,\eta \to 0$, the solutions for $v_k(\eta)$ and $u_k(\eta)$ in (3.11) can be compared with the general solutions (3.3) to arrive at the following expressions for the quantities A_k, B_k, C_k and D_k:

$$A_k = \frac{C_k}{\sqrt{2\,\epsilon_1}\,M_{_{\rm Pl}}} = \frac{2^{-(\gamma+1/2)}}{\Gamma(\gamma+3/2)}\,\frac{(-k\,\eta_1)^{\gamma+1}}{\sqrt{2\,\epsilon_1}\,a_1\,M_{_{\rm Pl}}}\,\mathcal{A}_k, \tag{3.13a}$$

$$B_k = \sqrt{2\,\epsilon_1}\,M_{_{\rm Pl}}\,D_k = -\,\frac{(2\,\gamma+1)\,2^{\gamma+1/2}}{\Gamma(-\gamma+1/2)}\,\frac{\sqrt{2\,\epsilon_1}\,a_1\,M_{_{\rm Pl}}}{\eta_1}\,(-k\,\eta_1)^{-\gamma}\,\mathcal{B}_k. \tag{3.13b}$$

Moreover, the scalar and tensor power spectra in power law inflation, evaluated in the super-Hubble limit, can be shown to be

$$\mathcal{P}_{_{\rm S}}(k) = \frac{k^3}{2\,\pi^2}\,|A_k|^2 = \frac{\mathcal{P}_{_{\rm T}}(k)}{16\,\epsilon_1}, \tag{3.14}$$

a well known result that is also valid in slow roll inflation [1, 12].

We now have all the quantities required to arrive at an estimate for the super-Hubble contributions to the parameters $C^{\mathcal{R}}_{_{\rm NL}}$ and $C^{\gamma}_{_{\rm NL}}$ [cf. Eqs. (3.2a) and (3.2b)] in power law inflation. Let us restrict ourselves to the equilateral limit, *i.e.* $k_1 = k_2 = k_3$, for simplicity. In such a case, upon using the results we have obtained above, we can show, after a bit of algebra [54, 55], that

$$\begin{aligned} C^{\mathcal{R}\,({\rm se})}_{_{\rm NL}} &= \frac{3}{4}\,C^{\gamma\,({\rm se})}_{_{\rm NL}} \\ &= \frac{3}{16\,\pi}\,\Gamma^2\left(\gamma+\frac{1}{2}\right)\,2^{2\,\gamma+1}\,(2\,\gamma+1)\,(\gamma+2)\,|\gamma+1|^{-2\,(\gamma+1)}\,\sin\left(2\,\pi\,\gamma\right) \\ &\quad\times\left[1-\frac{H_{\rm s}}{H_{\rm e}}\,{\rm e}^{-3\,(N_{\rm e}-N_{\rm s})}\right]\,\left(\frac{k}{a_{\rm s}\,H_{\rm s}}\right)^{-(2\,\gamma+1)}, \end{aligned} \tag{3.15}$$

where $(N_{\rm s}, N_{\rm e})$ and $(H_{\rm s}, H_{\rm e})$ denote the number of e-folds and the Hubble parameter at the conformal times $(\eta_{\rm s}, \eta_{\rm e})$. We should also add that, in arriving at the above expression, we have ignored overall factors involving $\Pi^{\boldsymbol{k}}_{mn,ij}$, which can be assumed to be of order unity without any loss of generality. Further, we have set the constant a_1 to be $a_{\rm s}$, *viz.* the scale factor at the time $\eta_{\rm s}$. If we now choose $\gamma \simeq -(2+\delta)$, where $\delta \ll 1$, we obtain that

$$C^{\mathcal{R}\,({\rm se})}_{_{\rm NL}} = \frac{3}{4}\,C^{\gamma\,({\rm se})}_{_{\rm NL}} \simeq -\,\delta^2\,\left(\frac{k_{\rm s}}{a_{\rm s}\,H_{\rm s}}\right)^3 \lesssim 10^{-19}, \tag{3.16}$$

where $k_{\rm s}$ is the largest wavenumber of interest and, in arriving at the final inequality, we have assumed that $k_{\rm s}/(a_{\rm s}\,H_{\rm s}) = 10^{-5}$ and $\delta \simeq 10^{-2}$. As we shall see later, this value always proves to be considerably smaller than the corresponding values generated as the modes

leave the Hubble radius during inflation. This implies that we can safely ignore the super-Hubble contributions to the scalar-tensor cross correlations and the tensor bi-spectrum as well as the corresponding non-Gaussianity parameters.

3.3.2 Details of the numerical method

Let us now turn to discuss the numerical procedure for evaluating the three-point functions. It should be clear by now that evaluating the three-point functions and the non-Gaussianity parameters involves solving for the evolution of the background and the perturbations and, eventually, computing the integrals involved. Given the inflationary potential $V(\phi)$ that describes the scalar field and the values for the parameters, the background evolution is completely determined if the initial conditions on the scalar field are specified. Typically, the initial value of the scalar field is chosen so that one achieves about 60 or so e-folds of inflation (as is required to overcome the horizon problem) before the accelerated expansion is terminated as the field approaches a minima of the potential. Further, the initial velocity of the field is often chosen such that the field starts on the inflationary attractor (in this context, see, for example, Refs. [41]).

Once the background has been solved for, the scalar and the tensor perturbations are evolved from the standard Bunch-Davies initial conditions using the governing equations (1.21) [1, 12, 38]. Then, in order to arrive at the three-point functions, it is a matter of being able to carry out the various integrals involved. Recall that, when calculating the power spectra, the initial conditions are imposed on the modes when they are sufficiently inside the Hubble radius, typically, when $k/(a\,H) \simeq 10^2$. The spectra are evaluated in the super-Hubble domain, when the amplitudes of the modes have reached a constant value, which often occurs when $k/(a\,H) \simeq 10^{-5}$ (see, for instance, Refs. [41, 66]). Since the super-Hubble contributions to the three-point functions are negligible, as in the purely scalar case discussed in the previous chapter, it suffices to carry out the integrals from the earliest time $\eta_{\rm i}$ when the smallest of the three wavenumbers (k_1, k_2, k_3) is well inside the Hubble radius to the final time $\eta_{\rm s}$ when the largest of them is sufficiently outside. However, there is one point that needs to be noted. In the extreme sub-Hubble domain, the modes oscillate rapidly and, theoretically, a cut-off is required in order to identify the correct perturbative vacuum [23, 24, 25]. This proves to be handy numerically, as the introduction of a cut-off ensures that the integrals converge quickly (for the original discussion on this point, see Refs. [92]). Motivated by the consistent results arrived at earlier in the case of the scalar bi-spectrum [55], we introduce a cut-off of the form $\exp - [\kappa\, k/(a\,H)]$,

where κ is a small parameter. As we shall discuss below, a suitable combination of κ, $\eta_{\rm i}$ and $\eta_{\rm s}$ (or, $N_{\rm i}$ and $N_{\rm s}$, in terms of e-folds) ensure that the final results are fairly robust against changes in their values.

We solve the background and the perturbation equations using the fifth order Runge-Kutta algorithm (see, for instance, Ref. [95]), with e-folds as the independent variable. We carry out the integrals involved using the so-called Bode's rule to arrive at the three-point functions and the non-Gaussianity parameters[2]. In Figs. 3.1 and 3.2, with the help of an example (*viz.* the three different contributions to the cross-correlation $G^{m_3 n_3}_{\mathcal{R}\mathcal{R}_\gamma}(\boldsymbol{k}_1, \boldsymbol{k}_2, \boldsymbol{k}_3)$, evaluated in the equilateral limit), we demonstrate the robustness of the procedure we have described above for a specific mode evolving in the popular quadratic potential. In arriving at the first figure, we have fixed the values of $N_{\rm i}$ and κ, and varied $N_{\rm s}$, whereas the second figure corresponds to a few different values of $N_{\rm i}$, but a fixed value of $N_{\rm s}$. It is clear from the figures that the choice of $N_{\rm s}$ corresponding to $k/(a\,H)$ of 10^{-5}, and the combination of $N_{\rm i}$ corresponding to $k/(a\,H)$ of 10^2 and κ of 0.1 leads to consistent results.

We have carried out similar exercises for all the models that we shall discuss in this chapter, and we have found that the above set of values for $N_{\rm i}$, $N_{\rm s}$ and κ lead to robust results in all the cases. Also, as we shall illustrate in the following subsection, the numerical results arrived at in such a fashion are consistent with the various analytical results that are available. Actually, we find that, the numerical results obtained with a κ of 0.1 and an N_i corresponding to $k/(a\,H)$ of 10^2 matches the analytical results at the level of 5%, just as it had in the case of the scalar bi-spectrum [55]. The match improves to 1–2$\%$ if we work with a κ of, say, 0.02, and simultaneously integrate from an N_i corresponding to $k/(a\,H)$ of 10^3. We should emphasize here that we have worked with these set of values in arriving at all the latter figures (*i.e.* Fig. 3.3 and thereafter).

3.3.3 Comparison with the analytical results

In this section, as it was done in the context of the scalar bi-spectrum (see Ref. [55]), we shall compare the numerical results for the three-point functions (or, equivalently, for the non-Gaussianity parameters) with the spectral dependence that can be arrived at in power law inflation in the equilateral and the squeezed limits and the results for an arbitrary triangular configuration that can be obtained in the slow roll scenario (as applied to

[2]There seems to be some confusion in the literature regarding whether it is the Bode's or the Boole's rule! Following Ref. [95], we have called it the Bode's rule.

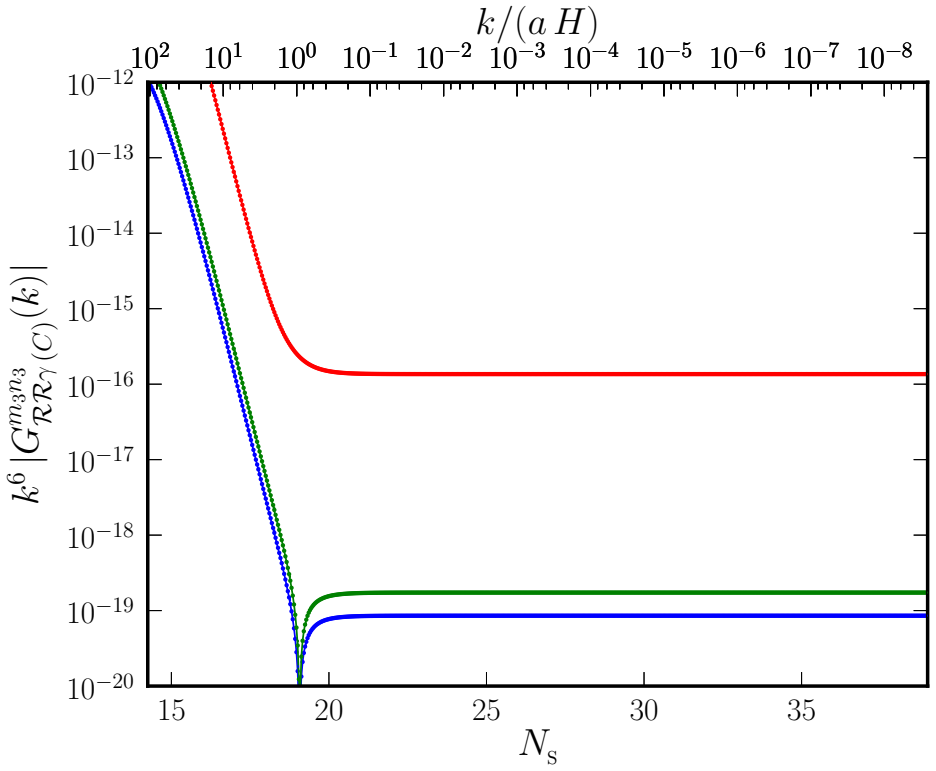

Figure 3.1: The absolute value of the different contributions to the scalar-scalar-tensor cross-correlation evaluated in the equilateral limit, *i.e.* $k^6\,G^{m_3n_3}_{\mathcal{R}\mathcal{R}_\gamma}(k)$, have been plotted for a specific mode (which leaves the Hubble radius at about 18 e-folds), evolving in the background driven by the conventional quadratic potential, as a function of the upper limit of integration $N_{\rm s}$. In this figure and in the three figures that follow, we shall adopt the following choice of colors to represent the different contributions to the three-point functions. The first, the second and the third terms of the three-point functions will always be represented by red, green and blue curves, in that order, respectively. We should also mention here that we shall ignore factors such as $\Pi^{\mathbf{k}}_{mn,ij}$ in plotting these quantities. It is clear from the above figure that the different contributions settle down to their final value soon after the mode has emerged from the Hubble radius [say, by $k/(a\,H) \simeq 10^{-2}$]. We find that all the contributions to the other three-point functions too exhibit the same behavior.

the case of the quadratic potential). With the motivation to consider a nontrivial situation involving departures from slow roll, we shall also evaluate the three-point functions for the case of the Starobinsky model analytically and compare them with the corresponding numerical results. We shall relegate some of the details of the calculation in the case of the Starobinsky model to Appendix A.

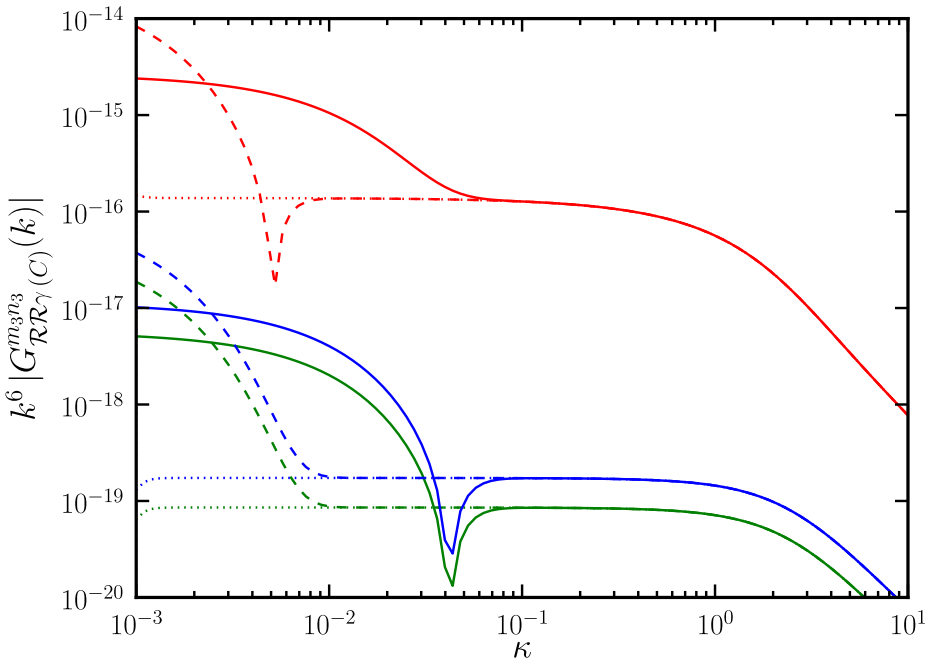

Figure 3.2: The absolute value of the different contributions to the scalar-scalar-tensor cross-correlation in the equilateral limit, *viz.* $k^6\,G^{m_3 n_3}_{\mathcal{R}\mathcal{R}\gamma}(k)$, discussed in the previous figure, have been plotted for the same model and mode for a few different combinations of $N_{\rm i}$ and κ, but with a fixed $N_{\rm s}$ [corresponding to $k/(a\,H)$ of 10^{-5}]. The solid, the dashed and the dotted lines correspond to integrals evaluated from different $N_{\rm i}$, corresponding to $k/(a\,H)$ of 10^2, 10^3 and 10^4, respectively. We should point out that too large a value of κ (say, much beyond $\kappa \simeq 0.1$) brings down the values of the integrals, as it then essentially kills the contributions that occur as the modes leave the Hubble radius. It is also evident that the choice of $\kappa = 0.1$ and an $N_{\rm i}$ corresponding to $k/(a\,H) = 10^2$ leads to consistent results (as all the curves converge over this domain). Again, we find that the same conclusions apply to all the contributions to the other three-point functions as well.

The case of power law inflation

As we have already discussed, power law inflation is described by the scale factor (2.6). Also, in such a scenario, the scalar and the tensor modes v_k and u_k can be obtained analytically [cf. Eq. (3.11)]. Note that these modes depend only on the combination $k\,\eta$. Due to this reason, interestingly, we find that, with a simple rescaling of variables, the spectral dependence (but, not the amplitudes) of all the contributions to the scalar-tensor cross correlations as well as the tensor bi-spectrum can be arrived at without actually having to evaluate the integrals involved [55]. Since the solutions to the scalar as well as the tensor modes are of the same form, in the equilateral limit, *i.e.* when $k_1 = k_2 = k_3 = k$, one finds that all the contributions to the three-point functions have the same spectral dependence,

viz. $k^6\, G_{\mathsf{ABC}\,(C)}(k) \propto k^{4\,(\gamma+2)}$.

In fact, in power law inflation, we find that the spectral dependence of all the contributions can also be arrived at in the squeezed limit, which corresponds to setting two of the wavenumbers to be the same, while allowing the third to vanish. Note that, as far as the cross-correlations go, in the squeezed limit, there exist two possibilities. We can either consider the limit wherein the wavenumber of a scalar mode goes to zero or we can consider the situation wherein the wavenumber of a tensor mode vanishes. We obtain the following behavior for $G^{m_3 n_3}_{\mathcal{R}\mathcal{R}\gamma\,(C)}(\boldsymbol{k}_1, \boldsymbol{k}_2, \boldsymbol{k}_3)$ when $k_1 = k_2 = k$ and $k_3 \to 0$ (*i.e.* when the wavenumber of the tensor mode vanishes):

$$k^3\, k_3^3\, G^{m_3 n_3}_{\mathcal{R}\mathcal{R}\gamma\,(1)}(k, k_3) \;\propto\; k^{2\,(\gamma+2)}\, k_3^{2\,(\gamma+2)}, \tag{3.17a}$$

$$k^3\, k_3^3\, G^{m_3 n_3}_{\mathcal{R}\mathcal{R}\gamma\,(2)}(k, k_3) \;\propto\; k^{2\,(\gamma+1)}\, k_3^{2\,(\gamma+3)}, \tag{3.17b}$$

$$k^3\, k_3^3\, G^{m_3 n_3}_{\mathcal{R}\mathcal{R}\gamma\,(3)}(k, k_3) \;\propto\; k^{2\,(\gamma+1)}\, k_3^{2\,(\gamma+3)}, \tag{3.17c}$$

whereas we find that all the terms have the following spectral dependence as $k_1 \to 0$ (*i.e.* as the wavenumber of a scalar mode goes to zero) and $k_2 = k_3 = k$:

$$k_1^3\, k^3\, G^{m_3 n_3}_{\mathcal{R}\mathcal{R}\gamma\,(C)}(k_1, k) \propto k_1^{2\,\gamma+5}\, k^{2\,\gamma+3}. \tag{3.18}$$

Similarly, in the case of $G^{m_2 n_2 m_3 n_3}_{\mathcal{R}\gamma\gamma\,(C)}(\boldsymbol{k}_1, \boldsymbol{k}_2, \boldsymbol{k}_3)$, when $k_2 = k_3 = k$ and $k_1 \to 0$ (*i.e.* when the wavenumber of the scalar mode vanishes), we obtain that

$$k_1^3\, k^3\, G^{m_2 n_2 m_3 n_3}_{\mathcal{R}\gamma\gamma\,(1)}(k_1, k) \;\propto\; k_1^{2\,(\gamma+2)}\, k^{2\,(\gamma+2)}, \tag{3.19a}$$

$$k_1^3\, k^3\, G^{m_2 n_3 m_3 n_3}_{\mathcal{R}\gamma\gamma\,(2)}(k_1, k) \;\propto\; k_1^{2\,(\gamma+2)}\, k^{2\,(\gamma+2)}, \tag{3.19b}$$

$$k_1^3\, k^3\, G^{m_2 n_3 m_3 n_3}_{\mathcal{R}\gamma\gamma\,(3)}(k_1, k) \;\propto\; k_1^{2\,(\gamma+3)}\, k^{2\,(\gamma+1)}, \tag{3.19c}$$

whereas we find that all the terms have the following spectral dependence when $k_1 = k_2 = k$ and $k_3 \to 0$ (*i.e.* as the wavenumber of the tensor mode goes to zero):

$$k^3\, k_3^3\, G^{m_2 n_2 m_3 n_3}_{\mathcal{R}\gamma\gamma\,(C)}(k, k_3) \propto k^{2\,(\gamma+1)}\, k_3^{2\,(\gamma+3)}. \tag{3.20}$$

Lastly, we can show that in power law inflation, in the squeezed limit, say, when $k_2 = k_3 = k$ and $k_1 \to 0$, the two contributions to the tensor bi-spectrum behave as

$$k_1^3\, k^3\, G^{m_1 n_1 m_2 n_2 m_3 n_3}_{\gamma\gamma\gamma\,(C)}(k_1, k) \propto k_1^{2\,(\gamma+2)}\, k^{2\,(\gamma+2)}. \tag{3.21}$$

In Figs. 3.3 and 3.4, we have compared the spectral dependences obtained above in the equilateral and the squeezed limits for all the different contributions to the three-point functions of interest with the corresponding numerical results. We find the agreement between the analytical and the numerical results to be quite good (about 1-2%, as we have alluded to before).

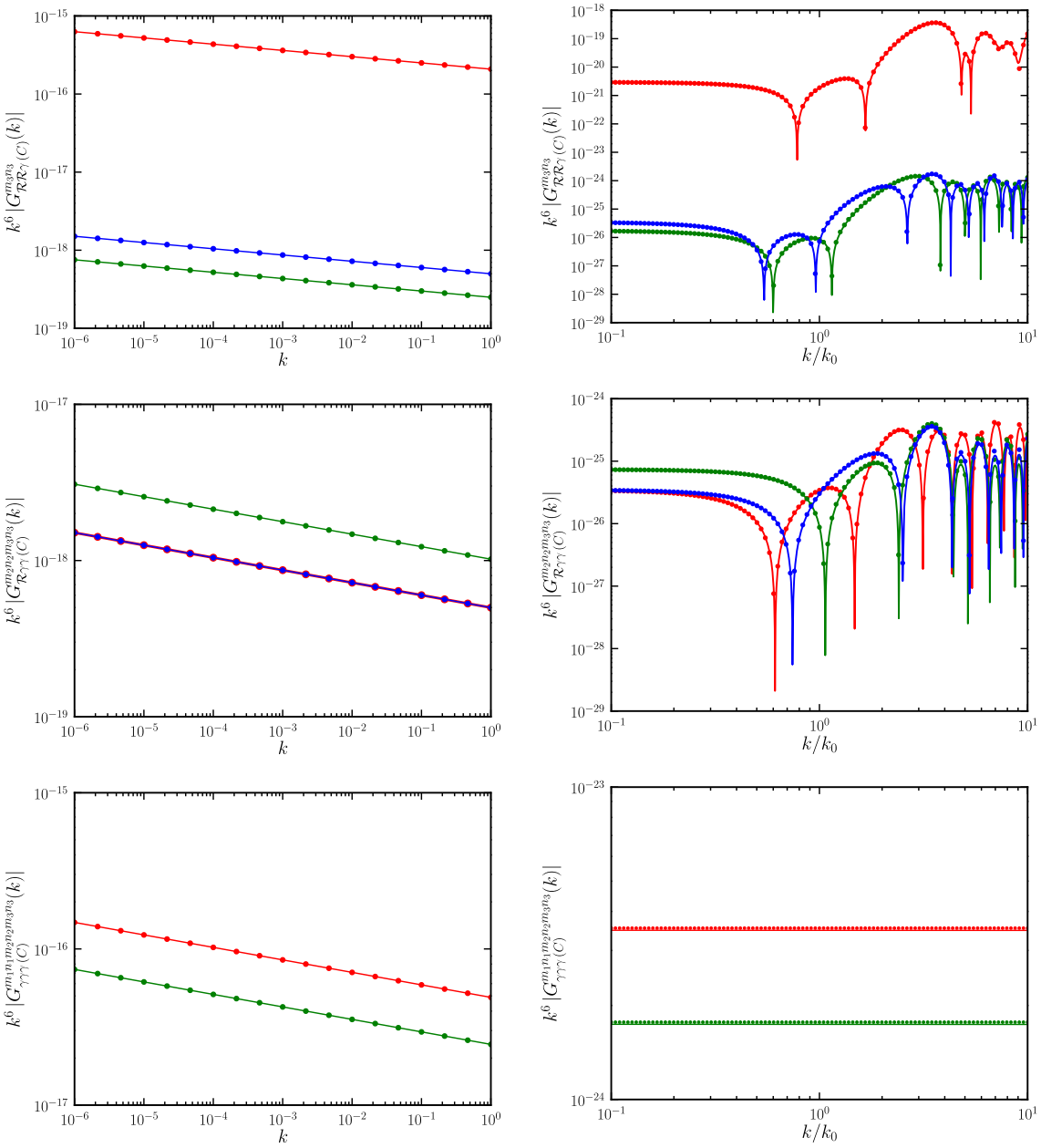

Figure 3.3: A comparison of the numerical results (plotted as solid lines) with the analytical results (marked with dots) for the various contributions to the three-points functions in the equilateral limit, *viz.* k^6 times the absolute values of $G^{m_3n_3}_{\mathcal{R}\mathcal{R}\gamma\,(C)}(k)$ (on top), $G^{m_2n_2m_3n_3}_{\mathcal{R}\gamma\gamma\,(C)}(k)$ (in the middle) and $G^{m_1n_1m_2n_2m_3n_3}_{\gamma\gamma\gamma\,(C)}(k)$ (at the bottom), for power law inflation (on the left) and the Starobinsky model (on the right). In the case of power law inflation, in plotting the analytical, spectral dependences, we have chosen the amplitude by hand so that they match the numerical result at a specific wavenumber. The hierarchy of the different contributions are clear from the above figure. Note that, in the cases of the scalar-tensor-tensor cross-correlation and the tensor bi-spectrum, as is expected from their dependence on the first slow roll parameter ϵ_1, the different contributions to these quantities prove to be of the same order. Whereas, in the case of the scalar-scalar-tensor cross-correlation, the second and the third terms are of the same order, but are sub-dominant to the first term.

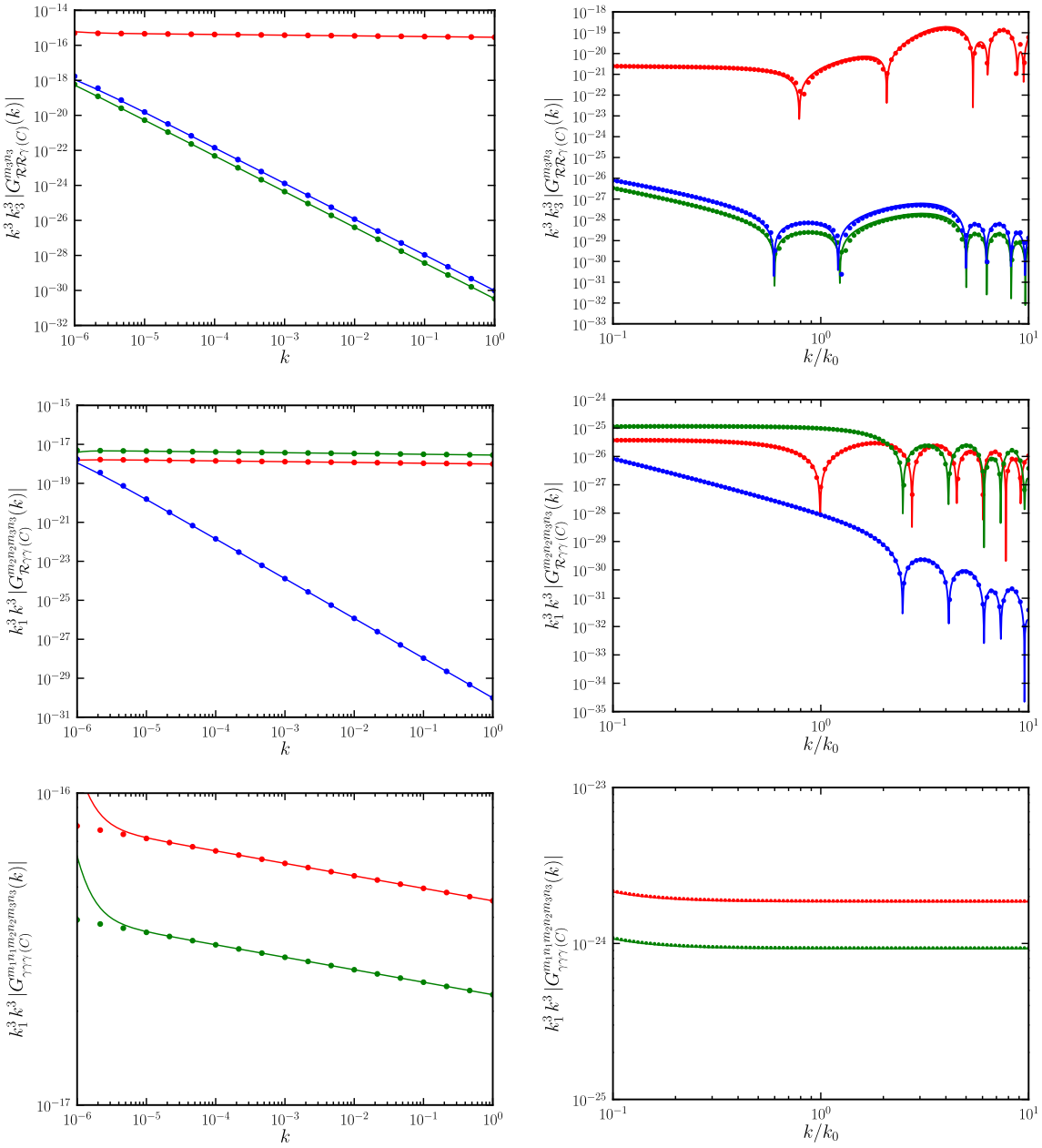

Figure 3.4: A comparison of the analytic and the numerical results in the squeezed limit for the same set of quantities and models as in the previous figure. Note that, in arriving at the theoretical spectral dependences in the squeezed limit, we have taken the wavenumber of the tensor mode to zero in the case of $G^{m_3 n_3}_{\mathcal{R}\mathcal{R}\gamma}(\boldsymbol{k}_1, \boldsymbol{k}_2, \boldsymbol{k}_3)$ and we have assumed that the wavenumber of the scalar mode vanishes in the case of $G^{m_2 n_2 m_3 n_3}_{\mathcal{R}\gamma\gamma}(\boldsymbol{k}_1, \boldsymbol{k}_2, \boldsymbol{k}_3)$. Clearly, the numerical results match the analytical results quite well in the equilateral limit. However, in the squeezed limit, while the match is good at large k, there is a noticeable difference between the theoretical and the numerical results at small k in some cases. This difference essentially arises because, to achieve the squeezed limit numerically, one has to work with a non-zero but suitably small value for the wavenumber that permits the evolution of the modes and the evaluation of the integrals. If needed, the match can be improved by working with a smaller wavenumber, but the effort can become taxing.

Comparison in the case of the Starobinsky model

As we have already discussed in the last chapter, the Starobinsky model is characterized by a linear potential with a sharp change in slope at a specific point [74]. In order to calculate the scalar-tensor three-point functions and the tensor bi-spectrum, in addition to the various quantities described in Subsec. 2.3.2, we shall also require the behavior of the tensor modes. As we had discussed, it is the term V_0 which dominates the potential over the domain of our interest. Hence, the behavior of the scale factor can be assumed to be that of de Sitter. Since the evolution of the tensor mode depends only on the scale factor [cf. Eq. (1.23b)], we can work with the de Sitter solution (1.53b) for the tensor modes throughout the evolution of the field, both before as well as after the transition. Due to this reason, the resulting tensor bi-spectrum will be given by the same expression that we had arrived at earlier in the slow roll approximation [cf. Eq. (1.59)].

Though the tensor modes behave in the same fashion before as well as after the transition, as we had discussed, the first slow roll parameter and the scalar modes behave differently on either side of the transition. Hence, while evaluating the scalar-tensor cross-correlations, we need to divide the integrals involved into two and carry out the integrals before and after the transition separately, just as it was done in the context of the scalar bi-spectrum [37, 75]. We find that the cross-correlations can be evaluated completely analytically for an arbitrary triangular configuration of the wavenumbers (which, in fact, proves to be difficult to carry out for the scalar bi-spectrum). Since the calculations and the expressions involved turn out to be rather long and cumbersome, we have relegated the calculations to Appendix A. In Figs. 3.3 and 3.4, we have compared the analytic results that we have obtained with the corresponding numerical results for the cross-correlations and the tensor bi-spectrum in the equilateral and the squeezed limits. Note that we have worked with the following values of the potential parameters in arriving at these results: $\phi_0/M_{_{\rm Pl}} = 0.707$, $V_0/M_{_{\rm Pl}}^4 = 2.37 \times 10^{-12}$, $A_+/M_{_{\rm Pl}}^3 = 3.35 \times 10^{-14}$ and $A_-/M_{_{\rm Pl}}^3 = 7.26 \times 10^{-15}$. These values have been chosen so that the assumptions of the Starobinsky model, under which the analytical results have been arrived at, are valid (in this context, see, for instance, Ref. [37]). We should also mention here that, in order to solve the problem numerically, the discontinuity in the potential of the Starobinsky model has been suitably smoothened [55, 76]. The figures suggest that the match between the analytic and the numerical results is very good.

The case of the quadratic potential

As is well known, the conventional quadratic potential leads to slow roll and hence, in this case, one can utilize the three-point functions evaluated in the slow roll limit (see Subsec. 1.5.4) to compare with the numerical results. For the sake of completeness, we shall write down the entire expressions for the non-Gaussianity parameters evaluated in the slow roll approximation. We find that, if we ignore factors involving $\Pi^{\boldsymbol{k}}_{mn,ij}$, they are given by

$$
\begin{aligned}
C^{\mathcal{R}}_{\rm NL} &= \left(k_{2|*}^{n_{\rm S}-1}\, k_{3|*}^{n_{\rm T}} + k_{2|1}^{3}\, k_{1|*}^{n_{\rm S}-1}\, k_{3|*}^{n_{\rm T}}\right)^{-1} \\
&\quad \times \left[k_{2|1}\, k_{{\rm T}|1}\left(1 - \frac{k_{2|1} + k_{3|1} + k_{2|1}\, k_{3|1}}{k_{{\rm T}|1}^{2}} - \frac{k_{2|1}\, k_{3|1}}{k_{{\rm T}|1}^{3}}\right) - \epsilon_1\, \frac{k_{2|1}\, k_{3|1}^{2}}{k_{{\rm T}|1}}\right] \\
&= \left(k_{1|3}^{3}\, k_{2|*}^{n_{\rm S}-1}\, k_{3|*}^{n_{\rm T}} + k_{2|3}^{3}\, k_{1|*}^{n_{\rm S}-1}\, k_{3|*}^{n_{\rm T}}\right)^{-1} \\
&\quad \times \left[k_{1|3}\, k_{2|3}\, k_{{\rm T}|3}\left(1 - \frac{k_{1|3} + k_{2|3} + k_{1|3}\, k_{2|3}}{k_{{\rm T}|3}^{2}} - \frac{k_{1|3}\, k_{2|3}}{k_{{\rm T}|3}^{3}}\right) - \epsilon_1\, \frac{k_{1|3}\, k_{2|3}}{k_{{\rm T}|3}}\right], \qquad \text{(3.22a)} \\
C^{\gamma}_{\rm NL} &= \frac{\epsilon_1}{4}\left(k_{3|1}^{3}\, k_{1|*}^{n_{\rm S}-1}\, k_{2|*}^{n_{\rm T}} + k_{2|1}^{3}\, k_{1|*}^{n_{\rm S}-1}\, k_{3|*}^{n_{\rm T}}\right)^{-1}\left(1 - k_{2|1}^{2} - k_{3|1}^{2} - \frac{8\, k_{2|1}^{2}\, k_{3|1}^{2}}{k_{{\rm T}|1}}\right) \\
&= \frac{\epsilon_1}{4}\left(k_{1|*}^{n_{\rm S}-1}\, k_{2|*}^{n_{\rm T}} + k_{2|3}^{3}\, k_{1|*}^{n_{\rm S}-1}\, k_{3|*}^{n_{\rm T}}\right)^{-1}\left(k_{1|3}^{3} - k_{1|3}\,\left(1 + k_{2|3}^{2}\right) - \frac{8\, k_{2|3}^{2}}{k_{{\rm T}|3}}\right), \qquad \text{(3.22b)} \\
h_{\rm NL} &= \left(k_{2|*}^{n_{\rm T}}\, k_{3|*}^{n_{\rm T}} + k_{2|1}^{3}\, k_{1|*}^{n_{\rm T}}\, k_{3|*}^{n_{\rm T}} + k_{3|1}^{3}\, k_{1|*}^{n_{\rm T}}\, k_{2|*}^{n_{\rm T}}\right)^{-1}\left(1 + k_{2|1} + k_{3|1}\right)\left(1 + k_{2|1}^{2} + k_{3|1}^{2}\right) \\
&\quad \times \left(1 - \frac{k_{2|1} + k_{3|1} + k_{2|1}\, k_{3|1}}{k_{{\rm T}|1^{2}}} - \frac{k_{2|1}\, k_{3|1}}{k_{{\rm T}|1}^{3}}\right), \qquad \text{(3.22c)}
\end{aligned}
$$

where $k_{i|j} = k_i/k_j$, $k_{i|*} = k_i/k_*$, $k_{{\rm T}|1} = 1+k_{2|1}+k_{3|1}$ and $k_{{\rm T}|3} = k_{1|3}+k_{2|3}+1$, and the quantity k_* denotes the pivot scale. Recall that, in the slow roll approximation, $n_{\rm S} = 1 - 2\,\epsilon_1 - \epsilon_2$, while $n_{\rm T} = -2\,\epsilon_1$. In Fig. 3.5, we have plotted the above analytical results for the non-Gaussianity parameters and the corresponding numerical results for an arbitrary triangular configuration of the wavenumbers for the case of the quadratic potential. There is clearly a striking similarity between the structure of the numerical results and the corresponding analytical estimates. We find that the numerical and analytical results match to better than 1% over a large region of the wavenumbers involved.

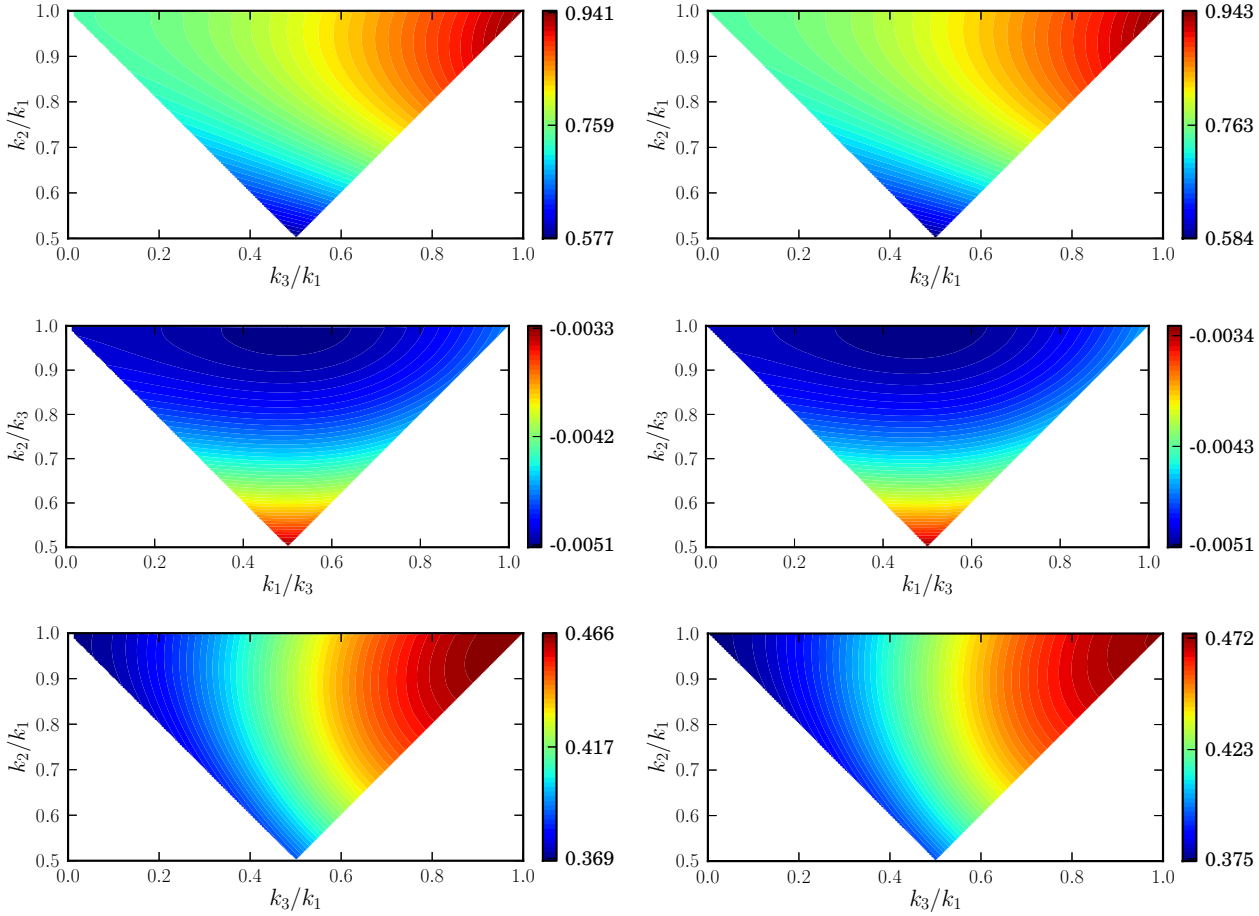

Figure 3.5: Density plots of the non-Gaussianity parameters $C^{\mathcal{R}}_{\rm NL}$ (on top), $C^{\gamma}_{\rm NL}$ (in the middle) and $h_{\rm NL}$ (at the bottom) for an arbitrary triangular configuration of the wavenumbers for the case of the conventional, quadratic potential. In arriving at the above figures, when k_1 and k_3 appear in the denominators of the two axes, we have chosen them to be the pivot scale k_*. Evidently, the strong similarity between the numerical results (on the left) and the corresponding quantities arrived at using the slow roll approximation (on the right) indicates the robustness of the numerical procedure we have adopted to compute the three-point functions. We find that the numerical results match the analytical estimates to better than 1% over a large domain of the wavenumbers of interest.

3.4 The three-point functions involving tensors in models leading to features

As we had discussed in Sec. 2.4, there has been considerable interest in studying the possibility of features in the scalar power spectrum over the last decade. Specifically, a large amount of attention has been focused on models leading to three types of features, *viz.* a sharp cut-off on large scales, a burst of oscillations over an intermediate range of scales and small but repeated oscillations over a wide range of scales (in this context, see Refs. [77, 78, 79, 80, 81, 82, 83, 84, 85, 86, 87, 88, 89]). Not surprisingly, it is exactly such classes of models have been considered by the Planck team [20, 21].

In this section, we shall utilize our code to study the behavior of the three-point functions of interest in models leading to deviations from slow roll. We shall consider the three different models which lead to features in the scalar power spectrum of the three types, *viz.* punctuated inflation, the quadratic potential with a step and the axion monodromy model, that we had discussed in the last chapter (see Sec. 2.4). We should mention that we have worked with the same values for the parameters of the models as we had done earlier, values which had led to an improved fit to the WMAP seven [4] or nine-year data [5]. It is important that we stress here that models such as the quadratic potential with the step and the axion monodromy model have very recently been compared with the Planck data (see Refs. [83, 89, 90]). These investigations suggest that the resulting features lead to an improved fit to the Planck data too. Moreover, models similar to punctuated inflation, which lead to suppression of power on large scales, continue to attract attention as well (in this context, see Refs. [80]). In Figs. 3.6, 3.7 and 3.8, we have plotted the density plots for the three non-Gaussianity parameters, *viz.* $C^{\mathcal{R}}_{\rm NL}$, $C^{\gamma}_{\rm NL}$ and $h_{\rm NL}$, for the cases of punctuated inflation, the quadratic potential with a step and the axion monodromy model, respectively.

Let us now highlight certain aspects of the results that we have obtained. We had earlier pointed out (see the caption of Fig. 3.3) the hierarchy of the various contributions to the three-point functions. We find that the hierarchy is maintained even when deviations from slow roll occur. This is not surprising because the tensor bi-spectrum is independent of the slow roll parameters, whereas the cross-correlations, at the most, depend on the first slow roll parameter ϵ_1. Since the first slow roll parameter cannot remain large for an extended period without completely terminating inflation, the hierarchy of the different contributions is preserved even in situations involving departures from slow roll.

It is clear from Figs. 3.6, 3.7 and 3.8 that the tensor bi-spectrum in the cases of the

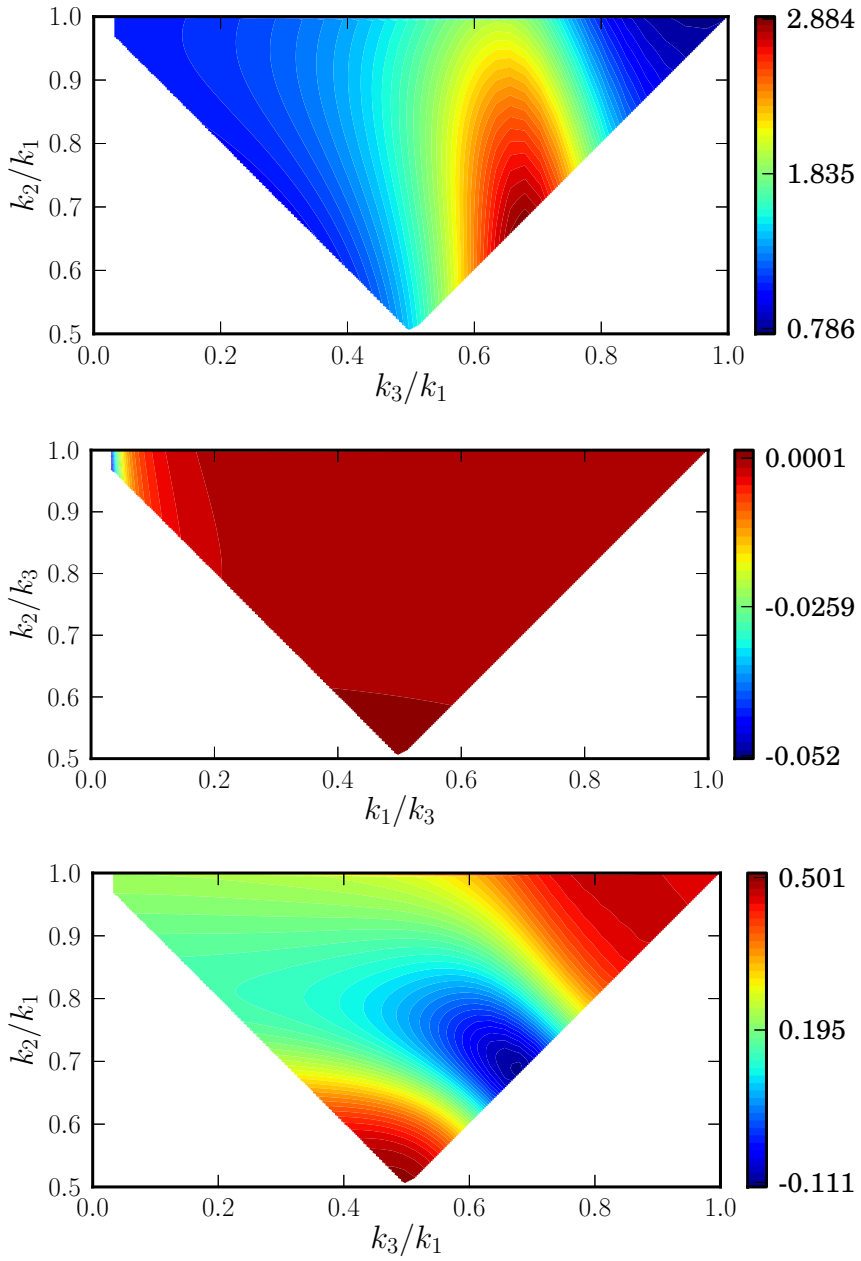

Figure 3.6: Density plots of the non-Gaussianity parameters $C^{\mathcal{R}}_{\rm NL}$ (on top), $C^{\gamma}_{\rm NL}$ (in the middle) and $h_{\rm NL}$ (at the bottom), evaluated numerically, have been plotted as function of k_3/k_1 and k_2/k_1 or k_1/k_3 and k_2/k_3, with a fixed value of k_1 or k_3 (when they appear in the denominators), for the case of the punctuated inflationary scenario. As discussed before, it should be evident that, in models leading to features, the shape of the three-point functions as plotted against k_3/k_1 and k_2/k_1 in the cases of $C^{\mathcal{R}}_{\rm NL}$ and $h_{\rm NL}$ or, against k_1/k_3 and k_2/k_3 in the case of $C^{\gamma}_{\rm NL}$, will depend on the choices of denominators k_1 and k_3. In order to capture the non-trivial shapes that this model leads to, we have fixed k_1 and k_3 (when appearing in the denominators) to be $10^{-3}\,\mathrm{Mpc}^{-1}$.

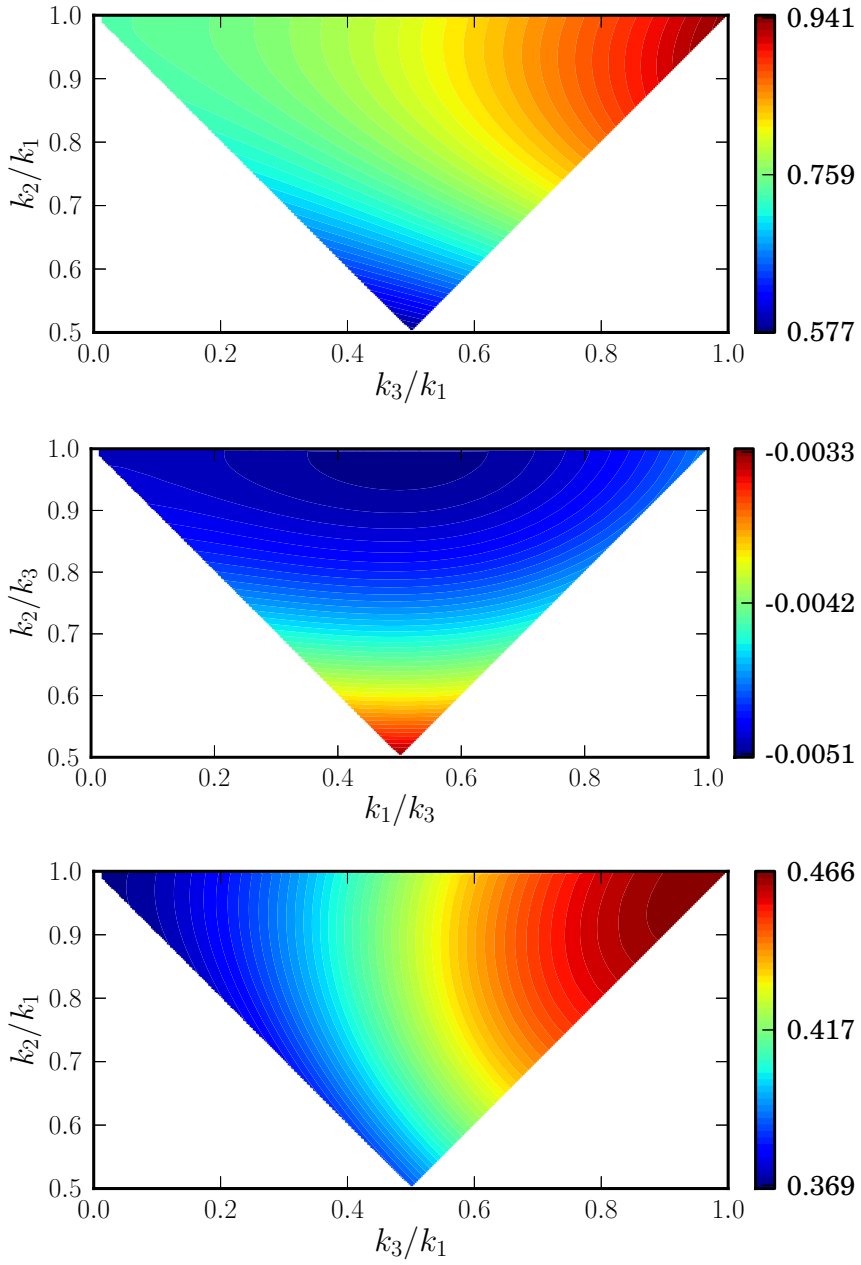

Figure 3.7: Density plots of the non-Gaussianity parameters $C^{\mathcal{R}}_{\rm NL}$ (on top), $C^{\gamma}_{\rm NL}$ (in the middle) and $h_{\rm NL}$ (at the bottom), plotted in the same fashion as in the previous figure, for the quadratic potential with a step. In order to capture the non-trivial shapes that this model leads to, we have fixed k_1 and k_3 (when they appear in the denominators) to be $2 \times 10^{-3}\,\mathrm{Mpc}^{-1}$.

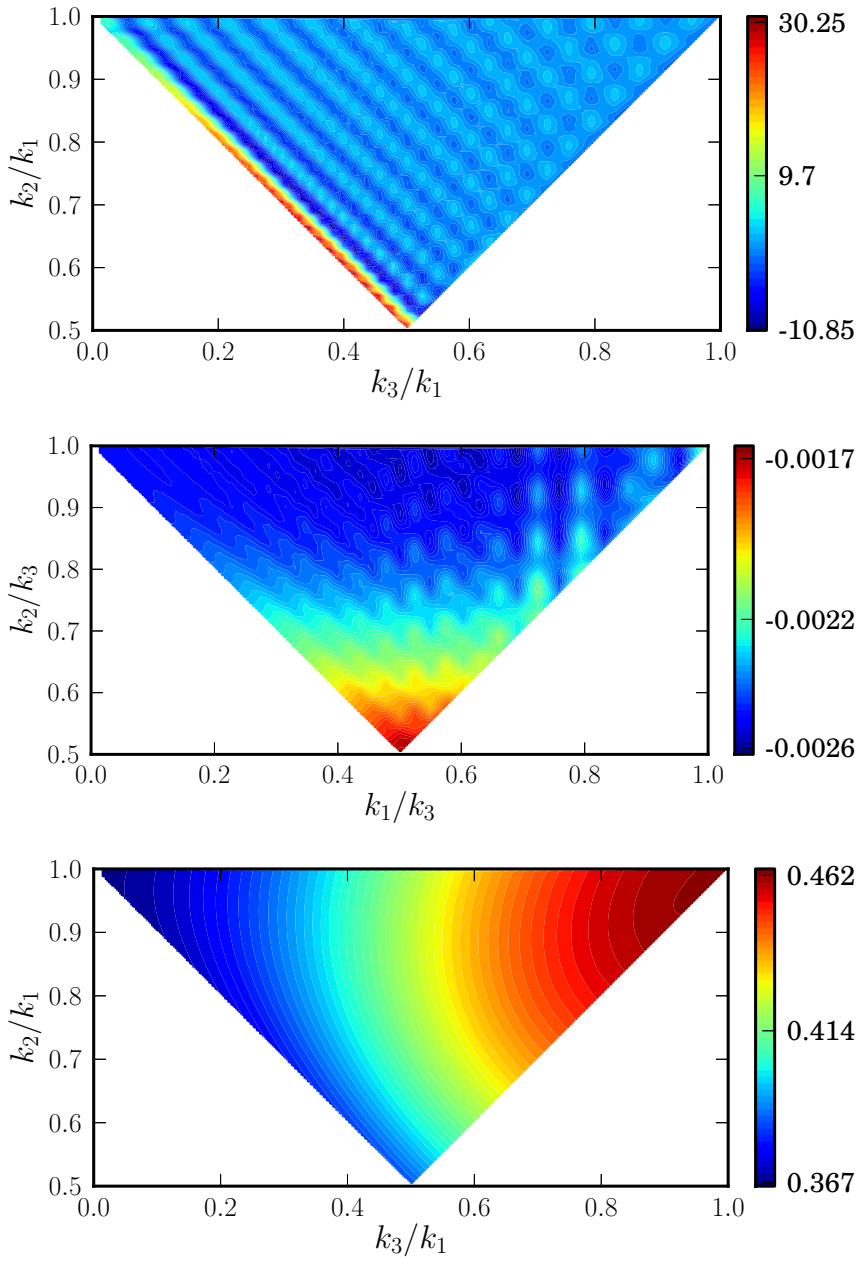

Figure 3.8: Density plots of the non-Gaussianity parameters $C^{\mathcal{R}}_{\rm NL}$ (on top), $C^{\gamma}_{\rm NL}$ (in the middle) and $h_{\rm NL}$ (at the bottom), plotted as in the last two figures, for the case of the axion monodromy model. In arriving at this figure, we have fixed k_1 and k_3 (when they appear in the denominators) to be $5 \times 10^{-2}\,\mathrm{Mpc}^{-1}$.

quadratic potential with a step and the axion monodromy model resemble each other very closely. In fact, they have virtually the same amplitude and shape as in the slow roll case illustrated in Fig. 3.5. This should not be surprising. After all, since the deviations from slow roll are rather minimal in these models, the tensors are hardly affected. In contrast, punctuated inflation, because of the brief departure from accelerated expansion that occurs, leads to a rather large effect on the tensors, with the tensor amplitude being considerably suppressed on small scales [79]. This is reflected in the non-trivial shape of the associated $h_{_{\rm NL}}$ parameter. The ringing effects on the scalars that arise due to the resonance encountered in the monodromy model (see, for example, Refs. [86, 88]) is clearly reflected in the amplitudes and shapes of the corresponding $C^{\mathcal{R}}_{_{\rm NL}}$ and the $C^{\gamma}_{_{\rm NL}}$ parameters. It is this resonance that leads to a substantially larger value for the $C^{\mathcal{R}}_{_{\rm NL}}$ parameter, as it does for the scalar non-Gaussianity parameter $f_{_{\rm NL}}$ (in this context, see, for instance, Ref. [55]). Note that, apart from the ringing, the shape of the $C^{\gamma}_{_{\rm NL}}$ parameter is somewhat similar in the cases of the quadratic potential with the step and the monodromy model. In the case of punctuated inflation, the shapes of the $C^{\mathcal{R}}_{_{\rm NL}}$ and $C^{\gamma}_{_{\rm NL}}$ parameters are considerably influenced by the contrasting fall and rise of the amplitudes of the scalar and the tensor power spectra at large scales. This behavior results in a larger value for the $C^{\mathcal{R}}_{_{\rm NL}}$ parameter than the corresponding value encountered in, say, the case of the model with a step.

3.5 The contributions during preheating

In most models of inflation, immediately after inflation and before the inflaton starts decaying, there exists a brief domain when the scalar field oscillates at the bottom of the potential and continues to dominate the background evolution. This brief epoch is referred to as preheating (see Sec. 1.6). Since the scalar field is the dominant source of the background, the perturbations (both scalar and tensor) continue to be governed by the same actions and equations of motion as they were during inflation. It is interesting then to investigate the contributions to the three-point functions that we have considered due to this epoch. In fact, the contributions to the scalar bi-spectrum during preheating in single field inflationary models were evaluated recently [54]. Our aim in this section is to extend the analysis to the case of the other three-point functions.

In order to do so, as should be clear by now, we shall require the behavior of the background as well as the perturbations during the epoch of preheating. If one considers single field inflationary models with quadratic minima, say, $V(\phi) \simeq m^2\,\phi^2/2$, it can be

shown that, during the epoch of preheating, the first slow roll parameter behaves as [54, 57, 58]

$$\epsilon_1 \simeq 3\,\cos^2(m\,t + \Delta), \tag{3.23}$$

where t is the cosmic time (measured since the end of inflation), while Δ is an arbitrary phase, chosen suitably to match the transition from inflation to preheating. The average value of the above slow roll parameter is $3/2$, which corresponds to a matter dominated era. Note that all perturbations of cosmological interest are on super-Hubble scales during the domain of preheating. Naively, one may imagine that the super-Hubble solutions for the scalar and the tensor perturbations during inflation, as given by Eqs. (3.3), will continue to hold during the epoch of preheating too. The tensor modes are governed by the quantity a''/a, which behaves monotonously during inflation as well as preheating. Therefore, the k^2 term in Eq. (1.23b) can indeed be ignored when compared to a''/a even during preheating, so that the super-Hubble solutions to the tensor modes, *viz.* Eq. (3.3b), continue to be applicable [58]. However, the quantity z''/z, as it involves the scalar field, behaves differently during inflation and preheating. While it grows monotonically during the later stages of inflation, the quantity can even vanish during preheating (since the scalar field is oscillating at the minimum of the potential). Hence, it is not a priori clear that the inflationary super-Hubble solutions will remain valid once the accelerated expansion has terminated. A careful analysis however illustrates that, under certain conditions which are easily achieved in quadratic minima (for details, see, for instance, Refs. [54, 58]), the inflationary super-Hubble solutions for the scalar modes continue to be applicable during preheating.

Recall that the contributions to the tensor bi-spectrum (and hence to the corresponding non-Gaussianity parameter $h_{_{\rm NL}}$) on super-Hubble scales during inflation is strictly zero. This is true even during the epoch of preheating. For simplicity, let us ignore the oscillations at the bottom of the quadratic minima and use the average value of the first slow roll parameter, *viz.* that $\epsilon_1 \simeq 3/2$. In such a case, if we focus on the equilateral limit, we can show that the contribution to the non-Gaussianity parameters $C^{\mathcal{R}}_{_{\rm NL}}$ and $C^{\gamma}_{_{\rm NL}}$ arising due to the evolution from the end of inflation to the e-fold, say, $N_{\rm f}$, during preheating can be expressed as

$$C^{\mathcal{R}\,({\rm ef})}_{_{\rm NL}}(k) = \left(\frac{4\,\gamma+5}{5\,\gamma+7}\right)\; C^{\gamma\,({\rm ef})}_{_{\rm NL}}(k) = \frac{12}{115}\,\left(\frac{4\,\gamma+5}{\gamma+2}\right)\; f^{({\rm ef})}_{_{\rm NL}}(k), \tag{3.24}$$

where $f^{({\rm ef})}_{_{\rm NL}}$ is the contribution due to preheating to the non-Gaussianity parameter asso-

ciated with the scalar bi-spectrum and is given by [55]

$$f_{\rm NL}^{\rm (ef)}(k) = \frac{115\,(\gamma+2)}{288\,\pi\,(\gamma+1)}\,\Gamma^2\left(\gamma+\frac{1}{2}\right)\,2^{2\,\gamma+1}\,(2\,\gamma+1)^2\,\sin\left(2\,\pi\,\gamma\right) \times\,|\gamma+1|^{-2\,(\gamma+1)}\,\left[1-{\rm e}^{-3\,(N_{\rm f}-N_{\rm e})/2}\right] \times\left[\left(\frac{\pi^2\,g_{\rm eff}}{30}\right)^{-1/4}\,(1+z_{\rm eq})^{1/4}\,\frac{\rho_{\rm cri}^{1/4}}{T_{\rm rh}}\right]^{-(2\,\gamma+1)}\,\left(\frac{k}{a_{\rm now}\,H_{\rm now}}\right)^{-(2\,\gamma+1)}. \quad (3.25)$$

We should mention here that we have arrived at this expression assuming inflation to be of the power law form, with the scale factor being given by Eq. (2.6) and with $\epsilon_1 = (\gamma+2)/(\gamma+1)$, as we have pointed out earlier. In the above expression, the quantity $g_{\rm eff}$ denotes the effective number of relativistic degrees of freedom at reheating, $T_{\rm rh}$ the reheating temperature and $z_{\rm eq}$ the redshift at the epoch of equality. Also, $\rho_{\rm cri}$, $a_{\rm now}$ and $H_{\rm now}$ represent the critical energy density, the scale factor and the Hubble parameter *today*, respectively[3]. It should be clear from the above expression that the contribution due to preheating is mainly determined by the quantity $\rho_{\rm cri}^{1/4}/T_{\rm rh}$. For an inflationary model wherein $\gamma \simeq -2$ and $T_{\rm rh} \simeq 10^{10}\,{\rm GeV}$, one obtains that $f_{\rm NL}^{\rm (ef)} \sim C_{\rm NL}^{\mathcal{R}\,{\rm (ef)}} \sim C_{\rm NL}^{\gamma\,{\rm (ef)}} \sim 10^{-60}$ for the modes of cosmological interest (*i.e.* for wavenumbers such that $k \simeq a_{\rm now}\,H_{\rm now}$). Needless to add, these values are simply unobservable (also see Ref. [96]; in this context, however, see Ref. [97]). In other words, as in the case of the scalar parameter $f_{\rm NL}$, the contribution to the other non-Gaussianity parameters due to the epoch of preheating is completely insignificant.

3.6 Summary

In this work, based on the Maldacena formalism and extending the recent effort towards calculating the scalar bi-spectrum, we have developed a numerical procedure for calculating the other three-point functions of interest. Motivated by the parameters often introduced to characterize the scalar and the tensor bi-spectra, we have introduced dimensionless non-Gaussianity parameters to describe the scalar-tensor cross-correlations. We have compared the performance of the code with the analytical results that are available in different situations and have utilized the code to calculate the three-point functions and the corresponding non-Gaussianity parameters in models that lead to features in the

[3]Since we have already made use of a_0 and H_0 to denote the scale factor at the transition and the Hubble parameter around the transition in the Starobinsky model, to avoid degeneracy, we have used the less conventional $a_{\rm now}$ and $H_{\rm now}$ to denote the scale factor and the Hubble parameter today!

scalar power spectrum. We have also shown that, as in the case of the scalar bi-spectrum, the contribution to the other three-point functions during the epoch of preheating proves to be completely negligible. In fact, we have made available a sample of the numerical code that we have worked with to arrive at the results discussed in this chapter at the following URL: *https://www.physics.iitm.ac.in/~sriram/tpf-code/registration.html*. The sample code corresponds to the specific case of the quadratic potential with a step that we have considered. The code can be easily extended to other inflationary models.

We believe that the non-Gaussianity parameters $C^{\mathcal{R}}_{\rm NL}$ and $C^{\gamma}_{\rm NL}$ which we have introduced here provide additional quantities to characterize an inflationary model. It will be interesting to arrive at constraints on these parameters as well from observational data and understand their implications. We are currently investigating these issues.

Chapter 4

The consistency relations for the scalar-tensor cross-correlations and the tensor bi-spectrum

4.1 Introduction

In the previous chapter, we had constructed a procedure (and developed a code) for numerically evaluating the three-point cross-correlations comprising of scalars and tensors as well as the tensor bi-spectrum for an arbitrary triangular configuration of the three wavenumbers involved [56]. We had also introduced dimensionless non-Gaussianity parameters, which we denoted as $C^{\mathcal{R}}_{\rm NL}$ and $C^{\gamma}_{\rm NL}$, to characterize the amplitude of the three-point scalar-tensor cross-correlations. As we had discussed in Chap. 2, in the squeezed limit, wherein one of the wavenumbers is much smaller than the other two, the inflationary scalar bi-spectrum generated by a single scalar field can be expressed completely in terms of the scalar power spectrum, a result that is referred to as a consistency relation (for the original results, see, for instance, Refs. [23, 61]; for more recent discussions in this context, see Ref. [62]; for similar results involving higher order correlation functions, see, for example, Ref. [63]). Equivalently, the scalar non-Gaussianity parameter $f_{\rm NL}$ can be written purely in terms of the scalar spectral index. However, most of the work on the consistency relations have focussed on the scalar bi-spectrum, and it seems natural to expect that similar consistency relations will be satisfied by the three-point functions that involve the tensor perturbations as well (in this context, see Refs. [23, 31, 32, 34]). Our aim in this chapter is to investigate the validity of consistency relations involving the three-point scalar-tensor cross-correlations and the tensor bi-spectrum. We shall first express the corresponding consistency relations as relations between the non-Gaussianity

parameters ($C^{\mathcal{R}}_{\rm NL}$ and $C^{\gamma}_{\rm NL}$ [56], and the quantity $h_{\rm NL}$ that is used to describe the purely tensor case [33]) and the scalar or the tensor spectral indices. We shall then analytically as well as numerically examine the validity of these consistency conditions in specific situations. As we shall illustrate, the consistency relations hold generically, and they prove to be valid even in scenarios involving substantial deviations from slow roll.

The structure of this chapter is as follows. In the following section, we shall quickly arrive at a few essential relations describing the three-point functions involving the tensor perturbations in the squeezed limit. In the subsequent section, we shall outline a proof of the consistency relations which describe the behavior of the three-point functions in the squeezed limit, wherein they can be expressed in terms of the scalar and the tensor power spectra. We shall also state the consistency conditions as relations between the non-Gaussianity parameters of interest, *viz.* $C^{\mathcal{R}}_{\rm NL}$, $C^{\gamma}_{\rm NL}$ and $h_{\rm NL}$, and the scalar and the tensor spectral indices $n_{\rm S}$ and $n_{\rm T}$. In Sec. 4.4, we shall explicitly establish the consistency relations for the three non-Gaussianity parameters in the two analytically tractable examples that we have considered before—the simple situation involving (a specific case of) power law inflation and the non-trivial scenario arising in the Starobinsky model. In Sec. 4.5, we shall numerically investigate the validity of the consistency relations involving $C^{\mathcal{R}}_{\rm NL}$, $C^{\gamma}_{\rm NL}$ and $h_{\rm NL}$ in models which permit deviations from slow roll. We shall consider the three models which we had focussed on in the last two chapters and show numerically that the consistency relations hold in each of these cases. Finally, in Sec. 4.6, we shall conclude with a brief discussion of the results.

4.2 The inflationary three-point functions involving tensors in the squeezed limit

In this section, we shall summarize the essential expressions describing the three-point functions involving the tensors in the squeezed limit. As we have discussed, the delta functions that appear in the definitions (1.34) of the three-point functions imply that the wavevectors $\boldsymbol{k}_1$, $\boldsymbol{k}_2$ and $\boldsymbol{k}_3$ form a triangle. The squeezed limit of the three-point functions corresponds to the situation wherein one of the three wavenumbers, *i.e.* k_1, k_2 or k_3, vanishes. In the two cases of the scalar-tensor cross-correlations, the squeezed limit can evidently be arrived at by choosing the wavenumber of either the scalar or the tensor mode to be zero. However, the contributions to the scalar-scalar-tensor three-point function either explicitly involve the wavenumber of the scalar mode or its time derivative, both of which go to zero in the large scale limit. As a result, the scalar-scalar-tensor three-

point function itself vanishes in the large scale limit of either of the scalar modes. For the same reason, we find that the scalar-tensor-tensor cross-correlation also vanishes in the limit wherein the wavenumber of any of the two tensor modes goes to zero. Therefore, in order to understand the behavior in the squeezed limit, we shall consider the large scale limits of the tensor and the scalar modes in the cases of the scalar-scalar-tensor and the scalar-tensor-tensor cross-correlations, respectively. In the squeezed limit, the expressions for the cross-correlations $G^{m_3n_3}_{\mathcal{R}\mathcal{R}\gamma}(\boldsymbol{k}_1, \boldsymbol{k}_2, \boldsymbol{k}_3)$ and $G^{m_2n_2m_3n_3}_{\mathcal{R}\gamma\gamma}(\boldsymbol{k}_1, \boldsymbol{k}_2, \boldsymbol{k}_3)$, and the tensor bi-spectrum $G^{m_1n_1m_2n_2m_3n_3}_{\gamma\gamma\gamma}(\boldsymbol{k}_1, \boldsymbol{k}_2, \boldsymbol{k}_3)$ can be written as [cf. Eqs. (1.46), (1.48) and (1.51)]

$$
\begin{aligned}
\lim_{k_3\to 0} G^{m_3n_3}_{\mathcal{R}\mathcal{R}\gamma}(\boldsymbol{k}_1, \boldsymbol{k}_2, \boldsymbol{k}_3) &= \lim_{k_3\to 0} \sum_{C=1}^{3} G^{m_3n_3}_{\mathcal{R}\mathcal{R}\gamma\,(C)}(\boldsymbol{k}, -\boldsymbol{k}, \boldsymbol{k}_3) \\
&= -\lim_{k_3\to 0} M_{_{\rm Pl}}^2\, \Pi^{\boldsymbol{k}_3}_{m_3n_3,ij}\, \hat{n}_i\, \hat{n}_j \sum_{C=1}^{3} \big[f_k(\eta_{_{\rm e}})\, f_k(\eta_{_{\rm e}})\, g_{k_3}(\eta_{_{\rm e}}) \\
&\quad \times \mathcal{G}^{C}_{\mathcal{R}\mathcal{R}\gamma}(\boldsymbol{k}, -\boldsymbol{k}, \boldsymbol{k}_3) + \text{ complex conjugate}\big], \qquad (4.1a) \\
\lim_{k_1\to 0} G^{m_2n_2m_3n_3}_{\mathcal{R}\gamma\gamma}(\boldsymbol{k}_1, \boldsymbol{k}_2, \boldsymbol{k}_3) &= \lim_{k_1\to 0} \sum_{C=1}^{3} G^{m_2n_2m_3n_3}_{\mathcal{R}\gamma\gamma\,(C)}(\boldsymbol{k}_1, \boldsymbol{k}, -\boldsymbol{k}) \\
&= \lim_{k_1\to 0} M_{_{\rm Pl}}^2\, \Pi^{\boldsymbol{k}}_{m_2n_2,ij}\, \Pi^{-\boldsymbol{k}}_{m_3n_3,ij} \sum_{C=1}^{3} \big[f_{k_1}(\eta_{_{\rm e}})\, g_k(\eta_{_{\rm e}})\, g_k(\eta_{_{\rm e}}) \\
&\quad \times \mathcal{G}^{C}_{\mathcal{R}\gamma\gamma}(\boldsymbol{k}_1, \boldsymbol{k}, -\boldsymbol{k}) + \text{complex conjugate}\big] \\
&= \lim_{k_1\to 0} 2\, M_{_{\rm Pl}}^2\, \Pi^{\boldsymbol{k}}_{m_2n_2,m_3n_3} \sum_{C=1}^{3} \big[f_{k_1}(\eta_{_{\rm e}})\, g_k(\eta_{_{\rm e}})\, g_k(\eta_{_{\rm e}}) \\
&\quad \times \mathcal{G}^{C}_{\mathcal{R}\gamma\gamma}(\boldsymbol{k}_1, \boldsymbol{k}, -\boldsymbol{k}) + \text{complex conjugate}\big], \qquad (4.1b) \\
\lim_{k_3\to 0} G^{m_1n_1m_2n_2m_3n_3}_{\gamma\gamma\gamma}(\boldsymbol{k}_1, \boldsymbol{k}_2, \boldsymbol{k}_3) &= \lim_{k_3\to 0} G^{m_1n_1m_2n_2m_3n_3}_{\gamma\gamma\gamma}(\boldsymbol{k}, -\boldsymbol{k}, \boldsymbol{k}_3) \\
&= -\lim_{k_3\to 0} M_{_{\rm Pl}}^2\, \Pi^{\boldsymbol{k}}_{m_1n_1,ij}\, \Pi^{-\boldsymbol{k}}_{m_2n_2,ij}\, \Pi^{\boldsymbol{k}_3}_{m_3n_3,ml}\, k_m\, k_l \\
&\quad \times \big[g_k(\eta_{_{\rm e}})\, g_k(\eta_{_{\rm e}})\, g_{k_3}(\eta_{_{\rm e}})\, \mathcal{G}_{\gamma\gamma\gamma}(\boldsymbol{k}, -\boldsymbol{k}, \boldsymbol{k}_3) \\
&\quad + \text{complex conjugate}\big] \\
&= -\lim_{k_3\to 0} 2\, M_{_{\rm Pl}}^2\, \Pi^{\boldsymbol{k}}_{m_1n_1,m_2n_2}\, \Pi^{\boldsymbol{k}_3}_{m_3n_3,ml}\, k_m\, k_l \\
&\quad \times \big[g_k(\eta_{_{\rm e}})\, g_k(\eta_{_{\rm e}})\, g_{k_3}(\eta_{_{\rm e}})\, \mathcal{G}_{\gamma\gamma\gamma}(\boldsymbol{k}, -\boldsymbol{k}, \boldsymbol{k}_3) \\
&\quad + \text{complex conjugate}\big], \qquad (4.1c)
\end{aligned}
$$

where, for simplicity, we have set $\boldsymbol{k}_1 = -\boldsymbol{k}_2 = \boldsymbol{k}$ in the first and the third expressions, and $\boldsymbol{k}_2 = -\boldsymbol{k}_3 = \boldsymbol{k}$ in the second. The overall minus sign in the above scalar-scalar-tensor correlation arises due to the fact that, in the squeezed limit, $\hat{n}_{1i} = -\hat{n}_{2i} = \hat{n}_i$.

The polarization factors in the tensor bi-spectrum simplify in the squeezed limit due to the transverse nature of the gravitational waves, *i.e.* $k_i\ \varepsilon^{s}_{ij}(\boldsymbol{k}) = 0$. Moreover, it is the normalization of the polarization tensor, *viz.* $\varepsilon^{r}_{ij}(\boldsymbol{k})\ \varepsilon^{s*}_{ij}(\boldsymbol{k}) = 2\ \delta^{rs}$, that leads to the overall factor of two in the cases of the scalar-tensor-tensor correlation and the tensor bi-spectrum. Note that the two three-point cross-correlations contain three independent terms. It is straightforward to argue that, in the squeezed limit of the tensor mode, it is only the first term that contributes in the case of the scalar-scalar-tensor correlation (as the other two contributions either depend explicitly on the wavenumber of the squeezed mode or its time derivative). Similarly, in the case of the scalar-tensor-tensor correlation, we find that the third term does not contribute in the squeezed limit of the scalar mode.

In the next section, we shall briefly outline a proof of the consistency relations obeyed by the different three-point functions and the corresponding non-Gaussianity parameters in the squeezed limit.

4.3 Consistency relations in the squeezed limit

A consistency relation basically links the three-point function to the two-point function in a particular limit of the wavenumbers involved[1]. As we saw in Chap. 2, the scalar bi-spectrum obeys a consistency relation in the squeezed limit [23, 61, 62]. In terms of the scalar non-Gaussianity parameter $f_{\rm NL}$, it can be expressed as $f_{\rm NL} = 5\ (n_{\rm S} - 1)/12$, where $n_{\rm S}$ is the scalar spectral index [cf. Eq. (1.27)]. The scalar consistency relation is expected to be valid for any single field inflationary model, irrespective of the detailed dynamics of the field [61]. As we had discussed earlier, this essentially occurs because of the fact that the amplitude of the long wavelength scalar modes freezes on super-Hubble scales. Due to this reason, their effects on the smaller wavelength modes can be treated as though they are evolving in a background with modified spatial coordinates. Since the tensor modes too behave in the same fashion as the scalar modes when they are sufficiently outside the Hubble radius (*i.e.* their amplitudes freeze as well), it seems natural to expect that there should exist similar consistency relations describing the three-point scalar-tensor cross-correlations and the tensor bi-spectrum [31, 32, 34]. In the remainder of this section, we shall arrive at the consistency relations governing the three-point functions involving the tensors in the squeezed limit.

[1]In fact, depending on the symmetries associated with the action governing the field(s) of interest, quantum field theory suggests such relations can exist between generic N-point and $(N-1)$-point correlation functions. Clearly, similar connections can be expected to arise for the various correlation functions generated during inflation as well (in this context, see, for instance, Refs. [63]).

As we have already pointed out, the amplitude of a long wavelength scalar or tensor mode would be a constant, since it would be well outside the Hubble radius (in this context, see, for instance, Refs. [66]). Due to the fact that the amplitude has frozen, it can be treated as a background as far as the smaller wavelength modes are concerned. Let us denote the constant amplitudes (*i.e.* as far as their time dependence is concerned) of the long wavelength scalar and tensor modes as, say, $\mathcal{R}^{\rm B}$ and $\gamma_{ij}^{\rm B}$, respectively. In the presence of such modes, the *background* metric will take the form

$$\mathrm{d}s^2 = -\mathrm{d}t^2 + a^2(t)\, \mathrm{e}^{2\,\mathcal{R}^{\rm B}}\, [\mathrm{e}^{\gamma^{\rm B}}]_{ij}\, \mathrm{d}\boldsymbol{x}^i\, \mathrm{d}\boldsymbol{x}^j, \tag{4.2}$$

i.e. the long wavelength modes lead to modified spatial coordinates. Such a modification is, in fact, completely equivalent to a spatial transformation of the form $\boldsymbol{x}' = \Lambda\, \boldsymbol{x}$, with the components of the matrix Λ being given by $\Lambda_{ij} = \mathrm{e}^{\mathcal{R}^{\rm B}}\, [\mathrm{e}^{\gamma^{\rm B}/2}]_{ij}$. Under such a spatial coordinate transformation, we can easily show that the Fourier modes of the small wavelength scalar and tensor perturbations transform as follows: $\mathcal{R}_{\boldsymbol{k}} \to \det\,(\Lambda^{-1})\, \mathcal{R}_{\Lambda^{-1}\,\boldsymbol{k}}$ and $\gamma_{ij}^{\boldsymbol{k}} \to \det\,(\Lambda^{-1})\, \gamma_{ij}^{\Lambda^{-1}\,\boldsymbol{k}}$, where, evidently, Λ^{-1} represents the inverse of the original matrix Λ. Upon using the property that the determinant of the exponential of a matrix is the exponential of its trace and the fact that γ_{ij} is traceless, we arrive at the result $\det\,(\Lambda^{-1}) = \mathrm{e}^{-3\,\mathcal{R}^{\rm B}}$. At the leading order in $\mathcal{R}^{\rm B}$ and $\gamma^{\rm B}$, we can also obtain that $|\Lambda^{-1}\,\boldsymbol{k}| = [1 - \mathcal{R}^{\rm B} - \gamma_{ij}^{\rm B}\, k_i\, k_j/(2\,k^2)]\; k$, where, as we have clarified earlier, k_i denotes the component of the wavevector $\boldsymbol{k}$ along the i-spatial direction. Moreover, since $\delta^{(3)}(\Lambda^{-1}\,\boldsymbol{k}_1 + \Lambda^{-1}\,\boldsymbol{k}_2) = \det\,(\Lambda)\; \delta^{(3)}(\boldsymbol{k}_1 + \boldsymbol{k}_2)$, on combining the above results, we find that the scalar and the tensor two-point functions in the presence of a long wavelength mode denoted by, say, the wavenumber k, can be written as

$$\begin{aligned}
\langle \hat{\mathcal{R}}_{\boldsymbol{k}_1}\, \hat{\mathcal{R}}_{\boldsymbol{k}_2} \rangle_k &= \frac{(2\,\pi)^2}{2\,k_1^3}\, \mathcal{P}_{\rm S}(k_1)\; \delta^{(3)}(\boldsymbol{k}_1 + \boldsymbol{k}_2) \\
&\quad \times \left[1 - (n_{\rm S} - 1)\, \mathcal{R}^{\rm B} - \left(\frac{n_{\rm S} - 4}{2}\right)\, \gamma_{ij}^{\rm B}\, \hat{n}_{1i}\, \hat{n}_{1j}\right], \qquad (4.3a) \\
\langle \hat{\gamma}_{m_1 n_1}^{\boldsymbol{k}_1}\, \hat{\gamma}_{m_2 n_2}^{\boldsymbol{k}_2} \rangle_k &= \frac{(2\,\pi)^2}{2\,k_1^3}\, \frac{\Pi_{m_1 n_1, m_2 n_2}^{\boldsymbol{k}_1}}{4}\, \mathcal{P}_{\rm T}(k_1)\; \delta^{(3)}(\boldsymbol{k}_1 + \boldsymbol{k}_2) \\
&\quad \times \left[1 - n_{\rm T}\, \mathcal{R}^{\rm B} - \left(\frac{n_{\rm T} - 3}{2}\right)\, \gamma_{ij}^{\rm B}\, \hat{n}_{1i}\, \hat{n}_{1j}\right], \qquad (4.3b)
\end{aligned}$$

where, as we have mentioned, $\hat{n}_{1i} = k_{1i}/k_1$.

The above expressions for the two-point functions can then be utilized to arrive at the three-point functions involving the tensors in the squeezed limit. We find that, in the

presence of a long wavelength mode, the three-point functions can be obtained to be

$$\begin{aligned}
\langle\, \hat{\mathcal{R}}_{\boldsymbol{k}_1}\, \hat{\mathcal{R}}_{\boldsymbol{k}_2}\, \hat{\gamma}^{\boldsymbol{k}_3}_{m_3n_3}\,\rangle_{k_3} &\equiv \langle\, \langle \hat{\mathcal{R}}_{\boldsymbol{k}_1}\, \hat{\mathcal{R}}_{\boldsymbol{k}_2}\,\rangle_{k_3}\, \hat{\gamma}^{\boldsymbol{k}_3}_{m_3n_3}\,\rangle \\
&= -\frac{(2\,\pi)^{5/2}}{4\,k_1^3\,k_3^3}\,\left(\frac{n_{_{\rm S}}-4}{8}\right)\,\mathcal{P}_{_{\rm S}}(k_1)\,\mathcal{P}_{_{\rm T}}(k_3) \\
&\quad\times \Pi^{\boldsymbol{k}_3}_{m_3n_3,ij}\,\hat{n}_{1i}\,\hat{n}_{1j}\,\delta^3(\boldsymbol{k}_1+\boldsymbol{k}_2), \qquad (4.4a)\\
\langle\, \hat{\mathcal{R}}_{\boldsymbol{k}_1}\, \hat{\gamma}^{\boldsymbol{k}_2}_{m_2n_2}\, \hat{\gamma}^{\boldsymbol{k}_3}_{m_3n_3}\,\rangle_{k_1} &\equiv \langle\, \hat{\mathcal{R}}_{\boldsymbol{k}_1}\, \langle\, \hat{\gamma}^{\mathbf{k_2}}_{m_2n_2}\, \hat{\gamma}^{\boldsymbol{k}_3}_{m_3n_3}\,\rangle_{k_1}\,\rangle \\
&= -\frac{(2\,\pi)^{5/2}}{4\,k_1^3\,k_2^3}\,\frac{n_{_{\rm T}}}{4}\,\mathcal{P}_{_{\rm S}}(k_1)\,\mathcal{P}_{_{\rm T}}(k_2)\,\Pi^{\mathbf{k_2}}_{m_2n_2,m_3n_3}\,\delta^3(\boldsymbol{k}_2+\boldsymbol{k}_3), \qquad (4.4b)\\
\langle\, \hat{\gamma}^{\boldsymbol{k}_1}_{m_1n_1}\, \hat{\gamma}^{\boldsymbol{k}_2}_{m_2n_2}\, \hat{\gamma}^{\boldsymbol{k}_3}_{m_3n_3}\,\rangle_{k_3} &\equiv \langle\, \langle\, \hat{\gamma}^{\boldsymbol{k}_1}_{m_1n_1}\, \hat{\gamma}^{\boldsymbol{k}_2}_{m_2n_2}\,\rangle_{k_3}\, \hat{\gamma}^{\boldsymbol{k}_3}_{m_3n_3}\,\rangle \\
&= -\frac{(2\,\pi)^{5/2}}{4\,k_1^3\,k_3^3}\,\left(\frac{n_{_{\rm T}}-3}{32}\right)\,\mathcal{P}_{_{\rm T}}(k_1)\,\mathcal{P}_{_{\rm T}}(k_3) \\
&\quad\times \Pi^{\boldsymbol{k}_1}_{m_1n_1,m_2n_2}\,\Pi^{\boldsymbol{k}_3}_{m_3n_3,ij}\,\hat{n}_{1i}\,\hat{n}_{1j}\,\delta^3(\boldsymbol{k}_1+\boldsymbol{k}_2), \qquad (4.4c)
\end{aligned}$$

where, in the cases of the scalar-scalar-tensor cross-correlation and the tensor bi-spectrum, we have considered $\boldsymbol{k}_3$ to be the squeezed mode, while we have considered $\boldsymbol{k}_1$ to be the squeezed mode in the case of the scalar-tensor-tensor cross-correlation. Upon making use of the above expressions for the three-point functions in the definitions (3.2) for the non-Gaussianity parameters, we can express the consistency relations in the squeezed limit as follows:

$$\begin{aligned}
\lim_{k_3\to 0}\, C^{\mathcal{R}}_{_{\rm NL}}(\boldsymbol{k},-\boldsymbol{k},\boldsymbol{k}_3) &= \left[\frac{n_{_{\rm S}}(k)-4}{4}\right]\,\left(\Pi^{\boldsymbol{k}_3}_{m_3n_3,\bar{m}\bar{n}}\right)^{-1}\,\Pi^{\boldsymbol{k}_3}_{m_3n_3,ij}\,\hat{n}_i\,\hat{n}_j, \qquad (4.5a)\\
\lim_{k_1\to 0}\, C^{\gamma}_{_{\rm NL}}(\boldsymbol{k}_1,\boldsymbol{k},-\boldsymbol{k}) &= \frac{n_{_{\rm T}}(k)}{2}\,\left(\Pi^{\boldsymbol{k}}_{m_2n_2,m_3n_3}\right)^{-1}\,\Pi^{\boldsymbol{k}}_{m_2n_2,m_3n_3}, \qquad (4.5b)\\
\lim_{k_3\to 0}\, h_{_{\rm NL}}(\boldsymbol{k},-\boldsymbol{k},\boldsymbol{k}_3) &= \left[\frac{n_{_{\rm T}}(k)-3}{2}\right]\,\Big(2\,\Pi^{\boldsymbol{k}}_{m_1n_1,m_2n_2}\,\Pi^{\boldsymbol{k}_3}_{m_3n_3,\bar{m}\bar{n}}+\Pi^{\boldsymbol{k}}_{m_1n_1,\bar{m}\bar{n}}\,\Pi^{\boldsymbol{k}_3}_{m_3n_3,m_2n_2} \\
&\quad+\Pi^{\boldsymbol{k}}_{\bar{m}\bar{n},m_2n_2}\,\Pi^{\boldsymbol{k}_3}_{m_3n_3,m_1n_1}\Big)^{-1} \\
&\quad\times \Pi^{\boldsymbol{k}}_{m_1n_1,m_2n_2}\,\Pi^{\boldsymbol{k}_3}_{m_3n_3,ij}\,\hat{n}_i\,\hat{n}_j, \qquad (4.5c)
\end{aligned}$$

where we have explicitly illustrated the point that $n_{_{\rm S}}$ and $n_{_{\rm T}}$ are, in general, dependent on the wavenumber [a dependence which can be arrived at from the corresponding power spectra through the expressions (1.27)]. It is useful to note here that, during slow roll inflation, while the non-Gaussianity parameter $C^{\gamma}_{_{\rm NL}}$ is of the order of the first slow roll parameter [cf. Eq. (3.22b)], the quantities $C^{\mathcal{R}}_{_{\rm NL}}$ and $h_{_{\rm NL}}$ prove to be of the order of unity [cf. Eqs. (3.22a) and (3.22c)]. This does not imply that the parameters $C^{\mathcal{R}}_{_{\rm NL}}$ and $h_{_{\rm NL}}$ are

'large'. They are of the order of unity due to the manner in which they have been introduced.

Finally, we would like to stress here the fact that we have arrived at the above consistency relations essentially assuming that the perturbations are initially in the Bunch-Davies vacuum and that the amplitudes of the scalar and the tensor perturbations are frozen on super-Hubble scales. While we have focussed on single field models of inflation driven by the canonical scalar field, the amplitude of the perturbations are known to be conserved in any single field model. For this reason, one can expect the consistency relations to hold even in non-canonical models of inflation, provided the perturbations are in the Bunch-Davies vacuum [32].

4.4 Analytical examples

In this section, we shall explicitly confirm the validity of the above consistency relations involving the tensors in two analytically tractable examples. We shall first consider a particular case of power law inflation and then discuss the Starobinsky model which, as we have seen, permits a brief period of departure from slow roll.

4.4.1 A power law case

Power law inflation corresponds to the situation wherein the scale factor is given by Eq. (2.6). In such a situation, as the first slow roll parameter proves to be a constant, $z \propto a$ and, hence, the scalar and the tensor modes can be described in terms of the same Hankel function [see Eq. (2.7)]. The perturbation spectra in power law inflation can be arrived at from the amplitudes of the Hankel functions, evaluated at late times, *i.e.* as $\eta \to 0$ [cf. Eq. (2.8)]. The tensor power spectrum is related to the scalar power spectrum as follows: $\mathcal{P}_{_{\rm T}}(k) = 16\,\epsilon_1\,\mathcal{P}_{_{\rm S}}(k)$, with the scalar power spectrum being given by Eq. (2.9). Note that the scalar and tensor spectral indices corresponding to these power spectra are constants, and are given by $n_{_{\rm S}} - 1 = n_{_{\rm T}} = 2\,(\gamma + 2)$. If the consistency relations (4.5) are indeed satisfied, then, upon setting each of the factors involving the polarization of the tensor perturbations to be unity, the above spectral indices would lead to the following

values of non-Gaussianity parameters of our interest:

$$C^{\mathcal{R}}_{\rm NL} = \frac{n_{\rm S}-4}{4} = \frac{2\,\gamma+1}{4}, \tag{4.6a}$$

$$C^{\gamma}_{\rm NL} = \frac{n_{\rm T}}{2} = \gamma+2, \tag{4.6b}$$

$$h_{\rm NL} = \frac{n_{\rm T}-3}{8} = \frac{2\,\gamma+1}{8}, \tag{4.6c}$$

which are constants independent of the wavenumber. Our task now would be to evaluate the three-point functions using the Maldacena formalism and examine if we indeed arrive at these values in the squeezed limit.

Ideally, it would have been desirable to arrive at analytic expressions describing the three-point functions in power law inflation for an arbitrary index γ. This clearly requires having to calculate the various integrals describing the correlations that we had summarized earlier in Subsec. 1.5.3. In fact, the spectral dependences of the three-point functions in power law inflation can be easily arrived at (in, say, the equilateral and the squeezed limits) without actually having to carry out the integrals involved (in this context, see Subsec. 3.3.3) [55, 56]. These results for the squeezed limit then immediately point to the fact that the non-Gaussianity parameters would be independent of scale. But, in order to be able to establish the consistency conditions (4.6) explicitly, apart from the spectral dependences, we shall require the amplitude of the integrals as well. But care is required in handling the integrals in the extreme sub-Hubble limit (*i.e.* as $\eta \to -\infty$) wherein the integrands oscillate with increasing frequency. This aspect seems to make it difficult to carry out the integrals and express them in a closed analytic form for a generic γ.

For the above reason, in order to establish the consistency relations, we shall focus on the specific case of $\gamma = -3$ or, equivalently, $\nu = -5/2$. In this case, the scalar and tensor modes simplify to

$$f_k(\eta) = \frac{g_k(\eta)}{\sqrt{2}} = -\frac{1}{\sqrt{2\,k^5}\,M_{\rm Pl}}\,\frac{1}{a_1\,\eta_1^2}\,\left(3+3\,i\,k\,\eta-k^2\,\eta^2\right)\,{\rm e}^{-i\,k\,\eta}, \tag{4.7}$$

so that the corresponding derivatives are given by

$$f_k'(\eta) = \frac{g_k'(\eta)}{\sqrt{2}} = \frac{-i}{\sqrt{2\,k^3}\,M_{\rm Pl}}\,\frac{1}{a_1\,\eta_1^2}\,\left(k^2\,\eta^2-i\,k\,\eta\right)\,{\rm e}^{-i\,k\,\eta}. \tag{4.8}$$

As $\eta \to 0$, the scalar and tensor modes reduce to

$$\lim_{\eta\to 0} f_k(\eta) = \lim_{\eta\to 0}\,\frac{g_k(\eta)}{\sqrt{2}} = -\frac{3}{\sqrt{2\,k^5}\,M_{\rm Pl}}\,\frac{1}{a_1\,\eta_1^2}. \tag{4.9}$$

We can arrive at the three-point functions of interest upon substituting the above scalar and tensor modes, their derivatives and their asymptotic behavior at late times, in the expressions (1.46), (1.48) and (1.51), and evaluating the various integrals involved. We find that, upon setting the factors containing the polarization tensor to be unity, in the squeezed limit, the three-point functions of interest are given by

$$\lim_{k_3\to 0} k^3\, k_3^3\, G^{m_3 n_3}_{\mathcal{R}\mathcal{R}\gamma}(\boldsymbol{k}, -\boldsymbol{k}, \boldsymbol{k}_3) = \frac{5}{4}\left(\frac{3}{M_{_{\rm Pl}}\, a_1\, \eta_1^2}\right)^4 \frac{1}{k^2\, k_3^2}, \tag{4.10a}$$

$$\lim_{k_1\to 0} k_1^3\, k^3\, G^{m_2 n_2 m_3 n_3}_{\mathcal{R}\gamma\gamma}(\boldsymbol{k}_1, \boldsymbol{k}, -\boldsymbol{k}) = \left(\frac{3}{M_{_{\rm Pl}}\, a_1\, \eta_1^2}\right)^4 \frac{1}{k_1^2\, k^2}, \tag{4.10b}$$

$$\lim_{k_3\to 0} k^3\, k_3^3\, G^{m_1 n_1 m_2 n_2 m_3 n_3}_{\gamma\gamma\gamma}(\boldsymbol{k}, \boldsymbol{k}, -\boldsymbol{k}_3) = \frac{5}{2}\left(\frac{3}{M_{_{\rm Pl}}\, a_1\, \eta_1^2}\right)^4 \frac{1}{k^2\, k_3^2}. \tag{4.10c}$$

The non-Gaussianity parameters corresponding to these three-point functions can be easily obtained to be $C^{\mathcal{R}}_{_{\rm NL}} = -5/4$, $C^{\gamma}_{_{\rm NL}} = -1$ and $h_{_{\rm NL}} = -5/8$. These values exactly match the results (4.6) with $\gamma = -3$, which implies that the consistency conditions are indeed satisfied in this case.

4.4.2 The case of the Starobinsky model

The second example that we shall consider is the Starobinsky model. In order to calculate the three-point functions of our interest, evidently, we shall require the behavior of the scale factor, the first slow roll parameter ϵ_1, and the scalar and the tensor modes [cf. Eqs. (1.46), (1.48) and (1.51)]. The forms of all these quantities except that of the tensor mode have been discussed in Subsec. 2.3.2. As we had discussed in Subsec. 3.3.3, since the scale factor behaves as in de Sitter, the tensor modes can be assumed to be given by the de Sitter solution, *viz.* Eq. (1.53b).

Upon using the background quantities and the expression (2.22a) for the scalar mode after the transition, we can arrive at the scalar power spectrum [cf. Eq. (2.25)] and the corresponding scalar spectral index $n_{_{\rm S}}$ [cf. Eq. (2.27)] in the Starobinsky model. From the expression for $n_{_{\rm S}}$, upon suitably ignoring overall factors containing the polarization tensor, we can obtain the non-Gaussianity parameter $C^{\mathcal{R}}_{_{\rm NL}}$ to be

$$\begin{aligned} C^{\mathcal{R}}_{_{\rm NL}}(k) &= \frac{n_{_{\rm S}}(k) - 4}{4} \\ &= \frac{1}{8}\left[\mathcal{I}(k) + \mathcal{I}_{_{\rm C}}(k)\, \cos\left(\frac{2\,k}{k_0}\right) + \mathcal{I}_{_{\rm S}}(k)\, \sin\left(\frac{2\,k}{k_0}\right)\right]^{-1} \Bigg\{\mathcal{J}(k) - 8\,\mathcal{I}(k) \\ &\quad + \left[\mathcal{J}_{_{\rm C}}(k) - 8\,\mathcal{I}_{_{\rm C}}(k)\right]\, \cos\left(\frac{2\,k}{k_0}\right) + \left[\mathcal{J}_{_{\rm S}}(k) - 8\,\mathcal{I}_{_{\rm S}}(k)\right]\, \sin\left(\frac{2\,k}{k_0}\right)\Bigg\}, \end{aligned} \tag{4.11}$$

where the functions $[\mathcal{I}(k), \mathcal{I}_{\rm c}(k), \mathcal{I}_{\rm s}(k)]$ and $[\mathcal{J}(k), \mathcal{J}_{\rm c}(k), \mathcal{J}_{\rm s}(k)]$ are given by Eqs. (2.26) and (2.28). We shall require the tensor spectral index $n_{_{\rm T}}$ in order to evaluate the other two non-Gaussianity parameters $C^{\gamma}_{_{\rm NL}}$ and $h_{_{\rm NL}}$ using the consistency relations (4.5). Since the tensor modes are described by the standard de Sitter solution, the resulting tensor spectrum is given by

$$\mathcal{P}_{_{\rm T}}(k) = \frac{2\,H_0^2}{\pi^2\,M_{_{\rm Pl}}^2}, \tag{4.12}$$

where $H_0^2 \simeq V_0/(3\,M_{_{\rm Pl}}^2)$. In other words, the tensor power spectrum is strictly scale invariant at the level of approximation we are working with. Therefore, the corresponding spectral index $n_{_{\rm T}}$ vanishes identically. Moreover, note that as the tensor modes remain unaffected by the transition, the tensor bi-spectrum will be of the same form as in the de Sitter case, a situation wherein it is easy to establish analytically that $h_{_{\rm NL}} = -3/8$ in the squeezed limit (see, for instance, Refs. [23, 33, 56]). In order to establish the consistency relation for the parameter $C^{\gamma}_{_{\rm NL}}$, we shall evaluate the tensor spectral index numerically, and compare the result with the analytical expressions that we shall obtain from the Maldacena formalism for the three-point functions in the squeezed limit.

The scalar-scalar-tensor cross-correlation in the Starobinsky model can be calculated analytically by dividing the integrals involved into two parts, corresponding to the epochs before and after the transition, and making use of the expressions for the first slow roll parameter and the scalar and the tensor modes. In the squeezed limit of the tensor mode, on ignoring the polarization tensors, we find that the scalar-scalar-tensor three-point function can be written as

$$\begin{aligned}\lim_{k_3\to 0}\, k^3\, k_3^3\, G^{m_3 n_3}_{\mathcal{R}\mathcal{R}_\gamma}(\boldsymbol{k}, -\boldsymbol{k}, \boldsymbol{k}_3) \;\; = \;\; & \frac{9\,H_0^8}{8\,M_{_{\rm Pl}}^2\,A_-^2}\Bigg\{8\,\mathcal{I}(k) - \mathcal{J}(k) + [8\,\mathcal{I}_{\rm c}(k)\; - \mathcal{J}_{\rm c}(k)]\,\cos\left(\frac{2\,k}{k_0}\right) \\ & + [8\,\mathcal{I}_{\rm s}(k)\; - \mathcal{J}_{\rm s}(k)]\,\sin\left(\frac{2\,k}{k_0}\right)\Bigg\},\end{aligned} \tag{4.13}$$

with $\mathcal{J}(k)$, $\mathcal{J}_{\rm c}(k)$ and $\mathcal{J}_{\rm s}(k)$ being given by Eqs. (2.28). Upon making use of this expression and the power spectra (2.25) and (4.12) in the definition (3.2a) of the parameter $C^{\mathcal{R}}_{_{\rm NL}}$ (and suitably ignoring the factors involving the polarization tensors), we find that one exactly arrives at the result (4.11), thereby establishing the consistency relation for this case.

Similarly, in the squeezed limit of the scalar mode, the scalar-tensor-tensor correlation in the Starobinsky model can be obtained to be

$$\lim_{k_1\to 0}\, k_1^3\, k^3\, G^{m_2 n_2 m_3 n_3}_{\mathcal{R}\gamma\gamma}(\boldsymbol{k}_1, \boldsymbol{k}, -\boldsymbol{k}) = \frac{H_0^4}{8\,M_{_{\rm Pl}}^4}\,\left[\mathcal{K}(k) + \mathcal{K}_{\rm c}(k)\,\cos\left(\frac{2\,k}{k_0}\right) + \mathcal{K}_{\rm s}(k)\,\sin\left(\frac{2\,k}{k_0}\right)\right], \tag{4.14}$$

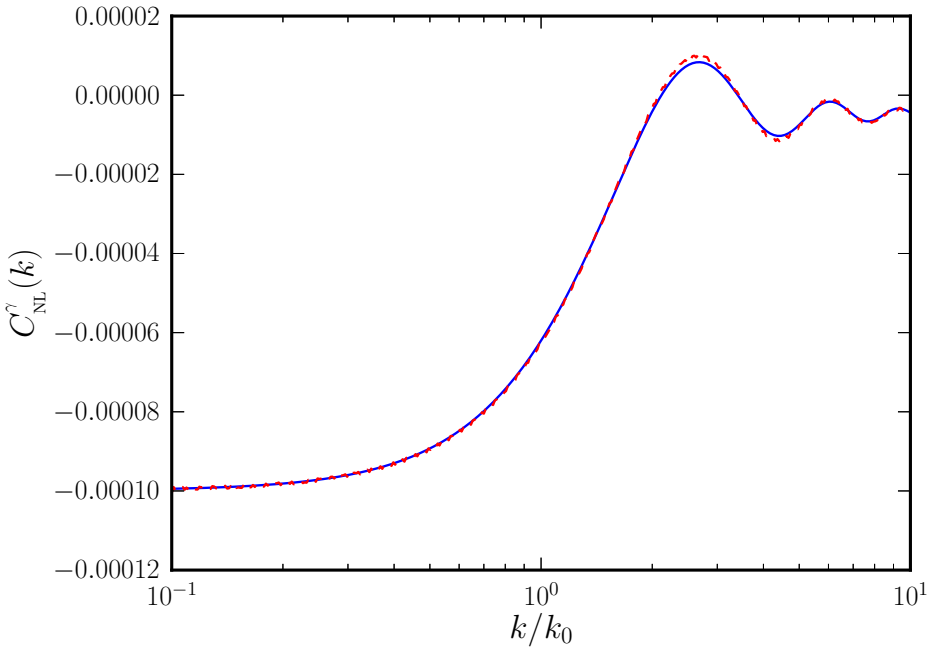

Figure 4.1: The non-Gaussianity parameter $C^{\gamma}_{\rm NL}$ in the Starobinsky model, evaluated in the squeezed limit, has been plotted as a function of k/k_0. The solid blue curve represents the parameter arrived at from the analytical results for the scalar-tensor-tensor cross-correlation (obtained using the Maldacena formalism) and the scalar and the tensor power spectra. The dashed red curve corresponds to the non-Gaussianity parameter obtained from consistency condition (4.5b), with the tensor spectral index being determined numerically. Evidently, there is good agreement between the two results, indicating that the consistency relation holds even when departures from slow roll occur. Note that we have worked with the same values of the potential parameters of the Starobinsky model as we had in the previous chapter.

where the quantities $\mathcal{K}(k)$, $\mathcal{K}_{\rm c}(k)$ and $\mathcal{K}_{\rm s}(k)$ are given by

$$\mathcal{K}(k) = 4\left(\frac{A_-}{A_+}\right)^2 + 9\left(\frac{\Delta A}{A_+}\right)^2\left(\frac{k_0}{k}\right)^6, \tag{4.15a}$$

$$\mathcal{K}_{\rm c}(k) = \frac{3\,\Delta A}{A_+}\left(\frac{k_0}{k}\right)^2\left[2 + 6\,\frac{\Delta A}{A_+}\left(\frac{k_0}{k}\right)^2 - \frac{3\,\Delta A}{A_+}\left(\frac{k_0}{k}\right)^4\right], \tag{4.15b}$$

$$\mathcal{K}_{\rm s}(k) = \frac{3\,\Delta A}{A_+}\left(\frac{k_0}{k}\right)^3\left[\left(\frac{3\,A_-}{A_+} - 4\right) - \frac{6\,\Delta A}{A_+}\left(\frac{k_0}{k}\right)^2\right]. \tag{4.15c}$$

In Fig. 4.1, we have plotted the $C^{\gamma}_{\rm NL}$ that results from the above analytical expression for the scalar-tensor-tensor cross-correlation and the power spectra (2.25) and (4.12). In the same figure, we have also plotted the $C^{\gamma}_{\rm NL}$ that arises from the numerical determination of

the tensor spectral index and the consistency condition (4.5b). It is clear from the figure that these two quantities match very well, indicating the fact that the consistency relation is valid in this case as well.

4.5 Numerical investigation of scenarios involving deviations from slow roll

In the last section, we had investigated the validity of the consistency relations comprising the tensor perturbations in two specific situations that had proved to be analytically tractable. It is well known that the scalar consistency relation is valid in slow roll inflation [23, 61, 62], and its applicability in situations containing departures from slow roll was thoroughly discussed in Chap. 2. Our general arguments in Sec. 4.3 as well as the analysis of the Starobinsky model in the previous section suggest that the consistency relations involving tensors too can be expected to be valid even in scenarios consisting of deviations from slow roll. It will be interesting to explicitly examine these relations in different models containing brief periods of fast roll. We shall consider for our investigation the three models that had been considered in the previous two chapters, *viz.* punctuated inflation, the quadratic potential with a step, and the axion monodromy model (see Subsec. 2.4.1).

We shall now numerically examine the validity of the consistency relations involving the tensor perturbations in the above-mentioned models. As we had described in the previous chapter, we have developed a numerical procedure and constructed a Fortran code for evaluating the three-point scalar-tensor cross-correlations and the tensor bi-spectrum [56]. We shall make use of the code to compute the three-point functions in the squeezed limit as well as the scalar and the tensor spectral indices, in order to check the consistency conditions (4.5). We shall work with values of the parameters for the potentials that have been shown to lead to an improved fit to the CMB data (cf. Subsec. 2.4.1). Also, we shall essentially follow the numerical procedure outlined in the last chapter. However, there are three points that we need to emphasize in this regard. Firstly, to achieve higher levels of numerical accuracy, say, of the order of 1–3% or better, for the three-point functions, one may have to integrate from a time when the modes are deeper inside the Hubble radius than $k/(a\,H) \simeq 10^2$. In our calculations, we shall choose to integrate from $k/(a\,H) \simeq 10^3$ in the cases of punctuated inflation and the quadratic potential with a step. The oscillating nature of the potential in the axion monodromy model leads to certain resonant behavior (see the first of the references in Ref. [68] and

Refs. [55, 56]), and it typically requires one to integrate from further deep inside the Hubble radius, even in the case of the power spectrum. For this reason, we shall choose to integrate from $k/(a\,H) \simeq 10^4$ in this case. Secondly, as we have discussed, due to the rapid oscillations of the modes when they are inside the Hubble radius, a cut-off in the integrands is required to regulate the integrals at early times. As earlier, we shall work with a cut off of the form $\exp -[\kappa\, k/(a\,H)]$, with the parameter κ to be chosen according to the initial time from which the integrations are to be carried out. For instance, the earlier the initial time, the smaller the quantity κ has to be [55, 56]. Since we shall integrate from $k/(a\,H) \simeq 10^3$ in the cases of punctuated inflation and the quadratic potential with a step, we shall work with $\kappa = 1/50$ in these cases, which is known to lead to a good accuracy [55, 56]. However, as we integrate from deeper inside the Hubble radius in the axion monodromy model, we shall work with $\kappa = 1/500$ in this case. The third and the last point concerns the implementation of the squeezed limit. To achieve this limit, we shall work with the smallest wavenumber (say, the largest scale mode that leaves the Hubble radius at the earliest possible time) that is numerically tenable, as we had done while examining the scalar consistency relation in Chap. 2. As a result, inherently, there will arise a weak wavenumber dependent effect when attempting to establish the consistency conditions numerically, with the smaller scale modes satisfying the condition better than the longer ones.

In Figs. 4.2, 4.3 and 4.4 we have plotted the numerical results for the non-Gaussianity parameters $C^{\mathcal{R}}_{\rm NL}$, $C^{\gamma}_{\rm NL}$ and $h_{\rm NL}$ for the three models discussed above. We find that the results from the spectral indices match the numerical results for the non-Gaussianity parameters obtained using Maldacena formalism at the level of 3% or better in the cases of punctuated inflation and the quadratic potential with the step, with the largest differences arising for the smallest wavenumbers for the reasons discussed above. The match is slightly poorer in the axion monodromy model (with differences of about 7% for some wavenumbers), but the match improves if we carry out the integrals over a longer duration in time. (We should mention here that the seeming difference in the cases of the model with the step and the axion monodromy model in the last row of Figs. 4.3 and 4.4 is due to the fact that the non-Gaussianity parameter $h_{\rm NL}$ has been plotted over a rather small range in amplitude to highlight the mild variations.) Clearly, the consistency relations hold true even in inflationary models that contain deviations from slow roll inflation.

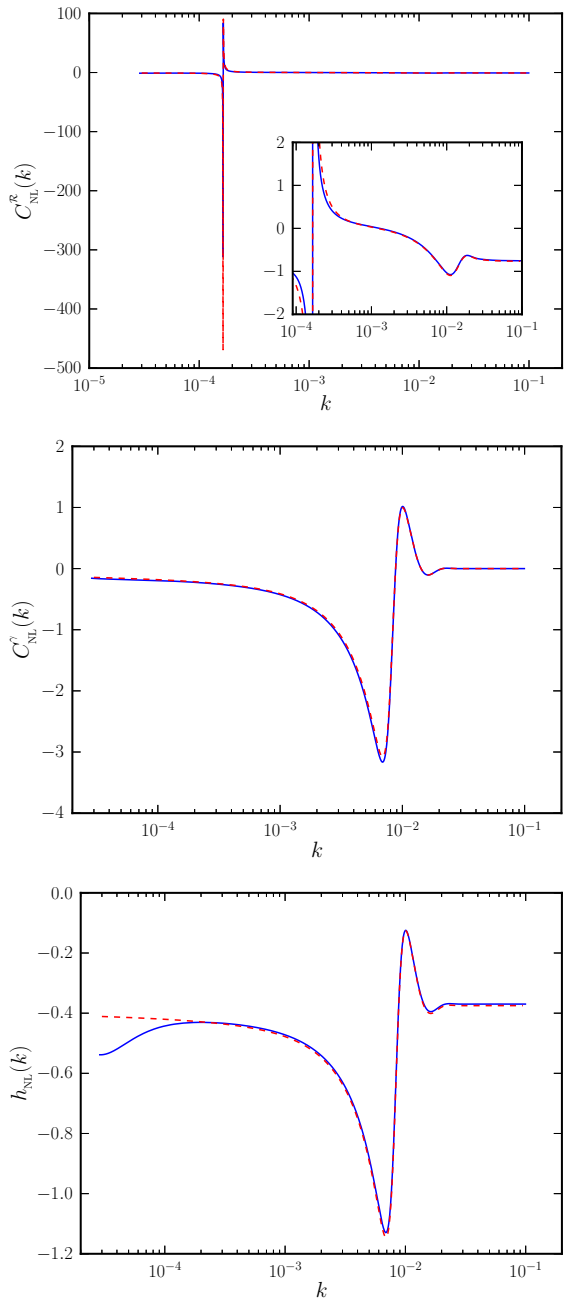

Figure 4.2: The non-Gaussianity parameters, $C^{\mathcal{R}}_{\rm NL}$ (on top), $C^{\gamma}_{\rm NL}$ (in the middle) and $h_{\rm NL}$ (at the bottom), arrived at using the Maldacena formalism and from the scalar and tensor spectral indices through the consistency conditions, have been plotted as a function of the wavenumber for the case of punctuated inflation. While the solid blue lines correspond to the numerical results for the parameters obtained using the Maldacena formalism, the dashed red lines represent the values arrived at from the spectral indices and the consistency relations. The two results match at the level of 3% or better, with the largest differences arising for the smallest wavenumbers due to the inherent limitation in implementing the squeezed limit numerically.

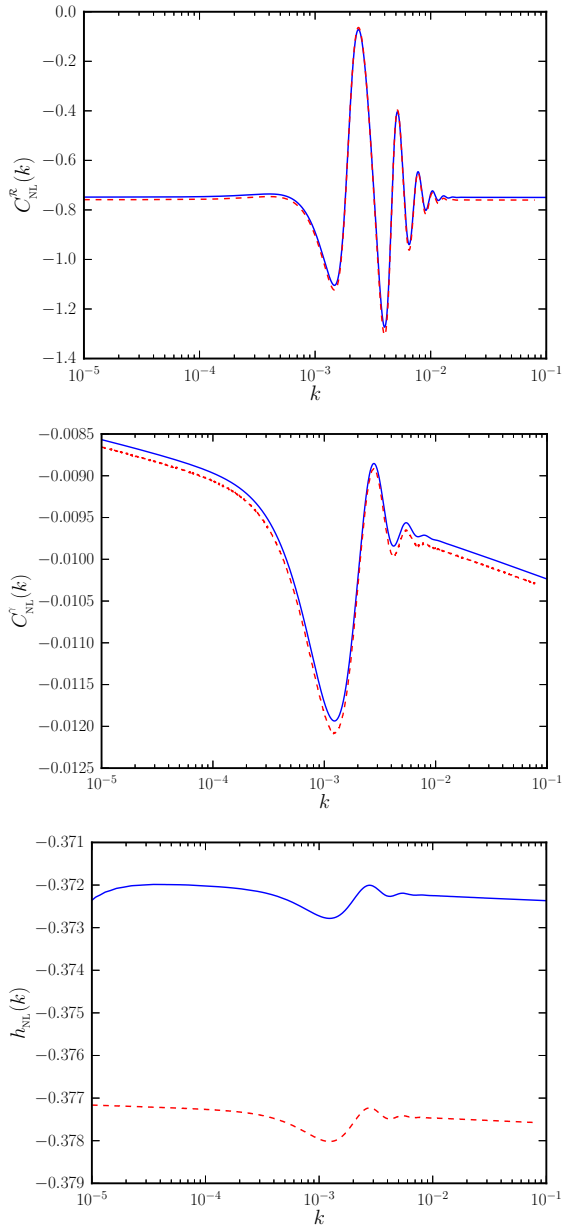

Figure 4.3: The non-Gaussianity parameters, $C^{\mathcal{R}}_{\rm NL}$ (on top), $C^{\gamma}_{\rm NL}$ (in the middle) and $h_{\rm NL}$ (at the bottom), plotted as in previous figure for the case of the quadratic potential with a step. At a first look, the difference in the last row may seem striking. But, we should clarify here that it is simply due to the fact that the non-Gaussianity parameter $h_{\rm NL}$ has been plotted over a rather small range in amplitude to highlight the mild variations.

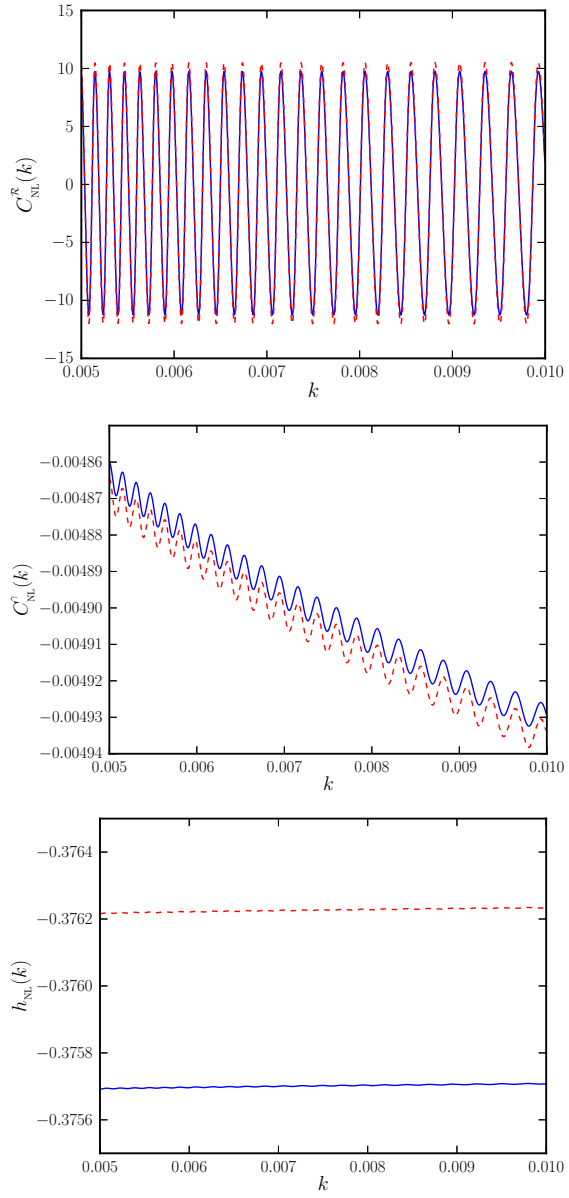

Figure 4.4: The non-Gaussianity parameters, $C^{\mathcal{R}}_{\rm NL}$ (on top), $C^{\gamma}_{\rm NL}$ (in the middle) and $h_{\rm NL}$ (at the bottom), have been plotted for the case of axion monodromy model as in the previous two figures. Though the match that we obtain is slightly poorer in this model (with differences of the order of 7% for certain wavenumbers), we find that the match can be improved by integrating for a longer duration. Further, as clarified in the previous figure, the seemingly large difference in the last row is simply due to the fact that the non-Gaussianity parameter $h_{\rm NL}$ has been plotted over a rather small range in amplitude to highlight the mild variations. Needless to add, these three figures confirm the validity of the consistency relations in single field inflationary models even in situations that allow strong departures from slow roll.

4.6 Discussion

Consistency relations link the three-point functions in the squeezed limit to the scalar and tensor power spectra. They essentially indicate that, in the squeezed limit, the three-point functions carry the same amount of information as the two-point functions do. Evidently, the consistency conditions can be conveniently expressed as relations between the non-Gaussianity parameters (two of which we had introduced in the last chapter) and the scalar or the tensor spectral indices. The consistency relations arise essentially because of the fact that inflaton is the only clock in single field inflationary models. Due to this reason, the amplitude of the long wavelength modes freeze in such situations. As we had discussed in Sec. 4.3, this implies that in the squeezed limit of interest, the long wavelength modes simply modify the background spatial coordinates. In this chapter, we have explicitly examined, both analytically and numerically, the validity of the consistency relations involving the tensor perturbations in single field inflationary models. Corroborating the general arguments that have been outlined earlier, we find that the consistency conditions hold true even in non-trivial scenarios involving drastic deviations from slow roll, such as what occurs in the case of punctuated inflation.

Chapter 5

Summary and outlook

With the emergence of increasingly precise cosmological data, it has been recognized that correlation functions beyond the power spectrum can act as powerful probes of the early universe. However, as we had discussed in the introductory section, despite the relatively strong bounds that have been arrived at on the scalar non-Gaussianity parameter $f_{\rm NL}$, there exists a wide range of models that remains consistent with the data. In such a situation, the possible observational bounds on the three-point functions involving tensors and the consistency relations involving the three-point functions can be expected to play a crucial role in arriving at a smaller class of viable inflationary models. With this goal in mind, in this thesis, we have investigated the computation and characteristics of inflationary three-point functions in general and those involving the tensors in particular.

In Chap. 2, we had investigated the scalar consistency relation in models involving deviations from slow roll. The consistency relations can play a very important role in constraining inflationary models. For instance, if the consistency relations are observationally confirmed, they can rule out many multi-field models of inflation and even, possibly, alternate scenarios such as the bouncing models (in this context, see, for instance, Refs. [19, 98] and references therein). In the chapter, we had analytically showed that the scalar consistency relation is valid in the cases of power law inflation and the Starobinsky model. Further, we had first numerically evaluated the complete scalar bi-spectra generated in punctuated inflation, the quadratic potential with a step and the axion monodromy model. We had then computed their squeezed limits and explicitly showed that the scalar consistency relation is valid even in situations involving deviations from slow roll.

In Chap. 3, we had constructed a numerical procedure to evaluate the inflationary three-point functions involving the tensor perturbations. Along the lines of the param-

eter $f_{\rm NL}$ that is used to characterize the scalar bi-spectrum, we had introduced two new parameters, *viz.* $C^{\mathcal{R}}_{\rm NL}$ and $C^{\gamma}_{\rm NL}$, to quantify the extent of non-Gaussianity in the three-point scalar-tensor cross-correlations. In addition, we had considered the parameter $h_{\rm NL}$ to describe the amplitude of the tensor bi-spectrum. We had utilized the numerical procedure to compute these quantities for the various models that we had considered earlier in Chap. 2. Lastly, we had estimated the contribution to these parameters due to the epoch of preheating in the case of inflationary potentials with a quadratic minimum.

In Chap. 4, we had studied the consistency relations obeyed by the three-point functions involving the tensors in the squeezed limit. We had expressed the consistency relations in terms of the newly introduced non-Gaussianity parameters and had examined the relations explicitly in a class of examples that we had discussed in the previous two chapters. We had found that, as in the purely scalar case considered in Chap. 2, the consistency conditions involving the tensors prove to be valid even away from slow roll.

In the light of the work described in this thesis, there are several open issues that can be pursued in the near future. In this thesis, we had described a numerical procedure and a code to compute the inflationary three-point functions involving tensors. As we had discussed, there already exists a fast and efficient code, BINGO [54], to calculate the scalar bi-spectrum for any inflationary model involving a single canonical scalar field. We need to modify and parallelize our code and integrate it with BINGO. Such a code will provide us with an effective code to calculate all the four non-Gaussianity parameters for any canonical single field inflationary model. Further, the codes need to be extended to include other classes of models such as those involving non-canonical scalar fields and models containing more than one field.

Consistency conditions, as described in this thesis, arise due to the fact that the amplitude of the perturbations freeze as they exit the Hubble radius during inflation. Such a soft, frozen, mode acts as a spatial diffeomorphism as far as the other modes are concerned, leading to these relations. Currently, it is understood that the consistency relations involving the three point functions are a particular case of a larger property which connects $(N+1)$-point functions to N-point functions in the presence of a soft scalar or tensor mode. It has been shown that these conditions arise from a master relation which is derived from the Slavnov-Taylor identity associated with the spatial diffeomorphisms (see Refs. [63], especially, the fourth reference). It would be interesting to explore the consistency relations from this perspective. Moreover, while the scalar consistency relation is known to hold in most situations involving single field inflationary models, there exist exceptions. An important class of exceptions are scenarios where in the field is evolving

away from the attractor [70]. In such a case, the supposedly decaying mode begins to grow on super-Hubble scales, causing a violation of the consistency relations. It will be interesting to examine the validity of the consistency relations involving tensors in these situations as well as in other scenarios such as the bouncing models. It also seems worthwhile to closely investigate the conditions under which the consistency relations hold in, say, two-field models (see, for example, Ref. [99]) and, in particular, examine in some detail the role the iso-curvature perturbations may play in this regard.

In all the calculations we have performed in this thesis, we have assumed that the perturbations are in the standard Bunch-Davies vacuum. However, it has been argued that high energy effects can lead to a situation wherein the perturbations can be in an excited state above the Bunch-Davies vacuum (in this context, see, for instance, Ref. [100]). The effect of such initial conditions on the inflationary scalar bi-spectrum has been explored to some extent. However, the corresponding effects on the three-point functions involving the tensors do not seem to have been studied adequately. For instance, it will be worthwhile to investigate if the consistency relations hold true when the perturbations are in an excited state above the Bunch-Davies vacuum [71].

In this thesis, we had evaluated the contribution to the three-point functions involving tensors due to preheating, wherein a single scalar field was oscillating in potentials with a quadratic minimum. It would be interesting to extend our analysis to scenarios wherein the inflaton is coupled to another scalar field, as in two-field models [97]. Furthermore, it would be important to carry out in detail a careful analysis of the effects of other post-inflationary scenarios, such as reheating, on the three-point functions [58, 59].

As we have repeatedly discussed, the comparison of models with the CMB data has been carried out mostly at the level of the power spectrum. A similar comparison at the level of the three-point functions can be numerically taxing. Due to this reason, one works with certain analytical templates for the scalar bi-spectrum to arrive at constraints on the extent of primordial non-Gaussianity [cf. Eqs. (1.60)]. However, the templates often considered cover only a limited range of possibilities (see, for instance, Ref. [101]). With future applications in mind, it will be helpful to arrive at similar templates for a wider range of models, including those which permit deviations from slow roll.

Lastly, needless to say, the efforts to introduce new non-Gaussianity parameters, such as those to characterize the three-point cross-correlations, will remain incomplete unless one also attempts to arrive at constraints on the values of these parameters. With such a goal in mind, it becomes necessary to systematically calculate the imprints of the inflationary three-point functions consisting of scalars and tensors on the CMB angular

three-point functions.

We are presently exploring along these directions.

Appendix A

Three-point functions involving tensors in the Starobinsky model

In this appendix, we shall provide some of the essential details for arriving at the analytical results for the three-point functions involving the tensors in the case of the Starobinsky model [37, 74, 75]. In Subsecs. 2.3.2 and 3.3.3, we have already discussed the behavior of the background as well as the perturbations in the model. It is just a matter of substituting the various quantities in the integrals that describe the three-point functions and being able to carry out the integrals involved. As we had pointed out earlier, due to the transition at the discontinuity in the potential, the integrals need to be divided into two. The integrals up to the transition essentially lead to the slow roll results, but with suitable modifications that arise because of the reason that the integrals are not to be carried out until late times. Though slow roll is violated briefly due to the discontinuity, we find that all the integrals can be evaluated in terms of simple functions to arrive at the three-point correlations. Since the scale factor is always of the de Sitter form, as we had mentioned, the tensor bi-spectrum proves to be the same as the one arrived at in the slow roll approximation [23, 33]. Therefore, we do not discuss it here. In what follows, we shall list out the results of the integrals involved in arriving at the two cross-correlations.

A.1 Calculation of $\mathcal{G}^{C}_{\mathcal{R}\mathcal{R}\gamma}$

Evidently, the quantities $\mathcal{G}^{C}_{\mathcal{R}\mathcal{R}\gamma}(\boldsymbol{k}_1, \boldsymbol{k}_2, \boldsymbol{k}_3)$, with $C = (1, 2, 3)$ [cf. Eqs. (1.47a)–(1.47c)], need to be first evaluated in order to arrive at the cross-correlation $G^{m_3 n_3}_{\mathcal{R}\mathcal{R}_\gamma}(\boldsymbol{k}_1, \boldsymbol{k}_2, \boldsymbol{k}_3)$. Upon dividing the integrals into two, we find that the contributions before the transition are

given by the following expressions:

$$\mathcal{G}^{1+}_{\mathcal{R}\mathcal{R}\gamma}(\boldsymbol{k}_1,\boldsymbol{k}_2,\boldsymbol{k}_3) = \frac{H_0}{2\,M_{_{\rm Pl}}^3\,\sqrt{k_1^3\,k_2^3\,k_3^3}}\,k_1\,k_2\,\Bigg[k_0+\frac{i\,(k_1\,k_2+k_1\,k_3+k_2\,k_3)}{k_{_{\rm T}}} - \frac{k_1\,k_2\,k_3}{k_{_{\rm T}}\,k_0}+\frac{i\,k_1\,k_2\,k_3}{k_{_{\rm T}}^2}\Bigg]\,{\rm e}^{-i\,k_{_{\rm T}}/k_0}, \tag{A.1a}$$

$$\mathcal{G}^{2+}_{\mathcal{R}\mathcal{R}\gamma}(\boldsymbol{k}_1,\boldsymbol{k}_2,\boldsymbol{k}_3) = \frac{A_+^2}{144\,H_0^3\,M_{_{\rm Pl}}^5\,\sqrt{k_1^3\,k_2^3\,k_3^3}}\,k_1\,k_2\,k_3^2 \times\,\left[\frac{i}{k_{_{\rm T}}}-\frac{k_3}{k_{_{\rm T}}\,k_0}+\frac{i\,k_3}{k_{_{\rm T}}^2}\right]\,{\rm e}^{-i\,k_{_{\rm T}}/k_0}, \tag{A.1b}$$

$$\mathcal{G}^{3+}_{\mathcal{R}\mathcal{R}\gamma}(\boldsymbol{k}_1,\boldsymbol{k}_2,\boldsymbol{k}_3) = -\frac{A_+^2}{144\,H_0^3\,M_{_{\rm Pl}}^5\,\sqrt{k_1^3\,k_2^3\,k_3^3}}\,k_1\,k_2\,k_3^2\,\Bigg[\left(-\frac{i}{k_{_{\rm T}}}+\frac{k_1}{k_{_{\rm T}}\,k_0}-\frac{i\,k_1}{k_{_{\rm T}}^2}\right) + \left(-\frac{i}{k_{_{\rm T}}}+\frac{k_2}{k_{_{\rm T}}\,k_0}-\frac{i\,k_2}{k_{_{\rm T}}^2}\right)\Bigg]\,{\rm e}^{-i\,k_{_{\rm T}}/k_0}, \tag{A.1c}$$

where, as we have indicated earlier, $k_{_{\rm T}} = k_1+k_2+k_3$. Similarly, after the transition, upon substituting the corresponding modes describing the perturbations, we find that, we can write

$$\mathcal{G}^{1-}_{\mathcal{R}\mathcal{R}\gamma}(\boldsymbol{k}_1,\boldsymbol{k}_2,\boldsymbol{k}_3) = \frac{H_0}{2\,M_{_{\rm Pl}}^3\,\sqrt{k_1^3\,k_2^3\,k_3^3}}\,k_1\,k_2\,\Big[\alpha^*_{k_1}\,\alpha^*_{k_2}\,\mathcal{I}^{11}_{\mathcal{R}\mathcal{R}\gamma}(k_1,k_2,k_3) - \alpha^*_{k_1}\,\beta^*_{k_2}\,\mathcal{I}^{12}_{\mathcal{R}\mathcal{R}\gamma}(k_1,k_2,k_3) - \beta^*_{k_1}\,\alpha^*_{k_2}\,\mathcal{I}^{13}_{\mathcal{R}\mathcal{R}\gamma}(k_1,k_2,k_3) + \beta^*_{k_1}\,\beta^*_{k_2}\,\mathcal{I}^{14}_{\mathcal{R}\mathcal{R}\gamma}(k_1,k_2,k_3)\Big], \tag{A.2a}$$

$$\mathcal{G}^{2-}_{\mathcal{R}\mathcal{R}\gamma}(\boldsymbol{k}_1,\boldsymbol{k}_2,\boldsymbol{k}_3) = -\frac{H_0}{8\,M_{_{\rm Pl}}^3\,\sqrt{k_1^3\,k_2^3\,k_3^3}}\,\frac{k_3^2}{k_1\,k_2}\,\Big[\alpha^*_{k_1}\,\alpha^*_{k_2}\,\mathcal{I}^{21}_{\mathcal{R}\mathcal{R}\gamma}(k_1,k_2,k_3) - \alpha^*_{k_1}\,\beta^*_{k_2}\,\mathcal{I}^{22}_{\mathcal{R}\mathcal{R}\gamma}(k_1,k_2,k_3) - \beta^*_{k_1}\,\alpha^*_{k_2}\,\mathcal{I}^{23}_{\mathcal{R}\mathcal{R}\gamma}(k_1,k_2,k_3) + \beta^*_{k_1}\,\beta^*_{k_2}\,\mathcal{I}^{24}_{\mathcal{R}\mathcal{R}\gamma}(k_1,k_2,k_3)\Big], \tag{A.2b}$$

$$\mathcal{G}^{3-}_{\mathcal{R}\mathcal{R}\gamma}(k_1,k_2,k_3) = -\frac{H_0}{8\,M_{_{\rm Pl}}^3\,\sqrt{k_1^3\,k_2^3\,k_3^3}}\,k_1\,k_2\,\Bigg\{\frac{k_3^2}{k_2^2}\,\Big[\alpha^*_{k_1}\,\alpha^*_{k_2}\,\mathcal{I}^{31}_{\mathcal{R}\mathcal{R}\gamma}(k_1,k_2,k_3) - \alpha^*_{k_1}\,\beta^*_{k_2}\,\mathcal{I}^{32}_{\mathcal{R}\mathcal{R}\gamma}(k_1,k_2,k_3) - \beta^*_{k_1}\,\alpha^*_{k_2}\,\mathcal{I}^{33}_{\mathcal{R}\mathcal{R}\gamma}(k_1,k_2,k_3) + \beta^*_{k_1}\,\beta^*_{k_2}\,\mathcal{I}^{34}_{\mathcal{R}\mathcal{R}\gamma}(k_1,k_2,k_3)\Big] + \frac{k_3^2}{k_1^2}\,\Big[\alpha^*_{k_1}\,\alpha^*_{k_2}\,\mathcal{J}^{31}_{\mathcal{R}\mathcal{R}\gamma}(k_1,k_2,k_3) - \alpha^*_{k_1}\,\beta^*_{k_2}\,\mathcal{J}^{32}_{\mathcal{R}\mathcal{R}\gamma}(k_1,k_2,k_3) - \beta^*_{k_1}\,\alpha^*_{k_2}\,\mathcal{J}^{33}_{\mathcal{R}\mathcal{R}\gamma}(k_1,k_2,k_3) + \beta^*_{k_1}\,\beta^*_{k_2}\,\mathcal{J}^{34}_{\mathcal{R}\mathcal{R}\gamma}(k_1,k_2,k_3)\Big]\Bigg\}. \tag{A.2c}$$

The expressions for the functions $\mathcal{I}^{1i}_{\mathcal{R}\mathcal{R}\gamma}(k_1,k_2,k_3)$, $\mathcal{I}^{2i}_{\mathcal{R}\mathcal{R}\gamma}(k_1,k_2,k_3)$ and $\mathcal{I}^{3i}_{\mathcal{R}\mathcal{R}\gamma}(k_1,k_2,k_3)$ as well as $\mathcal{J}^{3i}_{\mathcal{R}\mathcal{R}\gamma}(k_1,k_2,k_3)$, where $i=1,2,3,4$, are furnished in the last sub-section.

A.2 Calculation of $\mathcal{G}^{C}_{\mathcal{R}\gamma\gamma}$

In this case, the contributions before the transition are given by

$$\begin{aligned}
\mathcal{G}^{1+}_{R\gamma\gamma}(k_1,k_2,k_3) &= \frac{i\,A_+}{24\,H_0\,M_{_{\rm Pl}}^4\,\sqrt{2\,k_1^3\,k_2^3\,k_3^3}}\,k_2^2\,k_3^2 \\
&\quad\times\left(\frac{1}{k_{_{\rm T}}}+\frac{i\,k_1}{k_{_{\rm T}}\,k_0}+\frac{k_1}{k_{_{\rm T}}^2}\right)\,{\rm e}^{-i\,k_{_{\rm T}}/k_0}, \qquad \text{(A.3a)}\\
\mathcal{G}^{2+}_{R\gamma\gamma}(k_1,k_2,k_3) &= \frac{i\,A_+}{24\,H_0\,M_{_{\rm Pl}}^4\,\sqrt{2\,k_1^3\,k_2^3\,k_3^3}}\,(\boldsymbol{k}_2\cdot\boldsymbol{k}_3) \\
&\quad\times\left(-i\,k_0+\frac{k_1\,k_2+k_1\,k_3+k_2\,k_3}{k_{_{\rm T}}}+\frac{i\,k_1\,k_2\,k_3}{k_{_{\rm T}}\,k_0}+\frac{k_1\,k_2\,k_3}{k_{_{\rm T}}^2}\right) \\
&\quad\times{\rm e}^{-i\,k_{_{\rm T}}/k_0}, \qquad \text{(A.3b)}\\
\mathcal{G}^{3+}_{R\gamma\gamma}(k_1,k_2,k_3) &= -\frac{i\,A_+}{24\,H_0\,M_{_{\rm Pl}}^4\,\sqrt{2\,k_1^3\,k_2^3\,k_3^3}} \\
&\quad\times\left[(\boldsymbol{k}_1\cdot\boldsymbol{k}_2)\,k_3^2\,\left(\frac{1}{k_{_{\rm T}}}+\frac{i\,k_2}{k_{_{\rm T}}\,k_0}+\frac{k_2}{k_{_{\rm T}}^2}\right)\right. \\
&\quad\left.+\,(\boldsymbol{k}_1\cdot\boldsymbol{k}_3)\,k_2^2\,\left(\frac{1}{k_{_{\rm T}}}+\frac{i\,k_3}{k_{_{\rm T}}\,k_0}+\frac{k_3}{k_{_{\rm T}}^2}\right)\right]{\rm e}^{-i\,k_{_{\rm T}}/k_0}. \qquad \text{(A.3c)}
\end{aligned}$$

The corresponding quantities after the transition are found to be

$$\begin{aligned}
\mathcal{G}^{1-}_{R\gamma\gamma}(k_1,k_2,k_3) &= \frac{i\,A_-}{24\,H_0\,M_{_{\rm Pl}}^4\,\sqrt{2\,k_1^3\,k_2^3\,k_3^3}}\,k_2^2\,k_3^2 \\
&\quad\times\left[\alpha^*_{k1}\,\mathcal{M}_1(k_1,k_2,k_3)-\beta^*_{k1}\,\mathcal{M}_1(-k_1,k_2,k_3)\right], \qquad \text{(A.4a)}\\
\mathcal{G}^{2-}_{R\gamma\gamma}(k_1,k_2,k_3) &= -\frac{i\,A_-}{24\,H_0\,M_{_{\rm Pl}}^4\,\sqrt{2\,k_3\,k_2^3\,k_3^3}}\,(\boldsymbol{k}_2\cdot\boldsymbol{k}_3) \\
&\quad\times\left[\alpha^*_{k1}\,\mathcal{M}_2(k_1,k_2,k_3)-\beta^*_{k1}\,\mathcal{M}_2(-k_1,k_2,k_3)\right], \qquad \text{(A.4b)}\\
\mathcal{G}^{3-}_{R\gamma\gamma}(k_1,k_2,k_3) &= -\frac{i\,A_-}{24\,H_0\,M_{_{\rm Pl}}^4\,\sqrt{2\,k_1^3\,k_2^3,k_3^3}} \\
&\quad\times\left\{\frac{(\boldsymbol{k}_1\cdot\boldsymbol{k}_2)\,k_3^2}{k_1^2}\,\left[\alpha^*_{k1}\,\mathcal{M}_3(k_1,k_3,k_2)-\beta^*_{k1}\,\mathcal{M}_3(-k_1,k_3,k_2)\right]\right. \\
&\quad\left.+\,\frac{(\boldsymbol{k}_1\cdot\boldsymbol{k}_3)\,k_2^2}{k_1^2}\,\left[\alpha^*_{k1}\,\mathcal{M}_3(k_1,k_2,k_3)-\beta^*_{k1}\,\mathcal{M}_3(-k_1,k_2,k_3)\right]\right\}. \qquad \text{(A.4c)}
\end{aligned}$$

The forms of the expressions $\mathcal{M}_i(k_1, k_2, k_3)$ with $i = 1, 2, 3$ are given in the next subsection.

A.3 Evaluation of integrals

The quantity $\mathcal{I}^{11}_{\mathcal{R}\mathcal{R}\gamma}(k_1, k_2, k_3)$ is described by the integral

$$\mathcal{I}^{11}_{\mathcal{R}\mathcal{R}\gamma}(k_1, k_2, k_3) = \int_{-k_0^{-1}}^{0} \frac{\mathrm{d}\eta}{\eta^2}\, (1 - i\, k_1\, \eta)\, (1 - i\, k_2\, \eta)\, (1 - i\, k_3\, \eta)\, \mathrm{e}^{i\, k_{\mathrm{T}}\, \eta}, \tag{A.5}$$

which can be easily evaluated to be

$$\begin{aligned}\mathcal{I}^{11}_{\mathcal{R}\mathcal{R}\gamma}(k_1, k_2, k_3) &= \lim_{\eta_{\mathrm{e}} \to 0} \left(-\frac{\mathrm{e}^{i\, k_{\mathrm{T}}\, \eta_{\mathrm{e}}}}{\eta_{\mathrm{e}}}\right) \\ &\quad - \left(k_0 + \frac{i\, (k_1 k_2 + k_1\, k_3 + k_2\, k_3)}{k_{\mathrm{T}}} - \frac{k_1\, k_2\, k_3}{k_{\mathrm{T}}\, k_0} + i\, \frac{k_1\, k_2\, k_3}{k_{\mathrm{T}}^2}\right) \mathrm{e}^{-i\, k_{\mathrm{T}}/k_0} \\ &\quad + \frac{i\, (k_1\, k_2 + k_1\, k_3 + k_2\, k_3)}{k_{\mathrm{T}}} + \frac{i\, k_1\, k_2\, k_3}{k_{\mathrm{T}}^2}. \end{aligned} \tag{A.6}$$

We find that the rest of the functions $\mathcal{I}^{1i}_{\mathcal{R}\mathcal{R}\gamma}(k_1, k_2, k_3)$ with $i = 2, 3, 4$ can be expressed in terms of $\mathcal{I}^{11}_{\mathcal{R}\mathcal{R}\gamma}(k_1, k_2, k_3)$ as follows: $\mathcal{I}^{12}_{\mathcal{R}\mathcal{R}\gamma}(k_1, k_2, k_3) = \mathcal{I}^{11}_{\mathcal{R}\mathcal{R}\gamma}(k_1, -k_2, k_3)$, $\mathcal{I}^{13}_{\mathcal{R}\mathcal{R}\gamma}(k_1, k_2, k_3) = \mathcal{I}^{11}_{\mathcal{R}\mathcal{R}\gamma}(-k_1, k_2, k_3)$ and $\mathcal{I}^{14}_{\mathcal{R}\mathcal{R}\gamma}(k_1, k_2, k_3) = \mathcal{I}^{11}_{\mathcal{R}\mathcal{R}\gamma}(-k_1, -k_2, k_3)$.

The quantity $I^{21}_{\mathcal{R}\mathcal{R}\gamma}(k_1, k_2, k_3)$ is described by the integral

$$\begin{aligned}\mathcal{I}^{21}_{\mathcal{R}\mathcal{R}\gamma}(k_1, k_2, k_3) &= \frac{A_{-}^2}{18\, H_0^4\, M_{\mathrm{Pl}}^2} \int_{-k_0^{-1}}^{0} \frac{\mathrm{d}\eta}{\eta^2}\, \left(1 + \rho^3 \eta^3\right)^2 (1 - i\, k_3\, \eta) \\ &\quad \times \left[\frac{\epsilon_{2-}}{2\, \eta}\, (1 - i\, k_1\, \eta) + k_1^2\, \eta\right] \left[\frac{\epsilon_{2-}}{2\, \eta}\, (1 - i\, k_2\, \eta) + k_2^2\, \eta\right], \end{aligned} \tag{A.7}$$

with ϵ_{2-} being given by Eq. (2.17b). We find that this quantity can be written as

$$\begin{aligned}\mathcal{I}^{21}_{\mathcal{R}\mathcal{R}\gamma}(k_1, k_2, k_3) &= \frac{A_{-}^2}{18\, H_0^4\, M_{\mathrm{Pl}}^2} \Big[\mathcal{A}_1(k_1, k_2, k_3) + \mathcal{A}_2(k_1, k_2, k_3) \\ &\quad + \mathcal{A}_3(k_1, k_2, k_3) + \mathcal{A}_4(k_1, k_2, k_3)\Big], \end{aligned} \tag{A.8}$$

where

$$
\begin{aligned}
\mathcal{A}_1(k_1,k_2,k_3) &= 9\,\rho^6 \int_{-k_0^{-1}}^{0} \mathrm{d}\eta\; \eta^2\; (1-i\,k_1\,\eta)\; (1-i\,k_2\,\eta)\; (1-i\,k_3\,\eta)\; \mathrm{e}^{i\,k_{\mathrm{T}}\,\eta} \\
&= 9\,\rho^6 \left\{ \frac{8\,i}{k_{\mathrm{T}}^3} + \frac{24\,i\;(k_1\,k_2+k_1\,k_3+k_2\,k_3)}{k_{\mathrm{T}}^5} + \frac{120\,i\,k_1\,k_2\,k_3}{k_{\mathrm{T}}^6} \right. \\
&\quad + \left[\frac{4\,i}{k_{\mathrm{T}}\,k_0^2} - \frac{8\,i}{k_{\mathrm{T}}^3} - \frac{1}{k_0^3} + \frac{8}{k_{\mathrm{T}}^2 k_0} \right. \\
&\quad - (k_1\,k_2+k_1\,k_3+k_2\,k_3) \left(\frac{i}{k_{\mathrm{T}} k_0^4} + \frac{4}{k_{\mathrm{T}}^2\,k_0^3} - \frac{12\,i}{k_{\mathrm{T}}^3\,k_0^2} - \frac{24}{k_{\mathrm{T}}^4 k_0} + \frac{24\,i}{k_{\mathrm{T}}^5} \right) \\
&\quad \left. + k_1\,k_2\,k_3 \left(\frac{1}{k_{\mathrm{T}} k_0^5} - \frac{5\,i}{k_{\mathrm{T}}^2 k_0^4} - \frac{20}{k_{\mathrm{T}}^3\,k_0^3} + \frac{60\,i}{k_{\mathrm{T}}^4 k_0^2} + \frac{120}{k_{\mathrm{T}}^5 k_0} - \frac{120\,i}{k_{\mathrm{T}}^6} \right) \right] \\
&\quad \left. \times\, \mathrm{e}^{-i\,k_{\mathrm{T}}/k_0} \right\}, \qquad \text{(A.9a)}
\end{aligned}
$$

$$
\begin{aligned}
\mathcal{A}_2(k_1,k_2,k_3) &= -3\,\rho^3\,k_2^2 \int_{-k_0^{-1}}^{0} \mathrm{d}\eta\; \eta\; \left(1+\rho^3\,\eta^3\right)\; (1-i\,k_1\,\eta)\; (1-i\,k_3\,\eta)\; \mathrm{e}^{i\,k_{\mathrm{T}}\,\eta} \\
&= -3\,\rho^3\,k_1^2 \left(\frac{1}{k_{\mathrm{T}}^2} + \frac{2\,(k_1+k_3)}{k_{\mathrm{T}}^3} + \frac{6\,k_1\,k_3}{k_{\mathrm{T}}^4} - \frac{24\,i\,\rho^3}{k_{\mathrm{T}}^5} - \frac{120\,i\,\rho^3\,(k_1+k_3)}{k_{\mathrm{T}}^6} \right. \\
&\quad - \frac{720\,i\,\rho^3\,k_1\,k_3}{k_{\mathrm{T}}^7} + \left\{ -\frac{i}{k_{\mathrm{T}}\,k_0} - \frac{1}{k_{\mathrm{T}}^2} - i\;(k_1+k_3) \left(\frac{i}{k_{\mathrm{T}}\,k_0^2} + \frac{2}{k_{\mathrm{T}}^2\,k_0} - \frac{2\,i}{k_{\mathrm{T}}^3} \right) \right. \\
&\quad -k_1\,k_3 \left(-\frac{i}{k_{\mathrm{T}}\,k_0^3} - \frac{3}{k_{\mathrm{T}}^2\,k_0^2} + \frac{6\,i}{k_{\mathrm{T}}^3\,k_0} + \frac{6}{k_{\mathrm{T}}^4} \right) \\
&\quad + \rho^3 \left[\frac{i}{k_{\mathrm{T}}\,k_0^4} + \frac{4}{k_{\mathrm{T}}^2\,k_0^3} - \frac{12\,i}{k_{\mathrm{T}}^3\,k_0^2} - \frac{24}{k_{\mathrm{T}}^4\,k_0} + \frac{24\,i}{k_{\mathrm{T}}^5} \right. \\
&\quad -i\;(k_1+k_3) \left(-\frac{i}{k_{\mathrm{T}}\,k_0^5} - \frac{5}{k_{\mathrm{T}}^2\,k_0^4} + \frac{20\,i}{k_{\mathrm{T}}^3\,k_0^3} + \frac{60}{k_{\mathrm{T}}^4\,k_0^2} - \frac{120\,i}{k_{\mathrm{T}}^5\,k_0} - \frac{120}{k_{\mathrm{T}}^6} \right) \\
&\quad \left. \left. -k_1\,k_3 \left(\frac{i}{k_{\mathrm{T}}\,k_0^6} + \frac{6}{k_{\mathrm{T}}^2\,k_0^5} - \frac{30\,i}{k_{\mathrm{T}}^3\,k_0^4} - \frac{120}{k_{\mathrm{T}}^4\,k_0^3} + \frac{360\,i}{k_{\mathrm{T}}^5\,k_0^2} + \frac{720}{k_{\mathrm{T}}^6\,k_0} - \frac{720\,i}{k_{\mathrm{T}}^7} \right) \right] \right\} \\
&\quad \left. \times\, \mathrm{e}^{-i\,k_{\mathrm{T}}/k_0} \right), \qquad \text{(A.9b)}
\end{aligned}
$$

$$
\begin{aligned}
\mathcal{A}_3(k_1,k_2,k_3) &= -3\,\rho^3\,k_1^2 \int_{-k_0^{-1}}^{0} \mathrm{d}\eta\,\eta\; \left(1+\rho^3\,\eta^3\right)\; (1-i\,k_3\,\eta)\; (1-i\,k_2\,\eta)\; \mathrm{e}^{i\,k_{\mathrm{T}}\,\eta} \\
&= \mathcal{A}_2(k_2,k_1,k_3), \qquad \text{(A.9c)}
\end{aligned}
$$

$$
\begin{aligned}
\mathcal{A}_4(k_1,k_2,k_3) &= k_1^2\,k_2^2\int_{-k_0^{-1}}^{0}\mathrm{d}\eta\,\left(1+\rho^3\,\eta^3\right)^2\,(1-i\,k_3\,\eta)\,\mathrm{e}^{i\,k_{\mathrm{T}}\,\eta}\\
&= k_1^2\,k_2^2\left\{-\frac{i}{k_{\mathrm{T}}}-\frac{12\,\rho^3}{k_{\mathrm{T}}^4}+\frac{720\,i\,\rho^6}{k_{\mathrm{T}}^7}-\frac{i\,k_3}{k_{\mathrm{T}}^2}-\frac{48\,k_3\,\rho^3}{k_{\mathrm{T}}^5}+\frac{5040\,i\,k_3\,\rho^6}{k_{\mathrm{T}}^8}\right.\\
&\quad+\left[\frac{i}{k_{\mathrm{T}}}-\frac{2\,i\,\rho^3}{k_{\mathrm{T}}\,k_0^3}-\frac{6\,\rho^3}{k_{\mathrm{T}}^2\,k_0^2}+\frac{12\,i\,\rho^3}{k_{\mathrm{T}}^3\,k_0}+\frac{12\,\rho^3}{k_{\mathrm{T}}^4}+\frac{i\,\rho^6}{k_{\mathrm{T}}\,k_0^6}+\frac{6\,\rho^6}{k_{\mathrm{T}}^2\,k_0^5}-\frac{30\,i\,\rho^6}{k_{\mathrm{T}}^3\,k_0^4}\right.\\
&\quad-\frac{120\,\rho^6}{k_{\mathrm{T}}^4\,k_0^3}+\frac{360\,i\,\rho^6}{k_{\mathrm{T}}^5\,k_0^2}+\frac{720\,\rho^6}{k_{\mathrm{T}}^6\,k_0}-\frac{720\,i\,\rho^6}{k_{\mathrm{T}}^7}+i\,k_3\,\left(\frac{i}{k_{\mathrm{T}}\,k_0}+\frac{1}{k_{\mathrm{T}}^2}\right)\\
&\quad-2\,i\,k_3\,\rho^3\,\left(\frac{i}{k_{\mathrm{T}}\,k_0^4}+\frac{4}{k_{\mathrm{T}}^2\,k_0^3}-\frac{12\,i}{k_{\mathrm{T}}^3\,k_0^2}-\frac{24}{k_{\mathrm{T}}^4\,k_0}+\frac{24\,i}{k_{\mathrm{T}}^5}\right)\\
&\quad-i\,k_3\,\rho^6\left(-\frac{i}{k_{\mathrm{T}}\,k_0^7}-\frac{7}{k_{\mathrm{T}}^2\,k_0^6}+\frac{42\,i}{k_{\mathrm{T}}^3\,k_0^5}+\frac{210}{k_{\mathrm{T}}^4\,k_0^4}-\frac{840\,i}{k_{\mathrm{T}}^5\,k_0^3}-\frac{2520}{k_{\mathrm{T}}^6\,k_0^2}\right.\\
&\quad\left.\left.\left.+\frac{5040\,i}{k_{\mathrm{T}}^7\,k_0}+\frac{5040}{k_{\mathrm{T}}^8}\right)\right]\mathrm{e}^{-i\,k_{\mathrm{T}}/k_0}\right\}. \qquad \text{(A.9d)}
\end{aligned}
$$

Moreover, it can be shown that $\mathcal{I}^{22}_{\mathcal{R}\mathcal{R}\gamma}(k_1,k_2,k_3) = \mathcal{I}^{21}_{\mathcal{R}\mathcal{R}\gamma}(k_1,-k_2,k_3)$, $\mathcal{I}^{23}_{\mathcal{R}\mathcal{R}\gamma}(k_1,k_2,k_3) = \mathcal{I}^{21}_{\mathcal{R}\mathcal{R}\gamma}(-k_1,k_2,k_3)$ and $\mathcal{I}^{24}_{\mathcal{R}\mathcal{R}\gamma}(k_1,k_2,k_3) = \mathcal{I}^{11}_{\mathcal{R}\mathcal{R}\gamma}(-k_1,-k_2,k_3)$.

The quantity $\mathcal{I}^{31}_{\mathcal{R}\mathcal{R}\gamma}(k_1,k_2,k_3)$ is described by the integral

$$
\mathcal{I}^{31}_{\mathcal{R}\mathcal{R}\gamma}(k_1,k_2,k_3) = \int_{-k_0^{-1}}^{0}\mathrm{d}\eta\,\frac{\epsilon_{1-}}{\eta}\,\left[\frac{\epsilon_{2-}}{2\,\eta}\,(1-i\,k_1\,\eta)\,(1-i\,k_2\,\eta)+k_2^2\,\eta\,(1-i\,k_1\,\eta)\right]\mathrm{e}^{i\,k_{\mathrm{T}}\,\eta}, \qquad \text{(A.10)}
$$

where ϵ_{1-} is the slow roll parameter after the transition, which is given by Eq. (2.16b). The above integral can be evaluated to yield

$$
\begin{aligned}
\mathcal{I}^{31}_{\mathcal{R}\mathcal{R}\gamma}(k_1,k_2,k_3) &= \frac{A_-^2}{18\,H_0^4\,M_{\mathrm{Pl}}^2}\left(-3\,\rho^3\left\{\frac{1}{k_{\mathrm{T}}^2}+\frac{2\,(k_1+k_2)}{k_{\mathrm{T}}^3}+\frac{6\,k_1\,k_2}{k_{\mathrm{T}}^4}-\frac{24\,i\,\rho^3}{k_{\mathrm{T}}^5}\right.\right.\\
&\quad-\frac{120\,i\,\rho^3\,(k_1+k_2)}{k_{\mathrm{T}}^6}-\frac{720\,i\,k_1\,k_2\,\rho^3}{k_{\mathrm{T}}^7}\\
&\quad+\left[-\frac{i}{k_{\mathrm{T}}\,k_0}-\frac{1}{k_{\mathrm{T}}^2}-i\,(k_1+k_2)\,\left(\frac{i}{k_{\mathrm{T}}\,k_0^2}+\frac{2}{k_{\mathrm{T}}^2\,k_0}-\frac{i2}{k_{\mathrm{T}}^3}\right)\right.\\
&\quad\left.\left.-k_1\,k_2\left(-\frac{i}{k_{\mathrm{T}}\,k_0^3}-\frac{3}{k_{\mathrm{T}}^2\,k_0^2}+\frac{6\,i}{k_{\mathrm{T}}^3\,k_0}+\frac{6}{k_{\mathrm{T}}^4}\right)\right.\right.
\end{aligned}
$$

$$
\begin{aligned}
&+\rho^3\left(\frac{i}{k_{\rm T}\,k_0^4}+\frac{4}{k_{\rm T}^2\,k_0^3}-\frac{12\,i}{k_{\rm T}^3\,k_0^2}-\frac{24}{k_{\rm T}^4\,k_0}+\frac{24\,i}{k_{\rm T}^5}\right)\\
&-i\,(k_1+k_2)\,\rho^3\left(-\frac{i}{k_{\rm T}\,k_0^5}-\frac{5}{k_{\rm T}^2\,k_0^4}+\frac{20\,i}{k_{\rm T}^3\,k_0^3}+\frac{60}{k_{\rm T}^4\,k_0^2}-\frac{120\,i}{k_{\rm T}^5\,k_0}-\frac{120}{k_{\rm T}^6}\right)\\
&-\rho^3\,k_1\,k_2\left[\frac{i}{k_{\rm T}\,k_0^6}+\frac{6}{k_{\rm T}^2\,k_0^5}-\frac{30\,i}{k_{\rm T}^3 k_0^4}-\frac{120}{k_{\rm T}^4\,k_0^3}+\frac{360\,i}{k_{\rm T}^5\,k_0^2}+\frac{720}{k_{\rm T}^6\,k_0}-\frac{720\,i}{k_{\rm T}^7}\right)\Bigg]\\
&\times{\rm e}^{-i\,k_{\rm T}/k_0}\Bigg\}\\
&+k_2^2\left\{-\frac{i}{k_{\rm T}}-\frac{12\,\rho^3}{k_{\rm T}^4}+\frac{720\,i\,\rho^6}{k_{\rm T}^7}-\frac{i\,k_1}{k_{\rm T}^2}-\frac{48\,k_1\,\rho^3}{k_{\rm T}^5}+\frac{5040\,i\,k_1\,\rho^6}{k_{\rm T}^8}\right.\\
&+\left[\frac{i}{k_{\rm T}}+2\,\rho^3\left(-\frac{i}{k_{\rm T}k_0^3}-\frac{3}{k_{\rm T}^2\,k_0^2}+\frac{6\,i}{k_{\rm T}^3\,k_0}+\frac{6}{k_{\rm T}^4}\right)\right.\\
&+\rho^6\left(\frac{i}{k_{\rm T}\,k_0^6}+\frac{6}{k_{\rm T}^2\,k_0^5}-\frac{30\,i}{k_{\rm T}^3\,k_0^4}-\frac{120}{k_{\rm T}^4\,k_0^3}+\frac{360\,i}{k_{\rm T}^5\,k_0^2}+\frac{720}{k_{\rm T}^6\,k_0}-\frac{720\,i}{k_{\rm T}^7}\right)\\
&+i\,k_1\left(\frac{i}{k_{\rm T}\,k_0}+\frac{1}{k_{\rm T}^2}\right)\\
&-2\,i\,k_1\,\rho^3\left(\frac{i}{k_{\rm T}\,k_0^4}+\frac{4}{k_{\rm T}^2\,k_0^3}-\frac{12\,i}{k_{\rm T}^3\,k_0^2}-\frac{24}{k_{\rm T}^4\,k_0}+\frac{24\,i}{k_{\rm T}^5}\right)\\
&-i\,k_1\,\rho^6\left(-\frac{i}{k_{\rm T}\,k_0^7}-\frac{7}{k_{\rm T}^2\,k_0^6}+\frac{42\,i}{k_{\rm T}^3\,k_0^5}+\frac{210}{k_{\rm T}^4\,k_0^4}-\frac{840\,i}{k_{\rm T}^5\,k_0^3}-\frac{2520}{k_{\rm T}^6\,k_0^2}\right.\\
&\left.\left.\left.+\frac{5040\,i}{k_{\rm T}^7\,k_0}+\frac{5040}{k_{\rm T}^8}\right)\right]{\rm e}^{-i\,k_{\rm T}/k_0}\right\}\Bigg).
\end{aligned}
\tag{A.11}
$$

We find that the rest of the quantities can be written in terms of $\mathcal{I}^{31}_{\mathcal{RR}\gamma}(k_1,k_2,k_3)$ as follows: $\mathcal{I}^{32}_{\mathcal{RR}\gamma}(k_1,k_2,k_3)=\mathcal{I}^{31}_{\mathcal{RR}\gamma}(k_1,-k_2,k_3)$, $\mathcal{I}^{33}_{\mathcal{RR}\gamma}(k_1,k_2,k_3)=\mathcal{I}^{31}_{\mathcal{RR}\gamma}(-k_1,k_2,k_3)$, $\mathcal{I}^{34}_{\mathcal{RR}\gamma}(k_1,k_2,k_3)=\mathcal{I}^{31}_{\mathcal{RR}\gamma}(-k_1,-k_2,k_3)$, $\mathcal{J}^{31}_{\mathcal{RR}\gamma}(k_1,k_2,k_3)=\mathcal{I}^{31}_{\mathcal{RR}\gamma}(k_2,k_1,k_3)$, $\mathcal{J}^{32}_{\mathcal{RR}\gamma}(k_1,k_2,k_3)=\mathcal{J}^{31}_{\mathcal{RR}\gamma}(k_1,-k_2,k_3)$, $J^{33}_{\mathcal{RR}\gamma}(k_1,k_2,k_3)=\mathcal{J}^{31}_{\mathcal{RR}\gamma}(-k_1,k_2,k_3)$ and $\mathcal{J}^{34}_{\mathcal{RR}\gamma}(k_1,k_2,k_3)=\mathcal{J}^{31}_{\mathcal{RR}\gamma}(-k_1,-k_2,k_3)$.

Lastly, the quantities $\mathcal{M}_i(k_1,k_2,k_3)$, with $i=1,2,3$, are given by

$$
\begin{aligned}
\mathcal{M}_1(k_1,k_2,k_3) \;=\;& \frac{1}{k_{\rm T}}+\frac{k_1}{k_{\rm T}^2}-\frac{6\,i\,\rho^3}{k_{\rm T}^4}-\frac{24\,i\,k_1\,\rho^3}{k_{\rm T}^5}-\left[\frac{1}{k_{\rm T}}+k_1\left(\frac{i}{k_{\rm T}\,k_0}+\frac{1}{k_{\rm T}^2}\right)\right.\\
&+\rho^3\left(-\frac{1}{k_{\rm T}\,k_0^3}+\frac{3\,i}{k_{\rm T}^2\,k_0^2}+\frac{6}{k_{\rm T}^3\,k_0}-\frac{6\,i}{k_{\rm T}^4}\right)\\
&\left.+\rho^3\,k_1\left(-\frac{i}{k_{\rm T}k_0^4}-\frac{4}{k_{\rm T}^2\,k_0^3}+\frac{12\,i}{k_{\rm T}^3\,k_0^2}+\frac{24}{k_{\rm T}^4\,k_0}-\frac{24\,i}{k_{\rm T}^5}\right)\right]{\rm e}^{-i\,k_{\rm T}/k_0},
\end{aligned}
\tag{A.12a}
$$

$$
\begin{aligned}
\mathcal{M}_2(k_1,k_2,k_3) \;=\;& \lim_{\eta_{\rm e}\to 0}\left(-\frac{i\,e^{i\,k_{\rm T}\,\eta_{\rm e}}}{\eta_{\rm e}}\right) - \frac{k_1\,k_2+k_1\,k_3+k_2\,k_3}{k_{\rm T}} - \frac{k_1\,k_2\,k_3}{k_{\rm T}^2} + \frac{3\,i\,\rho^3}{k_{\rm T}^2} \\
& + \frac{6\,i\,\rho^3\;(k_1\,k_2+k_1\,k_3+k_2\,k_3)}{k_{\rm T}^4} + \frac{24\,i\,\rho^3\,k_1\,k_2\,k_3}{k_{\rm T}^5} \\
& - \Bigg[i\,k_0 - \frac{(k_1\,k_2+k_1\,k_3+k_2\,k_3)}{k_{\rm T}} \\
& - \frac{i\,k_1\,k_2\,k_3}{k_{\rm T}\,k_0} - \frac{k_1\,k_2\,k_3}{k_{\rm T}^2} - \frac{i\,\rho^3}{k_0^2} - \frac{3\,\rho^3}{k_{\rm T}\,k_0} + \frac{3\,i\,\rho^3}{k_{\rm T}^2} \\
& - i\,\rho^3\;(k_1\,k_2+k_2\,k_3+k_2\,k_3)\left(\frac{i}{k_{\rm T}\,k_0^3} + \frac{3}{k_{\rm T}^2\,k_0^2} - \frac{6\,i}{k_{\rm T}^3\,k_0} - \frac{6}{k_{\rm T}^4}\right) \qquad \text{(A.12b)} \\
& - \rho^3\,k_1\,k_2\,k_3\left(-\frac{i}{k_{\rm T}\,k_0^4} - \frac{4}{k_{\rm T}^2\,k_0^3} + \frac{12\,i}{k_{\rm T}^3\,k_0^2} + \frac{24}{k_{\rm T}^4\,k_0} - \frac{24\,i}{k_{\rm T}^5}\right)\Bigg]\,{\rm e}^{-i\,k_{\rm T}/k_0}, \\
\mathcal{M}_3(k_1,k_2,k_3) \;=\;& -\frac{3\,i\,\rho^3}{k_{\rm T}^2} - \frac{6\,i\,\rho^3\;(k_1+k_3)}{k_{\rm T}^3} - \frac{18\,i\,\rho^3\,k_1\,k_3)}{k_{\rm T}^4} \\
& + k_1^2\left(\frac{1}{k_{\rm T}} + \frac{k_3}{k_{\rm T}^2} - \frac{6\,i\,\rho^3}{k_{\rm T}^4} - \frac{24\,i\,\rho^3\,k_3}{k_{\rm T}^5}\right) \\
& + \Bigg[-\frac{3\,\rho^3}{k_{\rm T}\,k_0} + \frac{3\,i\,\rho^3}{k_{\rm T}^2} + 3\,\rho^3\;(k_1+k_3)\left(-\frac{i}{k_{\rm T}\,k_0^2} - \frac{2}{k_{\rm T}^2\,k_0} + \frac{2\,i}{k_{\rm T}^3}\right) \\
& - 3\,i\,\rho^3\,k_1\,k_3\left(\frac{i}{k_{\rm T}\,k_0^3} + \frac{3}{k_{\rm T}^2\,k_0^2} - \frac{6\,i}{k_{\rm T}^3\,k_0} - \frac{6}{k_{\rm T}^4}\right) \\
& - \frac{k_1^2}{k_{\rm T}} - k_1^2\,k_3\left(\frac{i}{k_{\rm T}\,k_0} + \frac{1}{k_{\rm T}^2}\right) \\
& - i\,\rho^3\,k_1^2\left(\frac{i}{k_{\rm T}k_0^3} + \frac{3}{k_{\rm T}^2k_0^2} - \frac{i6}{k_{\rm T}^3k_0} - \frac{6}{k_{\rm T}^4}\right) \qquad \text{(A.12c)} \\
& - \rho^3\,k_1^2\,k_3\left(-\frac{i}{k_{\rm T}\,k_0^4} - \frac{4}{k_{\rm T}^2\,k_0^3} + \frac{12\,i}{k_{\rm T}^3\,k_0^2} + \frac{24}{k_{\rm T}^4\,k_0} - \frac{24\,i}{k_{\rm T}^5}\right)\Bigg]\,{\rm e}^{-i\,k_{\rm T}/k_0}.
\end{aligned}
$$

Bibliography

[1] E. W. Kolb and M. S. Turner, *The Early Universe* (Addison-Wesley, Redwood City, California, 1990); S. Dodelson, *Modern Cosmology* (Academic Press, San Diego, U.S.A., 2003); V. F. Mukhanov, *Physical Foundations of Cosmology* (Cambridge University Press, Cambridge, England, 2005); S. Weinberg, *Cosmology* (Oxford University Press, Oxford, England, 2008); R. Durrer, *The Cosmic Microwave Background* (Cambridge University Press, Cambridge, England, 2008); D. H. Lyth and A. R. Liddle, *The Primordial Density Perturbation* (Cambridge University Press, Cambridge, England, 2009); P. Peter and J-P. Uzan, *Primordial Cosmology* (Oxford University Press, Oxford, England, 2009); H. Mo, F. v. d. Bosch and S. White, *Galaxy Formation and Evolution* (Cambridge University Press, Cambridge, England, 2010); D. Baumann and L. McAllister, *Inflation and String Theory*, arXiv:1404.2601 [hep-th].

[2] C. L. Bennet *et al.*, Astrophys. J. Suppl. **436**, 423 (1994); E. L. Wright *et al.*, Astrophys. J. Suppl. **436**, 443 (1994); K. M. Gorski, Astrophys. J. Suppl. **430**, L85 (1994); K. M. Gorski *et al.*, Astrophys. J. Suppl. **430**, L89 (1994);

[3] J. Dunkley *et al.*, Astrophys. J. Suppl. **180**, 306 (2009); E. Komatsu *et al.*, Astrophys. J. Suppl. **180**, 330 (2009).

[4] D. Larson *et al.*, Astrophys. J. Suppl. **192**, 16 (2011); E. Komatsu *et al.*, Astrophys. J. Suppl. **192**, 18 (2011).

[5] C. L. Bennett *et al.*, Astrophys. J. Suppl. **208**, 20 (2013); G. Hinshaw *et al.*, Astrophys. J. Suppl. **208**, 19 (2013).

[6] P. A. R. Ade *et al.*, arXiv:1303.5075 [astro-ph.CO].

[7] M. Colless *et al.*, Mon. Not. Roy. Astron. Soc. **328**, 1039 (2001).

[8] K. Abazajian *et al.*, Astrophys. J. Suppl. **182**, 543 (2009).

[9] P. Sarkar, J. Yadav, B. Pandey and S. Bharadwaj, Mon. Not. Roy. Astron. Soc. **399**, L128 (2009)

[10] J. Yang, M. S. Turner, G. Steigman, D. N. Schramm and K. A. Olive, Astrophys. J. **281**, 493 (1984); S. Burles, K. M. Nollett, M. S. Turner, Astrophys. J. **552**, L1 (2001); S. Burles, K. M. Nollett, M. S. Turner, Phys. Rev. D **63**, 063512 (2001).

[11] K. A. Olive, G. Steigman and T. P. Walker, Phys. Rep. **333**, 389 (2000).

[12] H. Kodama and M. Sasaki, Prog. Theor. Phys. Suppl. **78**, 1 (1984); V. F. Mukhanov, H. A. Feldman and R. H. Brandenberger, Phys. Rep. **215**, 203 (1992);J. E. Lidsey, A. Liddle, E. W. Kolb, E. J. Copeland, T. Barreiro and M. Abney, Rev. Mod. Phys. **69**, 373 (1997); A. Riotto, arXiv:hep-ph/0210162; W. H. Kinney, astro-ph/0301448; J. Martin, Lect. Notes Phys. **738**, 193 (2008); J. Martin, Lect. Notes Phys. **669**, 199 (2005); J. Martin, Braz. J. Phys. **34**, 1307 (2004); B. Bassett, S. Tsujikawa and D. Wands, Rev. Mod. Phys. **78**, 537 (2006); W. H. Kinney, arXiv:0902.1529 [astro-ph.CO]; L. Sriramkumar, Curr. Sci. **97**, 868 (2009) [arXiv:0904.4584 [astro-ph.CO]]; D. Baumann, arXiv:0907.5424v1 [hep-th].

[13] S. Perlmutter *et al.*, Astrophys. J. **517**, 565 (1999);

[14] J. Guy *et al.*, Astron. Astrphys. **523**, A7 (2010); M. Sullivan *et al.*, Astrophys. J. **737**, 102 (2011).

[15] P. A. R. Ade *et al.*, arXiv:1303.5076 [astro-ph.CO].

[16] P. A. R. Ade *et al.*, arXiv:1502.01589 [astro-ph.CO].

[17] P. A. R. Ade *et al.*, arXiv:1502.01590 [astro-ph.CO]

[18] F. Finelli and R. Brandenberger, Phys. Rev. D **65**, 103522 (2002); P. J. Steinhardt and N. Turok, Phys. Rev. D **65**, 126003 (2002).

[19] R. H. Brandenberger, arXiv:1206.4196 [astro-ph.CO]; D. Battefeld and P. Peter, arXiv:1406.2790 [astro-ph.CO].

[20] P. A. R. Ade *et al.*, arXiv:1303.5082 [astro-ph.CO].

[21] P. A. R. Ade *et al.*, arXiv:1502.02114 [astro-ph.CO].

[22] A. Gangui, F. Lucchin, S. Matarese and S. Mollerach, Astrophys. J. **430**, 447 (1994); A. Gangui, Phys. Rev. D **50**, 3684 (1994); A. Gangui and J. Martin, Mon. Not. Roy. Astron. Soc. **313**, 323 (2000); L. Wang and M. Kamionkowski, Phys. Rev. D **61**, 063504 (2000).

[23] J. Maldacena, JHEP **0305**, 013 (2003).

[24] D. Seery and J. E. Lidsey, JCAP **0506**, 003 (2005); X. Chen, Phys. Rev. D **72**, 123518 (2005); X. Chen, M.-x. Huang, S. Kachru and G. Shiu, JCAP **0701**, 002 (2007); D. Langlois, S. Renaux-Petel, D. A. Steer and T. Tanaka, Phys. Rev. Lett. **101**, 061301 (2008); Phys. Rev. D **78**, 063523 (2008).

[25] X. Chen, Adv. Astron. **2010**, 638979 (2010); Y. Wang, arXiv:1303.1523 [hep-th].

[26] E. Komatsu and D. N. Spergel, Phys. Rev. D **63**, 063002 (2001); E. Komatsu, D. N. Spergel and B. D. Wandelt, Astrophys. J. **634**, 14 (2005); D. Babich and M. Zaldarriaga, Phys. Rev. D **70**, 083005 (2004); M. Liguori, F. K. Hansen, E. Komatsu, S. Matarrese and A. Riotto, Phys. Rev. D **73**, 043505 (2006); C. Hikage, E. Komatsu and T. Matsubara, Astrophys. J. **653** (2006) 11 (2006); J. R. Fergusson and E. P. S. Shellard, Phys. Rev. D **76**, 083523 (2007); A. P. S. Yadav, E. Komatsu and B. D. Wandelt, Astrophys. J. **664**, 680 (2007); P. Creminelli, L. Senatore and M. Zaldarriaga, JCAP **0703**, 019 (2007); A. P. S. Yadav and B. D. Wandelt, Phys. Rev. Lett. **100**, 181301 (2008); C. Hikage, T. Matsubara, P. Coles, M. Liguori, F. K. Hansen and S. Matarrese, Mon. Not. Roy. Astron. Soc. **389**, 1439 (2008); O. Rudjord, F. K. Hansen, X. Lan, M. Liguori, D. Marinucci and S. Matarrese, Astrophys. J. **701**, 369 (2009); K. M. Smith, L. Senatore and M. Zaldarriaga, JCAP **0909**, 006 (2009); J. Smidt, A. Amblard, C. T. Byrnes, A. Cooray, A. Heavens and D. Munshi, Phys. Rev. D **81**, 123007 (2010); J. R. Fergusson, M. Liguori and E. P. S. Shellard, arXiv:1006.1642v2 [astro-ph.CO].

[27] M. Liguori, E. Sefusatti, J. R. Fergusson and E. P. S. Shellard, Adv. Astron. **2010**, 980523 (2010); A. P. S. Yadav and B. D. Wandelt, arXiv:1006.0275v3 [astro-ph.CO]; E. Komatsu, Class. Quantum Grav. **27**, 124010 (2010).

[28] P. A. R. Ade *et al.*, arXiv:1303.5084 [astro-ph.CO].

[29] P. A. R. Ade *et al.*, arXiv:1502.01592 [astro-ph.CO].

[30] X. Gao, T. Kobayashi, M. Shiraishi, M. Yamaguchi, J. Yokoyama and S. Yokoyama, arXiv:1207.0588 [astro-ph.CO].

[31] D. Jeong and M. Kamionkowski, Phys. Rev. Lett. **108**, 251301 (2012); L. Dai, D. Jeong and M. Kamionkowski, Phys. Rev. D **87**, 103006 (2013); Phys. Rev. D **88**, 043507 (2013).

[32] S. Kundu, arXiv:1311.1575 [astro-ph.CO].

[33] J. Maldacena and G. L. Pimentel, JHEP **1109**, 045 (2011); X. Gao, T. Kobayashi, M. Yamaguchi and J. Yokoyama, Phys. Rev. Lett. **107**, 211301 (2011).

[34] T. Tanaka and Y. Urakawa, JCAP **1105**, 014 (2011).

[35] D. J. Schwarz, C. A. Terrero-Escalante and A. A. Garcia, Phys. Lett. B **517**, 243 (2001); S. M. Leach, A. R. Liddle, J. Martin and D. J. Schwarz, Phys. Rev. D **66**, 023515 (2002).

[36] R. Arnowitt, S. Deser and C. W. Misner, Phys. Rev. **117**, 1595 (1960).

[37] J. Martin and L. Sriramkumar, JCAP **1201**, 008 (2012).

[38] T. Bunch and P. C. W. Davies, Proc. Roy. Soc. Lond. A **360**, 117 (1978).

[39] E. D. Stewart and D. H. Lyth, Phys. Lett. B **302**, 171 (1993); J. Martin and D. J. Schwarz, Phys. Rev. D, **62**, 103520 (2000).

[40] I. S. Gradshteyn and I. M. Ryzhik, *Table of Integrals, Series and Products*, Seventh Edition (Acedemic Press, New York, 2007).

[41] D. S. Salopek, J. R. Bond and J. M. Bardeen, Phys. Rev. D **40**, 1753 (1989); C. Ringeval, Lect. Notes Phys. **738**, 243 (2008).

[42] E. F. Bunn, A. R. Liddle and M. J. White, Phys. Rev. D **54**, R5917 (1996).

[43] A. Lewis and S. Bridle, Phys. Rev. D **66**, 103511 (2002).

[44] D. Blas, J. Lesgourgues and T. Tram, JCAP **07**, 034 (2011).

[45] A. A. Starobinsky, Phys. Lett. B **91**, 99 (1980).

[46] J. Martin, C. Ringeval and R. Trotta, Phys. Rev. D **83**, 063524 (2011); M. J. Mortonson, H. V. Peiris and R. Easther, Phys. Rev. D **83**, 043505 (2011); R. Easther and H. Peiris, Phys. Rev. D **85**, 103533 (2012); J. Norena, C. Wagner, L. Verde, H. V. Peiris and R. Easther, Phys. Rev. D **86**, 023505 (2012).

[47] J. Martin, C. Ringeval and V. Vennin, arXiv: 1303.3787 [astro-ph.CO].

[48] J. Martin, C. Ringeval, R. Trotta and V. Vennin, JCAP **1403**, 039 (2014).

[49] J. Martin, C. Ringeval and V. Vennin, arXiv:1407.4034 [astro-ph.CO].

[50] P. A. R. Ade *et al.*, arXiv:1403.4302 [astro-ph.CO].

[51] P. A. R. Ade *et al.*, Phys. Rev. Lett. **112**, 241101 (2014).

[52] R. Adam *et al.*, arXiv:1409.5738 [astro-ph.CO].

[53] P. A. R. Ade *et al.*, arXiv:1502.00612 [astro-ph.CO].

[54] D. K. Hazra, J. Martin and L. Sriramkumar, Phys. Rev. D **86**, 063523 (2012).

[55] D. K. Hazra, L. Sriramkumar and J. Martin, JCAP **05**, 026 (2013).

[56] V. Sreenath, R. Tibrewala and L. Sriramkumar, JCAP **1312**, 037 (2013).

[57] M. S. Turner, Phys. Rev. D **28**, 1243 (1983); A. Albrecht, P. J. Steinhardt, M. S. Turner and F. Wilczek, Phys. Rev. Lett. **48**, 1437 (1982); J. H. Traschen and R. H. Brandenberger, Phys. Rev. D **42**, 2491 (1990); Y. Shtanov, J. H. Traschen and R. H. Brandenberger, Phys. Rev. D **51**, 5438 (1995); L. Kofman, A. D. Linde, and A. A. Starobinsky, Phys. Rev. D **56**, 3258 (1997); D. I. Podolsky and A. A. Starobinsky, Grav. Cosmol. Suppl. **8N1**, 13 (2002); D. I. Podolsky, G. N. Felder, L. Kofman, and M. Peloso, Phys. Rev. D **73**, 023501 (2006).

[58] F. Finelli and R. H. Brandenberger, Phys. Rev. Lett. **82**, 1362 (1999); K. Jedamzik, M. Lemoine and J. Martin, JCAP **1009**, 034 (2010); JCAP **1004**, 021 (2010); R. Easther, R. Flauger and J. B. Gilmore, JCAP 1104, 027 (2011); R. K. Jain, P. Chingangbam and L. Sriramkumar, Nucl. Phys. B **852**, 366 (2011).

[59] J. Martin, C. Ringeval and V. Vennin, arXiv: 1410.7958 [astro-ph.CO].

[60] E. Komatsu and D. N. Spergel, Phys. Rev. D **63**, 063002 (2001).

[61] P. Creminelli and M. Zaldarriaga, JCAP **0410**, 006 (2004).

[62] C. Cheung, A. L. Flitzpatrick, J. Kaplan and L. Senatore, JCAP **0802**, 021 (2008); S. Renaux-Petel, JCAP **1010**, 020 (2010); J. Ganc and E. Komatsu, JCAP **1012**, 009 (2010); P. Creminelli, G. D'Amico, M. Musso and J. Norena, JCAP **1111**, 038 (2011); D. Chialva, JCAP **1210**, 037 (2012); K. Schalm, G. Shiu and T. van der Aalst, JCAP **1303**, 005 (2013); E. Pajer, F. Schmidt and M. Zaldarriaga, Phys. Rev. D **88**, 083502 (2013).

[63] L. Senatore and M. Zaldarriaga, JCAP **1208**, 001 (2012); P. Creminelli, J. Norena and M. Simonovoc, JCAP **1207**, 052 (2012); P. Creminelli, A. Perko, L. Senatore, M. Simonovic and G. Trevisan, JCAP **1311**, 015 (2013); L. Berezhiani and J. Khoury, JCAP **1402**, 003 (2014); L. Berezhiani, J. Khoury and J. Wang, arXiv:1401.7991 [hep-th]; H. Collins, R. Holman and T. Vardanyan, arXiv:1405.0017 [hep-th].

[64] V. Sreenath and L. Sriramkumar, JCAP **1410**, 021 (2014).

[65] S. W. Hawking, Phys. Lett. B **115**, 295 (1982); A. A. Starobinsky, Phys. Lett. B **117**, 175 (1982); A. Guth and S.-Y. Pi, Phys. Rev. Lett. **49**, 1110 (1982); V. N. Lukash, Sov. Phys. JETP **52**, 807 (1980); D. H. Lyth, Phys. Rev. D **31**, 1792 (1985).

[66] S. M. Leach and A. R. Liddle, Phys. Rev. D **63**, 043508 (2001); S. M. Leach, M. Sasaki, D. Wands and A. R. Liddle, *ibid.* **64**, 023512 (2001); R. K. Jain, P. Chingangbam and L. Sriramkumar, JCAP **0710**, 003 (2007).

[67] H. Motohashi, A. A. Starobinsky and J. Yokoyama, arXiv:1411.5021v1 [astro-ph.CO].

[68] J. Martin, H. Motohashi and T. Suyama, Phys. Rev. D **87**, 023514 (2013); M. H. Namjoo, H. Firouzjahi and M. Sasaki, Europhys. Lett. **101**, 39001 (2013); M. G. Jackson and G. Shiu, Phys. Rev. D **88**, 123511 (2013)

[69] P. Adshead, W. Hu, C. Dvorkin and H. V. Peiris, Phys. Rev. D **84**, 043519 (2011); A. Achucarro, J-O. Gong, G. A. Palma and S. P. Patil, Phys. Rev. D **87**, 121301 (2013); J. Gong, K. Schalm and G. Shiu, Phys. Rev. D **89**, 063540 (2014).

[70] M. H. Namjoo, H. Firouzjahi and M. Sasaki, Europhys. Lett. **101**, 39001 (2013); X. Chen, H. Firouzjahi, M. Namjoo and M. Sasaki, Europhys. Lett. **102**, 59001 (2013).

[71] J. Ganc, Phys. Rev. D **84**, 063514 (2011); I. Agullo and L. Parker, Phys. Rev. D **83**, 063526 (2011); Gen. Rel. Grav. **43**, 10 (2011).

[72] V. Sreenath D. K. Hazra and L. Sriramkumar, arXiv:1410.0252 [astro-ph.CO], to appear in JCAP.

[73] L. F. Abbott and M. B. Wise, Nucl. Phys. B **244**, 541 (1984); D. H. Lyth and E. D. Stewart, Phys. Lett. B **274**, 168 (1992); J. Martin and D. J. Schwarz, Phys. Rev. D **57**, 3302 (1998); L. Sriramkumar and T. Padmanabhan, Phys. Rev. D 71, 103512 (2005).

[74] A. A. Starobinsky, Sov. Phys. JETP Lett. **55**, 489 (1992).

[75] F. Arroja, A. E. Romano and M. Sasaki, Phys. Rev. D **84**, 123503 (2011); F. Arroja and M. Sasaki, JCAP **1208**, 012 (2012).

[76] J. Martin, L. Sriramkumar and D. K. Hazra, JCAP **1409**, 039 (2014).

[77] B. Feng and X. Zhang, Phys. Lett. B **570**, 145 (2003); M. Kawasaki and F. Takahashi, Phys. Lett. B **570**, 151 (2003); R. Sinha and T. Souradeep, Phys. Rev. D **74**, 043518 (2006); M. J. Mortonson and W. Hu, Phys. Rev. D **80**, 027301 (2009).

[78] J. M. Cline, P. Crotty and J. Lesgourgues, JCAP **0309**, 010 (2003); C. R. Contaldi, M. Peloso, L. Kofman and A. Linde, JCAP **0307**, 002 (2003); D. Boyanovsky, H. J. de Vega and N. G. Sanchez, Phys. Rev. D **74**, 123006 (2006); Phys. Rev. D **74**, 123007 (2006); B. A. Powell and W. H. Kinney, Phys. Rev. D **76**, 063512 (2007); C. Destri, H. J. de Vega and N. G. Sanchez, Phys. Rev. D **78**, 023013 (2008).

[79] R. K. Jain, P. Chingangbam, J.-O. Gong, L. Sriramkumar and T. Souradeep, JCAP **0901**, 009 (2009); R. K. Jain, P. Chingangbam, L. Sriramkumar and T. Souradeep, Phys. Rev. D **82**, 023509 (2010).

[80] L. Lello, D. Boyanovsky and R. Holman, arXiv:1307.4066 [astro-ph.CO]; M. Cicoli, S. Downes and B. Dutta, arXiv:1309.3412 [hep-th]; F. G. Pedro and A. Westphal, arXiv:1309.3413 [hep-th].

[81] J. A. Adams, B. Cresswell and R. Easther, Phys. Rev. D **64**, 123514 (2001); L. Covi, J. Hamann, A. Melchiorri, A. Slosar and I. Sorbera, Phys. Rev. D **74**, 083509 (2006); J. Hamann, L. Covi, A. Melchiorri and A. Slosar, Phys. Rev. D **76**, 023503 (2007); M. J. Mortonson, C. Dvorkin, H. V. Peiris and W. Hu, Phys. Rev. D **79**, 103519

(2009); M. Joy, V. Sahni and A. A. Starobinsky, Phys. Rev. D **77**, 023514 (2008); M. Joy, A. Shafieloo, V. Sahni and A. A. Starobinsky, JCAP **0906**, 028 (2009).

[82] D. K. Hazra, M. Aich, R. K. Jain, L. Sriramkumar and T. Souradeep, JCAP **1010**, 008 (2010).

[83] M. Benetti, M. Lattanzi, E. Calabrese and A. Melchiorri, Phys. Rev. D **84**, 063509 (2011); M. Benetti, arXiv:1308.6406 [astro-ph.CO].

[84] J. Martin and C. Ringeval, Phys. Rev. D **69**, 083515 (2004); Phys. Rev. D **69**, 127303 (2004); JCAP **0501**, 007 (2005); M. Zarei, Phys. Rev. D **78**, 123502 (2008).

[85] C. Pahud, M. Kamionkowski and A. R. Liddle, Phys. Rev. D **79**, 083503 (2009).

[86] R. Flauger, L. McAllister, E. Pajer, A. Westphal and G. Xu, JCAP **1006**, 009 (2010).

[87] T. Kobayashi and F. Takahashi, JCAP **1101**, 026 (2011).

[88] M. Aich, D. K. Hazra, L. Sriramkumar and T. Souradeep, Phys. Rev. D **87**, 083526 (2013).

[89] H. Peiris, R. Easther and R. Flauger, arXiv:1303.2616 [astro-ph.CO]; R. Easther and R. Flauger, arXiv:1308.3736 [astro-ph.CO].

[90] P. D. Meerburg, D. N. Spergel and B. D. Wandelt, arXiv:1308.3704 [astro-ph.CO]; P. D. Meerburg and D. N. Spergel, arXiv:1308.3705 [astro-ph.CO].

[91] D. K. Hazra, A. Shafieloo and T. Souradeep, JCAP **1307**, 031 (2013); P. Hunt and S. Sarkar, arXiv:1308.2317 [astro-ph.CO].

[92] X. Chen, R. Easther and E. A. Lim, JCAP **0706**, 023 (2007); JCAP **0804**, 010 (2008).

[93] S. Hotchkiss and S. Sarkar, JCAP **1005**, 024 (2010); S. Hannestad, T. Haugbolle, P. R. Jarnhus and M. S. Sloth, JCAP **1006**, 001 (2010); R. Flauger and E. Pajer, JCAP **1101**, 017 (2011); P. Adshead, W. Hu, C. Dvorkin and H. V. Peiris, Phys. Rev. D **84**, 043519 (2011); X. Chen, JCAP **1201**, 038 (2012); P. Adshead, W. Hu and V. Miranda, Phys. Rev. D **88**, 023507 (2013); J. S. Horner and C. R. Contaldi, arXiv:1311.3224 [astro-ph.CO].

[94] P. Ramachandran and G. Varoquaux, IEEE Computing in Science and Engineering **13**, 40 (2011)

[95] W. H. Press, S. A. Teukolsky, W. T. Wetterling and B. P. Flannery, *Numerical Recipes: The Art of Scientific Computing* (Cambridge University Press, Cambridge, England, 2007).

[96] K. Kohri, D. H. Lyth, C. A. Valenzuela-Toledo, JCAP **1002**, 023 (2010); Erratum-ibid. **1009**, E01 (2011).

[97] A. Chambers and A. Rajantie, JCAP **0808**, 002 (2008).

[98] X. Gao, M. Lilley and P. Peter, arXiv:1406.4119 [gr-qc].

[99] V. Assassi, D. Baumann and D. Green, JCAP **1211**, 047 (2012).

[100] R. H. Brandenberger and J. Martin, Class. Quantum Grav. **30**, 113001 (2013).

[101] J. R. Fergusson, H. F. Gruetjen, E. P. S. Shellard and B. Wallisch, arXiv:1412.6152 [astro-ph.CO]; M. Münchmeyer, P. D. Meerburg and B. D. Wandelt, arXiv:1412.3461 [astro-ph.CO].

List of papers on which this thesis is based

Papers in Refereed Journals

1. **V. Sreenath**, R. Tibrewala and L. Sriramkumar, *Numerical evaluation of the three-point scalar-tensor cross-correlations and the tensor bi-spectrum*, JCAP **1312**, 037 (2013) [arXiv:1309.7169 [astro-ph.CO]].

2. **V. Sreenath** and L. Sriramkumar, *Examining the consistency relations describing the three-point functions involving tensors*, JCAP **1410**, 021 (2014) [arXiv:1406.1609 [astro-ph.CO]].

3. **V. Sreenath**, D. K. Hazra and L. Sriramkumar, *On the scalar consistency relation away from slow roll*, JCAP **1502**, 029 (2015) [arXiv:1410.0252 [astro-ph.CO]].

Presentations in Conferences

1. A talk on *Scalar-tensor cross correlations and tensor bi-spectra in models involving deviations from slow roll* in **Twenty-Seventh Meeting of the Indian Association for General Relativity and Gravitation**, Department of Physics, H. N. Bahuguna Garhwal University, Srinagar (Garhwal), Uttarakhand, India, March 7–9, 2013.

2. A talk on *On the consistency relations describing the three-point functions involving tensors* in **Particle Cosmology after Planck**, DESY, Hamburg, Germany, September 23–26, 2014.